

ISSN 1857-1727

Volume 9

No. 1, 2014

CHEMISTRY

JOURNAL OF MOLDOVA

General, Industrial and Ecological Chemistry

Editor-in-chief: Gheorghe DUCA

Academy of Sciences of Moldova
Institute of Chemistry
State University of Moldova

Academy of Sciences of Moldova, Institute of Chemistry
State University of Moldova, Faculty of Chemistry and Chemical Technology

CHEMISTRY JOURNAL OF MOLDOVA

General, Industrial and Ecological Chemistry

Editor-in chief: Academician Gheorghe DUCA, Academy of Sciences of Moldova
Editors: Corr. member Tudor LUPASCU, Academy of Sciences of Moldova
Corr. member Mihail REVENCO, State University of Moldova

Local Editorial Board:

Dr. Hab. A. ARICU
Academy of Sciences of Moldova

Dr. Hab. D. BATIR
Academy of Sciences of Moldova

Acad. I. BERSUKER
Academy of Sciences of Moldova

Dr. G. DRAGALINA
State University of Moldova

Dr. V. GLADCHI
State University of Moldova

Dr. Hab. M. GONTA
State University of Moldova

Acad. A. GULEA
State University of Moldova

Dr. Hab. F. MACAEV
Academy of Sciences of Moldova

Dr. R. NASTAS, scientific secretary
of the editorial board,
Academy of Sciences of Moldova

Dr. Hab. I. POVAR
Academy of Sciences of Moldova

Dr. Hab. R. STURZA
Technical University of Moldova

Acad. C. TURTA
Academy of Sciences of Moldova

Acad. P. VLAD
Academy of Sciences of Moldova

International Editorial Board:

Acad. S. ALDOSHIN
Russian Academy of Sciences

Acad. S. ANDRONATI
National Academy of Sciences of Ukraine

Prof. V. ARION
University of Vienna, Austria

Prof. M. BAHADIR
Technical University of Braunschweig, Germany

Prof. J. de BOER
Vrije University Amsterdam, The Netherlands

Prof. L. CHIBOTARU
Katholieke Universiteit Leuven, Belgium

Prof. F. FRIMMEL
University of Karlsruhe, Germany

Acad. V. GONCHEARUK
National Academy of Sciences of Ukraine

Acad. I. HAIDUC
Romanian Academy, Bucharest, Romania

Acad. F. LAKHVICH
National Academy of Sciences of Belarus

Acad. J. LIPKOWSKI
Polish Academy of Sciences

Acad. V. LUNIN
Lomonosov Moscow State University, Russia

Prof. M. MACOVEANU
"Gh. Asachi" Technical University, Iasi, Romania

Acad. B. SIMIONESCU
Romanian Academy, Iasi, Romania

Editorial office address:

Institute of Chemistry, Academy of Sciences of Moldova, 3, Academiei Str., MD-2028, Chisinau, Republic of Moldova
Tel: + 373 22 725490; Fax: +373 22 739954; e-mail: chemjm@asm.md, chemjm@gmail.com
Web: www.cjm.asm.md

ISSUE CONTENTS LIST WITH GRAPHICAL ABSTRACTS

SPECIAL ISSUE DEDICATED TO THE INTERNATIONAL CONFERENCE DEDICATED TO THE 55th ANNIVERSARY FROM THE FOUNDATION OF THE INSTITUTE OF CHEMISTRY OF THE ACADEMY OF SCIENCE OF MOLDOVA

EDITORIAL

7

PREFACE

REVIEW PAPER

ORGANIC CHEMISTRY

8

ROLE OF CYCLODEXTRINS IN NEW ANTIMYCOBACTERIAL FORMULATIONS

Veaceslav Boldescu, Fliur Macaev, Gheorghe Duca

This paper is dedicated to the role of cyclodextrins in new formulations for the treatment of infections with *Mycobacterium tuberculosis* that are in the process of design and development. Cyclodextrins play the role of solubilizing agents and promoters of the antimycobacterial substances penetration inside the mycobacterial cell.



REVIEW PAPER

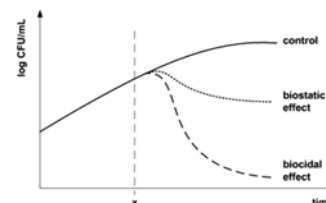
ORGANIC CHEMISTRY

14

ANTIMICROBIAL REAGENTS AS FUNCTIONAL FINISHING FOR TEXTILES INTENDED FOR BIOMEDICAL APPLICATIONS. I. SYNTHETIC ORGANIC COMPOUNDS

Madalina Zanoaga, Fulga Tanasa

This article offers an overview of some contemporary antimicrobial (biocides and biostatics) agents used as functional finishing for textiles intended for biomedical applications. It reviews only synthetic agents, namely quaternary ammonium compounds, halogenated phenols, polybiguanides, N-halamines, and renewable peroxides, as a part of an extensive study currently in progress.



FULL PAPER

ECOLOGICAL CHEMISTRY

33

ACTIVATED CARBONS FROM VEGETAL RAW MATERIALS TO SOLVE ENVIRONMENTAL PROBLEMS

Viktor Mukhin, Tudor Lupascu, Nadejda Voropaeva, Yuriy Spiridonov, Nicolay Bogdanovich, Vasiliy Gur'janov

Technologies for active carbons obtaining from vegetable by-products such as straw, nut shells, fruit stones, sawdust, hydrolysis products of corn cobs and sunflower husks have been developed. The physico-chemical characteristics, structural parameters and sorption characteristics of obtained active carbons were determined. The ability of carbonaceous adsorbents for detoxification of soil against pesticides, purification of surface waters and for removal of organic pollutants from wastewaters has been evaluated. The obtained results reveal the effectiveness of their use in a number of environmental technologies.

FULL PAPER

ECOLOGICAL CHEMISTRY

37

EURASIAN MINERAL WATER: MATHEMATICAL MODELING, CLASSIFICATION AND ASSESSMENT OF THEIR IMPACT ON THE BIOCHEMICAL COMPOSITION OF HUMAN BLOOD

Nikolay Kornilov, Elena Kornilova, Elena Stepanenko

In the article the results of comparative analysis of the composition of the Eurasian hydromineral resources and the assessment of their impact on the physiological condition of a human organism according to biochemical studies of venous blood are presented. Processing of initial data on the composition and properties of mineral waters chloride-hydrocarbonate, sulphate- hydrocarbonate and chloride-sulphate types and venous blood are made using the method of mathematical modelling, developed by the authors of this article. It is shown that in the balneological impact of hydromineral resources on the body in the blood increases the haemoglobin and oxygen, decreases glucose, and acid-base pH shifted to high alkalinity.

FULL PAPER

ECOLOGICAL CHEMISTRY

42

EVALUATION OF WATER POLLUTION STATUS IN SIRET HYDROGRAPHICAL BASIN (SUCEAVA REGION) DUE TO AGRICULTURAL ACTIVITIES

Carmen Zaharia

The study presents data concerning the water pollution status of Siret hydrographical basin (i.e. surface and ground waters, lakes) in Suceava County area (different controlling/monitoring sections) due to agricultural productive activities, especially regarding some quality indicators (nitrogen-based nutrient concentrations) evaluated for 2008. These data are recommending the necessity of continuous monitoring of water quality in the Siret River hydrographical basin, in all existing control sections, for identification of any pollution episodes, non-reported by polluters to the local environmental regulators.

FULL PAPER

ECOLOGICAL CHEMISTRY

53

VALORIZATION OF LOW-COST NATURAL MATERIALS IN DEPOLLUTION PROCESSES OF WASTEWATER

Laura Bulgariu, Igor Cretescu, Dumitru Bulgariu, Matei Macoveanu

In this paper, are presented the adsorptive characteristics of a low-cost material that are abundant in our region, namely: Romanian peat moss from Poiana Stampei (Romania), for the removal of different toxic heavy metal ions (Pb(II), Hg(II), Co(II) and Ni(II)) and oil products from aqueous media. The experiments have concerned the influence of several experimental parameters (initial solution pH, adsorbent dose, initial heavy metals concentration, contact time, and temperature) on the heavy metals and oil products removal efficiency. The most important conditions for desorption of heavy metal ions from loaded-materials, required for their regeneration are also presented.

FULL PAPER

ECOLOGICAL CHEMISTRY

59

QUANTIFICATION AND BIOREMEDIATION OF ENVIRONMENTAL SAMPLES BY DEVELOPING A NOVEL AND EFFICIENT METHOD

Mohammad Osama, Felicia Armstrong, Peter Norris, Habiba Tahira Hussain

Pleurotus ostreatus, a white rot fungus, is capable of bioremediating a wide range of organic contaminants including Polycyclic Aromatic Hydrocarbons. Ergosterol is produced by living fungal biomass and used as a measure of fungal biomass. The first part of this work deals with the extraction and quantification of PAHs from contaminated sediments by Lipid Extraction Method. The second part consists of the development of a novel extraction method (Ergosterol Extraction Method), quantification and bioremediation.

FULL PAPER

INDUSTRIAL CHEMISTRY

74

REMOVAL OF REMAZOL ROSSO RB DYE FROM AQUEOUS EFFLUENTS BY HOMOGENOUS FENTON OXIDATION PROCESSES

Carmen Zaharia, Victoria Fedorcea, Adrian Beda, Victor Amarandei, Augustin Muresan

The paper presents some data from our laboratory-setup experiments of homogenous oxidative processes with hydrogen peroxide (i.e. advanced Fenton oxidation processes) applied for Remazol Rosso RB dye-containing aqueous systems, especially textile effluents. Therefore, some different operating parameters (including pH, concentration of dye, H₂O₂ and ferrous ions, oxidation time, temperature, stirring regime, among its) were tested for determination of the best performance in effluent discoloration and dye removal, meaning the optimal values of each studied parameters for highest discoloration or dye removal.

FULL PAPER

INDUSTRIAL CHEMISTRY

80

RADIATION CHEMICAL CONVERSION OF OIL DERIVED FROM OIL-BITUMEN ROCK

Lala Jabbarova, Islam Mustafaev, Rauf Rzayev, Zarqalam Nabizade, Navoi Ibadov, Saida Akhmedbekova

The results of research in the radiation processing of synthetic oil derived from oil-bitumen rock of the Balakhany deposit in Azerbaijan are presented. The study has been conducted on a ⁶⁰Co gamma-source at a dose rate of P = 0.5 Gy/s and various absorbed doses of D = 43–216 kGy. Samples of synthetic oil from natural bitumen rocks have been analyzed by chromatography, gas chromatography–mass spectrometry, and IR-spectroscopy, and their radiation resistance has been evaluated. The results of the study allow for both assessment of the feasibility of manufacturing petrochemicals for various applications by radiation processing and use of these materials for isolating radioactive sources to preclude their impact on the environment.

FULL PAPER

INDUSTRIAL CHEMISTRY

85

THE DIMINISHING OF THE CONTENT OF TEXTILE DIRECT DYES AND AUXILIARY COMPOUNDS DURING THEIR CATALYTIC OXIDATION

Maria Gonta, Gheorghe Duca, Vera Matveevici, Larisa Mocanu

Advanced oxidation methods of organic compounds lead to their partial mineralization and increase of the adsorption process efficiency on the surface of oxidized activated carbon. We have studied the oxidation process using model solutions containing mixture of dye direct brown, ethylene glycol and sodium lauryl sulfate under the action of Fenton reagent, in the presence and absence of UV irradiation or under the action of electric current (in the electrochemical cell). The same studies were performed by replacing the iron (II) ion with titanium dioxide.

FULL PAPER

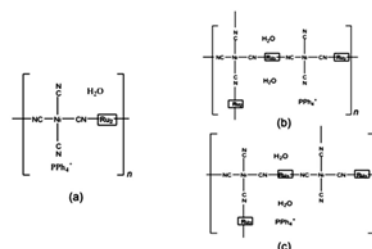
INORGANIC AND COORDINATION CHEMISTRY

93

MIXED-METAL COMPLEXES OF MIXED-VALENT DINUCLEAR RUTHENIUM(II,III) CARBOXYLATE AND TETRACYANIDONICKELATE(II)

Masahiro Mikuriya, Yusuke Tanaka, Daisuke Yoshioka, Makoto Handa

Mixed-metal chain complexes constructed from lantern-type dinuclear ruthenium(II,III) carboxylate unit and tetracyanonickelate(II), $(\text{PPh}_4)_n[\text{Ru}_2(\text{O}_2\text{CCH}_3)_4\text{Ni}(\text{CN})_4]_n \cdot n\text{H}_2\text{O}$ (**1**) and $(\text{PPh}_4)_n[\text{Ru}_2\{\text{O}_2\text{CC}(\text{CH}_3)_3\}_4]_{3n}[\text{Ni}(\text{CN})_4]_{2n} \cdot 2n\text{H}_2\text{O}$ (**2**), where very weak antiferromagnetic interaction is operating, were synthesized and characterized by elemental analysis and IR and UV-vis spectroscopies and temperature dependence of magnetic susceptibilities (4.5—300K).



FULL PAPER

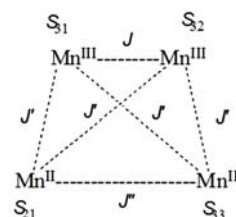
INORGANIC AND COORDINATION CHEMISTRY

100

MIXED-VALENT TETRANUCLEAR $\text{Mn}^{\text{II}}\text{Mn}^{\text{III}}$ COMPLEX WITH 1,3-DIAMINO-2-HYDROXYPROPANE- N,N',N'',N''' -TETRAACETIC ACID

Masahiro Mikuriya, Nobuyuki Nagao, Satoshi Kurahashi, Atsushi Tabuchi, Seiki Tomohara, Motohiro Tsuboi, Daisuke Yoshioka, Hiroshi Sakiyama, Akira Fuyuhiko

Mixed-valent tetranuclear $\text{Mn}^{\text{II}}\text{Mn}^{\text{III}}$ complex with 1,3-dimino-2-hydroxypropane- N,N',N'',N''' -tetracetic acid, $\text{Ca}_2[\text{Mn}_4\{\mu\text{-OHO}\}(\text{dhpta})_2(\text{CH}_3\text{COO})_2]$, where considerable antiferromagnetic interactions are operating, was synthesized and characterized by elemental analysis and IR and UV-vis spectroscopies, temperature dependence of magnetic susceptibilities (4.5—300K), and single-crystal X-ray crystallography.



FULL PAPER

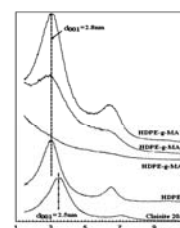
ORGANIC CHEMISTRY

106

STUDY OF PROPERTIES OF SOME POLYETHYLENE-CLAY NANOCOMPOSITES: INFLUENCE OF PREPARATION METHOD ON THE DEGREE OF CLAY INTERCALATION/EXFOLIATION

Fulga Tanasa, Madalina Zanoaga

Nanocomposites based on HDPE and HDPE-g-MA, as matrix, and nanoclay Cloisite 20A, as filler, were obtained by melt compounding and solution blending, and their properties were comparatively studied in order to establish the dependence of the clay degree of exfoliation/intercalation on the preparation procedure.



FULL PAPER

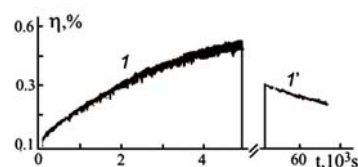
PHYSICAL CHEMISTRY AND CHEMICAL PHYSICS

112

HOLOGRAPHIC INFORMATION MEDIA BASED ON AZO-POLYMERS WITH DIFFERENT STRUCTURES

Irina Davidenko

Polarization sensitive holographic recording was accomplished in new synthesized azobenzene polymer composites with Co metallic polycomplexes of different structure.



FULL PAPER

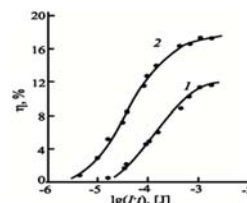
PHYSICAL CHEMISTRY AND CHEMICAL PHYSICS

117

HOLOGRAPHIC RECORDING MEDIA BASED ON ELECTRONS DONOR OLIGOMERS

Nicolay Davidenko, Irina Davidenko, Nicolay Chuprina, Yuriy Getmanchuk, Leonid Kostenko, Elena Mokrinskaya, Valeriy Pavlov, Sergey Studzinsky, Larisa Tonkopiieva

Information properties of recording media based on electrons donor oligomer of different structure for thermoplastic technique are investigated.



FULL PAPER

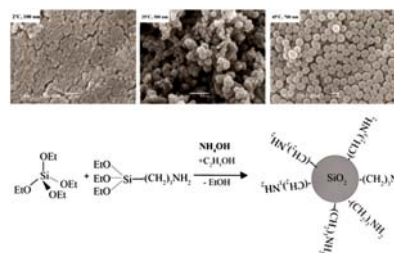
PHYSICAL CHEMISTRY AND CHEMICAL PHYSICS

123

AMINOSILICA NANO- AND SUBMICROSOPHERES: ANALYSIS OF FACTORS INFLUENCING MORPHOLOGY, STRUCTURE AND PROPERTIES

Inna Melnyk

Current paper focuses on the analysis of influence of main factors (stages of the synthesis, the ratio of the reacting components, the order of their introduction, the concentration of water and ammonia, the synthesis temperature) on the morphology, size and content of functional groups of aminosilicic nano- and submicrospheres. The recommendations for the synthesis of particles with predetermined properties were done. It is shown, that the ratio of the reacting components mainly affects the content of 3-aminopropyl functional groups and the temperature of the hydrolytic polycondensation reaction - the size of the particles.



FULL PAPER

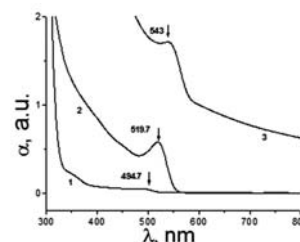
PHYSICAL CHEMISTRY AND CHEMICAL PHYSICS

128

SYNTHESIS AND CHARACTERIZATION OF CdSe COLLOIDAL QUANTUM DOTS IN ORGANIC SOLVENT

Ion Geru, Olga Bordian, Constantin Loshmansky, Ion Culeac, Constantin Turta

In this paper we present experimental results on preparation and characterization of colloidal CdSe quantum dots in organic solvent. CdSe QDs were synthesized following a modified literature method. CdSe QDs have been characterized by UV-Vis absorption and photoluminescent (PL) spectroscopy. The average CdSe particles size estimated from the UV-Vis absorption spectra was found to be in the range 2.28-2.92 nm which is in good agreement with PL measurements.



FULL PAPER

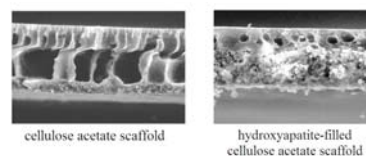
SUPRAMOLECULAR CHEMISTRY

132

BIOMATERIALS BASED ON NANOHYDROXYAPATITE

Gabriela Ciobanu, Constantin Luca, Octavian Ciobanu

In this study, the porous hydroxyapatite-filled cellulose acetate scaffolds were prepared via dry-wet phase inversion method by dispersing hydroxyapatite nanoparticles in the polymeric matrix. The calcined hydroxyapatite prepared by wet precipitation method has the crystal size smaller than 50 nm. The unfilled and hydroxyapatite-filled cellulose acetate scaffolds have an asymmetric structure consisting of two layers, the dense top layer (active layer) supported by the porous sub-layer (substructure). The cross-sectional SEM images revealed that hydroxyapatite nanoparticles were well dispersed in the cellulose acetate matrix.



INSTRUCTIONS FOR AUTHORS

136

PREFACE

We would like to welcome you, the participants of the *International Conference dedicated to the 55th anniversary from the foundation of the Institute of Chemistry of the Academy of Sciences of Moldova*. We wish you a pleasant and useful stay in the capital of our country, Chisinau.

The Institute of Chemistry of the Academy of Sciences of Moldova was founded in 1959 on the basis of the departments of organic chemistry, of inorganic chemistry and the laboratory of analytical chemistry of the Moldovan Branch of the Academy of Sciences of the USSR.

The cornerstones of scientific directions of the Institute were laid down by famous researchers, members of the Academy, founders of scientific schools in Moldova: A.V. Ablov (1905-1978) – School of Coordination Compounds Chemistry; G.V. Lazurievski (1906-1987) – School of Organic and Bioorganic Chemistry, Yu.S. Lealicov (1909-1976), organizer and leader of research related to physical-chemical methods of analysis – School of Polarography.

Later, new scientific schools were created: School of Quantum Chemistry – headed by academician I. Bersuker; School of Organic, Bioorganic Chemistry, Chemistry of Natural and Physiologically Active Compounds – headed by academician P. Vlad; School of Coordination Chemistry, Macrocyclic and Supramolecular Compounds – headed by academician N. Garbalau; School of Ecological Chemistry – headed by academician Gh. Duca and School of Bioinorganic Chemistry – headed by academician C. Turta. In addition, the Scientific School in the field of Chemistry of Adsorbents was created by the corresponding member T. Lupascu.

The research directions of the Institute of Chemistry are: (i) the synthesis and study of new polyfunctional substances; (ii) the study of chemical, physico-chemical processes; (iii) the development of environmental protection methods. At the Institute of Chemistry there are 117 researchers, including 4 Full Members of the Academy of Science of Moldova, 2 Corresponding Members of the Academy of Science of Moldova, 19 Doctors Habilitate and 49 Doctors.

In 2006, the Institute of Chemistry launched the publication (in English) of the peer-reviewed scientific journal “*Chemistry Journal of Moldova. General, Industrial and Ecological Chemistry*”.

The International Conference dedicated to the 55th anniversary from the foundation of the Institute of Chemistry of the Academy of Sciences of Moldova will serve as the main arena for discussion, experience and ideas exchange of recent achievements in chemistry. About 200 scientists from different countries (Romania, Switzerland, Poland, France, United Kingdom, Czech Republic, Republic of Moldova, Ukraine, Russian Federation, Azerbaijan, Japan, USA etc.) have expressed their wish to be registered at the Conference and attend its sessions. The Conference topics are:

- ✓ Inorganic and Physical Chemistry
- ✓ Analytical and Ecological Chemistry
- ✓ Organic and Bioorganic Chemistry.

A valuable contribution to Conference organization was provided by the following sponsors: ICS “Nitech” SRL; “Ecochimie” SRL; ÎEP “Știința”; “Unidecor” SRL; “Polivalent-95” SRL; “Stimed Plus” SRL.

We would like to wish good luck and successful results to all participants of the Conference!

Editorial Board
Chemistry Journal of Moldova

Instructions for authors

Please follow these instructions carefully to ensure that the review and publication of your paper are as swift and efficient as possible. These notes may be copied freely.

Journal policy

“Chemistry Journal of Moldova. General, Industrial and Ecological Chemistry” seeks to publish experimental or theoretical research results of outstanding significance and timeliness in all fields of Chemistry, including Industrial and Ecological Chemistry. The main goal of this edition is strengthening the Chemical Society of Moldova, following development of research in Moldovan chemical institutions and promotion of their collaboration with international chemical community. Publications may be in the form of *Short Communications*, *Full Papers* and *Review Papers*.

The contents of papers are the sole responsibility of the authors, and publication shall not imply the concurrence of the Editors or Publisher.

Short Communications should describe preliminary results of an investigation and for their significance are due to rapid communication. For this kind of publications, experimental confirmation is required only for the final conclusion of the communication. Maximum allowed length – 2 pages.

Full Papers should describe original research in chemistry of high quality and timeliness. Experimental work should be accompanied by full experimental details. Priority will be given to those contributions describing scientific work having as broad appeal as possible to the diverse readership. Maximum allowed length – 6 pages.

Review Papers are specially commissioned reviews of research results of topical importance. Maximum allowed length – 20 pages.

The language of submission is English, articles in other languages will not be considered. Papers are submitted on the understanding that the subject matter has not been previously published and is not being submitted elsewhere. Authors must accept full responsibility for the factual accuracy of the data presented and should obtain any authorization necessary for publication. All papers are sent to referees who advise the Editor on the matter of acceptance in accordance with the high standards required.

Referees' names are not disclosed, but their views are forwarded by the Editor to the authors for consideration. Authors are strongly encouraged to suggest the names and addresses of suitable referees.

Journal conventions

Nomenclature: Authors will find the following reference books and websites useful for recommended nomenclature. It is the responsibility of the author to provide correct chemical nomenclature.

- IUPAC Nomenclature of Organic Chemistry; Rigaudy, J.; Klesney, S. P., Eds; Pergamon: Oxford, 1979.
- A Guide to IUPAC Nomenclature of Organic Compounds (Recommendations 1993); Panico, R.; Powell, W. H.; Richer, J. C., Eds; Blackwell Publishing: Oxford, 1993.
- <http://www.acdlabs.com/iupac/nomenclature>
- <http://www.chem.qmul.ac.uk/iupac/>

X-ray crystallographic data: Prior to submission of the manuscript, the author should deposit crystallographic data for organic and metal-organic structures with the Cambridge Crystallographic Data Centre. The data, without structure factors, should be sent by e-mail to: deposit@ccdc.cam.ac.uk, as an ASCII file, preferably in the CIF format. Hard copy data should be sent to CCDC, 12 Union Road, Cambridge CB2 1EZ, UK. A checklist of data items for deposition can be obtained from the CCDC Home Page on the World Wide Web (<http://www.ccdc.cam.ac.uk/>) or by e-mail to: fileserv@ccdc.cam.ac.uk, with the one-line message, send me checklist. The data will be acknowledged, within three working days, with one CCDC deposition number per structure deposited. These numbers should be included with the following standard text in the manuscript: Crystallographic data (excluding structure factors) for the structures in this paper have been deposited with the Cambridge Crystallographic Data Centre as supplementary publication numbers CCDC Copies of the data can be obtained, free of charge, on application to CCDC, 12 Union Road, Cambridge CB2 1EZ, UK [fax: 144-(0)1223-336033 or e-mail: deposit@ccdc.cam.ac.uk]. Deposited data may be accessed by the journal and checked as part of the refereeing process. If data are revised prior to publication, a replacement file should be sent to CCDC.

Experimental: Authors should be as concise as possible in experimental descriptions. The Experimental section must contain all the information necessary to guarantee reproducibility. An introductory paragraph containing information concerning solvents, sources of less common starting materials, special equipment, etc. should be provided. The procedures should be written in the past tense and include the weight, mmol, volume, etc. in brackets after the names of the substances or solvents. General reaction conditions should be given only once. The title of an experiment should include the chemical name and compound number of the product prepared: subsequently, these compounds should be identified by their number. Details of the work up procedure must be included. An experimental procedure is not normally required for known compounds prepared by a literature procedure; in such cases, the reference will suffice. For known compounds prepared by a novel procedure, comparative data together with the literature reference are required (e.g. m.p. and published m.p. with a reference to the latter).

Characterization of new compounds: All new compounds should be fully characterized with relevant physical and spectroscopic data, normally including compound description, m.p./b.p. if appropriate, IR, NMR, MS and $[\alpha]_D$ values for enantiopure compounds. In addition, microanalyses should be included whenever possible (normally $\pm 0.4\%$). Under appropriate circumstances, and at the Editor's discretion, high resolution mass data (normally to ± 5 ppm) may serve in lieu of microanalyses; in this case a statement must be included regarding the purity of the products and how this was determined [e.g. all new compounds were determined to be $>95\%$ pure by HPLC (or GLC or ^1H NMR spectroscopy)]. For compound libraries prepared by combinatorial methods, a significant number of diverse examples must be fully characterized (normally half of the members for libraries up to 40 compounds, 20 representative examples for bigger libraries). Resin-bound intermediates do not have to be fully characterized if acceptable characterization of released products is provided. No supplementary data are accepted in addition to the basic material.

Manuscript preparation

Please follow these guidelines for manuscript preparation. An example of manuscript formatting is provided after the descriptive part of the document.

General requirements: Manuscripts will be accepted only in electronic form in A4 format, orientation *Portrait*, one column layout, single-spaced, margins 2.5 cm on all sides (see the sample formatting page). Pages must be numbered. The corresponding author's full mailing address, plus phone and fax numbers and e-mail address should be included. The manuscript should be compiled in the order depending on the paper type.

A theoretical or physicochemical paper normally contains the *Title, Authors, Affiliations, Abstract, Keywords*, a brief *Introduction* and formulation of the problem, an *Experimental* (or methodological part), *Results and discussion, Conclusions*, followed by *Acknowledgments and References*.

A paper devoted to synthesis contains the *Title, Authors, Affiliations, Abstract, Keywords, Introduction, Results and discussion, Conclusions, Experimental, Acknowledgments and References*.

Graphical Abstract: Authors must supply a graphical abstract at the time the paper is first submitted. It will include the article title and authors with the same formatting as in the article. The abstract body should summarize the contents of the paper in a concise, pictorial form designed to capture the attention of a wide readership and for compilation of databases. Carefully drawn chemical structures are desired that serve to illustrate the theme of the paper. Authors may also provide appropriate text, not exceeding 50 words. The whole graphical abstract should be kept within an area of 5cm by 16 cm. Authors must supply the graphical abstract on a separate page integrated in the article file. The graphics which is a part of the graphical abstract should be sent separately in its original format.

Title: The title should be brief, specific and rich in informative words; it should not contain any literature references or compound numbers. The title is in size 14 pt Bold (all capital letters).

Authors and affiliations: Include all authors in a single list. The style for the names is: first name, last name (full names, without initials). The names of the authors must be written in size 12 pt and separated by a comma. Indicate all the authors in order of their affiliation and provide affiliation address after the author's names. Affiliations should be as detailed as possible and must include the country name and must be written in size 9 pt Italic. The corresponding author should be indicated with an asterisk, and contact details (fax, e-mail) should be placed after nomination of the authors. There should be only one corresponding author.

Abstract: Authors must include a short abstract of approximately four to six lines that states briefly the purpose of the research, the principal results and major conclusions. References and compound numbers should not be mentioned in the abstract unless full details are given. The abstract body is 9 pt in size with the heading in bold.

Keywords: Authors are expected to provide a maximum of 5 keywords, separated by a comma (10 pt, Normal). These keywords will facilitate database searching. Avoid general, plural terms and multiple concepts (avoid, for example, “and”, “of”).

Text: Text should be subdivided in the simplest possible way consistent with clarity. Headings should reflect the relative importance of the sections. Ensure that all tables, figures and schemes are cited in the text in numerical order. The graphics and artworks should be integrated in the paper.

Trade names should have an initial capital letter, and trademark protection should be acknowledged in the standard fashion, using the superscripted characters TM and ® for trademarks and registered trademarks respectively (although not for words which have entered common usage, e.g. pyrex).

All measurements and data should be given in SI units.

Authors are requested to draw attention to hazardous materials or procedures by adding the word CAUTION followed by a brief descriptive phrase and literature references if appropriate.

The experimental information should be as concise as possible, while containing all the information necessary to guarantee reproducibility. The text body is 10 pt in size with the heading in bold.

Abbreviations: Within the text, abbreviations must be defined at the first mention and used consistently thereafter.

Acknowledgments: This is an optional section. The authors have to decide acknowledgement of certain collaborators, funds or programs who contributed in a way to the research described in the paper.

References: In the text, references should be indicated by Arabic numerals taken in square brackets, which run consecutively through the paper and appear before any punctuation; ensure that all references are cited in the text and vice versa. References should be numbered in the text in the order they are cited [1]. Multiple consecutive references may be abbreviated as [2-5].

Do not cite references in the abstract.

References should be written in English only. If it's in a different language then the reference must be translated with an appropriate title in English. The original language must be indicated in round brackets.

Complete bibliographic information for all cited references is required. If abbreviated names of the journals are used then authors are expected to consult American Chemical Society guidelines (The ACS Style Guide; Dodd, J. S.; Solla, L.; Berard, P.M. Ed.: American Chemical Society: Washington, DC, 2006) or the policy of the cited journal.

All references must be edited in the same style.

Each reference should contain only one literature citation.

The following style must be used for all contributions:

Books:

1. Katritzky, A.R. Handbook of Organic Chemistry. Pergamon: Oxford, 1985, 200 p.
2. Wipke, W.T.; Heller, S.R.; Feldmann, R.J.; Hyde, E. Eds. Computer representation and manipulation of chemical information. John Wiley: New York, 1974, pp. 287–298.

Symposia volumes:

3. Bravo-Suárez, J.; Kidder, M.K.; Schwartz, V. Novel Materials for Catalysis and Fuels Processing. ACS Symposium Series; American Chemical Society: Washington, DC, 2013, vol. 1132, 400 p.

Translated journal papers:

4. Garaba V. Problems of water supply in rural localities. Environment, 2005, 19, pp. 19-22 (in Romanian).
5. Magerramov, A.M.; Ramazanov, M.A.; Gadzhiyeva, F.V. Investigation of the structure and dielectric properties of nanocomposites based on polypropylene and zirconia nanoparticles. Surface Engineering and Applied Electrochemistry, 2013, 49(5), pp. 1-5 (in Russian).

Journal papers:

6. Shin, S.; Yoon, H.; Jang, J. Polymer-encapsulated iron oxide nanoparticles as highly efficient Fenton catalysts. *Catalysis Communications*, 2008, 10, pp. 178–182.

Patents:

7. Grant P. Device for Elementary Analyses. USA Patent, 1989, No. 123456.

Theses:

8. Cato, S.J. Thermodynamic study of polymer solutions. Ph.D. Thesis, University of Florida, Florida, USA, 1987.

Legal regulations and laws, organizations:

9. EC Directive, Directive 2000/76/EC of the European Parliament and of the Council of 4 December 2000, on the incineration of waste, Annex V, Official Journal of the European Communities, L 332/91, 28.12.2000, Brussels.

Web references:

The full URL should be given in text as a citation, if no other data are known. It should be accompanied by a sentence indicating the explanation of the content. When you are indicating the URL you should remove the Hiperlink, this can be achieved by selecting the URL then click the right button of the mouse and chose from the menu *Remove Hyperlink*.

10. Spectral Database for Organic Compounds, SDBS. http://sdb.sdb.aist.go.jp/sdb/cgi-bin/cre_index.cgi.

Footnotes: Footnotes should appear at the bottom of the appropriate page and be indicated by the following symbols:

*, †, ‡, §, ¶, k.

Tables: Table must fit in a size of a page A4, orientation: *Portrait*. All tables should be cited in the text, and numbered in order of appearance with Arabic numerals. All table columns should have a brief explanatory heading and appropriate units of measurement. Vertical lines should not be used. Footnotes to tables should be typed below the table, each on a separate line, and should be referred to by superscript letters.

Artwork: Only black and white artwork will be accepted. Figures, schemes and equations must be cited in the text and numbered in order of appearance with Arabic numerals; other graphics should be placed at a particular position in the text but not specifically referenced. All graphics (including chemical structures) must be supplied in digital format integrated into the paper. If graphics are created using ChemDraw the preferred settings is RSC-1997.cds set (File/Apply settings/RSC-1997.cds): font 7 pt Arial, chain angle 120°, bond spacing 20% of length, fixed length 0.43 cm, bold width 0.056 cm, line width 0.016 cm, margin width 0.044 cm and hash spacing 0.062 cm. Compound numbers should be in bold face. Computer-generated illustrations, halftones and line/tones should also be provided where possible.

Figures must be submitted in a very good resolution (but do not submit graphics that are disproportionately large for the content).

The following points should be taken into consideration when preparing electronic graphic files:

Preferred graphics programs: ChemDraw, CorelDraw 6 and 7, Photoshop. *Restricted use:* ChemWindow, ISIS-Draw.

Unusable: *.doc files, Excel graphics, C-Design, Origin, ClarisDraw, ChemIntosh, MacDraw Pro. *Acceptable formats of all graphics programs:* TIFF, WMF, BMP, CDX, CDR.

Files of scanned line graphics can be accepted at a minimum resolution of 1000 dpi, for scanned halftones, 300 dpi, and scanned line/tones.

Equations and formulas: To typeset your formulae or equations use Equation Editor or MathType (version 1999-2003). Quote them on the right side, between brackets. Equation must be cited in text as “Eq.(1)”, “Eq.(2)”.

$$I = 2d \sin\left(\frac{\Theta}{2}\right) \quad (2)$$

Please use size 10 pt and *Italic* for symbols, bold face for vectors and normal fonts for standard functions (i.e. log, ln, exp) and subscripts (i.e. $//_{app}$ i).

SI units must be used throughout.

In order to avoid possible confusion between the numeral 1 (one) and the lower-case letter l (el) please use the capital letter L to express liter units.

Decimal numbers should be expressed using punctuation (do not use commas).

Large and complex chemical formulae should be presented in text as figures.

Please follow the IUPAC nomenclature for your chemical compound.

Copyright guidelines

Upon acceptance of an article the copyright transfer will be automatic. This transfer will ensure the widest possible dissemination of information. If excerpts from other copyrighted works are included, the Author(s) must obtain written permission from the copyright owners and credit the source(s) in the article.

Submission of manuscripts

Please send your contribution as an e-mail attachment to:

Journal Editor, Academician Gheorghe DUCA
e-mail: chemjm@asm.md / chemjm@gmail.com

using Microsoft Word (Office 97 or higher for PCs) word processing soft.

Please prepare a single file (allowed formats: *.doc or *.rtf) containing on a separate page a short accompanying letter to the Editor, justifying why your article should appear in "Chemistry Journal of Moldova. General, Industrial and Ecological Chemistry", followed by the article body with all schemes, figures, tables integrated in the text (though not crystallographic CIF files). On the last page of this file please provide the Graphical Abstract. Submission of figures and artwork in separate files is mandatory in their native formats.

Authors should indicate the research field of their paper (see below) as well as the nature of contribution (Short Communication, Full Paper or Review Article) in their accompanying letters, along with their mailing address, daytime phone number and fax if available. Names and addresses of three potential referees are welcomed. Authors will be notified by email if their contribution is received and accepted.

Proofs: Proofs will be dispatched via e-mail and should be returned to the publisher with corrections as quickly as possible, normally within 48 hours of receipt.

Fields of research:

- | | | |
|-------------------------|--|--|
| 1. Analytical chemistry | 4. Industrial chemistry | 7. Organic chemistry |
| 2. Ecological chemistry | 5. Inorganic and coordination chemistry | 8. Physical chemistry and chemical physics |
| 3. Food chemistry | 6. Natural product chemistry and synthesis | 9. Supramolecular chemistry |

CHEMISTRY JOURNAL OF MOLDOVA. GENERAL, INDUSTRIAL AND ECOLOGICAL CHEMISTRY (14 pt Bold, CAPITAL LETTERS)

First Author^a, Second Author^{a*}, Third Author^b (12 pt Normal) (no titles please)

^a*First Organization, First Address (9 pt, Italic)*

^b*Second Organization; Second Address (9 pt, Italic)*

^{*}*e-mail, phone and fax numbers of the corresponding author*

Abstract. This document is an example of a contribution to be submitted to "Chemistry Journal of Moldova. General Industrial and Ecological Chemistry". This is the abstract in font size: 9 pt with the heading in bold. Please use the Times New Roman font. The title is in size 14 pt Bold (all capital letters), the names of the authors are in size 12 pt Normal and the name of the organization and its address are in size 9 pt Italic. The rest of the text is in single-space, typed in a one column layout and font size 10 pt.

Keywords: Insert a maximum of 5 keywords separated by a comma (10 pt, Normal). These keywords will facilitate database searching. Avoid general, plural terms and multiple concepts (avoid, for example, "and", "of").

Introduction

Contributions should comprise an even number of pages. There are no limits to the contribution size. Authors are also kindly requested to adhere to the formatting instructions for font size and layout.

How to prepare your paper

Please ensure that the required formats for text and figure submission are followed strictly. MS Word template can be found on the web page of Chemistry Journal of Moldova (www.cjm.asm.md). Use of this template is mandatory.

A theoretical or physico-chemical paper normally contains the *Title, Authors, Affiliations, Abstract, Keywords*, a brief *Introduction* and formulation of the problem, an *Experimental* (or methodological part), *Results and discussion*, *Conclusions*, followed by *Acknowledgments* and *References*.

In MS Word, under the *File* menu, choose *Page setup* and set the *Top, Bottom, Left & Right Margins* as 2.5 cm, the *Gutter* as 0 cm, and the *Header* and *Footer* to 1.2 cm and choose *Apply to: Whole Document*. Then select the "*Paper Size*" tab and set the *Paper Size: A4* and *Orientation: Portrait*.

Ensure that each new paragraph is clearly indicated, using TAB at 1.25 pts.

Title

The title is in size 14 pt Bold, all capital letters. Title should be concise and informative. Avoid the abbreviations where is possible.

Author list

Include all authors in a single list. The style for the names is: first name, last name (full names, without initials). The names of the authors must be written in size 12 pt and separated by a comma.

Text

Use the 10-point Times New Roman font. Use the automatic page numbering function to number the pages.

Abbreviations

If you are using abbreviations, please define them at the first mention in the text and use them consistently thereafter.

Figures and Tables

Figure and table titles must be typed in Bold and should appear below the figures and above the tables. If you are using previously published material please include the source in the form of reference citation at the end of the figure caption and/or table titles.

Tables

Before editing tables please consider the following requirements:

- Tables should be centered and they should occupy the full width of the page.
- Table must fit in a size of a page A4, *Portrait*.
- If your table transfers partially to the next page you should mention on the next page that this is a continuation

of the table and you must indicate the headings.

- All table columns should have a brief explanatory heading typed in bold and where appropriate, units of measurement.
- Vertical lines should not be used.
- Use the punctuation at the end of the table title.

All tables should be cited in the text, and numbered in order of appearance with Arabic numerals. Tables should be numbered sequentially—"Table 1", "Table 2", and should be cited in the text as "Table 1", "Table 2".

Figures

Only black and white artwork will be accepted. Individual figures should normally be centered. It is also more convenient for referees of your article if figures are placed as close as possible, and ideally after, the point where they are first mentioned in the text. Figures should be numbered sequentially—"Figure 1", "Figure 2", and should be cited in the text as "Figure 1", "Figure 2". We recommend you to place figures and their captions in a table with no margins.

Each figure should have a concise caption describing accurately what figure depicts. Figure captions begin with the term Figure in bold type, followed by figure number and punctuation, also in bold type. Also, use the punctuation at the end of the caption.

Figures must be submitted in a very good resolution (but do not submit graphics that are disproportionately large for the content).

Equations and formulae

To typeset your formulae or equations use Equation Editor or MathType (version 1999-2003). Quote them on the right side, between brackets. Equation must be cited in text as "Eq.(1)", "Eq.(2)".

Please use size 10 pt and *Italic* for symbols, bold face for vectors and normal fonts for standard functions (i.e. log, ln, exp) and subscripts (i.e. $_{app}$ i).

SI units must be used throughout.

In order to avoid possible confusion between the numeral 1 (one) and the lower-case letter l (el) please use the capital letter L to express liter units.

Decimal numbers should be expressed using punctuation (do not use commas).

Large and complex chemical formulae should be presented in text as figures.

Please follow the IUPAC nomenclature for your chemical compound, using the following resources:

- IUPAC Nomenclature of Organic Chemistry; Rigaudy, J.; Klesney, S. P., Eds; Pergamon: Oxford, 1979;
- A Guide to IUPAC Nomenclature of Organic Compounds (Recommendations 1993); Panico, R.; Powell, W. H.; Richer, J. C., Eds; Blackwell Publishing: Oxford, 1993;
- <http://www.acdlabs.com/iupac/nomenclature>;
- <http://www.chem.qmul.ac.uk/iupac/>.

Acknowledgments (optional)

You can acknowledge certain collaborators, funds or programs who contributed in a way to the research described in the paper.

References

References should be written in English only. If you are using references written in other languages please indicate them with an appropriate title in English. The original language should be indicated in round brackets.

Complete bibliographic information for all cited references is required. If you use abbreviated names of the journals then you should consult American Chemical Society guidelines (The ACS Style Guide; Dodd, J. S.; Solla, L.; Berard, P.M. Ed.: American Chemical Society: Washington, DC, 2006) or the policy of the cited journal. All references must be edited in the same style.

Graphical Abstract

Authors must supply a graphical abstract at the time the paper is first submitted. It will include the article title and authors with the same formatting as in the article. The abstract body should summarize the contents of the paper in a concise, pictorial form designed to capture the attention of a wide readership and for compilation of databases. Carefully drawn chemical structures are desired that serve to illustrate the theme of the paper. Authors may also provide appropriate text, not exceeding 50 words. The title is in size 10 pt Bold (all capital letters), the names of the authors are in size 9 pt. The abstract body must be written in font size 9 pt. The whole graphical abstract should be kept within an area of 5cm by 16cm. Authors must supply the graphical abstract on a separate page integrated in the article file. The graphics which is a part of the graphical abstract should be sent separately in its original format.

MS Word template of the graphical abstract can be found on the web page of Chemistry Journal of Moldova (www.cjm.asm.md).

ROLE OF CYCLODEXTRINS IN NEW ANTIMYCOBACTERIAL FORMULATIONS

Veaceslav Boldescu*, Fliur Macaev, Gheorghe Duca

Institute of Chemistry of Academy of Science of Moldova, 3, Academiei str., Chisinau MD2028, Republic of Moldova

**veaceslav.boldescu@gmail.com; phone: (+373 22) 73 97 58; fax: (+373 22) 73 99 54*

Abstract. This paper is dedicated to the role of cyclodextrins in new formulations for the treatment of infections with *Mycobacterium tuberculosis* that are in the process of design and development. Cyclodextrins play the role of solubilizing agents and promoters of the antimycobacterial substances penetration inside the mycobacterial cell. Different formulations and their advantages and disadvantages are discussed.

Keywords: cyclodextrin, nano-encapsulation, tuberculosis, mycobacteria, cholesterol.

Introduction

Tuberculosis is one of the deadliest infectious diseases killing annually 1.5 million people worldwide. The major problems connected with the tuberculosis treatment are: strong side effects of the majority of the existent antituberculosis drugs, long duration of treatment, high dosage, unpleasant organoleptic properties and high frequency of administration. These factors very often cause the lack of compliance of the patient with treatment. The last fact in association with low bioavailability and insufficient enantiomeric purity of some antituberculosis drugs, all together, lead to development of drug-resistant (DRTB), multiple drug-resistant (MDRTB), and extensively drug-resistant (XTRB) tuberculosis.

The problem with tuberculosis puts the Republic of Moldova among the top five European countries with high rate of new infections. The current situation becomes more complicated because of high percentage (approx. 25%) of MDRTB infections, with proportion of previously treated cases that became MDRTB reaching 65.1% [1].

In order to resolve the problem a multidisciplinary approach is needed. One of the possibilities can be introduction of more patient-friendly types of antituberculosis drugs with lower frequency of administrations, shorter time of treatment, lower doses and fewer side effects. For the development of such drugs a wide knowledge in phthiology and tuberculosis drugs chemistry is needed.

For improvement of the efficiency of new antituberculosis formulations and reduction of their side effects and time of treatment, new formulations with cyclodextrins have been proposed. Different formulations and their advantages and disadvantages are further discussed.

Different approaches to improve the efficiency of antituberculosis drugs

In order to reduce duration of treatment, frequency and quantity of the administered doses of drugs, to avoid first pass effect and to reduce the side effects, new antituberculosis drug entities and different micro- and nanoparticle based systems for nebulisation have been proposed.

Thus, in the field of the micro- and nanoparticulate systems, a lyposomal system loaded with rifampicin is known. The system contains phosphatidile choline and cholesterol as main vehicles. In order to increase the specificity of the system accumulation in macrophages, it has been covered with macrophag-specific ligands – O-stearyl amylopectin and maleylated bovine serum albumin [2].

The main disadvantages of this system are:

- susceptibility to phospholipid oxidation, and as consequence, lower stability;
- increased costs of the production technology;
- short half-life time in the body.

Many similar compositions developed by the leading specialists in the field are known [3-8].

The closest by composition known microparticulate systems are gelatin based microparticles covered with manosyl groups and loaded with isoniazid [9], and microspheres based on alginate-chitozan used for transport of different anti-tuberculosis drugs [10].

The main disadvantage of these systems is the fact that they only facilitate accumulation of drugs in the macrophages, but do not facilitate their penetration in the mycobacterial cell.

In the field of new anti-mycobacterial drugs, recently, many groups of researchers have proposed entities from different chemical classes: thiolactomycins [11], benzothiazones [12], substituted quinoliny chalcones [13], cinnamic derivatives [14].

Development of new classes of anti-tuberculosis drugs is in permanent emergency since the resistance to older ones appears sooner than the new ones are registered.

Cyclodextrins and their role in anti-mycobacterial formulations

Cyclodextrins are a family of cyclic natural oligosaccharides and their semi-synthetic derivatives. Naturally occurring α -, β -, and γ -cyclodextrins are torus-like macro-rings built up from 6, 7, and 8 glucopyranose units, respectively (Table 1). As a consequence of 4C_1 conformation of the glucopyranose moieties, all the primary hydroxyl groups are situated on the one edge of the torus, while all the secondary ones are situated on the other. The internal cavity of the cyclodextrins is lined by the hydrogen atoms and the glycosidic oxygen bridges, which produce a high electron density, causing some hydrophobicity [15].

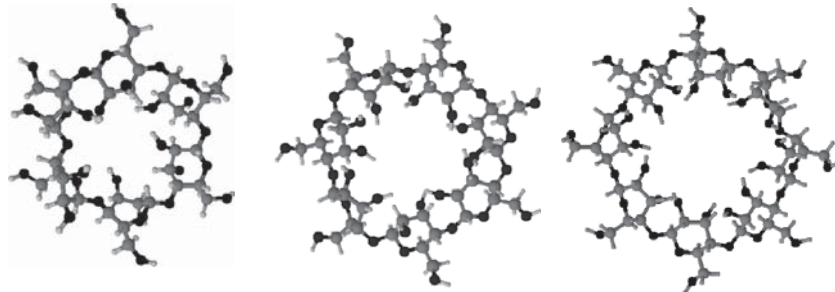
In an aqueous solution, the cyclodextrins' cavity is filled with water molecules that are energetically unfavored due to polar-non-polar interactions and, therefore, can be readily substituted by any less polar guest-molecule added to the solution.

The main reasons of cyclodextrins popularity as hosts for inclusion of different substances are:

- they are produced from a renewable natural material (starch) applying environmental-friendly technologies (enzymatic conversion);
- they are relatively cheap and are produced in amounts of thousands of tons per year;
- they are nontoxic in consumable concentrations and their secondary toxic effects can be easily eliminated by an appropriate chemical modification;
- they are biodegradable and do not pollute the environment [15].

Table 1

Properties of cyclodextrins [15].

			
Parameters	α -cyclodextrin	β -cyclodextrin	γ -cyclodextrin
Number of glucopyranose fragments	6	7	8
Molecular weight	973	1135	1297
Internal cavity diameter (nm)	0.47–0.53	0.60–0.66	0.75–0.83
External diameter (nm)	1.46 \pm 0.04	1.54 \pm 0.04	1.75 \pm 0.04
Torus height (nm)	0.79 \pm 0.01	0.79 \pm 0.01	0.79 \pm 0.01
Cavity volume approx. (mL/mol)	104	157	256
$[\alpha]_D$ at 25°C	150 \pm 0.5	162.5 \pm 0.5	177.4 \pm 0.5
Water solubility (g/100 mL at 25°C)	14.5	1.85	23.2

Previously, a number of antimycobacterial formulations containing cyclodextrins have been proposed. Many of them contain complexes of an antimycobacterial drug with cyclodextrin with purpose to increase the solubility of the drug and reduce its toxicity. Thus complexes of rifampicin with sucralose and β -cyclodextrins have been proposed for pulmonary delivery [16, 17]. The role of the cyclodextrins under this study was to enhance the solubility and permeation of poorly water soluble rifampicin through the biological membranes. As such, cyclodextrins act as permeation enhancers by carrying the drug through the aqueous barriers which exists before the lipophilic surface of biological membranes [16].

Similar complexes have been obtained for other antituberculosis agents: pirazinamide [18], isoniazid [19, 20].

Another formulation includes cyclodextrin nanoparticles/microparticles containing rifabutin is implied for oral, intravenous or intramuscular administration. According to the invention authors, the main role of cyclodextrins in this formulation is to enhance solubility of rifabutin [21].

Besides the use of cyclodextrins as pharmaceutical auxiliary agents, they have started to attract a lot of attention due to their intrinsic biological activity or physiological effects that are specific for their derivatives. Thus, carboxyl thio

ether derivatives of γ CD are used as a new class of selective relaxant binding agents [22]. Some β CD derivatives proved to inhibit anthrax lethal toxin by blocking the transmembrane pore formed by its protective antigen subunit [23, 24], others are effective in inhibition of α -hemolysin playing important role in the pathogenesis of *Staphylococcus aureus*, a bacteria that causes severe forms of pneumonia [25]. Interestingly, cyclodextrins have also been proven to have lysis activity against certain strains of *Bacillus*, but not against other Gram-positive or Gram-negative bacteria [26].

The types of biological activity of cyclodextrins important for their use in medicine were classified in [27] as follows:

- effects based on the ability of cyclodextrins to form inclusion complexes with exogenous substances as guest molecules;
- effects based on the ability of cyclodextrins to form inclusion complexes with endogenous substances as guest molecules;
- effects based on the chemical nature of cyclodextrins and their derivatives;
- effects based on the ability of cyclodextrins to block endogenous and exogenous macromolecules.

All these types of activity have been analyzed by us as useful for antifungal formulations [28].

We have suggested that complexation of cholesterol by cyclodextrins can be used to increase the permeability of the mycobacterial cell wall for penetration by antimycobacterial compounds. Thus, we have proposed to obtain new nano-encapsulated in cyclodextrins antituberculosis remedies with higher efficiency and fewer side effects as compared to the existing drugs [29]. In the proposed formulation, cyclodextrins play the roles of solubilizing agents and promoters of the antimycobacterial substances penetration inside the mycobacterial cell. The nano-encapsulated drugs are then loaded into the alginate-chitosan microparticles that help them penetrate into macrophages infected with *M. tuberculosis* [30].

Preliminary results (unpublished) of the biological tests of antimycobacterial activity of the obtained substances and systems have demonstrated that antituberculosis efficiency of the studied substances changes in association with different cyclodextrins. Thus, β -cyclodextrin, one of the naturally occurring cyclodextrins, seems to enhance antituberculosis activity of the associated oxadiazole derivative, while sulfobutyl ether of β -cyclodextrin does not have this influence. This observation might be explained by the fact that sulfobutyl ether of β -cyclodextrin possesses certain level of charge of the molecule due to the presence of sulfobutyl ether groups, which makes it less suitable for cholesterol complexation than simple β -cyclodextrin. Namely cholesterol complexation is considered to be in the core of mechanism of cyclodextrins activity as promoters of antituberculosis compounds penetration through the mycobacterial cell wall (Figure 1).

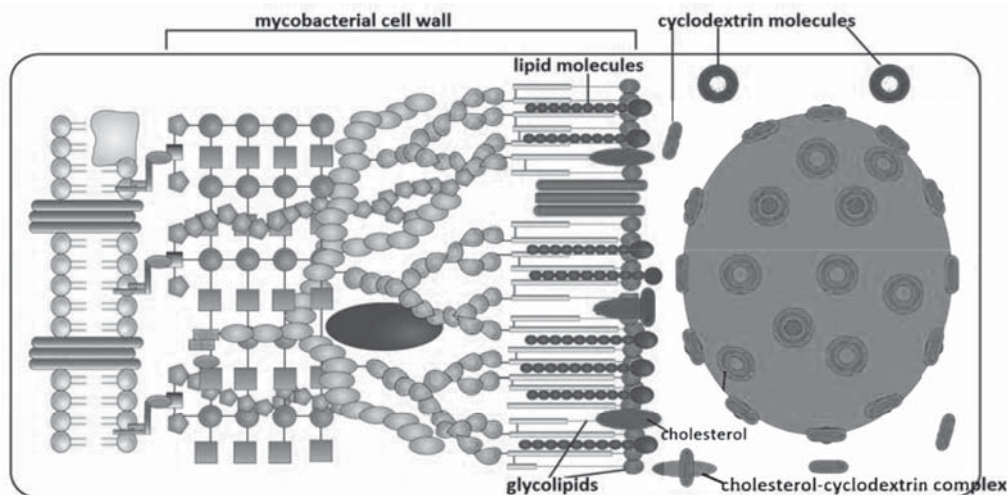


Figure 1. Extraction of cholesterol molecules from the mycobacterial cell wall.

It has been demonstrated before that in the case of *Mycobacterium tuberculosis* cyclodextrins extract cholesterol deposited in the mycobacterial cell wall [31] that leads to disorganization of the protective lipid bilayer and, thus, increases its permeability for drug molecules [32].

β CDs are particularly efficient sterol acceptors, apparently because the size of their inner hydrophobic cavity matches the size of the sterol molecule (Figure 2). As a more potent cholesterol-extracting agent, a randomly methylated derivative of β CD is usually used.

Thus, the studies performed by Castagne and collaborators [33] have shown that the high substituted dimethyl- β CD (D.S. 2.0) and randomly methylated β CD (D.S. 1.8) are efficient cholesterol solubilizers or extractors from cell membranes. Molecular modeling studies performed by this group have also indicated that 1:1 complexes of cholesterol

with these cyclodextrins are not favorable, while all four 1:2 conformations are possible. Trimethyl- β -cyclodextrin (D.S. 3.0) showed an unexpected behavior not being able to extract high amounts of cholesterol despite its good solubilizing properties. Moreover, only two of all the complexes conformations of this cyclodextrin with cholesterol gave favorable complexation energies, which could explain its difficulty to form complexes and to extract this sterol. Methylated derivative of β CD with low degree of substitution (D.S. 0.5) proved to have the lowest affinity towards cholesterol and the lowest solubilizing properties towards it. However, molecular modeling studies revealed that CD complexes, both 1:2 and 1:1, with cholesterol had the highest interaction or complexation energies [33].

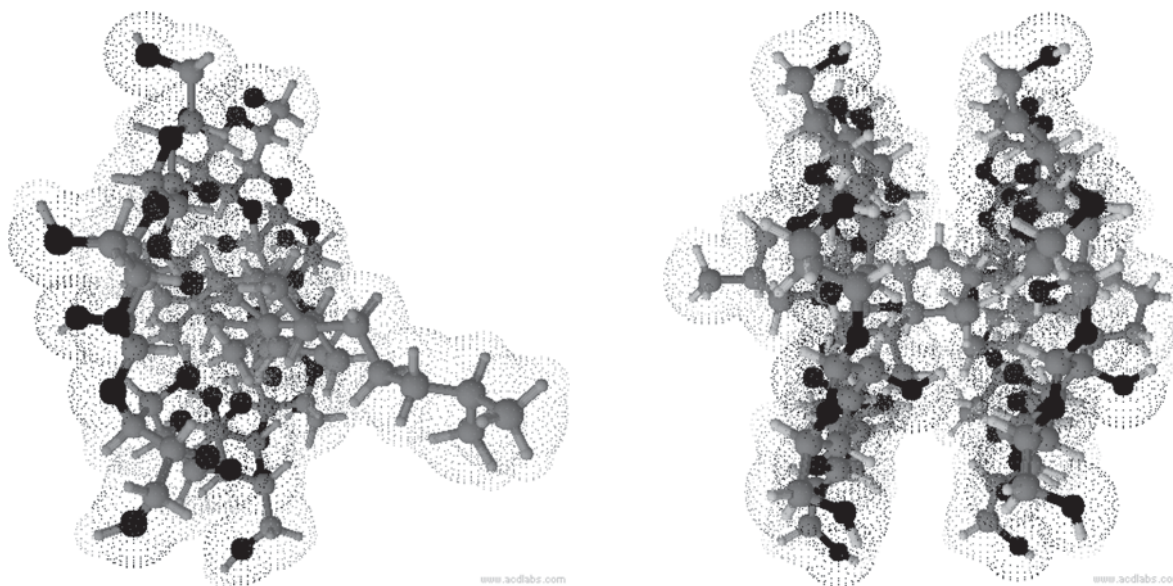


Figure 2. Schematic representation of 1:1 (left) and 1:2 (right) inclusion complexes of sterols with β CD.

Conclusions

Cholesterol complexation by cyclodextrins increases permeability of the mycobacterial cell wall and promotes penetration of antimycobacterial compounds inside. First results of the biological tests of antimycobacterial activity of the antimycobacterial compounds and their complexes with cyclodextrins have demonstrated that antituberculosis efficiency of the studied substances changes in association with different cyclodextrins. Thus, β -cyclodextrin, one of the naturally occurring cyclodextrins, seems to enhance antituberculosis activity of the associated oxadiazole derivative, while sulfobutyl ether of β -cyclodextrin does not have this influence. This observation might be explained by the fact that sulfobutyl ether of β -cyclodextrin possesses certain level of charge of the molecule due to the presence of sulfobutyl ether groups, which makes it less suitable for cholesterol complexation than unsubstituted β -cyclodextrin.

Acknowledgments

The authors are grateful for the funding of this research under the Moldovan State Program project 14.518.04.08A.

References

1. Zignol, M.; van Gemert, W.; Falzon, D.; Sismanidis, C.; Glaziou, P.; Floyd, K.; Raviglione, M. Surveillance of anti-tuberculosis drug resistance in the world: an updated analysis, 2007–2010. *Bulletin of the World Health Organization*, 2012, 90, pp. 111D–119D.
2. Vyas, S. P.; Kannan, M. E.; Jain, S. et al. Design of liposomal aerosol for improved delivery of rifampicin to alveolar macrophages. *International Journal of Pharmaceutics*, 2004, 269, pp. 37–49.
3. Pandey, R.; Sharma, S.; Khuller, G. K. Nebulization of liposome encapsulated antitubercular drugs in guinea pigs. *International Journal of Antimicrobial Agents*, 2004, 24, pp. 93–94.
4. Sharma, R.; Saxena, D.; Dwivedi, A. K. et al. Inhalable microparticles containing drug combinations to target alveolar macrophages for treatment of pulmonary tuberculosis. *Pharmaceutical Research*, 2001, 18, pp. 1405–1410.

5. Edwards, D.; Fiegel, J.; Sung J. Particles for treatment of pulmonary infection. USA Patent, 2007, No. 2007011396.
6. Shim, C. K.; Yang R. Pharmaceutical composition for lung targeting. Korea Patent, 2008, No. 20080043333.
7. Ahmad, Z.; Pandey, R.; Sharma, S.; Khuller, G.K. Alginate nanoparticles as antituberculosis drug carriers: formulation development, pharmacokinetics and therapeutic potential. *The Indian Journal of Chest Diseases & Allied Sciences*, 2006, 48, pp. 171–176.
8. Tiwari, S.; Chaturvedi, A.P.; Tripathi, Y.B.; Mishra, B. Macrophage-specific targeting of isoniazid through mannosylated gelatin microspheres. *AAPS PharmSciTech*, 2011, 12(3), pp. 900-908.
9. Saraogi, G.K.; Sharma, B.; Joshi, B.; Gupta, P.; Gupta, U.D.; Jain, N.K.; Agrawal, G.P. Mannosylated gelatin nanoparticles bearing isoniazid for effective management of tuberculosis. *Journal of Drug Targeting*, 2011, 19(3), pp. 219-227.
10. Pandey, R.; Khuller, G.K. Chemotherapeutic potential of alginate-chitosan microspheres as antitubercular drug carriers. *Journal of Antimicrobial Chemotherapy*, 2004, 53, pp. 635-640.
11. Kamal, A.; Azeeda, S.; Malik, M.S. et al. Efforts towards the development of new antitubercular agents: potential for thiolactomycin based compounds. *Journal of Pharmacy and Pharmaceutical Sciences*, 2008, 11, pp. 56(s)-80(s).
12. Makarov, V.; Manina, J.; Mikusova, K. et al. Benzothiazinones kill *Mycobacterium tuberculosis* by blocking arabinan synthesis. *Science*, 2009, 324, pp. 801-804.
13. Sharma, M.; Chaturvedi, V.; Manju, Y.K. et al. Substituted quinolinyl chalcones and quinolinyl pyrimidines as a new class of anti-infective agents. *European Journal of Medicinal Chemistry*, 2009, 44, pp. 2081-2091.
14. De, P.; Yoya, G.K.; Bedos-Belval, F.; Constant, P. et al. Design, synthesis and biological evaluation of new cinnamic derivatives as antituberculosis agents. *Journal of Medicinal Chemistry*, 2011, 54, pp. 1449-1461.
15. Szejtli, J. Past, present, and future of cyclodextrin research. *Pure and Applied Chemistry*, 2004, 76(10), pp. 1825-1845.
16. Patil, J.S.; Suresh, S. Physicochemical characterization, in vitro release and permeation studies of respirable rifampicin-cyclodextrin inclusion complexes. *Indian Journal of Pharmaceutical Science*, 2009, 71, pp. 638-643.
17. Nanduri, B.; Neelam S. K.; Kakulapati R.R.; Jhillu S.Y. Inclusion complex of anti-tubercular rifampicin with beta-cyclodextrin or 2-hydroxypropyl beta-cyclodextrin and a process for producing the same. *International Patent*, 2004, No. 2004041284.
18. Aree, T.; Chaichit, N. Inclusion complexes of β -cyclodextrin with pyrazinamide and piperazine: Crystallographic and theoretical studies. *Supramolecular Chemistry*, 2009, 21(5), pp. 384-393.
19. Terekhova, I. V.; Kumeev, R. S. Thermodynamics of inclusion complexes between cyclodextrins and isoniazid. *Russian Journal of Physical Chemistry A*, 2010, 84(1), pp. 1-6.
20. Teixeira, M. G.; De Assis, J. V.; Soares, C. G.; Venâncio, M. F.; Lopes, J. F.; Nascimento Jr, C. S.; De Almeida, W. B. Theoretical and Experimental Study of Inclusion Complexes Formed by Isoniazid and Modified β -Cyclodextrins: ^1H NMR Structural Determination and Antibacterial Activity Evaluation. *The Journal of Physical Chemistry B*, 2014, 118(1), pp. 81–93.
21. Geliperina, S.E.; Maxiennko, O.O.; Vanchugova, L.V.; Shipulo, E.V.; Babii, V.E.; Ignatiev, A.V. Pharmaceutical composition based on cyclodextrin nanoparticles containing rifabutin, method for its obtaining, method for treatment of mycobacteriosis and helicobacter infection. *Euroasian Patent*, 2010, No. 2010016410 (In Russian).
22. Welliver, M.; McDonough, J.; Kalynych, N.; Redfern, R. Discovery, development, and clinical application of sugammadex sodium, a selective relaxant binding agent. *Drug Design, Development and Therapy*, 2008, 2, pp. 49-59.
23. Karginov, V.A.; Nestorovich, E.M.; Yohannes, A.; Robinson, T.M.; Fahmi, N. E.; Schmidtman, F.; Hecht, S.M.; Bezrukov, S.M. Search for cyclodextrin-based inhibitors of anthrax toxins: synthesis, structural features, and relative activities. *Antimicrobial Agents and Chemotherapy*, 2006, 50(11), pp. 3740-3753.

24. Joshi, A.; Kate, S.; Poon, V.; Mondal, D.; Boggara, M.B.; Saraph, A.; Martin, J.T.; McAlpine, R.; Day, R., Garcia, A.E.; Mogridge, J.; Kane, R.S. Structure-based design of a heptavalent anthrax toxin inhibitor. *Biomacromolecules*, 2011, 12(3), pp. 791-796.
25. Ragle, B.E.; Karginov, V.A.; Wardenburg, J.B. Prevention and treatment of *Staphylococcus aureus* pneumonia with a β -cyclodextrin derivative. *Antimicrobial Agents and Chemotherapy*, 2010, 54(1), pp. 298-304.
26. Zhang, H.M.; Li, Z.; Uematsu, K.; Kobayashi, T.; Horikoshi, K. Antibacterial activity of cyclodextrins against *Bacillus* strains. *Archives of Microbiology*, 2008, 190(5), pp. 605-609.
27. Duca, G.; Ivancic, A.; Boldescu, V. Cyclodextrins – fields of application. Part II. *Chemistry Journal of Moldova*, 2012, 7(2), pp. 39-45.
28. Macaev, F.; Boldescu, V.; Geronikaki, A.; Sucman, N. Recent advances in the use of cyclodextrins in antifungal formulations. *Current Topics of Medicinal Chemistry*. 2013, 21, pp. 2677-2683.
29. Boldescu, V.; Bratu, I.; Borodi, Gh.; Kacso, I.; Duca, Gh.; Macaev, F.; Pogrebnoi, S.; Ribkovskaia, Z. Study of binary systems of beta-cyclodextrin with a highly potential anti-mycobacterial drug candidate. *Journal of Inclusion Phenomena and Macrocyclic Chemistry*, 2012, 74, pp. 129-135.
30. Boldescu, V. Nanoparticles and microparticles in tuberculosis treatment. *Akademios*, 2013, 1(28), pp. 108-111 (In Romanian).
31. Brzostek, A.; Pawelczyk, J.; Rumijowska-Galewicz, A.; Dziadek, B.; Dziadek, J. *Mycobacterium tuberculosis* is able to accumulate and utilize cholesterol. *Journal of Bacteriology*, 2009, 191(21), pp. 6584 – 6591.
32. Donova, M.N.; Nikolayeva, V.M.; Dovbnya, D.V. et al. Methyl- β -cyclodextrin alters growth, activity and cell envelope features of sterol-transforming Mycobacteria. *Microbiology*, 2007, 153, pp. 1981–1992.
33. Castagne, D.; Dive, G.; Evrard, B.; Frédérich, M.; Piel, G. Spectroscopic studies and molecular modeling for understanding the interactions between cholesterol and cyclodextrins. *Journal of Pharmacy and Pharmaceutical Sciences*, 2010, 13(2), pp. 362-377.

ANTIMICROBIAL REAGENTS AS FUNCTIONAL FINISHING FOR TEXTILES INTENDED FOR BIOMEDICAL APPLICATIONS.

I. SYNTHETIC ORGANIC COMPOUNDS

Madalina Zanoaga*, Fulga Tanasa

"Petru Poni" Institute of Macromolecular Chemistry, 41A, Grigore Ghica Voda Alley, Iasi, Romania

**email: zanoaga@icmpp.ro; phone: (+40 232) 21 74 54; fax: (+40 232) 21 12 99*

*Paper dedicated to the 65th anniversary of the
"Petru Poni" Institute of Macromolecular Chemistry of Romanian Academy, Iasi, Romania*

Abstract: This article offers an overview of some contemporary antimicrobial agents used as functional finishing for textiles intended for biomedical applications. It reviews only synthetic agents, namely quaternary ammonium compounds, halogenated phenols, polybiguanides, *N*-halamines, and renewable peroxides. These agents can be divided into several groups according to their mechanism of antimicrobial activity, toxicity, durability and ecological acceptability. Examples of commercial antimicrobial products are presented herein, as well as the corresponding finishing methods.

Keywords: antimicrobial agents, structure, fibers, medical textiles.

Introduction

Textiles are ubiquitous and are used throughout the world for various purposes every day. In 2008, the world *per capita* fiber consumption was 10.4 kg [1,2]. Nowadays, with the rapid changes in the social-economic structure of our society, textile materials (woven, nonwoven, knitted, and composites) have found various end-uses from apparels up to technical textiles [3]. The medical textiles sector, looked at in its broadest meaning, is undoubtedly one of the greatest success stories of recent years, in terms of the global technical textile industry. Medical textiles offer a variety of technical and functional properties, having applications in the field of medical and clinical care.

Common problem in hospitals and healthcare institutions is microbial contamination of surfaces, including textile fabrics, which can lead to infections and, consequently, to cross-infections. Irrespective of their applications, *internal* (surgical threads and various implants) or *external* (various extracorporeal devices such as catheters and hollow fibers for dialyzers, gauzes, bandages, nappies, tampons, and so on), medical textiles have to be comprised of basic bioactive properties, especially antimicrobial. Also, it is extremely important for *protective clothing* (surgical masks, caps, gowns, etc.) and *hospital linen* to meet the demands for antimicrobial protection.

Together, the abuse of antibiotics, new virus occurrence and prevalence of multi-resistant bacteria, such as methicillin-resistant *Staphylococcus aureus* (MRSA) and vancomycin-resistant *Enterococcus* (VRE), along with ageing of the population have generated the need for new and more efficient medical textiles.

Most synthetic textiles inherently resist against microorganisms (such as bacteria, fungi and mildew) attack, but are generally not inherently biocide. Further, the ability to inhibit growth of microorganisms does not reveal how fast or even whether the microorganism is destroyed. With natural fibers, however, there is a significant overlap of treatments which both protect the textile and attack the microorganisms [4,5]. Textile materials are susceptible anyway to microbial degradation because they provide an excellent environment for microorganisms to proliferate, because of their large surface area and ability to retain moisture. These microbes are found almost everywhere in the environment and can multiply quickly when basic requirements (such as moisture, nutrients and temperature) are met. Microbial load of textiles is maintained during storage and negatively affects the wearer during use, as well as the textile itself. These effects comprise product deterioration including discoloration, offensive odors, dermal infections, allergic responses and other diseases which are often associated. Therefore, it is highly desirable to minimize the growth of microbes on textiles during their use [4].

Accordingly, controlling the undesirable effects of microorganisms on textiles is becoming an important issue, especially within the medical textile industry. The detrimental effects can be controlled by durable antimicrobial finishing of textiles using broad-spectrum biocide or biostatic agents that prevent or inhibit the growth of microorganisms.

Estimations have shown that the production of antimicrobial textiles was in the magnitude of 30,000 tones in Western Europe and 100,000 tones worldwide in 2000 [5]. Furthermore, it was estimated that the production rate will increase, making it one of the fastest growing sectors of the textile market. Sportswear, socks, shoe linings and lingerie accounted for 85% of the total production. There is also a broader market for antimicrobial fibers, for instance, in medical textiles, outdoor textiles, air filters, automotive textiles, domestic home furnishings, etc. Consumers' attitude towards hygiene and active lifestyle has created a rapidly increasing market for antimicrobial textiles in order to protect the user from microorganism contamination. Another aspect of antimicrobial functional

finishing of textiles is the addition of a therapeutic value to the material, intended for example, for wound healing [6-8].

As a consequence, the number of different technological approaches, antimicrobial agents and methods of binding them to the substrate, suitable for textiles, has increased significantly. A survey [1] listed the consumption of biocidal substances in Europe as 1546 metric tonnes for use in fibers, leather, rubber and polymeric materials and the demand for functional textiles with achieved antimicrobial activity is increasing. The development of new antimicrobials with enhanced activity is an ongoing topic of research and targets products ranging from synthetic organic compounds up to naturally based biocids [9-11]: quaternary ammonium compounds, dyes and regenerable *N*-halamines, polyhexamethylene biguanides, triclosan, peroxyacids, metals and metal oxides (silver, copper, titanium, cobalt, etc.), chitosan, essential oils, enzymes, natural pigments, etc.

This article reviews some of the most known antimicrobial agents and the corresponding finishing techniques used in order to obtain functional textiles for biomedical applications.

Antimicrobial treatment of textiles: requirements and mode of action

There is a growing volume of literature describing the survival and growth of microorganisms in textiles and their dissemination as a health risk. Textiles are not only carriers of microorganisms, but also good media for their proliferation. When the fabric is worn next to skin, infestation may cause cross infections by pathogens and odors development.

The antimicrobial functional finishes are applied to textiles in order to protect the wearer and the fabric itself [12], several objectives being achieved by this:

- to prevent and control infestation, proliferation and cross infection;
- to reduce odors and stains formation due perspiration and degradative processes;
- to limit the deterioration of textiles, particularly fabrics made from natural fibers;
- to control the spread of disease and danger of infection, inside and outside hospitals.

In order to obtain the greatest benefit, an ideal antimicrobial treatment should not only destroy undesirable microorganisms, but also satisfy a number of requirements concerning their effectiveness against a broad spectrum of bacterial and fungal species, low toxicity towards consumers, etc. [4,7,13]. Thus, first and foremost, the safety criterion must be considered: the product should not be excessively toxic to humans and the environment, and should not cause skin allergy and irritations of any kind. Second, the compatibility is defining the treatment quality: the product must not influence negatively on the textile properties and appearance, and must be compatible with common fibers and fabrics, as well as manufacture technologies. Last but not least, the durability of the product is decisive for its service life: it should be able to endure numerous laundering cycles, drying, and leaching. Researchers are now focusing on safe, durable, and environmentally friendly natural substitutes [14, 15].

According to their mechanism of antimicrobial activity, toxicity, durability and ecological acceptability, these agents can be divided into different groups [16]:

- biocides and biostats,
- leaching and bound antimicrobials,
- controlled-release and barrier-forming agents,
- agents of poor and good washing resistance.

These antimicrobial agents differ in their chemical structure, effectiveness, method of application, and influence on users and the environment, as well as production costs [5, 17-20].

In general, antimicrobials are similar to antibiotics in that they both inhibit microbes growth. But while the purpose of antibiotics is to cure disease, antimicrobials aim to prevent transmission of disease-causing microorganisms [21]. In the case of the antimicrobial textile finishes, their activity can be **biocidal** or **biostatic**. The biocides (bactericides and fungicides) include agents that destroy bacteria and fungi, whilst the biostats (bacteriostats and fungistats) inhibit the proliferation of microorganisms. The mode of action is directly related to and strongly dependent upon the concentration of the active substance in the textile finishing. The **minimum inhibitory concentration** (MIC) is required for biostatic activity, but for biocidal activity the **minimum biocidal concentration** (MBC) should be exceeded [3,16].

A schematic illustration of different types of activity of an antimicrobial agent used for functional finishing of textiles is presented in Figure 1. As showed, antimicrobials may exert different actions onto pathogens depending on their inhibitory concentration (biostatic effect) or biocidal concentration (biocidal effect), yielding in a significant decrease in the number of CFU.

Antimicrobial reagents used for textiles

The growth rate of microbes can be astoundingly rapid. The bacteria population, for example, will double every 20 to 30 min under ideal condition (36-40°C, pH 5-9). At this rate, one single bacteria cell can increase to 1048576 cells in just 7 hours [22]. Therefore, antimicrobial finishes must be quick acting to be effective.

There are several classes of antimicrobial agents used for antimicrobial functionalization of textiles [1]. The most prevalent antimicrobials for textile use include quaternary ammonium compounds (QAC), halogenated phenols (such as triclosan), metal-organic complexes (such as zinc pyrithione), polybiguanides (such as polyhexamethylene biguanides, PHMB), *N*-halamine compounds, metals and their corresponding oxides and salts, regenerable peroxides, etc. [1,3,5,11,16], and some of them, namely synthetic organic compounds, are discussed below.

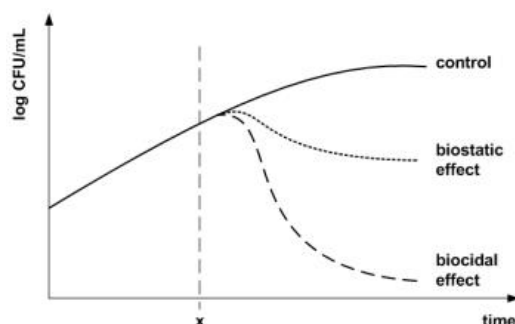


Figure 1. Effects of antibacterial agents on microbial growth rates (x - addition of an antimicrobial agent; CFU - colony forming unit) [3].

Quaternary Ammonium Compounds (QACs)

Quaternary ammonium compounds (QACs), particularly those containing chains of 12–18 carbon atoms, have been widely used as disinfectants. These compounds have a nitrogen atom bearing a positive charge which is responsible for the various detrimental effects on microorganisms. During bacterial inactivation, the quaternary ammonium groups remain intact and retain their antimicrobial activity as long as QACs are attached to textiles [5].

Cationic surface active agents (cationic surfactants), including particular quaternary ammonium salts (QASs), are important biocides known to be effective antiseptics [16]. As antimicrobial agents for textiles, monoammonium and "gemini" or "dimeric" ammonium surfactants (Figure 2) bearing alkyl, alkyl-aryl and perfluorinated hydrocarbon groups are used [23-25]. These are active against a broad spectrum of microorganisms such as Gram-positive and Gram-negative bacteria, fungi and certain types of viruses [26].

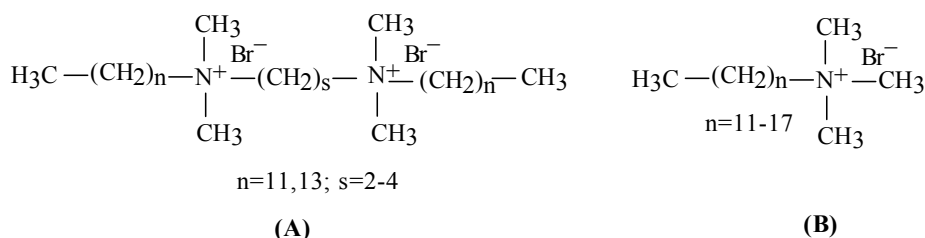


Figure 2. Chemical structure of monoquaternary ammonium salt, namely alkanediyl- α,ω -bis(dimethylalkylammonium bromide) (A) [24], and diquaternary ammonium salt, namely alkyltrimethylammonium bromide (B) [25].

The antimicrobial activity of QASs depends on a number of structural factors, as follows: the length of the alkyl chain, the presence of perfluorinated groups and the number of cationic ammonium groups in the molecule. The antimicrobial function arises from attractive interactions between the cationic ammonium group of the QAS and the negatively charged cell membrane of the microbe. These interactions consequently result in the formation of a surfactant-microbe complex. This, in turn, causes the interruption of all essential functions of the cell membrane and, thus, the interruption of cellular protein activity [27-29]. QASs also affect the bacterial DNA, causing a loss of multiplication ability [30].

If the QAS contains the cationic ammonium moiety bonded to a long hydrocarbon chain, two types of interactions between the agent and the microorganism can occur:

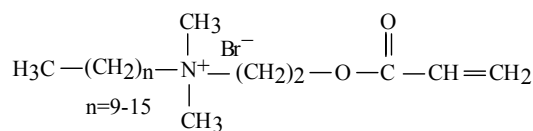
- a polar interaction with the nitrogen cation of the ammonium group, and
- a non-polar interaction with the long alkyl chain having hydrophobic character.

Penetration of the hydrophobic group into the microorganism occurs consequently, enabling the alkyl ammonium group to physically interrupt all the key functions of the cell.

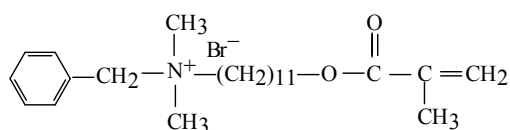
Despite many positive properties, QASs have an inherent disadvantage, namely leaching from the textile due to its weak bonding to fiber or fabric. There are no reactive functional groups in the structure of the QAS as to allow

its chemical bonding to the fibers. As consequence, leaching of the QAS from textile occurs, yielding in a fast decrease in concentration to values below the MIC. In addition, QASs have poor wash durability.

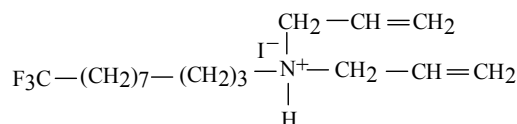
New and non-leaching, even permanently bonded, QAS biocidal groups have been designed especially for textile fibers. They are polymerizable QASs containing acrylate or methacrylate moieties, able to be incorporated in the fibers structure. Such QAS monomers have been named surfactant monomers or “*surfmers*”. Under appropriate conditions, surfmers polymerize into a bulky polymer network having a polycationic structure, including side QAS groups chemically bonded to the main polyacrylate chain [31-33]. Some examples are given in Figure 3.



(A)



(B)



(C)

Figure 3. Chemical structures of some surfmers:

A - alkyl(2-(acryloyloxy)ethyl)dimethyl ammonium bromide [31,32],

B - benzyl(11-(acryloyloxy)undecyl)dimethyl ammonium bromide [32],

C - N-(4,4,5,5,6,6,7,7,8,8,9,9,10, 10,11,11-heptafluoroundecyl)-N,N-diallylmethylammonium iodide [33].

QASs can act as a bio-barrier once they are chemically bonded to the textile surface and, therefore, kill microorganisms by contact. Furthermore, the formation of a polymer network on the fibers surface strongly increases the coupling durability and washing resistance of the biocide textile.

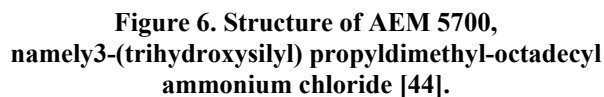
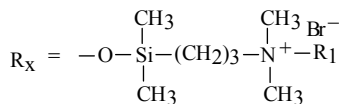
Different approaches were used to obtain antimicrobial textiles containing QASs, but the sol-gel technology has proven to be most appropriate because it enables the formation of a nanocomposite polymer network with an organic-inorganic hybrid structure [34-36]. Colloidal solutions (sols) have been prepared for this purpose, consisting of mixtures of tetraalkoxysilane ($\text{Si}(\text{OR})_4$) and QASs with different structures [37] or organic-inorganic hybrids, including alkyl-trialkoxysilanes ($\text{R}_x\text{-Si}(\text{OR})_3$), with incorporated quaternary ammonium groups [30, 38-43], as presented in Figure 4.

Alkoxysilanes are sol-gel precursors with alkoxy groups that can hydrolyze in the presence of a catalyst to form silanol ($-\text{SiOH}$) groups, which further condense among each other or with the hydroxyl ($-\text{OH}$) groups of the textile fibers. The formation of covalent bonds between $-\text{SiOH}$ groups of the sol-gel precursor and $-\text{OH}$ moieties of the textile fibers yields in increased durability and washing resistance for the nanocomposite network on the finished antibacterial textiles.

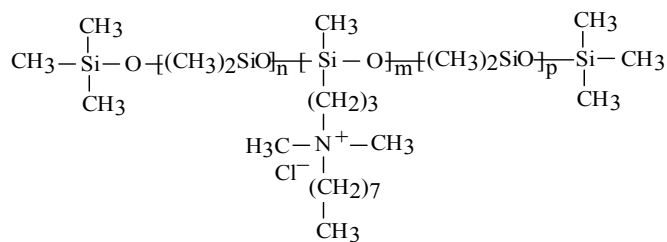


A commercial antimicrobial textile product using QAC as the active agent is the BIOGUARD® produced by AEGIS Environments. The active substance, 3-trimethoxy-silyl-propyl-dimethyl-octadecyl ammonium chloride (AEM 5700, formerly known as the Dow Corning 5700 Antimicrobial Agent; see Figure 6), has a MIC of 10–100 mg/l against Gram-positive and Gram-negative bacteria [46].

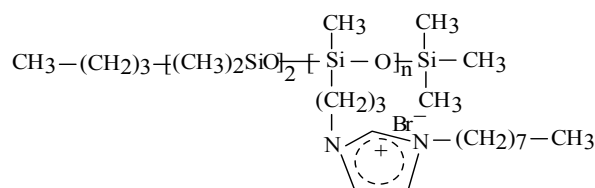
A commercial antimicrobial textile product using QAC as the active agent is the BIOGUARD® produced by AEGIS Environments. The active substance, 3-trimethoxy-silyl-propyl-dimethyl-octadecyl ammonium chloride (AEM 5700, formerly known as the Dow Corning 5700 Antimicrobial Agent; see Figure 6), has a MIC of 10–100 mg/l against Gram-positive and Gram-negative bacteria [46].



Other important antimicrobials for textile applications are substituted polycationic polysiloxanes with pendant QAS or imidazolium salt groups, which demonstrated biostatic effect. They are mostly copolymers consisting of polydimethylsiloxane, polymethylhydro-siloxane and QAS- or imidazolium-modified polysiloxanes in different molar ratios. Their structures are presented in Figure 7.



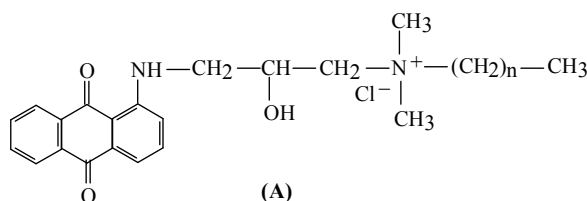
(A)



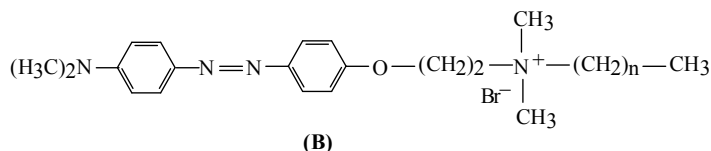
(B)

Figure 7. Substituted polycationic polysiloxane with pendant QAS (A) [45] and imidazolium salt (B) [49] groups.

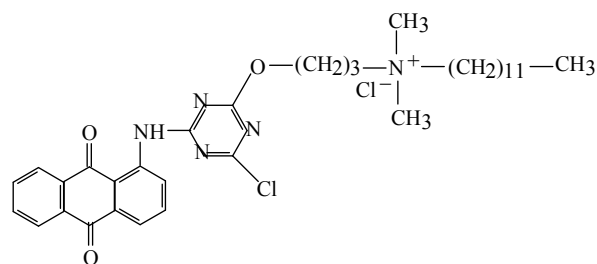
QACs with relevant antimicrobial activity are mono- and diazoic dyes, as well as anthraquinone-based dyes, containing one or even two QAS moieties with different structures (Figure 8).



(A)



(B)



(C)

Figure 8. Antimicrobial cationic anthraquinone-based dye (A) [50,51], monoazoic dye (B) [52] and anthraquinone-based reactive dye (C) [53] containing QAS.

These novel cationic dyes have biostatic activity due to the chemically bonded QAS groups [50-55]. Owing to the QAS content, the di-substituted dyes have higher antimicrobial activity than mono-substituted ones [50]. The other structural factor affecting QACs activity is the chain length: the longer the chain of the QAS groups in the dye structure, the more intense the antimicrobial activity [50, 54].

Cationic anthraquinone-based dyes can be effectively introduced into acrylic fibers in order to simultaneously achieve coloration and antimicrobial function. However, the wash durability of the treated acrylic fabric is low [51]. To improve the wash durability of antimicrobial dyes on cotton fibers, an anthraquinone cationic reactive dye (Figure 8C) has been synthesized by chemical binding a QAS group to the reactive *s*-triazine group of the dye by a nucleophilic substitution [53]. This reactive cationic dye has been applied to cotton fibers with high exhaustion and fixation rates, without the addition of any salt as electrolyte. Although the dyed cotton exhibits good color retention after washing, antimicrobial function decreased after repetitive washing, due to the deactivation of quaternary ammonium groups by their reaction with negatively charged anionic units from detergent.

The biocide action depends on both the size of the molecule and the functional group density. Larger molecules tend to have lower permeation through cell membranes and, thus, appear less biocidal. Dendrimers have attracted attention as possible antimicrobial agents due to their compact structure and availability of many end groups. Dendritic biocides containing quaternary ammonium groups are interesting because their functional group density increases with their size, suggesting that an optimal size and biocide activity can be reached [56-58]. The structure of a 4-generation poly(propyleneimine) dendrimer with 32 surface primary amine groups is shown in Figure 9.

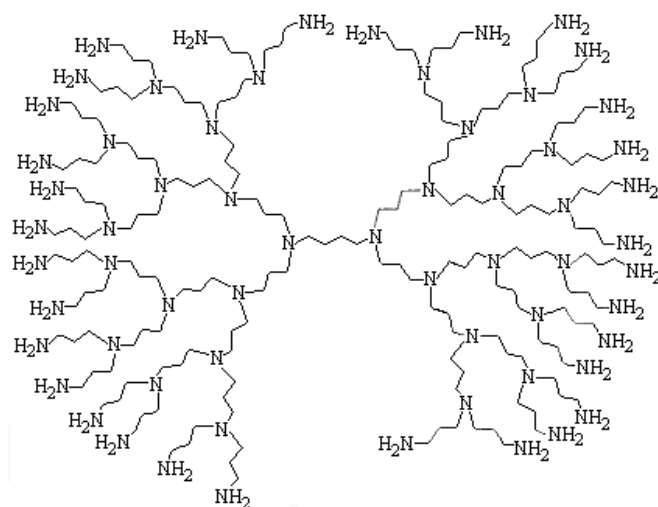


Figure 9. A 4-generation poly(propyleneimine) dendrimer with 32 surface primary amine groups (according to [56]).

Recently, a series of highly effective quaternary ammonium functionalized poly(propyleneimine) dendrimers was synthesized [56]. Their biocidal properties depend on the size of the dendrimers used, length of the hydrophobic chain in the quaternary group, and counter anion. It was observed that these novel biocides with bromide anions are more efficient than those with chloride anions.

The attachment of QACs to textile substrates is believed to take place predominantly by the ionic interaction between cationic groups in QACs and anionic ones at fibers surface [59,60].

Thus, for polyester fibers such as Acrilan® (from Acrilan) and Orlon® (from DuPont) which contain carboxylic or sulfonate groups, QACs can be directly bridged under specific conditions (near boiling temperature) [61-63].

Other synthetic fibers, such as nylon, contain fewer reactive sites and are quite resistant to chemical modification procedures, including antimicrobial finishing. QACs have been substantively bound to nylon fibers using acid dyes as bridge and the modified fibers achieved biocidal properties, but displayed some strength issues. It is considered that dye molecules may act as bridges to bind QACs to the fibers surface [64]. The fabrics were first dyed with acid dyes before QACs were applied under alkaline conditions. The ionic interaction between the dye molecules and the QAC was sufficiently strong to provide a semi-durable antimicrobial finishing [59, 60, 64].

Similarly, the glutamyl and aspartyl residues in wool provide carboxylic groups able to bind QACs. Particularly, cetylpyridinium chloride can render it antimicrobial activity to wool upon corresponding treatment, with durability up to 10 launderings [65, 66].

Nevertheless, attempts have been made to covalently attach QAC onto wool. A new QAC, *N*-dodecyl-amino-betaine-2-mercaptoethylamine hydrochloride (DABM) was synthesized [67,68] and it can react with wool by means of its thiol group, either with cysteine-S-sulphonate residues (Bunte salts) of sodium bisulphite pretreated wool or with the disulfide bond of cystine wool, forming an asymmetrical disulfide bond. Such covalent attachment of the quaternary ammonium surfactant provides antimicrobial activity.

Cotton fabrics have been treated in the presence of a 4-aminobenzenesulfonic acid-chlorotriazine adduct which increased the number of anionic sites on the fabric surface and facilitated the QACs binding [69]. In general, these studies considered the influence of the solution pH, the QAC concentration, temperature, and exhaustion time.

Some antimicrobial products for textile application are currently commercially available under specific trade names. Thus, Dow-Corning produced a series of quaternary amines which could be fixed to a surface via silane coupling reaction [70-72]. Aegis Environments (Midland, Michigan), a spin-off company, has developed the technology under the trade name Microprobe Shield[®]. The product is used in a wide cross-section of the textile industry – nonwovens, wipes, medical wear, socks, athletic apparel, uniforms, floor mats, ceiling tiles etc. Other companies are also involved in research and development of such antimicrobial agents for functional finishing of textiles [73].

Halogenated phenols

Halogenated phenols are a group of organic reagents known for their antimicrobial activity and, therefore, widely used as antiseptics and disinfectants, fungicides and pesticides. There are a few very famous members of this class, such as triclosan (2,4,4-trichloro-2-hydroxydiphenylether), diclosan (5-chloro-2-(4-chlorophenoxy)phenol), chloroxylenol (4-chloro-3,5-dimethylphenol, currently used in the Dettol formulation, along with other components), trichlorophenyl-methyl-iodosalicyl (also known as TCP and it combines antiseptic effects of both halogenated phenols and salicylic acid derivatives), as well as Tinosan[®] which encompasses active biocidal agents such as diclosan (see Figure 10).

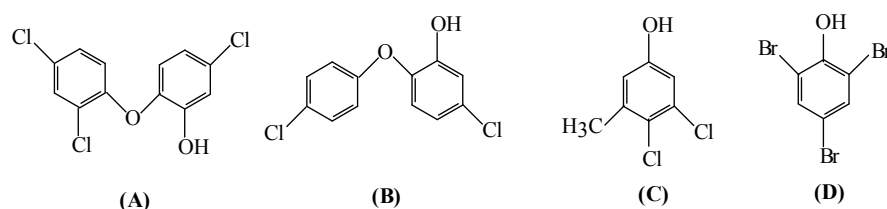


Figure 10. Structure of the most known halogenated phenols:

- A - triclosan (2,4,4-trichloro-2-hydroxydiphenylether) [3] (according to PubChem Compound, CID 5564),**
B - diclosan (5-chloro-2-(4-chlorophenoxy)phenol) (according to PubChem Compound, CID 18807),
C - chloroxylenol (4-chloro-3,5-dimethylphenol) (according to PubChem Compound, CID 2723),
D - 2,4,6-tribromophenol (according to PubChem Compound, CID 1483).

Recent investigations evidenced the efficiency of natural compounds with similar structure, such as 2,4,6-tribromophenol found in significant amounts in different species of Antarctic sponges [74].

Attention has been drawn to these compounds due not only to their biocide activity, but also to their structural similarity with highly toxic contaminants, such as dioxins and halogenated phenolic compounds (HPCs) (including hydroxylated polychlorobiphenyls (OH-PCBs) and hydroxylated polybromodiphenyl-ethers (OH-PBDEs) which are persistent organic pollutants [75]). The possibility of their conversion into these hazardous compounds may represent a potential health risk to human (e.g., dermal irritation) and wildlife, as well.

Among halogenated phenols, triclosan is the most widely used biocide; it is present in many contemporary consumer and personal health-care products, detergents and household objects, including textiles and plastics. At bactericidal concentration, triclosan is very effective against a broad range of microorganisms, including antibiotic-resistant bacteria, but it also has some antifungal and antiviral properties [16,21].

The mechanism of triclosan antimicrobial effect is based mainly on the inhibition of fatty acid biosynthesis through blocking lipid biosynthesis, as well as on the interaction with amino acid residues of the enzyme-active site within the membrane [76]. As the widespread use of triclosan could represent a potential risk in terms of the development of resistant microorganisms [16], strong binding to textiles surface and subsequent controlled release is required.

As a textile finish, it is mostly used for the protection of industrial and transport filters, the production of antimicrobial shoe-socks, socks, towels, cleaning wipes and for household textiles [3].

A cotton knitted fabric treated with 6% triclosan solution by the conventional exhaust process has shown an effective reduction of bacteria *Staphylococcus aureus* and *Escherichia coli*. After 50 laundering cycles, antimicrobial activity decreased, but the reduction was still over 70%. The activity in acidic, basic and synthetic urine conditions was also reduced [76].

Unlike most other cationic biocides used on textiles, triclosan is not ionized in solution. Triclosan has, therefore, been applied to cellulose fibers in combination with polycarboxylic acids as crosslinking agents [77]. The application of polycarboxylic acid to fibers previously finished with triclosan enhances the washing durability of the antimicrobial coating.

To achieve a more durable finishing, novel host–guest inclusion complexes have been prepared using triclosan and cationic β -cyclodextrins (torus-shaped cyclic oligosaccharides containing six to eight glucose units linked by α -1,4 bonds), based on the ability of small molecules to penetrate into the hydrophobic cavity of β -cyclodextrins (Figure 11).

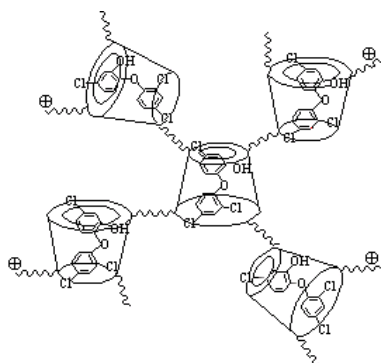


Figure 11. Schematic illustration of host–guest inclusion complexes of triclosan and β -cyclodextrin (according to [78]).

Water solubility, stability and antimicrobial activity have been determined for the host–guest complexes [78,79]. Owing to strong electrostatic attraction, the complexes are adsorbed to the surface of cellulose fibers almost completely.

In another approach, triclosan has been encapsulated in microspheres made of biodegradable polylactide and immobilized onto nonwoven viscose textiles [80].

Cotton and cotton blends can be submitted to functional finishing with triclosan mixed with a polyurethane resin and a plasticizer [81] with good results.

Being a relatively small molecule, triclosan can also act like a disperse dye and can be used by exhaustion prior to dyeing, together with dyeing or after dyeing of polyester and nylon fibers at 5%. During the fabric use, the agent migrates to the treated textiles surface at a slow, yet sustained, rate as to provide antimicrobial efficacy [82].

Triclosan can also be directly incorporated into synthetic polymers through melt-mixing or suspension polymerization [83,84]. A number of companies manufacture and market triclosan-based fibers, yarns or fabrics. For instance, the nylon and polyester products Tinosan AM 100[®] and CEL[®] (Ciba Speciality Chemicals), the Silfresh[®] cellulose acetate yarn (Novaceta) and Microban[®] textile products (Microban International), all contain triclosan as the active antimicrobial agent which is applied during the finishing stage or is incorporated into the fiber during extrusion [85,86]. Fibers using triclosan are available from Synthetic Industries (olefin), Sterling Fibers (acrylic), and Cydsa (acrylic), as well as from several other suppliers of acetate, olefin, and acrylic fibers. Finishes for fabrics including polyester and cellulose are available [87,88].

Literature is abundant in data concerning the bacterial resistance towards triclosan. Despite of its antimicrobial activity, triclosan breaks down into toxic compounds when exposed to sunlight in the environment (in example, 2,8-dichlorodibenzo-*p*-dioxin which is chemically related to other toxic polychlorinated dioxins). The chemical structure of triclosan is quite similar to that of diethylstilbestrol (DES), a non-steroidal estrogen, and it is raising concerns about its potential as an endocrine disruptor. Recent studies showed that triclosan can significantly affect the thyroid gland activity [89], at exposure levels equivalent to those currently found in the environment and human tissues, and exhibit weak androgenic effects [90]; there is no evidence that triclosan is a carcinogen or teratogen [91].

Due to the health and environmental issues, the scientific community is concerned about the long term effects [92] and analyses the opportunity to limit the triclosan use in textiles and some other products.

Polybiguanides

Polybiguanides are polymeric polycationic amines that include cationic biguanide repeating units separated by hydrocarbon chain linkers of identical or dissimilar length [16] (Figure 12). One of the most important antimicrobial agents among them is PHMB, poly(hexamethylenebiguanide) which has an average of 11 biguanide units (Figure 13) [93,94].

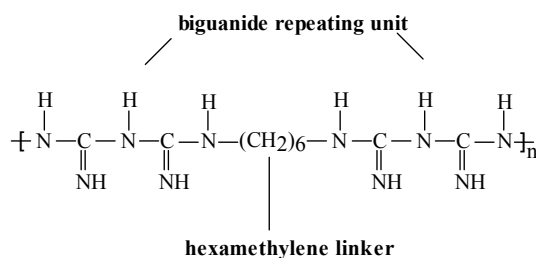


Figure 12. Structure of biguanide units linked by a hexamethylene spacer (according to [16]).

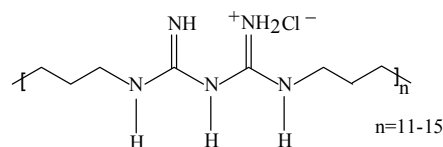


Figure 13. Poly(hexamethylenebiguanide) hydrochloride structure [94].

PHMB exhibits much greater antimicrobial activity than the corresponding monomeric or dimeric biguanides, chemical stability, and low toxicity, all at a reasonable cost. Its maximal biocidal efficiency is due to both cationic structure (H_2N^+) and flexible spacer, a hexamethylene group, between biguanide repeating units. PHMB is, therefore, widely used in medicine as an antiseptic agent for textiles, especially for preventing wound infection by antibiotic-resistant bacteria [95,96]. It also has several other interesting properties that make this material suitable as a building block for supramolecular chemistry and “smart” materials [97].

In a comparative investigation on the antiseptic efficacy, some of the most known and used antimicrobial agents were studied [98]:

- triclosan - a halogenated phenol (see section 3.2.),
- octenidine - a bis(dihydropyridinyl)-decane derivative, similar in its action to the quaternary ammonium compounds,
- PHMB,
- PVP-Iodine - a stable chemical complex of polyvinylpyrrolidone (PVP) and elemental iodine, and
- chlorhexidine digluconate - a cationic polybisbiguanide used primarily as its salts, namely dihydrochloride, diacetate and digluconate.

It was concluded that PHMB was the most effective and recommended when prolonged use is needed and/or when prolonged contact is feasible.

The biocide activity of PHMB was studied and it was highlighted that it acts through multiple mechanisms. The attachment of PHMB induces shifts in the physical properties of membranes. It disorganizes the cytoplasmatic membrane of microbes, leading to increased membrane permeability. The study reveals phase transitions (solid/liquid) in membranes into more fluid and rigid domains. The outer surface of bacteria is universally negatively charged and usually stabilized by divalent magnesium and calcium cations. PHMB replaces these ions and, therefore, has a natural affinity for the membranes of both Gram-positive and Gram-negative bacteria, as well as other microorganisms [99]. It was also demonstrated that PHMB activity increases on a weight basis with increasing levels of polymerization. To date, bacterial resistance to PHMB has rarely been observed, although resistance to the bisbiguanide chlorhexidine is well known [5,100].

Wound dressings are one of the most known textile applications of PHMB, due to its low toxicity ($\text{MIC}=0.5\text{--}10\text{ppm}$). The literature indicates that PHMB can bind to the anionic carboxylic groups of cellulose (Figure 14), which are formed through oxidation of glucose rings during pre-treatment processes, such as bleaching and mercerizing [16].

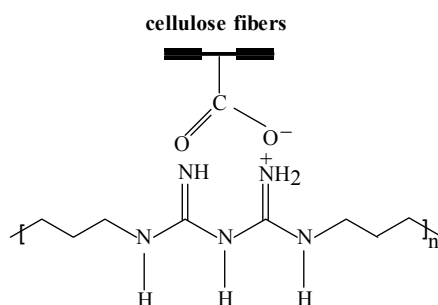


Figure 14. PHMB binding to the carboxylic group of cellulose [16].

At lower concentrations, electrostatic interactions between PHMB and carboxylic groups in the cellulose dominate; however, hydrogen bonding of PHMB with cellulose resulting in multilayer adsorption becomes increasingly dominant as the concentration of PHMB increases. The adsorption of PHMB increases if cellulose fibers

are previously dyed with anionic reactive dyes [94], which provide sulfonic acid sites able to link PHMB. However, strong PHMG-dye interactions cause a reduction in its antimicrobial activity, which is undesirable.

Another finishing approach for PHMB-treated cotton fibers involves an after-treatment with a strong organic acid used to increase durability, as well as to overcome fabric yellowing. PHMB can also be directly exhausted onto cotton at room temperature and neutral pH or applied in a pad-dry-cure process. PHMB needs to be applied in an amount of 2–4% for durable finishing and 0.25–1% for disposable items. The PHMB treatment was extended to synthetic fibers using a self cross-linkable resin and a catalyst [5].

Special grades of PHMB, namely Vantocil® and Reputex®, have been developed. The primary performance benefits of Vantocil® include: fast-acting and broad spectrum antimicrobial activity; no cross-resistance with therapeutic antibiotics; high level of retained biocidal activity in both soft and hard water conditions, and in the presence of organic load (bovine serum albumin, yeast extract, milk and sucrose); stable and effective performance over a pH range of 1–11; low surface activity; provide very low foaming [101]. Reputex® has a higher molecular weight than Vantocil®, containing an average of 16 biguanide units in the polymer. This longer polymer length not only results in higher biocide activity, but also provides more cationic sites per molecule for a possibly stronger binding to the textile surface. Reputex® was initially applied to cotton or its blends, using exhaust or pad-dry-cure processes, and more recently to polyester and nylon [102], under the trade name Purista®.

N-Halamines

N-halamines are heterocyclic organic compounds containing one or more nitrogen-halogen (N–X) covalent bonds that are normally formed by the halogenation of imide, amide, or amine groups. Other N-halamines containing different reactive groups, such as sterically hindered hydantoin, imidazolidones and oxazolidinones, proved to be effective for textile applications [73]. Their antimicrobial properties, proven for a broad spectrum of bacteria, fungi and viruses, are based on the release of chlorine by its electrophilic substitution with H in the N–Cl bond. This reaction can be carried out in the presence of water and results in the presence of free chlorine cations able to bind to the acceptor regions on microorganism and, subsequently, hinder their enzymatic and metabolic processes, leading to microorganism destruction. During the interaction with microbial membrane, the N-halamine bond is reversibly converted into N–H bond (which has no biocide activity) and has to be exposed to hypochlorite solution (*e.g.*, during bleaching or laundering) for its regeneration (as presented in Figure 15) and antimicrobial activity recovery [103,104].

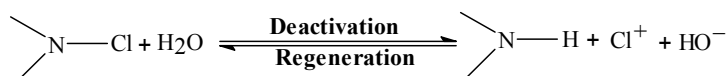


Figure 15. Reaction mechanism of N-halamine compounds [3,5].

N-halamines can be applied to various textile surfaces including cellulose [104], polyamide [105] and polyester [106] fibers. To increase their effectiveness and the durability of the antimicrobial finish [104], research has been oriented toward synthesis of N-halamide monomers with an incorporated vinyl reactive group (Figure 16) that can polymerize on cellulose fibers under appropriate conditions to form a coating with excellent durability after washing [16].

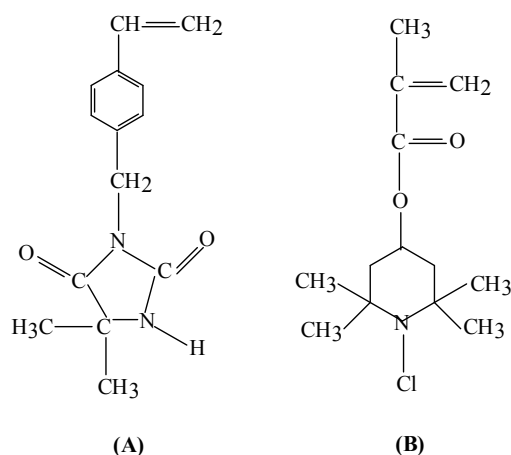


Figure 16. Chemical structure of 3-(4'-vinylbenzyl)-5,5-dimethylhydantoin (A) [106] and N-chloro-2,2,6,6-tetramethyl-4-piperidinyl methacrylate (B) [16].

Cellulose treated with methylol-5,5-dimethylhydantoin in combination with hypochlorite forms chloramines on the fiber surface [3]. Nevertheless, the fabrics yellowing and their strength loss occur when high concentrations of chloramines are used, affecting textiles not only from practical point of view (they become brittle), but also esthetic due to the unpleasant chlorine odor.

Moreover, covalent binding of *N*-halamines to the cellulose surface is ensured by two different methods:

- the preparation of *N*-halamine precursors containing two hydroxyl groups, which can be chemically bonded to hydroxyl groups from cellulose fibers surface in the presence of 1,2,3,4-butanetetracarboxylic acid (BTCA) as cross linking agent [107], or
- the synthesis of *N*-halamine siloxane monomer precursors, which allow the silanol groups to react with the cellulose hydroxyl groups to form a nanocomposite coating, as presented in Figure 17: A is 4-[3-triethoxysilylpropoxyl]-2,2,6,6-tetramethylpiperidine [108], B is 5,5-dimethyl-3-(3'-triethoxysilyl-propyl)-hydantoin [105], C is 3-(3-triethoxysilyl-propyl)-7,7,9,9-tetramethyl-1,3,8-triazaspiro[4.5]decane-2,4-dione [105].

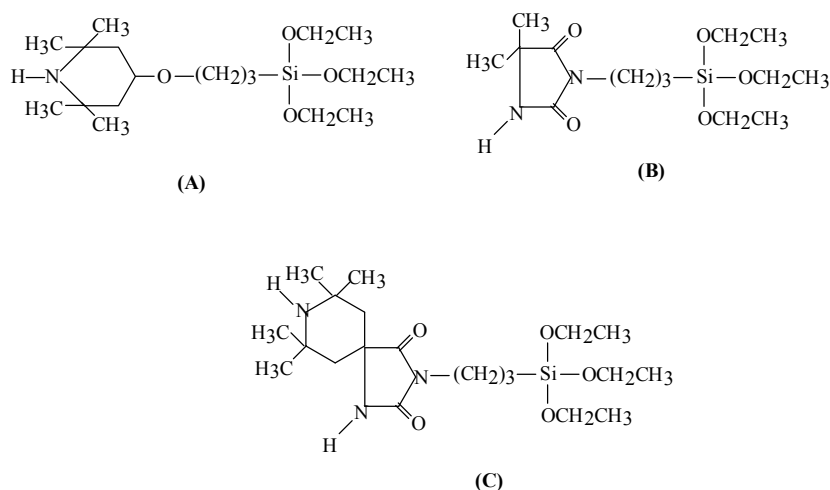


Figure 17. Chemical structure of different *N*-halamine siloxane precursors [105,108].

In addition, the study showed that copolymers incorporating *N*-halamine siloxane and QAS siloxane by synthesis, namely poly[3-(5,5-dimethylhydantoinylpropyl)siloxane-*co*-3-dimethyldodecylammoniumpropyl-siloxane chloride] (Figure 18), displayed enhanced antimicrobial behavior due to the synergistic action of these agents.

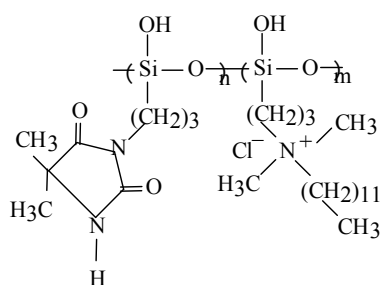


Figure 18. Chemical structure of hydantoinyl/quat siloxane copolymer [104].

Different heterocyclic *N*-halamine compounds have been covalently attached to various types of fibers, ranging from nylon [109] and polyester [110], to cotton [5] and keratinous fibers [111]. Another method to covalently attach these biocide compounds is to graft them onto cellulosic fabrics [3,5,16], as well as synthetic fabrics, mostly made of high performance polymer fibers such as: polyethylene terephthalate (PET), nylon-66 (PA), polypropylene (PP), acrylic fibers (Orlon), polyester/polyamide (PET/PA=70/30) blend microfibers, polyethylene (PE), Nomex (*m*-aramid fibers), Kermel (polyamid-imide fibers), poly-[2,2'-(*m*-phenylene)-5,5'-bisbenzimidazole]/Kevlar (PBI/*p*-aramid) blend fibers [112, 113]. A schematic illustration of the covalent bonding reaction of *N*-halamine compounds on polyamide and polyester fibers is presented in Figure 19.

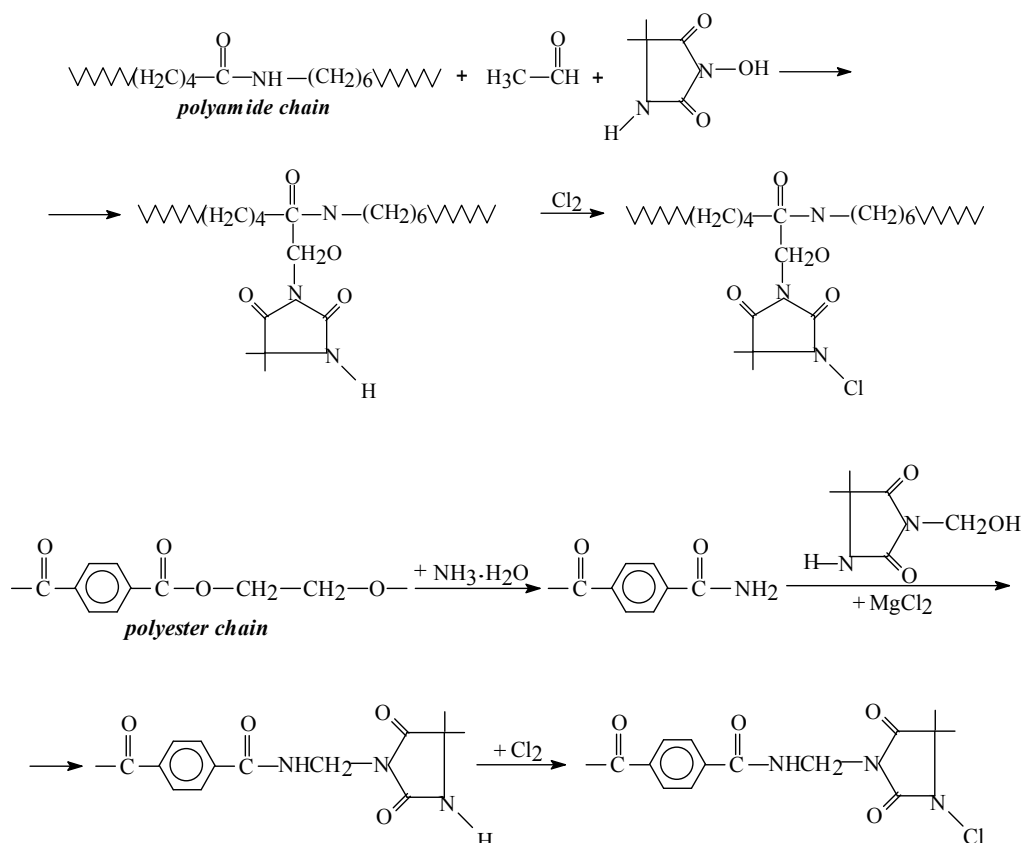


Figure 19. Reaction of *N*-halamine compounds with polyamide and polyester, respectively [73].

Antimicrobial nanofibrous nylon 6 membranes were fabricated with *N*-halamine additives through electrospinning. *N*-halamines generally contain one or more imide, amide or amine halamine bonds [114]. The antimicrobial activity of *N*-halamines increases in the following sequence: imide>amide>amine halamines, which is in a reverse order of their stability. Three structurally different *N*-halamines were introduced into the electrospinning dope of nylon 6 as antimicrobial additives:

- chlorinated 5,5-dimethylhydantoin (CDMH), containing an imide and amide halamine group;
- chlorinated 2,2,5,5-tetramethyl- imidazolidin-4-one (CTMIO), with an amide and amine halamine group and
- chlorinated 3-dodecyl-5,5-dimethylhydantoin (CDDMH), which has an amide halamine group and a long alkyl chain.

At same active chlorine content, CDMH-nylon 6 fibers proved to be the faster in antimicrobial action, while CDDMH-nylon 6 ones acted much slower, due to the slower reaction rate of chloro-amide group and the inhibition caused by the attached long alkyl chain. The antimicrobial action of electrospun CTMIO-nylon 6 membranes was of similar rate as that of CDDMH-nylon 6 ones.

In another comparative study, cellulose and *m*-aramid fibers, as well as composite cellulose/*m*-aramid fibers, were treated with an *N*-halamine as ionic liquid, namely 1-butyl-3-methyl-imidazolium chloride, in order to achieve biocide activity [115]. Stable and rechargeable composite cellulose/*m*-aramid fibers were prepared by dry-jet wet spinning of a mixed polymer solution. These fibers showed a much higher chlorination level than the pure *m*-aramid fiber and retained their antimicrobial properties for over 50 standard washing cycles.

As general procedure, the antimicrobial activity of functional textiles can be readily recovered by washing them in chlorine aqueous solution. The residual adsorbed (unbounded covalently) chlorine produces an unpleasant odor and discolors fabrics. A reduction step (i.e., with sodium sulfite) [116] may be used to remove the chlorine excess from the fabric surface, which is a convenient approach to overcome this problem.

Regenerable peroxides

Alternate methods for textiles functional finishing employ renewable antimicrobial agents. One example may be *N*-halamines. Another approach is using peroxydic moieties, such as peroxide and peroxyacids, which have been widely used as disinfectants in the food and beverage industries, as well as bleaching agents for textiles and paper [117]. A classic example is the peroxyacetic acid which is well known as a powerful disinfectant used in hospitals [118].

Peroxyacids are converted to carboxylic acid during their biocide action, but can be easily regenerated through the reaction with an oxidant (*e.g.*, hydrogen peroxide) [119], as showed in Figure 20.

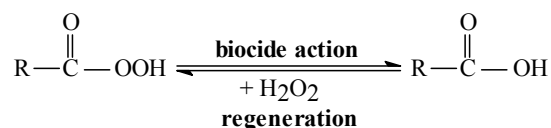


Figure 20. Regeneration reaction of peroxides [119].

As for their mode of action, peroxydic compounds attack the microbe cell membrane, get into the cytoplasm and affect the microorganism enzymes [120].

The formation of peroxyacids on cellulose fibers can be carried out in two steps: (1) grafting/crosslinking polycarboxylic acids (PCAs) onto cellulose, and (2) oxidation of unreacted free acid moieties of cellulose-linked PCAs up to the corresponding peroxyacid units [117]. This reaction (2) may be performed either in an oxygen bleach bath [118] or with strong oxidants, such as sodium perborate [121]. The feasibility of grafting BTCA (butane tetracarboxylic acid) or citric acid onto cotton fabrics by a pad-dry-cure process, similar to cotton durable press, was also investigated [119, 121].

Such functional finishing can be applied not only to cotton (cellulose) fibers, but to polyester fabrics, too [122]. It was proven that peroxyacids bonding to the fabrics was stable over extended periods of storage, whilst their antimicrobial activity appeared to be diminished after several washing and recharging cycles [118, 121].

Conclusions

Antimicrobial functional finishing for textiles intended for biomedical applications is becoming pervasive. Most major fibers and fabrics producers have added antimicrobial products to their product lines. Significant differences still remain in terms of efficacy, kinetics, and durability between various products, but this field is active as more improvements are still necessary.

Biocides are a chemically diverse group of agents. Critical features that govern interactions between microbes and biocides are: the physico-chemical characteristics of the chemical agent, cell morphology, and the microorganism physiology. Antibacterial action includes membrane disruption, macromolecule disfunction, and metabolic inhibition. Disinfection kinetics offer a measure to differentiate between various biocides. The increasingly demand for antimicrobial textiles requires more sophisticated biocidal systems. Modern approaches focus on combinations of various agents able to act synergistically, intracellular biocide delivery through cellular transport processes able to overcome cellular barriers, targeted discharge of biocide.

This paper presented, in a concise manner, only some synthetic agents, their mode of action and some applications, being a part of an extensive study currently in progress. Further papers will review other biocides, such as metals, their oxides and salts (silver, copper, cobalt, etc), metal-organic complexes (*e.g.*, zinc pyrithione), natural antimicrobials (chitosan), plant extracts (essential oils, dyes, germicides). Technological aspects will be also discussed, as well as particular aspects concerning methods of application and durability of these functional finishing treatments of textiles.

References

1. Windler, L.; Height, M.; Nowack, B. Comparative evaluation of antimicrobials for textile applications. *Environment International*, 2013, 53, pp. 62–73.
2. FAO, ICAC. A summary of the world apparel fiber consumption survey 2005–2008. Food and Agriculture Organization of the United Nation; International Cotton Advisory Committee; 2011. FAO and ICAC, 2011.
3. Ristić, T.; Zemljić, L. F.; Novak, M.; Kunčič, M. K.; Sonjak, S.; Cimerman, N. G.; Strnad, S. Antimicrobial efficiency of functionalized cellulose fibers as potential medical textiles. In *Science against microbial pathogens: communicating current research and technological advances*. Vol. 1 FORMATEX “Microbiology Series No. 3”, Badajoz, Spain, 2011, pp. 36-51.
4. Ali, N. F.; El-Mohamedy, R. S. R.; Rajput, S. Improvement of antimicrobial activity for onion natural dyed fabrics through chitosan pretreatment. *Journal of Applied Science Research*, 2013, 9(8), pp. 4993-5002.
5. Gao, Y.; Cranston, R. Recent advances in antimicrobial treatments of textiles. *Textile Research Journal*, 2008, 78(1), pp. 60-72.
6. Hebeish, A. A.; Ali, N. F.; Abd El- Thalouth, J. I. Green strategy for development of antimicrobial printed textile fabrics. *Research Journal of Textile & Apparel*, 2012, 16(1), pp. 77-85.
7. Pavlidou V., New Multifunctional Textiles: Antimicrobial Treatments. In “Proceedings of the Intelligent Textile Structures—Application, Production and Testing International Workshop”, Thessaloniki, Greece 2005, <http://centrum.tul.cz/centrum/itsapt/prezentace/wp2/113105EF.PPT> (accessed May 14-th 2014).

8. Antimicrobial Fabrics Help Fight War Against Germs, Press Release 2004-02-26, <http://www.textilesintelligence.com/til/press.cfm?prid=325> (accessed May 14-th 2014).
9. Bshena, O.; Heunis T. D. J.; Dicks, L. M. T.; Klumperman, B. Antimicrobial fibers: therapeutic possibilities and recent advances. *Future Medical Chemistry*, 2011, 3, pp. 1821–1847.
10. Dastjerdi, R.; Montazer, M. A review on the application of inorganic nano-structured materials in the modification of textiles: Focus on anti-microbial properties. *Colloids and Surfaces B*, 2010, 79, pp. 5-18.
11. Joshi, M.; Wazed, Ali, S.; Purwar, R. Ecofriendly antimicrobial finishing of textiles using bioactive agents based on natural products. *Indian Journal of Fibre & Textile Research*, 2009, 34, pp. 295–304.
12. Sadaf, S.; Saeed, M.; Kalsoom, S. Comparison of treated and untreated cotton fabric with antimicrobial finish. *Science International (Lahore)*, 2012, 24(3), pp. 293-297.
13. Williams, J. F.; Halo Source, V.; Cho, U. Antimicrobial functions for synthetic fibers: Recent developments. *American Association of Textile Chemists and Colorists Review (AATCC Review)*, 2005, 5(4), pp. 17-21.
14. Ye, W.; Xin, J. H.; Li, P.; Lee, K.-L. D.; Kwong, T.-L. Durable antibacterial finish on cotton fabric by using chitosan-based polymeric core-shell particles. *Journal Applied of Polymer Science*, 2006, 102, pp. 1787–1793.
15. Ranganath, A. S. A comparative evaluation of antimicrobial properties and durability to laundering of selected antimicrobial agents on a hospital textile. Ph.D. Thesis, Colorado State University, Colorado, USA, 2011.
16. Simoncic, B.; Tomsic, B. Structures of novel antimicrobial agents for textiles – A review. *Textile Research Journal*, 2013, 80(16), pp. 1721–1737.
17. Schindler, W. D., Hauser, P. J. *Chemical finishing of textiles*. Woodhead Publishing Ltd, Cambridge, 2004, 216 p.
18. Dring, I. Anti-microbial, rotproofing and hygiene finishes. In “Textile Finishing”, Heywood, D. (Ed.), Society of Dyers and Colourists, Bradford, 2003, pp. 351–371.
19. Mahltig, B.; Haufe, H.; Böttcher, H. Functionalization of textiles by inorganic sol-gel coatings. *Journal Materials Chemistry*, 2005, 15(41), pp. 4385–4398.
20. Vigo, T. L. Protection of Textiles from Biological Attack. In “Functional Finishes, Part A, Chemical Processing of Fibres and Fabrics, Handbook of Fiber Science and Technology, Vol. II”, Sello, S. B. (Ed.), Marcel Dekker: New York, 1983, pp. 367–426.
21. Glaser, A. The ubiquitous Triclosan – A common antibacterial agent exposed. *Pesticides and You*, 2004, 24(3), pp. 12-17.
22. Schindler, W. D.; Hauser, P. J. *Chemical finishing of textiles*. Woodhead Publishing Limited, Cambridge, 2004, 176 p.
23. Murguia, M. C.; Machuca, L. M.; Lura, M. C.; Cabrera M. I.; Grau, R. J. Synthesis and properties of novel antifungal gemini compounds derived from N-acetyl diethanolamines. *Journal of Surfactants and Detergents*, 2008, 11, pp. 223–230.
24. Laatiris, A.; El Achouri, M.; Infante, M. R.; Bensouda, Y. Antibacterial activity, structure and CMC relationships of alkanediyl α,ω -bis(dimethylammonium bromide) surfactants. *Microbiological Research*, 2008, 163, pp. 645–650.
25. Massi, L.; Guittard, F.; Levy, R.; Gêribaldi, S. Enhanced activity of fluorinated quaternary ammonium surfactants against *Pseudomonas aeruginosa*. *European Journal of Medicinal Chemistry*, 2009, 44, pp. 1615–1622.
26. Ahlström, B.; Chelminska-Bertilsson, M.; Thompson, R. A.; Edebo, L. Long-chain alkanoylcholines, a new category of soft antimicrobial agents that are enzymatically degradable. *Antimicrobial Agents and Chemotherapy*, 1995, 39(1), pp. 50–55.
27. Tiller, J. C.; Liao, C. J.; Lewis, J.; Klivanov, A.M. Designing surfaces that kill bacteria on contact. *Proceedings. Natl. Acad. Sci. U.S.A.*, 2001, vol. 98, pp. 5981–5985.
28. Ascenzi J. M. *Handbook of disinfectants and antiseptics*, Marcel Dekker: New York, 1996, 300 p.
29. Gilbert, P.; Moore, L. E. Cationic antiseptics: Diversity of action under a common epithet. *Journal of Applied Microbiology*, 2005, 99(4), pp. 703–715.
30. Marini, M.; Bondi, M.; Iseppi, R.; Toselli, M.; Pilati, F. Preparation and antibacterial activity of hybrid materials containing quaternary ammonium salts via sol-gel process. *European Polymer Journal*, 2007, 43(8), pp. 3621–3628.
31. Owusu-Adom K.; Guymon, C. A. Photopolymerization kinetics of poly(acrylate)–clay composites using polymerizable surfactants. *Polymer*, 49(11), 2008, pp. 2636–2643.
32. Caillier, L.; de Givenchy, E.T.; Levy, R.; Vandenberghe, Y.; Gêribaldi, S.; Guittard, F. Synthesis and antimicrobial properties of polymerizable quaternary ammoniums. *European Journal of Medicinal Chemistry*, 2009, 44(8), pp. 3201–3208.
33. Shao, H.; Jiang, L.; Meng, W. D.; Qing, F. L. Synthesis and antimicrobial activity of a perfluoroalkyl-containing quaternary ammonium salt. *Journal of Fluorine Chemistry*, 2003, 124, pp. 89–91.
34. Novak, B. M. Hybrid nanocomposite materials – between inorganic glasses and organic polymers. *Advanced Materials*, 1993, 5(6), pp. 422–433.

35. Judeinstein, P.; Sanchez, C. Hybrid organic–inorganic materials: A land of multidisciplinary. *Journal of Material Chemistry*, 1996, 6(4), pp. 511–525.
36. Nalwa H. S. *Handbook of Organic–Inorganic Hybrid Materials and Nanocomposites*; American Scientific Publisher, Stevenson Ranch, 2003, 382 p.
37. Wang, X.; Wang, C. The antibacterial finish of cotton via sols containing quaternary ammonium salts. *Journal of Sol–Gel Science and Technology*, 2009, 50, pp. 15–21.
38. Isquith, A. J.; Abbott, E. A.; Walters, P. A. Surface-bonded antimicrobial activity of an organosilicon quaternary ammonium chloride. *Applied Microbiology*, 1972, 24, pp. 859–863.
39. Tomšič, B.; Simončič, B. Antimicrobial activity of 3-(trimethoxysilyl)propyldimethyl-alkylammonium chloride. *Tekstilec*, 2005, 48, pp. 79–87.
40. Li, Z.; Lee, D.; Sheng, X.; Cohen, R. E.; Rubner, M. F. Two-level antibacterial coating with both release-killing and contact killing capabilities. *Langmuir*, 2006, 22, pp. 9820–9823.
41. Yu, M.; Gu, G.; Meng, W. D.; Qing, F. L. Superhydrophobic cotton fabric coating based on a complex layer of silica nanoparticles and perfluorooctylated quaternary ammonium silane coupling agent. *Applied Surface Science*, 2007, 253, pp. 3669–3673.
42. Jausovec, D.; Angelescu, D.; Vončina, B.; Nylander, T.; Lindman, B. The antimicrobial reagent role on the degradation of model cellulose film. *Journal of Colloid and Interface Science*, 2008, 327, pp. 75–83.
43. Pant, R. R.; Buckley, J. L.; Fulmer, A. P.; Wynne, J. H.; McCluskey, M. D.; Phillips, J. P. Hybrid siloxane epoxy coatings containing quaternary ammonium moieties. *Journal Applied Polymer Science*, 2008, 110, pp. 3080–3086.
44. Chojnowski, J.; Fortuniak, W.; Rosciszewski, P.; Werel, W.; Lukasiak, J.; Kamysz, W.; Halasa, R. Polysilsesquioxanes and oligosilsesquioxanes substituted by alkylammonium salts as antibacterial biocides. *Journal of Inorganic and Organometallic Polymers Materials*, 2006, 16, pp. 219–230.
45. Majumdar, P.; Lee, E.; Gubbins, N.; Stafslie, S. J.; Daniels, J.; Thorson, C. J.; Chisholm, B. J. Synthesis and antimicrobial activity of quaternary ammonium-functionalized POSS (Q-POSS) and polysiloxane coatings containing Q-POSS. *Polymer*, 2009, 50, pp. 1124–1133.
46. Russell, A. D. Bacterial adaptation and desistance to antiseptics, disinfectants and preservatives is not a new phenomenon. *Journal of Hospital Infection*, 2004, 57, pp. 97–104.
47. A New, Durable Antimicrobial Finish for Textiles, http://microbeshield.com/techdocs/New_Durable_Antimicrobial_Finish_for_Textiles_4A1-F.pdf (accessed June 2007).
48. Majumdar, P.; Lee, E.; Patel, N.; Stafslie, S. J.; Daniels, J.; Chisholm, B. J. Development of environmentally friendly, antifouling coatings based on tethered quaternary ammonium salts in a crosslinked polydimethylsiloxane matrix. *Journal of Coatings and Technology Research*, 2008, 5, pp. 405–417.
49. Mizerska, U.; Fortuniak, W.; Chojnowski, J.; Halasa, R.; Konopacka, A.; Werel, W. Polysiloxane cationic biocides with imidazolium salt (ImS) groups, synthesis and antibacterial properties. *European Polymer Journal*, 2009, 45, pp. 779–787.
50. Ma, M.; Sun, Y.; Sun, G. Antimicrobial cationic dyes. Part 1: Synthesis and characterization. *Dyes and Pigments*, 2003, 58, pp. 27–35.
51. Ma, M.; Sun, G. Antimicrobial cationic dyes. Part 3: Simultaneous dyeing and antimicrobial finishing of acrylic fabrics. *Dyes and Pigments*, 2005, 66, pp. 33–41.
52. Liu, S.; Ma, J.; Zhao, D. Synthesis and characterization of cationic monoazo dyes incorporating quaternary ammonium salts. *Dyes and Pigments*, 2007, 75, pp. 255–262.
53. Zhao, T.; Sun, G.; Song, X. An antimicrobial cationic reactive dye: synthesis and applications on cellulosic fibers. *Journal Applied of Polymer Science*, 2008, 108, pp. 1917–1923.
54. Liu, J.; Sun, G. The synthesis of novel cationic anthraquinone dyes with high potent antimicrobial activity. *Dyes and Pigments*, 2008, 77, pp. 380–386.
55. Liu, J.; Sun, G. The biocidal properties of anthraquininoid dyes. *Dyes and Pigments*, 2009, 81(3), pp. 231–234.
56. Chen C. Z.; Beck-Tan, N. C.; Dhurjati, P.; van Dyk, T. K.; LaRossa, R. A.; Cooper S. L. Quaternary ammonium functionalized Poly(propylene imine) dendrimers as effective antimicrobials: structure activity. *Biomacromolecules*, 2000, 1(3), pp. 473–480.
57. Hummelen J. C.; van Dongen, J. L. J.; Meijer, E. W. Electrospray mass spectroscopy of poly(propylene imine) dendrimers–The issue of dendrimeric purity or polydispersity. *Chemistry – A European Journal*, 1997, 3(9), pp. 1489–1493.
58. Weener J. W.; van Dongen, J. L. J.; Meijer, E. W. Enhanced contrast ratios and rapid switching in electrochromics based on poly(3,4-propylenedioxythiophene) derivatives. *Journal of the American Chemical Society*, 1999, 121(44), pp. 10346–10355.
59. Kim, Y. H.; Sun, G. Durable antimicrobial finishing of nylon fabrics with acid dyes and a quaternary ammonium salt. *Textile Research Journal*, 2001, 71, pp. 318–323.
60. Son, Y. A.; Sun, G. Durable antimicrobial nylon 66 fabrics: Ionic interactions with quaternary ammonium salts. *Journal Applied of Polymer Science*, 2003, 90, pp. 2194–2199.

61. Kim, Y. H.; Sun, G. Functional finishing of acrylic and cationic dyeable fabrics: intermolecular interactions. *Textile Research Journal*, 2002, 72, pp. 1052–1056.
62. Cai, Z. S.; Sun, G. Antimicrobial finishing of acrilan fabrics with cetylpyridinium chloride. *Journal Applied Polymer Science*, 2004, 94, pp. 243–247.
63. Cai, Z. S.; Sun, G. Antimicrobial finishing of acrilan fabrics with cetylpyridinium chloride: Affected properties and structures. *Journal Applied of Polymer Science*, 2005, 97, 1227–1236.
64. Kim, Y. H.; Sun, G. Dye molecules as bridges for functional modifications of nylon: Antimicrobial functions. *Textile Research Journal*, 2000, 70, pp. 728–733.
65. Zhu, P.; Sun, G. Antimicrobial finishing of wool fabrics using quaternary ammonium salts. *Journal Applied Polymer Science*, 2004, 93, pp. 1037–1041.
66. Zhao, T.; Sun, G. Antimicrobial finishing of wool fabrics with quaternary aminopyridinium salts. *Journal Applied Polymer Science*, 2006, 103, pp. 482–486.
67. Diz, M.; Jovic, D.; Infante, M. R.; Erra, P. Reaction of a new thiol cationic surfactant with Bunte salt in wool fibers. *Textile Research Journal*, 1997, 67, pp. 486–493.
68. Diz, M.; Infante, M. R.; Erra, P.; Manresa, A. Antimicrobial activity of wool treated with a new thiol cationic surfactant. *Textile Research Journal*, 2001, 71, pp. 695–700.
69. Son, Y. A.; Kim, B. S.; Ravikumar, K.; Lee, S. G. Imparting durable antimicrobial properties to cotton fabrics using quaternary ammonium salts through 4-aminobenzenesulfonic acid -chloro-triazine adduct. *European Polymer Journal*, 2006, 42, pp. 3059–3067.
70. Isquith, A. J.; Abbott, E. A.; Walters, P. A. Surface bonded antimicrobial activity of organosilicon quaternary ammonium chloride. *Applied Microbiology*, 1973, 25(2), pp. 253–256.
71. Abbott, E. A.; Isquith, A. J. Method of inhibiting the growth of bacteria and fungi using organosilicon amines. USA Patent, 1975, No 3860709.
72. Abbott, E. A.; Isquith, A. J.; Walters, P. A. Algicidal Surfaces. USA Patent, 1975, No. 3865728.
73. Broughton, R. M. Jr.; Worley, S. D.; Cho, U.; Lin J.; Sun G. Incorporation of antimicrobial materials in fabric. *Proceedings of INTC - International Nonwoven and Fibre Industries*, 2001, Baltimore, MD.
74. Vetter, W.; Janussen, D. Halogenated natural products in five species of Antarctic sponges: compounds with POP-like properties? *Environmental Science and Technology*, 2005, 39(11), pp. 3889–3895.
75. Montaña, M.; Gutleb, A. C.; Murk, A. J. Persistent toxic burdens of halogenated phenolic compounds in humans and wildlife. *Environmental Science and Technology*, 2013, 47(12), pp. 6071–6081.
76. Orhan M.; Kut, D.; Gunesoglu, C. Use of triclosan as antibacterial agent in textiles. *Indian Journal of Fibre and Textile Research*, 2007, 32, pp.114–118.
77. Orhan, M., Kut, D.; Gunesoglu, C. Improving the antibacterial activity of cotton fabrics finished with triclosan by the use of 1,2,3,4-butanetetracarboxylic acid and citric acid. *Journal of Applied Polymer Science*, 2009, 111, pp. 1344–1352.
78. Guan, Y.; Qian, L.; Xiao, H. Novel antimicrobial host-guest complexes based on cationic β -cyclodextrin polymers and triclosan/butylparaben. *Macromolecular Rapid Communications*, 2007, 28, pp. 2244–2248.
79. Qian, L.; Guan, Y.; Ziaee, Z.; He, B.; Zheng, A.; Xiao, H. Rendering cellulose fibers antimicrobial using cationic β -cyclodextrin-based polymers included with antibiotics. *Cellulose*, 2009, 16, pp. 309–317.
80. Goetzendorf-Grabowska, B.; Krolkowska, H.; Gadzinowski, M. Polymer microspheres as carriers of antibacterial properties of textiles: A preliminary study. *Fibres and Textiles in Eastern Europe*, 2004, 12, pp. 62–64.
81. Payne, S. A. Antimicrobial superfinish and method of making. USA Patent, 2004, No. 20040077747.
82. Mikolajczyk, T.; Wolowska-Czapnik D. Highly porous polyacrylonitrile fibres with antibacterial and antifungal properties. *Fibres and Textiles in Eastern Europe*, 2002, 10, pp. 18–22.
83. Kalyon, B. D.; Olgun, U. Antimicrobial efficacy of triclosan-incorporated polymers. *American Journal of Infection Control*, 2001, 29, pp. 123–125.
84. Iconomopoulou, S. M.; Andreopoulou, A. K.; Soto, A.; Kallitsis, J. K.; Voyiatzis, G. A. Incorporation of low molecular weight biocides into polystyrene-divinyl benzene beads with controlled release characteristics. *Journal of Controlled Release*, 2005, 102, pp. 223–233.
85. Mao, J. W.; Murphey, L. Durable freshness for textiles. 2001, American Association of Textile Chemists and Colorists Review (AATCC Review), 1, pp. 28–31.
86. Mansfield R. G. Keeping it fresh. *Textile World*, 2002, 152, pp. 42–45.
87. Windler, L.; Height, M.; Nowack, B. Review - Comparative evaluation of antimicrobials for textile applications. *Environment International*, 2013, 53, pp. 62–73.
88. Microban Products Company, <http://www.microban.com> (accessed May 14-th 2014).
89. Veldhoen, N.; Skirrow, R.; Osachoff, H.; Wigmore, H.; Clapson, D.; Gunderson, M.; van Aggelen, G.; Helbing, C. The bactericidal agent triclosan modulates thyroid hormone-associated gene expression and disrupts postembryonic anuran development. *Aquatic Toxicology*, 2006, 80, pp. 217–227.

90. Foran, C. M.; Bennett, E. R.; Benson, W. H. Developmental evaluation of a potential non-steroidal estrogen: triclosan. *Marine Environmental Research*, 2000, 50, pp. 153-156.
91. Bhargava, H. L. P. Triclosan: Applications and safety. *American Journal of Infection Control*, 1996, 24, pp. 209-218.
92. Calafat, A. M.; Ye, X.; Wong, L.-Y.; Reidy, J. A.; Needham, L. L. Urinary concentrations of triclosan in the U.S. population: 2003–2004. *Environmental Health Perspectives*, 2008, 116(3), pp. 303-307.
93. Krebs, F. C.; Miller, S. R.; Ferguson, M. L.; Labib, M.; Rando, R. F.; Wigdahl, B. Polybiguanides, particularly polyethylene hexamethylene biguanide, have activity against human immunodeficiency virus type 1. *Biomedicine and Pharmacotherapy*, 2005, 59, pp. 438–445.
94. Kawabata, A.; Taylor, J. A. The effect of reactive dyes upon the uptake and antibacterial efficacy of poly(hexamethylenebiguanide) on cotton. Part 3: Reduction in the antibacterial efficacy of poly(hexamethylene biguanide) on cotton dyed with bis(monochlorotriazinyl) reactive dyes. *Carbohydrate Polymers*, 2007, 67, pp. 375–389.
95. Mulder, G. D.; Cavorsi, J. P.; Lee, D. K. Polyhexamethylenebiguanide (PHMB): An addendum to current topical antimicrobials. *Wounds*, 2007, 19, pp. 173–182.
96. Moore, K.; Gray, D. Using PHMB antimicrobial to prevent wound infection. *Wounds UK*, 2007, 3, pp. 96–102.
97. de Paula, G. F.; Netto, G. I.; Mattoso, L. H. C. Physical and chemical characterization of poly(hexamethylene biguanide) hydrochloride. *Polymers*, 2011, 3, pp. 928-941.
98. Koburger, T.; Hübner, N.-O.; Braun, M.; Siebert, J.; Kramer, A. Standardized comparison of antiseptic efficacy of triclosan, PVP-iodine, octenidine dihydrochloride, polyhexanide and chlorhexidine digluconate. *Journal of Antimicrobial Chemotherapy*, 2010, 65, pp. 1712–1719.
99. Kaehn, K. Polihexanide: A safe and highly effective biocide. *Skin Pharmacology and Physiology*, 2010, 23(suppl. 1), pp. 7–16.
100. Blackburn, R. S.; Harvey, A. L.; Kettle, L.; Manian, A. P.; Payne, J. D.; Russell, S. J. Sorption of chlorhexidine on cellulose: mechanism of binding and molecular recognition. *Journal of Physical Chemistry, Part B*, 2007, 111, pp. 8775–8784.
101. <http://www.archbiocides.com/Products/Brand/vantocil.htm> (accessed May 14-th 2014).
102. <http://www.archbiocides.com/Splash/purista.htm> (accessed May 14-th 2014).
103. Qian, L.; Sun, G. Durable and regenerable antimicrobial textiles: chlorine transfer among halamine structures. *Industrial and Engineering Chemical Research*, 2005, 44, pp. 852–856.
104. Barnes, K.; Liang, J.; Wu, R.; Worley, S. D.; Lee, J.; Broughton, R. M.; Huang, T. S. Synthesis and antimicrobial applications of 5,50-ethylenebis[5-methyl-3-(3-triethoxysilylpropyl)hydantoin]. *Biomaterials*, 2006, 27, pp. 4825–4830.
105. Lin, J.; Cammarata, V.; Worley, S. D. Infrared characterization of biocidal nylon. *Polymer*, 2001, 42, pp. 7903–7906.
106. Ren, X.; Kocer, H. B.; Kou, L.; Worley, S. D.; Broughton, R.M.; Tzou, Y. M.; Huang, T. S. Antimicrobial polyester. *Journal of Applied Polymer Science*, 2008, 109, pp. 2756–2761.
107. Ren, X.; Kocer, H. B.; Worley, S. D.; Broughton, R. M.; Huang, T. S. Rechargeable biocidal cellulose: synthesis and application of 3-(2,3-dihydroxypropyl)-5,5-dimethylimidazo-lidine-2,4-dione. *Carbohydrate Polymers*, 2009, 75, pp. 683–687.
108. Liang, J.; Chen, Y.; Barnes, K.; Wu, R.; Worley, S. D.; Huang, T. S. N-halamine/quat siloxane copolymers for use in biocidal coatings. *Biomaterials*, 2006, 27, pp. 2495–2501.
109. Lin, J.; Winkelmann, C.; Worley, S. D.; Broughton, R. M.; Williams, J. F. Antimicrobial treatment of nylon. *Journal of Applied Polymer Science*, 2001, 81, pp. 943–947.
110. Lin, J.; Winkelmann, C.; Worley, S. D.; Kim, J. H.; Wei, C. I.; Cho, U. C.; Broughton, R. M.; Santiago, J. I.; Williams, J. F. Biocidal polyester. *Journal of Applied Polymer Science*, 2002, 85, pp. 177–182.
111. Wu, F. C. Regenerable antimicrobial animal fiber materials. USA Patent, 2002, No. 20020123281(2002).
112. Sun, Y. Y.; Sun, G. Novel regenerable N-halamine polymeric biocides. III. Grafting hydantoin-containing monomers onto synthetic fabrics. *Journal of Applied Polymer Science*, 2001, 81, pp. 1517–1525.
113. Sun, Y. Y.; Sun, G. Novel refreshable N-halamine polymeric biocides: Grafting hydantoin-containing monomers onto high performance fibers by a continuous process. *Journal of Applied Polymer Science*, 2003, 88, pp. 1032–1039.
114. Obendorf, S. K.; Sun, G. Development of antimicrobial membrane for protective clothing. NTC Project: C05-CR01. National Textile Center Research Briefs: June 2008. (<http://www.ntcresearch.org/projectapp/?project=C05-CR01>) (accessed May 14-th 2014).
115. Lee, J.; Broughton, R. M.; Worley, S. D.; Huang, T. S. Antimicrobial polymeric materials; cellulose and m-aramid composite fibers. *Journal of Engineered Fibers and Fabrics*, 2007, 2(4), pp. 25-32.
116. Li, S. Method of retaining antimicrobial properties on a halamine-treated textile substrate while simultaneously reducing deleterious odor and skin irritation effects. USA Patent, 2003, No. 6576154.

117. Huang, L. K.; Sun, G. Durable and rechargeable antimicrobial cellulose with peroxy moieties. In the Book of Abstract of the Conference of the Fiber Society, 2004 Fall, Cornell University, Ithaca, NY, USA (www.thefibersociety.org/httpdocs/Assets/Past_Meetings/BooksOfAbstracts/2004_Fall_abstracts.pdf) (accesed May 14-th 2014).
118. Dettenkofer, M.; Block, C. Hospital disinfection: efficacy and safety issues. *Current Opinion in Infectious Diseases*, 2005, 18, pp. 320–325.
119. Huang, L. K.; Sun, G. Durable and regenerable antimicrobial cellulose with oxygen bleach: concept proofing. *American Association of Textile Chemists and Colorists Review (AATCC Review)*, 2003, 3, pp. 17–21.
120. Ramachandran, T.; Rajendrakumar, K.; Rajendran, R. Antimicrobial textiles. An overview. *IE(I) Journal-TX*, 2004, 84, pp. 42-47.
121. Huang, L. K.; Sun, G. Durable and oxygen bleach rechargeable antimicrobial cellulose: sodium perborate as an activating and recharging agent. *Industrial and Engineering Chemical Research*, 2003, 42, pp. 5417–5422.
122. Sun, G.; Huang, L. K. Regenerable antimicrobial polymers and fibers with oxygen bleaches. USA Patent, 2005, No. 6962608.

ACTIVATED CARBONS FROM VEGETAL RAW MATERIALS TO SOLVE ENVIRONMENTAL PROBLEMS

Viktor Mukhin^{a*}, Tudor Lupascu^b, Nadejda Voropaeva^c, Yuriy Spiridonov^d,
Nicolay Bogdanovich^e, Vasiliy Gur'janov^a

^aENPO "Neorganika", 4, K. Marks str., Electrostal 144001, Russian Federation

^bInstitute of Chemistry, Academy of Sciences of Moldova, 3, Academiei str., Chisinau, MD 2028, Republic of Moldova

^cSRI of rapeseed RAAS, 26, Boevoi proezd, Lipetsk, 398037, Russian Federation

^dSRI of phytopathology of RAAS, Bolshie Vyazemy, 143050, Odintsovo district, Moscow Region, Russian Federation

^eNorth Arctic Federal University, 17, North Dvina Quay, Arhangelsk, 163002, Russian Federation

*e-mail: neorg.el@mail.ru

Abstract. Technologies for active carbons obtaining from vegetable byproducts such as straw, nut shells, fruit stones, sawdust, hydrolysis products of corn cobs and sunflower husks have been developed. The physico-chemical characteristics, structural parameters and sorption characteristics of obtained active carbons were determined. The ability of carbonaceous adsorbents for detoxification of soil against pesticides, purification of surface waters and for removal of organic pollutants from wastewaters has been evaluated. The obtained results reveal the effectiveness of their use in a number of environmental technologies.

Keywords: active carbon, vegetal raw byproducts, structural parameters, soil detoxification, water purification.

Introduction

Progressive environmental pollution has made ecological safety an important component of the national security as a whole.

Today, virtually the entire planet and especially the areas where people live are subject to serious environmental threats. The main ones are: radioactive contamination of territories, pollution of soil by acid rain, with chemicals and pesticides, oil spills on land and sea and the destruction of the atmosphere. Pollution of the biosphere dramatically reduces the quality of life and according to World Health Organization (2002), the factors affecting human health depend on: diet and lifestyle - 51 %, the environment - 39%, medicine - 10%.

In view of the above, the special attention should be paid to the environmental safety of the agrarian sector, providing the population with food, as farmland soils on the planet account for only 6% of the total land area, and the number of inhabitants at the end of the XXI century is expected to be 10 billions.

The problems of global environmental pollution were raised earlier by the Russian scientist Professor of MChTI "D. Mendeleev", N.V. Keltsev who offered the main way to solve the situation. He wrote: "At the moment when the question of life and death addresses not only the army, but all mankind, concerned by catastrophic pollution of the biosphere, it is time once again to turn for help to adsorption - one of the most effective methods of protecting the environment from pollution".

Due to their physico-chemical properties, carbonaceous adsorbents (activated carbons) are unique and ideal sorption materials, which allow solving a wide range of issues of chemical and biological safety, environmental and infrastructure issues [1].

Activated carbons (AC) - are highly porous materials obtained in the form of grains or powder of various carbon-based materials having high internal surface (up to 2500 m²/g) and high absorbency towards impurities in the treated media (air, gas, water and other liquids, soil).

Among a wide variety of raw materials for the production of active carbon, in recent years the various vegetal wastes are of particular interest, as a constantly renewable source of raw materials.

In this research the technologies for active carbons production from major tonnage plant wastes: straw, nut shells and fruit stones, sawdust and products of hydrolysis of corn stalks and sunflower husk have been developed. Our research showed the effectiveness of their use in a number of environmental technologies.

Experimental

Activated carbons obtained from straw. In order to obtain active carbons from straw, the wheat straw, oat straw and rapeseed straw have been chosen as raw material. The technique was as follows. The straw was milled, loaded into a steel retort, which was capped and placed in the electric furnace, feeding nitrogen into the vessel to create an inert atmosphere. The retort was heated at a rate of temperature rise 1-20 °C/min to 450-500°C and maintained at the final carbonization temperature for 30-60 min. After completing the process of carbonization the retort was switched to the mode of steam activation at 850-870 °C.

Testing of active carbons from straw. The effectiveness of active carbons for the detoxification of soil from residues of applied herbicide has been evaluated [2]. The experiments were conducted in the laboratory of artificial climate (LAC) of the State Research Institute of Phytopathology RAAS (Golitsino, Moscow region). In order to sowing sunflower test culture, the pots with a capacity of 600 g of soil were used. The samples of soil were contaminated with the Singer herbicide in a dose corresponding to 5 g/ha. The tested active carbons were injected in a dose of 100 kg per 1 ha. After 30 days the average weight of the test plant was evaluated.

Activated carbons obtained from fruit stones. Active carbons from peach and apricot stones were obtained by steam activation method [1], which are proposed for respiratory protection filters.

Activated carbons obtained from sawdust. Activated carbons of brand "Carboline" with a high surface area of 2500 m²/g, iodine adsorption capacity of 200-300 % and methylene blue absorption capacity of 600 mg/g have been obtained from sawdust or lignin by chemical activation method developed in the Northern Arctic Federal University (Arhangelsk).

Testing of active carbon "Carboline". Active carbon "Carboline" in its powder form is an indispensable adsorbent in the treatment of drinking water and waste waters. Laboratory tests were carried out in the laboratory of water purification at the Research Institute "Vodgeo" (Moscow).

Activated carbons obtained from hydrolysis products of corn cobs and sunflower husks. Preparation of activated carbon FAS was as follows: the mixture of furfural with sulfuric acid and active organic additives was performed in a mixer. Its volume was adjusted so that the residence time of the mixture therein didn't exceed the time of its gelation. The partially tarred composition flew by its gravity to a distributor and from its nozzles into a hot oil layer where it fragmented into droplets of the desired diameter depending on the viscosity. Final tarring and thermo set of the product in the reactor occurred in 15-18 seconds. The product separated by centrifugation from the oil, in the form of spherical grains of 2-3 mm, were sent to heat treatment and activation in a rotating electric furnace at a temperature of 850-870 °C.

Standard test methods, including evaluation of ash content [3], bulk density [4], strength to abrasion [2,5], adsorption capacity for iodine and methylene blue (MB) [2,5,6] have been used to characterize obtained activated carbon samples. Total pore volume (V_{Σ}) was determined by adsorption of water [7].

Sorption volume (W_s), micropore (V_{mi}) and mesopore volumes (V_{meso}) have been determined from nitrogen sorption isotherm by using the ASAP 2020 device (Micromeritics, USA) [2,8].

Results and discussion

Activated carbons obtained from straw (activated carbons of brand RAU)

Straw consumption by Russian economy significantly decreased. However, grain production gradually increases, and therefore increases the production of straw (in our country 80-100 million tons of straw accumulate each year only from grains and cereal crops). There is necessary for a rational solution to problems of post-harvest processing of soil and plant waste disposal, as currently they are simply burned or plowed into the ground.

Some physico-chemical characteristics of straw active carbons are presented in the Table 1. All obtained activated carbons are characterized by the development of the total pore volume (V_{Σ}), and a substantial expansion of the volume of sorption space (W_s), wherein the actual volume of micropores (V_{mi}) sized 0.8 nm is up to 0.16-0.20 cm³/g, providing good indexes of the adsorption capacity for iodine and methylene blue (MB).

Table 1

Characteristics of activated carbons obtained from straw.

Raw material	Bulk density, g/dm ³	Ash, wt%	Pore volume, cm ³ /g			Adsorption capacity	
			V_{Σ}	W_s	V_{mi}	Iodine, %	MB, mg/g
Wheat straw	66.5	12.2	3.61	0.73	0.20	64	52
Oat straw	72.5	28.2	3.97	0.44	0.16	50	44
Canola straw	135	16.5	4.17	0.48	0.16	39	87

The results of testing experiments of active carbons for detoxification of soils are shown in Table 2. Obtained results show that the growth inhibition (in comparison with blank control) in the case of the application of active carbons from wheat and oat straw, on soils contaminated by herbicides (using Singer as an example), represent only 4.9%, while in the case of the world- recognized active carbon Grosafe for soil destination, it reaches 12.2%. These results suggest that the effectiveness of active carbons obtained from straw is about 2.5 times higher than of the active carbon Grosafe used for soils detoxification.

Table 2

**Effect of activated carbons on the phytotoxicity of methsulfuron - methyl (Singer, SP)
on the example of sunflower plants (September, 2013).**

Experiment	Average mass, g	% to control
Singer, SP	1.1	73.2
Singer, SP + AC from oat straw	3.9	4.9
Singer, SP + AC from wheat straw	3.9	4.9
Singer, SP + AC from canola straw	3.2	21.9
Singer, SP + AC Grosafe	3.6	12.2
Control (no herbicides)	4.1	-

Activated carbons obtained from nutshells and fruit stones (activated carbons of brand MeKS)

It is known that the best active carbons from nutshells are ones derived from coconut shells. Because this kind of vegetal raw material is missing in Europe, we chose the same type of compacted plant material: stones of peach and apricot - and we obtained active carbon prototypes by steam activation. The physico-chemical and adsorption properties of obtained active carbons from fruit stones in comparison with activated carbons from coconut shells of brand GCN830 (Norit, The Netherlands) are presented in Table 3.

Table 3

Characteristics of activated carbons obtained from coconut shells and fruit stones.

Raw material	Bulk density, g/dm ³	Strength to abrasion, %	Ash, wt%	Pore volume, cm ³ /g		Adsorption capacity	
				V _Σ	V _{mi}	Iodine, %	MB, mg/g
Apricot	395	94.0	4.6	0.89	0.52	111	290
Peach	394	93.6	2.4	0.90	0.50	110	295
Coconut	410	90.3	2.7	0.85	0.57	110	270

As shown in Table 3, activated carbons from fruit stones (within the measurement error - 10%) are on the same level with the activated carbons from coconut shells. This gives us the opportunity to create on their basis individual and collective respiratory protection of filter type, since it is known that the best gas masks are created using activated carbons obtained from coconut shells.

Activated carbons obtained from sawdust (activated carbons of brand "Carboline")

The total volume of wood waste in Russia is around 150 million m³/year, the proportion of sawdust and lignin being not less than 50 million m³/year. The characteristics of the obtained activated carbons (by chemical method of activation) in comparison with industrial analogues are presented in Table 4. As follows from the obtained data, the value of the main quality indicators of "Carboline" is much higher than that for the traditionally used in Russia active carbons OU-A, UAF, in fact by 2-3 times.

Active carbon "Carboline" in its powder form is an indispensable adsorbent in the treatment of drinking water and sewage from organic pollutants. Test results of active carbon "Carboline" for compliance with active carbons used for purification of drinking water are presented in Table 5.

Table 4

Characteristics of activated carbon samples prepared by chemical activation.

Characteristics	"Carboline"	OU-A*	UAF**	World level PHOM200 (UK)
1. Raw material	Sawdust	Birch Coal	Black coal	Coconut shell
2. Adsorption capacity for iodine, %	235	70	70	103
3. Adsorption capacity for MB, mg/g	604	225	190	246
4. Ash content, %	2.3	10.0	11.5	2.6
5. Content of compounds of Fe ³⁺ , %	0.09	0.2	-	0.04
6. Water content, %	0.3	10.0	5.0	5.6
7. Bulk density, g/dm ³	212	-	-	320
8. Fineness (sieve residue 0.1 mm), %	18	5	5	1
9. pH	3	4-6	8-9	9-11

*Activated carbon obtained according to GOST 4453-74;

**Activated carbon obtained according to TS 2162-010-22931414-01.

Table 5

Results of testing “Carboline” activated carbons for compliance with requirements towards active carbons used for purification of drinking water.

No.	Characteristics	Required	Result
1	Adsorption capacity for iodine, mg/g, not less	880.0	1266.0
2	Adsorption capacity for MB, mg/g, not less	220.0	386.0
3	Water content, wt%, not more	10.0	3.9
4	Ash content, wt%, not more	10.0	2.35
5	Water-soluble ash, wt%, not more	2.0	0.5

Given that currently the use of powder forms of activated carbons is increasing on water channels in Russia and the rest of the world, the powdered coal “Carboline” with such high adsorption performance has great application prospects.

Activated carbons obtained from hydrolysis products of corn cobs and sunflower husks (activated carbons of brand FAS)

One of the most promising synthetic materials is furfural - product of primary processing of pentosane-containing plant material, primarily corn cobs and sunflower husks. Due to the availability of raw materials and the high reactivity of furfural, it is one of the most popular products on the world market for the production of a variety of monomeric and polymeric materials. Its presence in the Russian Federation, which has considerable and reproducible reserves of vegetal raw materials for large-scale production of furfural, proves the possibility of using it to develop an industrial technology for producing carbon adsorbents characterized by significantly improved mechanical and adsorptive properties in comparison with well-known brands of activated carbons.

The characteristics of activated carbons FAS of progressive activation are shown in Table 6, in comparison with two commercially available active carbons: (i) based on black coal - F- 400 (Calgon Carbon Corp., USA) and (ii) birch wood BAU-A (JSC “Sorbent”, Russian Federation).

Table 6

Comparative characteristics of the spherical carbonaceous adsorbent FAS with domestic and imported AC.

Sample	Bulk density, g/dm ³	Strength to abrasion, %	Ash, wt%	Pore volume				
				V _Σ , cm ³ /g	V _{mi} , cm ³ /g	cm ³ /cm ³	V _{meso} , cm ³ /g	cm ³ /cm ³
FAS	509	99.7	0.03	0.92	0.45	0.23	0.47	0.24
FAS	436	98.8	0.05	1.09	0.56	0.24	0.53	0.23
FAS	345	98.0	0.08	1.50	0.80	0.28	0.70	0.24
BAU-A	240	37.0	6.0	1.60	0.23	0.07	0.09	0.02
F-400	420	82.0	7.0	0.80	0.32	0.13	0.12	0.05

Outstanding strength and adsorption characteristics of FAS, especially micropore volume per unit volume (cm³/cm³) which are 2-3 times higher than of industrial active carbons, together with almost zero ash content, opens tremendous opportunities for solving problems of protection from atmospheric emissions, hydrosphere, lithosphere and the man himself as the main object of biosphere.

Conclusions

The performed research on the preparation and usage of activated carbons obtained from renewable raw materials reveals the ability of carbonaceous adsorbents for detoxification of soil against pesticides, purification of surface waters and for removal of organic pollutants from wastewaters.

References

1. Mukhin, V.M.; Klushin V.N. Production and use of carbonaceous adsorbents. Moscow: PHTU D.I. Mendeleev, 2012, 305 p. (in Russian).
2. Mukhin, V.M.; Tarasov A.V.; Klushin V.N. Active carbons of Russian Federation. Moscow: Metallurgy, 2000, 352 p. (in Russian).
3. GOST 12596-67 Method for determination of the ash content (in Russian).
4. GOST 16190-70 Method of bulk density determination (in Russian).
5. GOST 4453-74 Wood powder active carbon. Technical specifications (in Russian).
6. GOST 6217-74 Adsorption capacity towards iodine (in Russian).
7. GOST 17219-71 Method for determination of the total pore volume towards water (in Russian).
8. MI 6-16-2795-84 Determination of the effective volume micropore of activated carbons (in Russian).

EURASIAN MINERAL WATER: MATHEMATICAL MODELING, CLASSIFICATION AND ASSESSMENT OF THEIR IMPACT ON THE BIOCHEMICAL COMPOSITION OF HUMAN BLOOD

Nikolay Kornilov^{a*}, Elena Kornilova^b, Elena Stepanenko^a

^aStavropol State Agrarian University, 12, Zootechnicheskii per., Stavropol 355000, Russian Federation,

^bInnovative Company "Stavropol-ARSIO", 384, Lenina str., Stavropol 355006, Russian Federation,

*e-mail: nkornilov@26.ru; phone:(+7 903) 416 88 41; fax: (+7 865) 226 34 49

Abstract. In the article we give the results of comparative analysis of the composition of the Eurasian hydromineral resources and we implement the assessment of their impact on the physiological condition of an organism of the person according to biochemical studies of venous blood. Processing of initial data on the composition and properties of mineral waters chloride-hydrocarbonate, sulphate-hydrocarbonate and chloride-sulphate types and venous blood are made using the method of mathematical modeling, developed by the authors of this article. It is shown that in the balneological impact hydromineral resources on the body hemoglobin and oxygen in the blood increases, glucose decreases, and acid-base pH shifts to high alkalinity.

Keywords: minerals water, blood, modeling, classification.

Introduction

Natural mineral waters are natural resources widely applied in medicine, food industry and a number of other fields of manufacture. The geographical expansion of extraction, bottling and spa applications of medicinal mineral waters and mud, has led to the necessity of a system for monitoring and estimating parameters for: quality, origin, composition and properties of various mineral water and mud.

The biological efficacy of salted - waters systems upon human body is largely dependent on their composition and properties through a mathematical function, usually approximated by statistical methods of the linear regression equation. Nowadays it is important to assess the quality of mineral waters using experimental data of chemical and physico-chemical analysis (total salinity, ionic composition, acid-base balance, conductivity and some other characteristics). Generic requirements for the ionic composition and salinity for the different types of mineral waters given by national standards and data (on separate regional waters) are published in various scientific journals and on Internet sites.

However, until now, the general model of mineral waters' classification has not been developed which allows estimating quantitatively the conformity of regional mineral waters to the reference waters of certain types, groups and classes.

Quoted in the national standards in Russian Federation, CIS and EU tracts of mineral waters are divided into types, groups and subgroups (classes), mostly from the values of total salinity and ionic composition (of salt systems), in certain ranges of concentration, whose boundaries are chosen at random, and that is major disadvantage of existing systems standardization.

The purpose of this work consisted in the establishment of the quantitative dependences connecting composition and properties of the regional Eurasian mineral waters chloride-hydrocarbonate, sulphate-hydrocarbonate and chloride-sulfate type on the basis of a mathematical model developed by us for the classification of mineral waters, using the characteristic parameters calculated from experimental data on the chemical composition of waters [1].

The paper assessed the composition of some mineral waters in Russian Federation, CIS and the EU, the lake brine and squeezed water, medicinal sulphide mud and dark-gray clay sediments underlying dolomite marl, a natural impermeable horizon of salty lakes in Russian Federation and Romania.

The estimated characteristic parameters of the natural waters (Research method)

In order to estimate the applied parameters for water identification, we have been introduced the notions of the "characteristic indicator" of the water and their relation with the chemical composition and total salinity of waters [2].

The phrase "characteristic indicator" refers to those functions of the system, through which, or through whose derivatives, can be expressed in explicit form the composition and mass properties of water-salt systems. In this paper we are talking about Eurasian natural mineral waters of different genesis and metamorphism.

As the initial parameters accepted for the mathematical description of structure of water-salt systems of mineral waters, the following amounts have been entered:

1. \bar{M} - The total mineralization of water, g/dm³.

The value \bar{M} can be calculated from a known parity in chemistry:

$$\bar{M} = M \cdot C_n, \quad (1)$$

where: M - the gram-equivalent of a salt system of mineral water, g/eqv.; C_n – concentration of salts in solution, eqv/dm³.

The value M is calculated from equation (1) and is a function of one variable X_i/X_j .

2. The dependence M of the ratio X_i/X_j presented in the form of the equation:

$$M = a \left(\frac{X_i}{X_j} \right)^b, \quad (2)$$

where: X_i/X_j - the ratio of equivalent fractions anions $X_{Cl^-}/X_{HCO_3^-}$, $X_{SO_4^{2-}}/X_{HCO_3^-}$ and $X_{Cl^-}/X_{SO_4^{2-}}$; a and b - constants.

The value M adopted by us as the first characteristic indicator that has investigated the water of different ionic composition in a certain sequence in magnitude relations X_i/X_j . Characteristic parameter M is a well-defined value of the salt solution and depends on the nature of dissolved salts, the composition and concentration of ions, forming a salt solution.

We have previously shown that the dilution of the solution with a given value of demineralized water does not change its value. Solutions of different concentrations with similar values X_i/X_j belong to the same subgroup (class) of water. Solutions with close relationships X_i/X_j constitute a certain class of mineralized water.

3. The evaluation study of water supplies of a class of mineralized waters was carried out with characteristic indicator φ , calculated from the equation:

$$\varphi = A \left(\frac{X_i}{X_j} \right)^D, \quad (3)$$

where: A and D are the coefficients ($A = a^2 \cdot b$, $D = 2b - 1$).

Characteristic indicator φ can combine mineral water in a separate class of a certain group of mineral waters.

A logarithmic conversation of the equation (3) allows receiving the equation of linear regression for the processing units of the characteristic indicator φ methods of mathematical statistics. In this work the base computer program "Statistics-7" was applied.

Results and discussion

Calculation of characteristic indicator φ of different types of mineral water is made by the equations:

a) chloride-hydrocarbonate type $X_{Cl^-}/X_{HCO_3^-}$ [2]:

$$-\log \varphi \left(\frac{Cl}{HCO} \right) = 2.5807 - 1.1524 \log \left(\frac{X_{Cl^-}}{X_{HCO_3^-}} \right) \quad (4)$$

b) sulphate- hydrocarbonate type $X_{SO_4^{2-}}/X_{HCO_3^-}$ [4]:

$$-\log \varphi \left(\frac{SO_4^{2-}}{HCO_3^-} \right) = 3.3946 - 1.1301 \log \left(\frac{X_{SO_4^{2-}}}{X_{HCO_3^-}} \right) \quad (5)$$

c) chloride-sulfate type $X_{Cl^-}/X_{SO_4^{2-}}$ [5]:

$$-\log \varphi \left(\frac{Cl}{SO_4^{2-}} \right) = 3.3096 - 1.0572 \log \left(\frac{X_{Cl^-}}{X_{SO_4^{2-}}} \right) \quad (6)$$

Table 1

The values of the characteristic indicator φ of the composition of the some regional Eurasian water depending on the total mineralization and ionic composition.

No.	Mineral water, country	The total mineralization of water, \bar{M} , g/dm ³	The ratio X_i/X_j	The value of the characteristic indicator, φ
Chloride-hydrocarbonate type, $X_{Cl^-}/X_{HCO_3^-}$				
1.	Imperial, Spain	3.921	0.471	907
2.	Isti-Su Verkhni, Azerbaijan	6.082	0.614	668
3.	Keiser Friedrich Heilquelle, Germany	4.549	0.635	643
4.	Vesuvio, Italy	2.128	0.666	608
5.	Essentuki No.17, Russian Federation	12.057	0.728	549
6.	Biskirchener Karlsalssprudel, Germany	2.788	0.759	523
Sulphate-hydrocarbonate type, $X_{SO_4^{2-}}/X_{HCO_3^-}$				
1.	Sulphate Narzan, Russian Federation	5.219	0.794	3219
2.	Smirnovskaya, Russian Federation	3.615	0.847	2993
3.	Apenta, Italy	1.847	0.932	2686
4.	Azurra, Italy	0.522	0.935	2676
5.	Ueberkingen, Germany	3.848	0.953	2619
6.	Boario, Italy	0.726	0.996	2492
Chloride-sulfate type, $X_{Cl^-}/X_{SO_4^{2-}}$				
1.	Krakowianka, Poland	2.714	0.460	4617
2.	Feodosiiskaya, Russian Federation	3.957	0.540	3900
3.	Dax, France	0.987	0.575	3651
4.	Slanic-Moldova No. 5, Romania	0.212	0.658	3168
5.	Lysogorskaya, Russian Federation	18.165	0.744	2784
6.	Don, Russian Federation	2.850	0.791	2610

Table 1 shows the calculated values of the characteristic indicator φ .

This article also considers the possibility of applying the method of mathematical modeling and application of the characteristic indicator of the composition of φ for the estimation of the physiological state of the organism according to biochemical analysis of venous blood of patients of the sanatorium "Techirghiol" (Romania), described in the work [3].

In Tables 2 and 3 it is shown some biochemical indices of chemical composition and properties of blood before and after the adoption of balneological procedures, mud treatment of patients of the sanatorium "Techirghiol". Biochemical blood analysis is made with the device CCXS-6.

With the use of the experimental data (Tables 2 and 3) we calculated characteristic indicator of venous blood of patients of the sanatorium "Techirghiol" (Romania) before and after the Spa treatments with mud.

Characteristic indicator of the ion composition of blood φ^* before and after the procedures we calculated by the equation:

1. Original indicator φ^{*o}

$$-\log \varphi^{*o} \left(\frac{Cl^-}{HCO_3^-} \right) = 2.5718 - 1.1506 \log \left(\frac{X_{Cl^-}}{X_{HCO_3^-}} \right) \quad (7)$$

2. The value of characteristic indicator φ^* after procedures:

$$-\log \varphi^* \left(\frac{Cl^-}{HCO_3^-} \right) = 2.5033 - 1.1349 \log \left(\frac{X_{Cl^-}}{X_{HCO_3^-}} \right) \quad (8)$$

In the result of the comparative analysis of composition and properties of Eurasian natural mineral waters using the method of mathematical modeling and introduction of the characteristic indicator of φ we established the quantitative relations linking the evaluation of the integral indicator φ with mineralization and ionic composition of the water of various types and geographical location of the source of mineral water.

Table 2

Biochemical parameters of the chemical composition and properties of human blood before the procedures.							
No. of the patient	Ion concentration, mol/dm ³		pCO ₂ ,	pO ₂ ,	Glucose,	Hemoglobin,	pH
	HCO ₃ ⁻	Cl ⁻	mmHg	mmHg	mg/dL	g/dL	
1.	29.7526	100.755	48.2975	28.4012	180	14.7940	7.3936
2.	25.6601	105.293	44.2954	42.7791	80	13.6072	7.3669
3.	28.7327	105.032	48.4927	40.0465	87	15.0668	7.3767
4.	29.616	104.683	48.4537	33.3757	103	14.3005	7.4210
5.	26.0374	103.585	40.7284	43.7158	93	13.433	7.4097
6.	27.4314	105.802	48.9607	45.7622	98	14.0599	7.3524
7.	29.4035	107.669	47.4241	42.9389	106	14.2744	7.3964
8.	28.8403	108.196	50.3500	25.8367	123	14.4548	7.3620
9.	28.9969	107.348	48.6241	29.2395	122	14.6029	7.3795
10.	26.9461	108.952	40.9163	51.0594	144	14.4133	7.4226
11.	30.0801	107.939	49.0207	29.7467	91	15.2759	7.3919
12.	26.5423	107.551	40.9486	63.0600	132	18.3332	7.4157
13.	29.2089	104.550	43.8950	32.9255	257	13.7067	7.4271

Table 3

Biochemical parameters of the chemical composition and properties of human blood after the procedures.							
No. of the patient	Ion concentration, mol/dm ³		pCO ₂ ,	pO ₂ ,	Glucose,	Hemoglobin,	pH
	HCO ₃ ⁻	Cl ⁻	mmHg	mmHg	mg/dL	g/dL	
1.	32.4535	101.8046	48.7149	39.0512	117	14.7940	7.4618
2.	28.1153	105.3554	45.9244	30.0058	75	14.3457	7.3909
3.	25.9409	108.4871	41.3033	54.2744	84	12.7026	7.4020
4.	30.4505	105.2026	49.6929	38.1093	99	13.8033	7.4342
5.	26.8541	103.667	41.7745	57.4177	77	13.2129	7.4121
6.	29.0077	105.7348	49.5124	55.7568	83	14.0599	7.3718
7.	26.7567	108.6529	39.9790	87.7730	108	14.8729	7.4296
8.	25.1097	109.8214	37.6393	45.4035	81	15.2222	7.4282
9.	29.1084	105.4624	43.0842	27.8902	115	13.4303	7.4337
10.	26.6644	107.7174	36.8411	48.0840	108	14.5825	7.4636
11.	29.5132	107.4811	48.8783	36.4002	107	14.5903	7.3849
12.	26.7005	107.6161	38.7008	64.4981	108	18.4041	7.4428
13.	28.3394	105.4173	43.6908	41.7544	210	13.7601	7.4160

Studies have shown that the characteristic composition indicator of water-salt solutions φ determines the identity of the investigated water to a certain class waters of a group and can be used as the basis of identification of regional water and organization of the system of national monitoring.

Application of methods of mathematical modeling and using of characteristic indicator of φ for research of human body fluids, in particular venous blood has shown an opportunity of application of a method for computer diagnostics of the physiological condition of the human body based on the data of biochemical studies of blood [6].

Conclusions

The evaluation of the composition of the Eurasian mineral waters and human venous blood by using the characteristic indicator φ we can make the following conclusions:

1) we suggested mathematical model of water-salt systems regional water and the comparative assessment of their conformity with the reference groups waters chloride-hydrocarbonate, chloride-sulfate and sulfate-hydrocarbonate type;

2) we determined the correspondence of the ion composition of water-salt systems mineral waters chloride-hydrocarbonate type and human venous blood:

$$-\log \varphi(\text{water}) = 2.5807 - 1.1524 \log \left(\frac{X_{\text{Cl}^-}}{X_{\text{HCO}_3^-}} \right)$$

and

$$-\log \varphi(\text{blood}) = 2.5718 - 1.1506 \log \left(\frac{X_{\text{Cl}^-}}{X_{\text{HCO}_3^-}} \right);$$

3) it is shown that the impact of hydromineral resources and medicinal mud on the human body changes the indicators ionic composition and properties of venous blood: the ratio of chloride and hydrocarbonate ions, acid-base balance, blood oxygenation, the content of hemoglobin, glucose;

4) the characteristic indicator φ allows with a high degree of reliability to conduct computer diagnostics of the physiological state of the human body according to biochemical studies of blood.

Acknowledgements

The authors express their gratitude to PhD of medicine, associate professor of the Ovidius University (Romania) O. Surdu for the opportunity to participate in joint research on impact of hydroresources of Lake Techirghiol on the physiological state of the human body.

References

1. Vasil'tseva, O.N.; Kornilov, N.I.; Kornilova, E.N. Classification of natural chloride-hydrocarbonate mineral waters (mathematical model and principles of formation composition and characteristics); Agrus: Stavropol, 2009, 180 p. (in Russian).
2. Ermolenko, O.N.; Kornilov, N.I.; Kornilova, E.N. Identification of Eurasian mineral sodium chloride-bicarbonate waters. Natural and engineering sciences, 2008, 2, pp. 232-234 (in Russian).
3. Surdu, O. Evaluation of chemical factor of action in sapropelic mud from Techirghiol; Gramar: Bucharest, 2006, 47 p.
4. Kornilov, N.I.; Kudinov, R.A.; Ermolenko, O.N.; Kornilova, E.N. Comparative evaluation of natural sulphate-bicarbonate waters of Russia, CIS countries, Germany and Italy. Symposia volumes: Topical issues Ecology and Nature Management; Agrus: Stavropol, 2005, vol. 1, pp. 394-401 (in Russian).
5. Kornilov, N.I.; Surdu, O.; Kornilova, E.N.; Surdu, T.V. Monitoring of the Eurasian natural chlorides-sulfate water using a mathematical model classification of mineral water. Topical issues Ecology and Nature Management; 3-rd International scientific Conference, Paragraph: Stavropol, 2011, pp. 15-22.
6. Kornilov, N.I.; Kornilova, E.N.; Kudinov, R.A. Classification of water-salt systems physiological fluids of humans and animals. Problems Ecology and Protection Agricultural Plants; Symposia volumes, Agrus: Stavropol, 2006, pp. 25-39.

EVALUATION OF WATER POLLUTION STATUS IN SIRET HYDROGRAPHICAL BASIN (SUCEAVA REGION) DUE TO AGRICULTURAL ACTIVITIES

Carmen Zaharia

*“Gheorghe Asachi” Technical University of Iasi, Faculty of Chemical Engineering and Environmental Protection, Department of Environmental Engineering and Management, 73, Prof. dr. docent D. Mangeron, Iasi 700050, Romania
e-mail: czah@ch.tuiasi.ro or czaharia2003@yahoo.com; phone: (+40 232) 27 86 83 ext 2175; fax: (+40 232) 27 13 11*

Abstract. The study presents data concerning the water pollution status of Siret hydrographical basin (i.e. surface and ground waters, lakes) in Suceava County area (different controlling/monitoring sections) due to agricultural productive activities, especially regarding some quality indicators (nitrogen-based nutrient concentrations) evaluated for 2008. The real water pollution state in Siret hydrographical basin (Suceava region) is estimated by the global pollution index (I^*_{GP}), and corresponds to values of 1.234 - 1.523 for ground waters, 1.330 - 1.550 for surface water, and 1.330 - 1.435 for lakes based on collected data from representative water regulator authority of Siret River hydrographical basin. These values are indicating *an aquatic environment modified by agricultural activities within admissible limits*. The results of simple risk estimation are also summarized, being found minor referring to ammonia, nitrates and nitrites. These data are recommending the necessity of continuous monitoring of water quality in the Siret River hydrographical basin, in all existing control sections, for identification of any pollution episodes, non-reported by polluters to the local environmental regulators.

Keywords: agricultural activity, nutrient quality indicators, global pollution index (I^*_{GP}), real pollution status, Siret River, Suceava County area.

Introduction

Due to increasing environmental quality constraints and necessity of serious and more complicating natural water treatment for different purposes (mainly because presence of more and more diverse and complex polluting species), the control or monitoring of natural water resources in the whole hydrographical basins are becoming more important, together with its global evaluation of pollution status. Why? Because of necessity to sustainably develop and manage the natural water resources in their hydrographical basins [1-4] which is a complex, multidimensional phenomenon (more than triple dimensions - economical, social and environmental [5], in terms of multiple scales, domains and generations), with a breadth and depth that cannot be fully covered by the current portfolio of reductionist-oriented tools, needing at least triple (or multiple)-quantitatively assessment scale tools [6]. Most specialists/observers recognized that sustainability can be achieved not only by simple application of existing environmental laws to new polluting and developing or conservation problems, or by making incremental changes in those laws, but also by preparation of simple or complex/integrated local environmental impact reports for decisions to reduce or avoid impacts whenever feasible, or local responsibility/awareness to limit different emissions, discharges or evacuations in environment, application of good working practices in different domains to reduce and/or control environmental pollution, application of environmental integrated management scheme, local risk assessments and monitoring measures, or others.

Some of important categories of economical activities are those from agricultural field, and in all over the world it is recognized the existence, in some states, of aggressive and/or urban sustainable agriculture systems [7]. The positive and/or negative impact and risk of these agricultural activities to environment pollution, especially natural water resources pollution, must be always considered in condition of fresh water deficit or drought [5]. Moreover, there are significant computational challenges in integrated sustainability assessment (ISA) for design of policies, regulations and business practices for sustainable agricultural development [7]. Thus, there are proposed different types of assessments [6]: (i) a step-wise procedure that links the science with application of integrated sustainability assessment step by step; (ii) assessment based on development of holistic metrics (toolkit), methods and tools in a way that reflects stakeholder values, allowing key decision-makers to identify the most appropriate for their own projects and to combine the results based on their values (framework described by multi-criteria, systems perspective and engagement of relevant stakeholders). The majority of these assessments are based on computational tools, more and more complicated and dependent on level dimensions, domains, generations and interrelationships between them. Therefore, sometimes the certification of some realities in agricultural systems concluded some disagreements between modeled predicted agricultural development and the real agricultural developing system status, and important also it is the fact that environmental domain (environment conservation) is the key issue in proposing developing system with or without financial or social or other kind of supporting domains. This is the reason for why the environmental impact assessment caused by the agricultural development in the studied Romanian region is estimated by the global pollution

index (I^*_{GP}), and also the water quality expressed by a quality index (EQ_w), meaning scientific environmental analysis (e.g., physical, chemical analysis of environmental components).

This is one of the paper targets which are evaluating the whole agricultural activities in 2008 in order to follow the development strategy adopted by the local decision-makers and environmental authorities, considering environmental protection requirements in context of regional agricultural, social and environmental development strategy, precisely sustainable development strategy. Moreover, the water resource management is involving permanent monitoring actions concerning analysis of water quality (i.e. supervision, operational, or investigation monitoring depending of water bodies' importance) in different important hydrological basins of Romanian watercourses (e.g., in Moldova zone: Prut, Siret, Bistrita, etc.) [1-4], together with impact diagnosis against local aquatic environment pollution status due to local economic (agricultural, industrial, commercial, among others) and domestic activities included for sustainable development of investigated Romanian region.

The environmental impact assessment still remains one of the first stages in evaluation of sustainability of strategic development plan/program achieved at individual/mixed levels in a specific region. Therefore, the paper focuses on evaluation some reported data of water regional regulating authority (National Agency 'Romanian Waters' Co. - Siret Waters' Division, in Romanian: A.N. Apele Romane – Directia Apelor Siret) in terms of pollution status of Siret River hydrographical basin in Suceava region (i.e. ground waters - 12 control sections, 52 drilling wells; surface waters - 14 control sections; lakes - 5 control sections), and impact assessment of whole agricultural activities by the global pollution index (average value) in different strategic/control sections/domains for elucidation of real pollution status in the Siret hydrographical basin (Suceava region) towards aquatic life forms (as the most sensible pollution receptors) not abiotic solid media.

Experimental

Siret River Hydrographical Basin: Characterization and Controlling Sections

Siret River (15,157 km length, on Romanian territory) springs from Carpathian mountains of Northern Bucovina (altitude of 1,238 m from the sea level), in Ukraine (679 km length), and is considered as the most important influent of Danube River (nearly Galati town), having an average multiannual flow of about 250 m³/s and as the biggest hydrological basin from Romanian territory [2].

The surface water resources of Siret hydrological basin (Siret H.B.) represent about 17 % of the total volume of water resources of Romania (i.e. 28,116 km², with length of 10,280 km, average density of 0.37 km/km²), and are constituted, in principal, of Siret River and its influents (i.e. *right side*: Siretul Mic, Suceava, Moldova, Bistrita, Trotus, Putna, Buzau, and *left side*: Polocin and Barlad), together with its natural and accumulation lakes (32 lakes, with an useful volume of 1,847.63 mil. m³). The total estimated volume of natural water of Siret H.B. is of 6,868 mil. m³ from which: 5,800 mil. m³ - surface waters, and 1,068 mil. m³ - ground waters, deserving more than 2,500,867 inhabitants (39.6% in urban area) [2, 8].

The water quality of Siret River is periodically monitoring by A.N. Apele Romane Company – Siret Waters Sector, by analysing some groups of quality indicators daily, weekly, or monthly (pH; oxygen regime: dissolved oxygen, COD-Mn/CCO-Cr, BOD₅; mineralization level: fixed residues; nutrients' content: ammonia-NH₄⁺, nitrates-NO₃⁻, nitrites-NO₂⁻, etc.).

The location of control sections from where were periodically sampling water for local or laboratory analysis (PE or glass plastic recipients of 0.5 or 2 dm³ capacity, refrigerated or preserved/conserved samples) are [8-10]: (1) *Siret River - surface water*: 14 control sections organized in areas with significant agricultural activities (i.e. Siret, Mihoveni-Suceava, Vorniceni-Somuzu Mare, Gura Humorului-Moldova, Carlibaba-Bistrita, Dorna, Sadau, Strujinoasa-Putnisoara, Satu Mare-Pozen, Ostra-Brateasa, Stulpicani-Suha, Gainesti-Ciumarni, Crucea-Barnarel, Gura Negri-Neagra); *water lakes*: 5 control sections (i.e. natural lake: Lala, accumulation lakes: Rogojesti, Dragomirna, Bucecea, Solca), and *ground waters*: 12 control sections (i.e. Gramesti, Radauti, Darmanesti, Fantanele, Vicov, Dolhasca, Somuz, Campulung Moldovenesc, Poiana Stampei, Saru Dornei). For appreciation of water quality in 2008, there were mediated the average results registered for seasonal period (at least ten samples collected and analyzed monthly from each control section), these mediated values being considered further for assessment of environmental impact due to agricultural activities.

Materials and Methods

The laboratory analyses of some physical-chemical indicators, which very well-defined the significant impact of agricultural activities such as pH and nitrogen-based nutrients content, were performed according with Romanian standard methods internationally approved (SR ISO and/or SR EN), as well as the reference materials, chemical reagents, and operating parameters for spectrophotometer methodology used [11-12]: pH (SR ISO 10523-97); nitrates-NO₃⁻ (SR ISO 7890-1:1998, SR ISO 7890-2/3:2000), nitrites-NO₂⁻ (SR EN 26777: 2002), ammonia (STAS 6328-85 or SR ISO 7150-1/2001), total nitrogen (SR EN ISO 13395:2002). The values of investigated physical-chemical indicators were given at request by A.N. Apele Romane – Directia Ape Siret, Bacau) [8, 9].

Environmental impact assessment methodology

There were calculated the water quality index, EQ_i (Eq.(1)) [13, 14], and also the evaluation score, ES_i , expressed by marks between 1 and 10 attributed based on evaluation scale presented in Table 1 [16-18].

$$EQ_i = C_{i,measured} / MAC_i \quad (1)$$

where: i – identification of the specific quality indicator; $C_{i,measured}$ – measured/analyzed value of the quality indicator, and MAC_i – maximum admissible concentration of the quality indicator in accordance with the imposed limits of local environmental legislation or local water regulating authority.

Table 1

Correlation scale of quality index (EQ_i) with evaluation score (ES_i) and effects of pollution level on each environmental component (quality index scale) [13, 14].

Evaluation score, ES_i	Quality index, EQ_i	Effects on the aquatic environment and human health
10	0	The aquatic environment is not affected by the agricultural activity. Environment state: natural.
9	0.0-0.2	The aquatic environment is affected by the agricultural activity. The effect cannot be quantified.
8	0.2-0.7	The aquatic environment is affected, but under the maximum admissible limits – level 1. Alert level: potential effects.
7	0.7-1.0	The aquatic environment is affected, but into maximum admissible limits – level 2. Intervention level: potential effects.
6	1.0-2.0	The aquatic environment is affected, over the maximum admissible limits – level 1. The effects are pronounced.
5	2.0-4.0	The aquatic environment is affected, over the maximum admissible limits – level 2. The effects are harmful.
4	4.0-8.0	The aquatic environment is affected, over the maximum admissible limits – level 3. The harmful effects are pronounced.
3	8.0-12.0	Degraded aquatic environment – level 1. The effects are lethal to the average exposure.
2	12.0-20.0	Degraded aquatic environment – level 2. The effects are lethal at short times of exposure.
1	> 20.0	The aquatic environment is improper for life.

The cumulative effect of different nitrogen-based nutrients is expressed by the average arithmetic value (i.e. EQ_{water} or ES_{water}) of all nutrient indicators (EQ_i) or evaluation scores (ES_i). The environmental impact is quantified by the global pollution index (I_{GP}^*) (Eq.2), using the alternative assessment methodology proposed by Popa et al. [14].

$$I_{GP}^* = \frac{S_i}{S_r} = \frac{100 \cdot n}{ES_1 \cdot ES_n + \sum_{i=1}^{n-1} ES_i \cdot ES_{i+1}} = \frac{100}{\overline{ES_w}^2} \quad (2)$$

where: S_i – geometrical surface of non-affected natural state (ideal state of environment, a circle with ray of 10), S_r – geometrical surface of real environment state (real state, a circle with ray of ES_w), n - number of investigated quality indicators, ES_i - the evaluation score corresponding to i quality indicator, $\overline{ES_w}^2$ - average value of all values for $(ES_i)(ES_{i+1})$ ($i= 1, 2, \dots, n-1$) that can finally express the global aquatic environment evaluation score (ES_w) (Figure 1) [13-18].

The correlation between the global pollution index (I_{GP}^*), real state of water in the Siret River hydrographical basin (Suceava region), and real water pollution status is characterized in Table 2 [13-18].

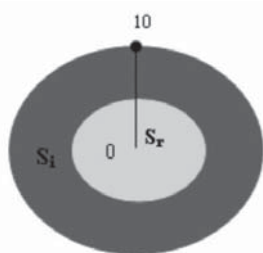


Figure 1. Alternative methodology of global pollution index (I_{GP}^*): graphical representation (S_i - ideal state and S_r - real state) [13-18].

Table 2

Correlation in the alternative methodology of global pollution index [13-22].

I_{GP}^* values	Real pollution status of water (e.g., surface water, ground water, lake)
$I_{GP}^* = 1$	Natural water, unaffected by all agricultural activities
$1 < I_{GP}^* < 2$	Natural water modified by all agricultural activities in admissible limits
$2 \leq I_{GP}^* \leq 3$	Natural water modified by all agricultural activities, with generation of discomfort effects
$3 \leq I_{GP}^* < 4$	Water modified by all agricultural activities, with stress generation against organisms
$4 \leq I_{GP}^* < 6$	Natural water modified by all agricultural activities, dangerous for organisms
$I_{GP}^* \geq 6$	Polluted natural water (degraded), improper for organisms

Results and discussion

The agricultural activities can directly and indirectly (by infiltration) affect the water quality in a hydrographical basin, e.g. Siret River hydrographical basin, in a specific region (e.g., Suceava region). The contamination level must be estimated in order to implement urgent remediation and control measures or environmental risk assessment.

The vulnerable zones to pollution with nitrates from agricultural activities in Siret River H.B. were established after evaluation of 203 localities (towns and villages, total ground of 10,527.33 km²) from (1) Siret Superior (168 locations, 8,165.69 km²) and (2) Siret Inferior (35 locations, 2,361.64 km²), being found **54** perimeters (mainly actual pollution sources, total 50,293 ha, with 33,094 ha of agricultural area) from which: **18** (villages) in Suceava county, 11 (villages) in Iasi county, 15 (villages) in Neamt county, and 10 (villages) in Bacau county.

The natural polluting sources are due to (1) precipitations (nitrogen oxides from atmosphere emitted by a flash of lightning, fuel combustion, or washing of rocks or ashes from uncontrolled vegetation burning etc. and introduced in natural water resources; (2) ammonia nitrification by nitrosomonas and nitrosococcus microorganisms (bacteria) and of nitrites by nitrobacter; (3) spring source as result of in-deep dissolution in rocks or nitrates-containing soil erosion etc.

The diffuse anthropogenic pollution sources with decreasing in-time significance in overall water pollution status (Suceava county area) are consisting of: (1) wrong fertilization (in excess) with fertilizer (chemical commercial products) and manure (natural product) or compost (Table 3) [8, 9]; (2) non respecting of some important rules of portioning and construction of stables and wells; (3) wrong/poor management of stable refuses (directly storage on soil, animal wastes and wastewaters from zootechnical sector, e.g., horned cattle, swine, fowls, sheep, not corresponding treated or untreated); (4) wrong/poor management of rural municipal wastes; (5) infiltrations of wastewaters produced from unstable tight-closing systems or individual toilets, or inexistence of functional rural wastewater collection and treatment systems.

Table 3

Evolution of fertilizers consumption in Suceava county area (2004-2008) [8, 9].

Fertilizer types	Consumption of fertilizers, kg/ha				
	2004	2005	2006	2007	2008
Nitrogen-based	69	70	72	80	51
Phosphorus-based	45	55	59	52	50
Potassium-based	41	6	71	52	40
Total	96	64	69	67	48

The mediated monitoring data in 2008 of Siret River hydrographical basin quality, in vulnerable zones to water pollution by nitrogen-based nutrient contents consisting in 12 control sections were presented in Table 4, and the calculated values of water quality indexes (EQ_i) and estimated values from compliance scale of evaluation scores (ES_i) in Table 5.

The measured/analyzed values of ammonia content in Siret River in Suceava region in all 14 control sections were varied between 0.148 and 0.971 mg/L NH_4^+ , the highest ammonia value being registered at Satu Mare control

section, and the lowest one at Carlibaba, five (i.e. Siret, Mihoveni, Vorniceni, Gura Humorului, and Satu Mare) of all control sections having surpassing the maximum admissible concentration (MAC). Therefore, the Siret River is affected by ammonia from agricultural activities but in admissible limits with potential effects that require measures for alert or intervention level (corresponding to ES_i values of 7-9), but sometimes the effects are pronounced exceeding the admissible limits (values of $ES_i=6$).

Table 4

Mediated/average values of nitrogen-based nutrient content in Siret River H.B. in Suceava county area (2008) in zones with significant agricultural activities (authorized statistic data, A.N. Apele Romane – Siret Waters Division [9]).

No.	Control section (mixing area with influents of Siret River)	Analyzed quality indicators, mg/L					
		NH_4^+		NO_3^-		NO_2^-	
		Measured	MAC	Measured	MAC	Measured	MAC
1	Siret (Siret)	0.729	0.5	2.953	50	0.024	0.5
2	Mihoveni (Suceava)	0.655	0.5	3.159	50	0.033	0.5
3	Vorniceni (Somuzu Mare)	0.604	0.5	2.684	50	0.029	0.5
4	Gura Humorului (Moldova)	0.840	0.5	2.772	50	0.020	0.5
5	Carlibaba (Bistrita)	0.148	0.5	0.639	50	0.014	0.5
6	Dorna (Dorna)	0.257	0.5	1.892	50	0.019	0.5
7	Sadau (Sadau)	0.328	0.5	0.903	50	0.011	0.5
8	Strujinoasa (Putnisoara)	0.242	0.5	0.894	50	0.016	0.5
9	Satu Mare (Pozen)	0.971	0.5	1.758	50	0.018	0.5
10	Ostra (Brateasa)	0.163	0.5	0.627	50	0.022	0.5
11	Stulpicani (Suha)	0.275	0.5	0.583	50	0.017	0.5
12	Gainesti (Ciumarni)	0.169	0.5	0.872	50	0.004	0.5
13	Crucea (Barnarel)	0.231	0.5	0.787	50	0.014	0.5
14	Gura Negri (Neagra)	0.184	0.5	0.469	50	0.008	0.5

For nitrates, in Suceava county area, the mediated values had values between 0.469 and 3.159 mg/L NO_3^- , the highest being registered at Mihoveni, and the lowest at Gura Negri, no surpassing admissible limits; the Siret River is affected by nitrates from agricultural activities, but in admissible limits and the effect cannot be yet quantified ($ES_i=9$).

The mediated values for nitrites are varied between 0.004 and 0.033 mg/L NO_2^- , the highest being registered at Mihoveni and the lowest at Gainesti, no surpassing admissible limits; the Siret River is affected by nitrites from agricultural activities but in admissible limits and the effect cannot be yet quantified ($ES_i=9$).

Table 5

Values of EQ_i and ES_i in Siret River H.B. in Suceava county area (2008) in zones with significant agricultural activities.

No.	Control section (mixing area with influents of Siret River)	Analyzed quality indicators, mg/L					
		NH_4^+		NO_3^-		NO_2^-	
		EQ_i	ES_i	EQ_i	ES_i	EQ_i	ES_i
1	Siret (Siret)	1.458	6	0.059	9	0.048	9
2	Mihoveni (Suceava)	1.31	6	0.063	9	0.066	9
3	Vorniceni (Somuzu Mare)	1.208	6	0.053	9	0.058	9
4	Gura Humorului (Moldova)	1.68	6	0.055	9	0.040	9
5	Carlibaba (Bistrita)	0.296	8	0.012	9	0.028	9
6	Dorna (Dorna)	0.514	8	0.037	9	0.038	9
7	Sadau (Sadau)	0.656	8	0.018	9	0.022	9
8	Strujinoasa (Putnisoara)	0.484	8	0.017	9	0.032	9
9	Satu Mare (Pozen)	1.942	6	0.035	9	0.036	9
10	Ostra (Brateasa)	0.326	8	0.012	9	0.044	9
11	Stulpicani (Suha)	0.56	8	0.011	9	0.034	9
12	Gainesti (Ciumarni)	0.338	8	0.017	9	0.008	9
13	Crucea (Barnarel)	0.462	8	0.015	9	0.028	9
14	Gura Negri (Neagra)	0.368	8	0.009	9	0.016	9

The application of alternative methodology of environmental impact assessment (EIM) by the global pollution index permits estimation of an aquatic environment of Siret River modified by the agricultural activities in admissible limits with I^*_{GP} values of 1.33 or 1.55 (Table 6) according with the collected data of environmental regulator for this zone.

The mediated monitoring data in 2008 of water quality in lakes (5 control sections) from Siret River H.B. concerning the nitrogen-based nutrient content are presented in the Table 7, and the calculated values of water quality indexes (EQ_i) and estimated values from compliance scale of evaluation scores (ES_i) in the Table 8.

Table 6

Values of evaluation scores (ES_i), global pollution indexes (I_{GP}^*) and water pollution status of Siret River H.B. in zones with significant agricultural activities.

Control Sections	\overline{ES}_1^2	ES_i	I_{GP}^*	Control sections	\overline{ES}_1^2	ES_i	I_{GP}^*	Real pollution status
Siret	64.5	8.031	1.550	Strujinoasa	75.166	8.669	1.330	<i>Water (Siret River) quality modified by all agricultural activities in admissible limits</i>
Mihoveni	64.5	8.031	1.550	Satu Mare	64.5	8.031	1.550	
Vorniceni	64.5	8.031	1.550	Ostra	75.166	8.669	1.330	
Gura Humorului	64.5	8.031	1.550	Stulpicani	75.166	8.669	1.330	
Carlibaba	75.166	8.669	1.330	Gainesti	75.166	8.669	1.330	
Dorna	75.166	8.669	1.330	Crucea	75.166	8.669	1.330	
Sadau	75.166	8.669	1.330	Gura Negri	75.166	8.669	1.330	

In Suceava county area, the lakes from Siret River H.B. were evaluated (in 2008) by the authorized regulator (A.N. Apele Romane – Siret Waters Division) as containing ammonia between 0.189 and 0.379 mg/L NH_4^+ (e.g., the highest ammonia value being registered in Rogosesti lake, and the lowest one in Solca lake; no surpassing admissible limits; the lakes are affected by ammonia from agricultural activities but in admissible limits and the effect are pronounced requiring measures for alert or intervention level ($ES_i=7-8$), nitrites between 0.529 and 0.894 mg/L NO_3^- (e.g., the highest nitrites value being registered in Dragomirna lake, and the lowest one in Bucecea lake; no surpassing admissible limits; the lakes are affected by nitrates from agricultural activities but in admissible limits and the effect cannot be yet quantified ($ES_i=9$), and nitrites between 0.010 and 0.019 mg/L NO_2^- (e.g., the highest nitrites value being registered in Dragomirna lake, and the lowest one in Lala lake; no surpassing admissible limits; the lakes are affected by nitrites from agricultural activities but in admissible limits and the effect cannot be yet quantified ($ES_i=9$), respectively.

Table 7

Mediated/average values of nitrogen-based nutrient content in lakes from Siret River H.B. in Suceava county area (2008) around zones with significant agricultural activities (authorized statistic data, A.N. Apele Romane – Siret Waters Division [9]).

No.	Lake	Type	Analyzed quality indicators, mg/L					
			NH_4^+		NO_3^-		NO_2^-	
			Measured	MAC	Measured	MAC	Measured	MAC
1	Lala	natural	0.256	0.5	0.746	50	0.010	0.5
2	Rogojesti	accumulation	0.303	0.5	0.538	50	0.012	0.5
3	Dragomirna	accumulation	0.379	0.5	0.894	50	0.019	0.5
4	Bucecea	accumulation	0.264	0.5	0.529	50	0.011	0.5
5	Solca	accumulation	0.189	0.5	0.629	50	0.017	0.5

Table 8

Values of EQ_i and ES_i in lakes from Siret River H.B. in Suceava county area (2008) around zones with significant agricultural activities.

No.	Lake	Type	Analyzed quality indicators, mg/L					
			NH_4^+		NO_3^-		NO_2^-	
			EQ_i	ES_i	EQ_i	ES_i	EQ_i	ES_i
1	Lala	natural	0.512	8	0.014	9	0.020	9
2	Rogojesti	accumulation	0.606	8	0.010	9	0.024	9
3	Dragomirna	accumulation	0.758	7	0.017	9	0.038	9
4	Bucecea	accumulation	0.528	8	0.010	9	0.022	9
5	Solca	accumulation	0.378	8	0.012	9	0.034	9

The application of alternative methodology of environmental impact assessment by the global pollution index permits estimation of an aquatic environment of lakes in Siret River H.B. modified by the agricultural activities in admissible limits with I_{GP}^* values of 1.33 or 1.435 (Table 9) according with the collected data of water regulator authority (A.N. Apele Romane – Siret Waters Division) for this zone (Suceava county area).

The mediated monitoring data in 2008 (May-August) of ground water quality in 12 control drilling wells from Siret River H.B. (Suceava, Somuz, Moldova, Dorna, Neagra Sarului) concerning the nitrogen-based nutrient content are presented in Table 10, and the calculated values of water quality indexes (EQ_i) and estimated values from compliance scale of evaluation scores (ES_i) in the Table 11.

Table 9

Values of evaluation scores (ES_i), global pollution indexes (I^*_{GP}) and water pollution status of lakes in Siret River H.B. around zones with significant agricultural activities.

Lakes	\overline{ES}_1^2	ES_i	I^*_{GP}	Control sections	\overline{ES}_1^2	ES_i	I^*_{GP}	Real pollution status
Lala	75.166	8.669	1.330	Bucecea	75.166	8.669	1.330	<i>Lakes modified by all agricultural activities in admissible limits</i>
Rogojesti	75.166	8.669	1.330	Solca	75.166	8.669	1.330	
Dragomirna	69.666	8.346	1.435					

In Suceava county area, the ground waters from Siret River H.B. (Suceava county area) were evaluated (in 2008) by the water authorized regulator (A.N. Apele Romane – Siret Waters Division) as containing ammonia between 0.00 and 6.05 mg/L NH_4^+ (e.g., the highest ammonia value being registered in F1 drilling well of Poiana Stampei control section, and the lowest one in Saru Dornei (F2-F5) control section; no surpassing admissible limits; the ground waters are not affected by ammonia from agricultural activities), nitrites between 0.45 and 21.47 mg/L NO_3^- (e.g., the highest nitrites value being registered in Campulung Moldovenesc-Moldova drilling wells, and the lowest one in Dolhasca-Somuz drilling wells; no surpassing admissible limits; the ground waters are not affected by nitrates from agricultural activities), and nitrites between 0.000 and 0.069 mg/L NO_2^- (e.g., the highest nitrites value being registered in Fantanele drilling wells, and the lowest one in Berchisesti-Moldova drilling wells; no surpassing admissible limits; the ground waters are not affected by nitrites from agricultural activities), respectively.

Table 10

Mediated/average values of nitrogen-based nutrient content in ground waters (control drilling wells) from Siret River H.B. in Suceava county area (2008) in zones with significant agricultural activities (authorized statistic data, A.N. Apele Romane – Siret Waters Division [9]).

No.	Control section	Drilling wells no.	Collection data	pH	Analyzed quality indicators, mg/L					
					NH_4^+		NO_3^-		NO_2^-	
					Measured	MAC	Measured	MAC	Measured	MAC
1	Gramesti – Suceava	F3	30.05	7.49	0.15	0.5	1.85	50	0.040	0.5
		F2	08.07	6.83	0.31	0.5	1.91	50	0.044	0.5
		F4	30.05	6.88	0.08	0.5	15.01	50	0.013	0.5
		F5	08.07	6.79	0.25	0.5	8.49	50	0.022	0.5
2	Radauti – Suceava	F6	03.06	7.04	0.11	0.5	0.62	50	0.0016	0.5
		F6	17.11	7.24	0.09	0.5	1.07	50	0.153	0.5
		F7	03.06	7.28	0.09	0.5	5.67	50	0.026	0.5
		F7	17.11	6.91	0.06	0.5	4.00	50	0.025	0.5
		F17	03.06	7.30	0.09	0.5	6.50	50	0.019	0.5
		F17	17.11	7.14	0.03	0.5	5.76	50	0.022	0.5
3	Darmanesti – Suceava	F2	26.05	6.68	0.03	0.5	2.15	50	0.010	0.5
		F2	17.11	7.09	0.31	0.5	0.48	50	0.014	0.5
		F4	26.05	6.69	0.51	0.5	3.47	50	0.010	0.5
		F4	17.11	7.16	0.31	0.5	4.53	50	0.039	0.5
4	Fantanele – Suceava	F6	24.05	7.28	0.17	0.5	0.77	50	0.069	0.5
		F6	15.11	6.80	3.45	0.5	10.52	50	0.022	0.5
		F8	24.05	6.85	0.15	0.5	2.56	50	0.037	0.5
		F8	15.11	6.96	0.92	0.5	1.98	50	0.012	0.5
5	Vicov – Suceava	F4	03.06	7.40	0.09	0.5	0.73	50	0.11	0.5
		F4	17.11	7.46	0.09	0.5	1.82	50	0.019	0.5
		F5	03.06	7.11	0.09	0.5	0.89	50	0.004	0.5
		F5	17.11	7.30	0.01	0.5	6.48	50	0.024	0.5
6	Dolhasca – Somuz	F3	15.07	7.26	0.17	0.5	0.45	50	0.002	0.5
		F3	01.12	7.24	0.29	0.5	5.99	50	0.17	0.5
		F3	01.12	7.13	0.12	0.5	5.79	50	0.007	0.5

Table 10 (Continuation)

No.	Control section	Drilling wells no.	Collection data	pH	Analyzed quality indicators, mg/L					
					NH ₄ ⁺		NO ₃ ⁻		NO ₂ ⁻	
					Measured	MAC	Measured	MAC	Measured	MAC
7	Somuz – Somuz	F2	15.07	7.80	0.19	0.5	12.28	50	0.018	0.5
		F2	01.12	7.11	0.13	0.5	11.16	50	0.004	0.5
		F3	15.07	7.50	0.15	0.5	3.08	50	0.046	0.5
		F3	01.12	7.13	0.12	0.5	5.79	50	0.007	0.5
8	Campulung Moldovenesc – Moldova	F2	31.05	7.93	0.03	0.5	20.94	50	0.015	0.5
		F2	30.11	6.79	0.06	0.5	4.59	50	0.008	0.5
		F3	31.05	7.82	0.05	0.5	21.47	50	0.024	0.5
		F3	30.11	6.76	0.08	0.5	4.33	50	0.019	0.5
9	Berchisesti – Moldova	F3	03.06	7.16	0.10	0.5	8.21	50	0.066	0.5
		F3	30.11	7.33	0.26	0.5	7.12	50	0.000	0.5
		F4	03.06	6.46	0.09	0.5	4.96	50	0.020	0.5
		F7	03.06	6.74	0.08	0.5	11.12	50	0.020	0.5
		F7	30.11	7.27	0.67	0.5	7.71	50	0.000	0.5
10	Bogdanesti – Moldova	F3	21.05	7.58	0.08	0.5	7.71	50	0.003	0.5
		F3	17.11	7.18	0.03	0.5	2.38	50	0.004	0.5
		F4	21.05	7.43	0.09	0.5	3.06	50	0.003	0.5
		F4	17.11	7.18	0.05	0.5	1.79	50	0.009	0.5
11	Poiana Stampei – Dorna	F1	14.09	6.42	0.00	0.5	6.07	50	0.020	0.5
		F1	12.10	6.30	6.05	0.5	0.69	50	0.041	0.5
		F2	14.09	6.21	0.00	0.5	1.38	50	0.006	0.5
		F2	12.10	6.14	0.10	0.5	0.60	50	0.017	0.5
12	Saru Dornei – Neagra Sarului	F2	14.09	6.46	0.00	0.5	1.26	50	0.009	0.5
		F2	12.10	6.28	0.17	0.5	0.60	50	0.011	0.5
		F5	14.09	6.30	0.00	0.5	1.26	50	0.017	0.5
		F3	12.10	6.42	2.93	0.5	1.32	50	0.023	0.5
		F4	14.09	6.11	0.00	0.5	1.20	50	0.012	0.5
		F4	12.10	6.42	0.14	0.5	0.80	50	0.035	0.5

The application of alternative methodology of environmental impact assessment by the global pollution index permits estimation of *an aquatic environment of ground waters from control drilling wells of Siret River H.B. not modified by the agricultural activities* with I^*_{GP} values between 1.234 and 1.523 (Table 12) according with the collected data of authorized water regulator/controller for this zone (Suceava county area).

The results of simple environmental risk estimation ($Risk = Probability \times Gravity$) for these relatively low nitrogen-based nutrients values (ammonia, nitrate and nitrite) indicated minor polluting risk ($Risk \leq 2$).

Table 11

Values of EQ_i and ES_i in ground waters (control drilling wells) from Siret River H.B. in Suceava county area (2008) in zones with significant agricultural activities (authorized statistic data, A.N. Apele Romane – Siret Waters Division [9]).

Analyzed quality indicators, mg/L									
No.	Control section	Drilling wells no.	Collection data	NH ₄ ⁺		NO ₃ ⁻		NO ₂ ⁻	
				<i>EQ_i</i>	<i>ES_i</i>	<i>EQ_i</i>	<i>ES_i</i>	<i>EQ_i</i>	<i>ES_i</i>
1	Gramesti – Suceava	F3	30.05	0.30	8	0.037	9	0.08	9
		F2	08.07	0.62	8	0.038	9	0.088	9
		F4	30.05	0.16	9	0.300	8	0.026	9
		F5	08.07	0.50	8	0.169	9	0.044	9
		Average	0.395	8.25	0.136	8.75	0.059	9	
2	Radauti – Suceava	F6	03.06	0.22	8	0.012	9	0.032	9
		F6	17.11	0.18	9	0.021	9	0.306	8
		F7	03.06	0.18	9	0.113	9	0.052	9
		F7	17.11	0.12	9	0.08	9	0.05	9
		F17	03.06	0.18	9	0.13	9	0.038	9
		F17	17.11	0.06	9	0.115	9	0.044	9
Average			0.157	8.83	0.078	9	0.087	8.83	

Table 11 (Continuation)

No.	Control section	Drilling wells no.	Collection data	Analyzed quality indicators, mg/L					
				NH ₄ ⁺		NO ₃ ⁻		NO ₂ ⁻	
				<i>EQ_i</i>	<i>ES_i</i>	<i>EQ_i</i>	<i>ES_i</i>	<i>EQ_i</i>	<i>ES_i</i>
3	Darmanesti – Suceava	F2	26.05	0.60	8	0.043	9	0.02	9
		F2	17.11	0.62	8	0.009	9	0.028	9
		F4	26.05	1.02	6	0.069	9	0.02	9
		F4	17.11	0.62	8	0.90	9	0.078	9
		Average		0.715	7.50	0.255	9	0.036	9
4	Fantanele – Suceava	F6	24.05	0.34	8	0.015	9	0.138	9
		F6	15.11	6.9	4	0.210	8	0.044	9
		F8	24.05	0.30	8	0.051	9	0.074	9
		F8	15.11	1.84	6	0.039	9	0.024	9
		Average		2.345	6/50	0.078	8.75	0.070	9
5	Vicov – Suceava	F4	03.06	0.18	9	0.014	9	0.022	9
		F4	17.11	0.18	9	0.036	9	0.038	9
		F5	03.06	0.18	9	0.017	9	0.008	9
		F5	17.11	0.02	9	0.129	9	0.048	9
		Average		0.14	9	0.049	9	0.029	9
6	Dolhasca – Somuz	F3	15.07	0.34	8	0.009	9	0.004	9
		F3	01.12	0.58	8	0.199	9	0.034	9
		F4	01.12	1.34	6	0.051	9	0.014	9
		Average		0.753	7.33	0.086	9	0.017	9
7	Somuz – Somuz	F2	15.07	0.38	8	0.245	8	0.036	9
		F2	01.12	0.26	8	0.223	8	0.008	9
		F3	15.07	0.30	8	0.061	9	0.092	9
		F3	01.12	0.24	8	0.115	9	0.014	9
		Average		0.295	8	0.161	8.50	0.037	9
8	Campulung Moldovenesc – Moldova	F2	31.05	0.06	9	0.418	8	0.03	9
		F2	30.11	0.12	9	0.091	9	0.016	9
		F3	31.05	0.10	9	0.429	8	0.048	9
		F3	30.11	0.16	9	0.086	9	0.038	9
		Average		0.11	9	0.256	8.50	0.033	9
9	Berchisesti – Moldova	F3	03.06	0.20	9	0.164	9	0.132	9
		F3	30.11	0.52	8	0.142	9	0	10
		F4	03.06	0.18	9	0.099	9	0.04	9
		F7	03.06	0.16	9	0.222	8	0.04	9
		F7	30.11	0.16	9	0.222	8	0.04	9
		Average		0.48	8.20	0.156	8.80	0.042	9.40
10	Bogdanesti – Moldova	F3	21.05	0.16	9	0.047	9	0.006	9
		F3	17.11	0.06	9	0.061	9	0.08	9
		F4	21.05	0.18	9	0.035	9	0.006	9
		F4	17.11	0.10	9	0.074	9	0.018	9
		Average		0.125	9	0.054	9	0.009	9
11	Poiana Stampei – Dorna	F1	14.09	0	10	0.121	9	0.040	9
		F1	12.10	12.1	2	0.013	9	0.082	9
		F2	14.09	0	10	0.027	9	0.012	9
		F2	12.10	0.20	9	0.012	9	0.034	9
		Average		3.075	7.75	0.043	9	0.042	9
12	Saru Dornei – Neagra Sarului	F2	14.09	0	10	0.025	9	0.018	9
		F2	12.10	0.34	8	0.012	9	0.022	9
		F5	14.09	0	10	0.025	9	0.034	9
		F3	12.10	5.86	4	0.026	9	0.046	9
		F4	14.09	0	10	0.024	9	0.024	9
		F4	12.10	0.28	8	0.016	9	0.07	9
		Average		1.08	8.33	0.021	9	0.035	9

As result of this impact evaluation due to agricultural activities against aquatic environment of Siret River H.B., it is recommended the implementation of preventive protection programme for each agricultural activity and permanent monitoring of nitrogen-based nutrient contents in all existing control sections, for identification of any pollution episodes, non-reported by polluters to the local environmental regulators.

Table 12

Values of evaluation scores (ES_i), global pollution indexes (I_{GP}^*) and water pollution status of ground waters (control drilling wells) from Siret River H.B. in zones with significant agricultural activities.

Control section (drilling wells)	\overline{ES}_1^2	ES_i	I_{GP}^*	Control sections	\overline{E}_1^2	ES_i	I_{GP}^*	Real pollution status
Gramesti – Suceava	75.135	8.668	1.330	Somuz – Somuz	72.291	8.502	1.383	<u>1.234 – 1.523</u>
Radauti – Suceava	78.874	8.886	1.266	Campulung Moldovenesc	78.041	8.834	1.281	
Darmanesti – Suceava	72.375	8.507	1.381	Berchisesti	77.500	9.00	1.234	Ground waters not modified by all agricultural activities
Fantanele – Suceava	65.656	8.102	1.523	Bogdanesti	81.000	9.00	1.234	
Vicov – Suceava	81.00	9.000	1.234	Poiana Stampei	73.760	8.588	1.355	
Dolhasca – Somuz	71.444	8.452	1.399	Saru Dornei	77.054	8.778	1.298	

Conclusions

Some collected data from the authorized water regulator/controller of Siret River hydrographical basin (A.N. Apele Romane în Directia Ape Siret) concerning the nitrogen-based nutrient concentration (*i.e.* ammonia, nitrates, nitrites) are interpreted in terms of environmental impact quantification due to agricultural activities in Suceava county area. In general, the water pollution status of Siret River hydrographical basin in Suceava county area is in admissible limits ($I_{GP}^* < 1.55$), and the risks are minor as illustrated below.

No. eval.	Water type from Siret River H.B. (Suceava county area)	I_{GP}^* values (min – max)	Real pollution status
1	Surface water of Siret River in zone of agricultural polluting sources (14 control sections)	1.330 – 1.550	Surface water modified by agricultural activities in admissible limits
2	Water from lakes in zone of agricultural polluting sources (5 control sections)	1.330 – 1.435	Lakes modified by agricultural activities in admissible limits
3	Ground waters in zone of agricultural pollution sources (12 control sections, 52 drilling wells) (Min – Bogdanesti, Vicov and Max – Fantanele)	1.234 – 1.523	Ground waters modified by agricultural activities in admissible limits

These data indicate the necessity of continuous water monitoring in Siret River hydrographical basin in all investigated control sections for identification of different pollution episodes, non-reported by polluters to the local environmental regulators.

References

- Teodosiu, C.; Cojocariu, C.; Musteret, C.P.; Dascalescu, I.G.; Caraene, I. Assessment of Human and Natural Impacts Over Water Quality in the Prut River Basin, Romania. *Environmental Engineering and Management Journal*, 2010, 8(3), pp. 1439-1450.
- Zaharia, C.; Radu, I. Control Study of Siret River Quality in Pascani County Area and Estimation of Its Pollution Level. *Acta Chemica Iasi*, 2013, 21(2), pp. 119-136. DOI: 10.2478/achi-2013-0011.
- Zaharia, C.; Teslaru, M.I. Control and analysis of some water quality indicators of Bahlui River in Iasi County area (spring season). *The Bulletin of the Polytechnic Institute from Iasi, series: Chemistry and Chemical Engineering Section*, 2012, LVIII(LXII) (2), pp. 69-79.
- Danalache, E.; Zaharia, C. Control of some quality indicators of Prut River in two control sections (Radauti and Darabani) (spring season). *Scientific papers, series: Horticulture*, 2013, 56(2), pp. 531-536.

5. Zaharia, C. The sustainable agricultural development – concepts, principles, eco-efficiency, eco-equity. *Agronomical Research in Moldavia*, 2010, vol. XLIII (143), 3, pp. 91-99.
6. Halog, A.; Manik, Y. Advancing Integrated Systems Modelling Framework for Life Cycle Sustainability Assessment. *Sustainability*, 2011, 3, pp. 469-499. DOI: 10.3390/su3020469.
7. Dernbach, J.C.; Mintz, J.A. Environmental Laws and Sustainability: An Introduction. *Sustainability*, 2011, 3, pp. 531-540. DOI: 10.3390/su3030531.
8. Siret River Monitoring. <http://www.apesiret.usv.ro>
9. Tilica, L. Quality and pollution level assessment in waters of Siret River hydrographical basin, Suceava County. Master Dissertation Thesis, 'Gheorghe Asachi' Technical University of Iasi, Romania, 2013, pp. 49-89 (in Romanian).
10. Zaharia, C. Elements of aquatic environment chemistry. *Performantica*: Iasi, 2011, pp. 45-80 (in Romanian).
11. Surpateanu, M.; Zaharia, C. Environmental chemistry. Manual of practice applications. Rotaprint, Gheorghe Asachi' Technical University Publishing House: Iasi, 1999, pp. 63-92.
12. Surpateanu, M.; Zaharia, C. ABC – Analysis Methods for Control of Environmental Factors. T Press: Iasi, 2002, pp. 63-140.
13. Zaharia, C. Evaluation of environmental impact produced by different economic activities with the global pollution index. *Environmental Science and Pollution Research*, 2012, 19(6), pp. 2448-2455.
14. Popa, C.; Cojocaru, C.; Macoveanu, M. Geometrical correlation method for global estimation of the ecosystem state. *Environmental Engineering and Management Journal*, 2005, 4(4), pp. 437-447.
15. Macoveanu, M. Methods and techniques of ecological impact assessment. *Ecozone*: Iasi, 2nd edition, 2005, pp. 54-88 (in Romanian).
16. Zaharia, C.; Murarasu, I. Environmental impact assessment induced by an industrial unit of basic chemical organic compounds synthesis using the alternative method of global pollution index. *Environmental Engineering and Management Journal*, 2009, 8(1), pp. 107-112.
17. Zaharia, C. Assessing the impact of some industrial and transport activities on soil by the global pollution index. *Environmental Engineering and Management Journal*, 2011, 10(3), pp. 387-391.
18. Mocanu, A.M.; Luca, C.; Odochian, L.; Zaharia, C.; Iordache, C. Assessment of environmental impact of some new aryloxyalkyl carboxylic acid derivatives. *Environmental Engineering and Management Journal*, 2012, 11(2), pp. 413-420.

VALORIZATION OF LOW-COST NATURAL MATERIALS IN DEPOLLUTION PROCESSES OF WASTEWATER

Laura Bulgariu^a, Igor Cretescu^{a*}, Dumitru Bulgariu^{b,c}, Matei Macoveanu^{a*}

^a"Gheorghe Asachi" Technical University of Iasi, Faculty of Chemical Engineering and Environmental Protection,
Department of Environmental Engineering and Management, 71A, D. Mangeron, Iasi 700050, Romania

^b"Alexandru Ioan Cuza" University, Faculty of Geography, Department of Geology, 20A, Carol I str., Iasi 700506, Romania

^cRomanian Academy, Branch of Iasi, Department of Geography, 18A, Carol I str., Iasi 700506, Romania

*e-mail: icre@tuiasi.ro; mmac@ch.tuiasi.ro; phone / fax: (+40 232) 27 17 59

Abstract. The adsorption on non-conventional and low-cost materials for removal of toxic heavy metals and oil products from aqueous media has become important in the last years, because is an efficient and cost-effective alternative compared to traditional chemical and physical remediation, and also other decontamination techniques. The good efficiency, minimization of secondary (chemical or biological) wastes and low cost of adsorbent materials, are only few main advantages of adsorption that can be used for the removal of such pollutants in high volumes of aqueous solutions, being thus more adequate for large scale applications. In this paper, are presented the adsorptive characteristics of a low-cost material that are abundant in our region, namely: Romanian peat moss from Poiana Stampei (Romania), for the removal of different toxic heavy metal ions (Pb(II), Hg(II), Co(II) and Ni(II)) and oil products from aqueous media. The experiments have concerned the influence of several experimental parameters (initial solution pH, adsorbent dose, initial heavy metals concentration, contact time, and temperature) on the heavy metals and oil products removal efficiency. The most important conditions for desorption of heavy metal ions from loaded-materials, required for their regeneration are also presented.

Keywords: heavy metals, oils products, low-cost natural materials, peat moss, wastewater treatment.

Introduction

The industrial effluents usually contain significant amounts of pollutants, such as heavy metals or oil products, which increase the environmental pollution problems and causing the deterioration of aquatic ecosystems. These pollutants are discharged from various industries, such as textile, pigments, storage batteries, plastics, mining, electroplating, metallurgical processes, combustible transportation and storage, etc. [1, 2], and are considered persistent environmental contaminants, because cannot be destroyed and degraded, or these processes occurs in a very long period of time [3]. In addition, due to their toxic effect and accumulation tendency throughout the food chain, the heavy metals and oil pollution represents an important problem with serious ecological and human health consequences. Thus, it is desirable to eliminate these compounds from industrial wastewaters, and this could be also important from economical considerations.

Various kinds of methods are currently used for the treatment of polluted aqueous effluents. In case of heavy metals the most important removal methods are chemical precipitation, flocculation, electrochemical treatment, ion exchange and adsorption [4-6]. In case of oil pollution, the dispersants, booms and skimmers can be used as cleanup methods to destroy or remove the oil slicks from water surface [7-9]. Unfortunately, many of these methods are not economically feasible even for small-scale industries, because require additional reagents or generate secondary wastes that required also a supplementary treatment.

In regards with its simplicity, the retention of pollutants on solid adsorbents is an effective method which can be used for the removal of heavy metals and oil products from wastewaters, in special when the utilized adsorbent is not very expensive [10]. From this perspective, natural materials which are available in large quantities or certain waste products from industrial or agricultural activities may have potential as inexpensive adsorbents. The peat moss is one example of such low-cost adsorbents which can be utilized for the removal of heavy metals and oil products from aqueous effluents [11, 12]. The major reasons that promote the use of peat moss and adsorbent material are: biodegradability, use of renewable resources, waste recycling of life cycle extension, lower cost per unit, lower impact on ecosystem if released or lost during clean-up operations, and public perception that the products are environmental friendly.

In general, peat moss is considered a complex solid material with organic matter in various stages of decomposition, which contains lignin, cellulose and humic substances as major constituents [13, 14]. These constituents, especially lignin, have numerous polar functional groups (ex. alcoholic, phenolic, carboxylic, aldehydic, ketonic, etheric, etc.) which can be involved in the chemical interactions with metal ions. Due to these properties, peat moss tends to have a high cation exchange capacity and is an effective adsorbent for various heavy metals [15-17]. On the other hand, due to these major components with long hydrocarbon chains, the peat moss has an accentuated hydrophobic character, compatible with the structure of oil products, and can be used for the removal of such compounds from aqueous solutions.

In this study, we have investigated the effectiveness of peat moss as adsorbent for the removal of several heavy metals (Pb(II), Hg(II), Co(II), Ni(II)) and oil products from aqueous media. The influence of various experimental parameters (initial solution pH, peat dose, contact time, temperature, viscosity, initial concentration, etc.) was considered. The experiments have been followed: (i) the influence of several experimental parameters on the efficiency of adsorption process, and (ii) conditions for desorption of heavy metal ions from loaded-materials, required for their regeneration. The studied adsorbent showed high efficiency and good selectivity for studied heavy metals and oil products and should be considered for the removal of these pollutants from wastewaters samples.

Experimental

The peat moss used for the adsorption experiments was drawing at 0.5 m depth from Poiana Stampei, Romania. It is of low decomposition degree, with the following characteristics: pH = 4.96 (in water), ash = 5.32 %, total organic carbon = 33.68 %, total oxygen = 14.14 %, total nitrogen = 0.75 %, total phosphorus = 2.34 %. The peat moss samples was dried in air for 6 hours at 70 ± 2 °C, grounded and sieved until the particle dimension was less than 1-2 mm, and then stored in desiccators for the further use.

Stock solutions of heavy metal ions (Pb(II), Hg(II), Co(II) and Ni(II)), containing 10^{-2} mol M(II) L⁻¹ were prepared by dissolving metal nitrate salts in double distilled water. The working solutions were obtained by diluting the stock solutions with double distilled water. Fresh dilutions were prepared and used for each experiment. The initial pH of working solutions was adjusted to required value with 0.1 mol L⁻¹ HNO₃ or NaOH solution, before mixing the adsorbent.

The adsorption experiments were performed for a single component by batch technique, mixing a constant amount of low-cost material (0.125-0.200 g peat moss) with volume of 25 mL of known heavy metals concentration, in 150 mL conical flasks, with intermittent stirring for a required time (usually, 24 hours). The effect of initial solution pH was investigated at room temperature, and constant initial concentration of heavy metal ions, adjusting the pH values between 2.0 and 6.0. This pH interval was chosen for all studied metal ions to remain free M²⁺ species in solution. A series of such conical flasks were intermittently shaken in water bath at three different temperatures, for 3-4 hours, in order to study the effect of temperature on the sorption process efficiency. For kinetic experiments, a constant amount of adsorbent (0.125-0.200 g) was mixed with 25 mL of known heavy metals initial concentration, at various time intervals between 5 and 180 min.

At the end of sorption procedure, the adsorbent was separated through filtration, and the heavy metals concentration in filtrate was determined spectrophotometrically (Digital Spectrophotometer S 104 D, 1 cm glass cell), using a specific method for each heavy metal ion [18].

The adsorption capacity of considered low-cost materials was quantitatively evaluated using the amount of heavy metal retained on weight unit of adsorbent (q , mmol/g) and the percent of heavy metal removed (R , %), calculated with the following equations:

$$q = \frac{(c_0 - c) \cdot (V/1000)}{m} \quad (1)$$

$$R\% = \frac{(c_0 - c)}{c_0} \cdot 100 \quad (2)$$

where: c_0 is the initial concentration of heavy metals solution (mmol/L), c is the equilibrium concentration of heavy metals solution (mmol/L), V is volume of solution (mL), and m is the adsorbent mass (g).

The petroleum-based liquid employed in the sorption tests was Light Fuel Oil (LFO) of regional production provided by PETROM Company (Romania). Three runs of the measurements were made at room temperature of 22 ± 2 °C. The test deals with determination of initial sorption capacity of sorbent as the pick-up ratio. It is expressed as the ratio between amount of oil (g) retained per unit mass of sorbent (g). The initial sorption capacity S (g oil /g sorbent) has been determined by gravimetric method of analysis using a digital balance with resolution of 0.001g and may be written as follows [23]:

$$S = \frac{W_{so} - W_s}{W_s} = \frac{W_o}{W_s} \quad (3)$$

where: W_s means the weight of fresh adsorbent sample (g), W_{so} denotes the weight of adsorbent saturated with oil product (g) and W_o is the weight of oil product retained into adsorbent matrix (g). Note that, under normal conditions, an adsorbent will not be exposed to sufficient oil layer thickness to become completely saturated. Therefore, this test gives the maximum possible sorption capacity data without the competing presence of water.

Results and discussion

Utilization of peat moss as low-cost material for the removal of heavy metals

Generally, the removal of metal ions from aqueous solution by adsorption takes places with maximum efficiency only in well-defined experimental conditions. From this reason, it is important to study the influence of several experimental parameters (such as initial solution pH, adsorbent dose, contact time or temperature) on the adsorption capacity of a given adsorbent.

One of the most important experimental parameter that should be establish is the initial solution pH, because many studies from literature have shown that low-cost materials act as a good adsorbent in a rather narrow pH range [19]. This is because the initial solution pH not only influenced the speciation and solubility of heavy metal ions, but also the dissociation degree of functional groups from adsorbent surface (ex: hydroxyl, carboxyl, carbonyl, amino, etc.), considered as adsorption sites.

In order to explain the influence of this parameter on the adsorption efficiency using peat moss as adsorbent, we must considering the following:

(i) at low pH values (acid media) – most of heavy metals are present as free positively charged cations (M^{n+}), that could interact with negatively charged functional groups from adsorbent surface. But, at low pH values most of functional groups from peat moss surface are un-dissociated or positively charged and cannot interact with metal ions from aqueous solution.

(ii) when pH is increased – the dissociation degree of functional groups from peat moss also increases, these become negatively charged, and will start to binds the positively charged metal ions from aqueous solution. Unfortunately, the increasing of pH determined the increasing of HO^- ions concentration from aqueous solution, and thus the speciation of metal ions can be changed. Experimental studies have been showed that if the pH value of aqueous solution is higher than 8, the hydrolysis of most metal ions occurs, accompanied by the formation of some insoluble aqua-complexes, and this is not desirable during of adsorption process.

In consequence, the increasing of initial solution pH will be done gradually, and the optimum value will correspond to the maximum of adsorption efficiency (Figure 1). For most studied adsorption systems, the maximum adsorption efficiency is obtained at an initial solution pH value of 6.0, and this was considered as optimum value and was used in all further experiments (Table 1).

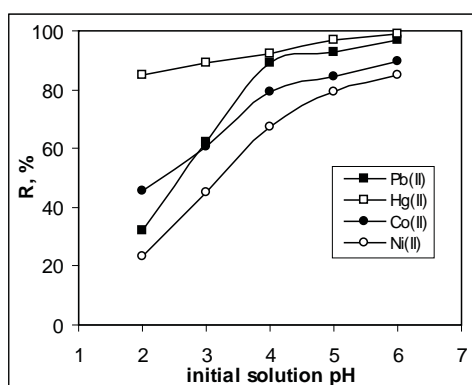


Figure 1. Influence of initial solution pH on the heavy metals adsorption onto peat moss.

Table 1

Optimum experimental conditions for the adsorption of heavy metals onto peat moss [20].

Heavy metal	pH	adsorbent dose (g/L)	Contact time (min)	Temperature (°C)
Pb(II)	6.0	5.0	50	22
Hg(II)	6.0	5.0	50	24
Co(II)	6.0	5.0	55	25
Ni(II)	6.0	5.0	60	25

The adsorbent dose is another important experimental parameter which has a great influence on the sorption process, and determines the potential of adsorbent through the binding sites available to remove heavy metal ions at a specific concentration [21]. By analyzing the dependences obtained in these experiments, it can be established that an

adsorbent dose of 5.0 g/L, can be considered sufficient for the quantitative removal of heavy metal ions from aqueous solutions (Table 1).

The contact time between the two phases required to reach the equilibrium state is also a parameter that should be optimized in adsorption processes of metal ions from aqueous solutions. Unsatisfactory value of this parameter drastically limits the practical use of a given sorption process, even if its efficiency in the heavy metal ions removal is high.

The effect of contact time between solid phase – adsorbent material and aqueous phase – heavy metal ions solution has been investigated at room temperature in considered optimum experimental conditions (initial solution pH, adsorbent dose), for a given value of initial concentration of metal ions. The adsorbents were kept in contact with metal-bearing solution for different period of time (between 5 and 180 min) and the experimental dependences obtained for the adsorption of several heavy metal ions on peat moss are illustrated in Figure 2.

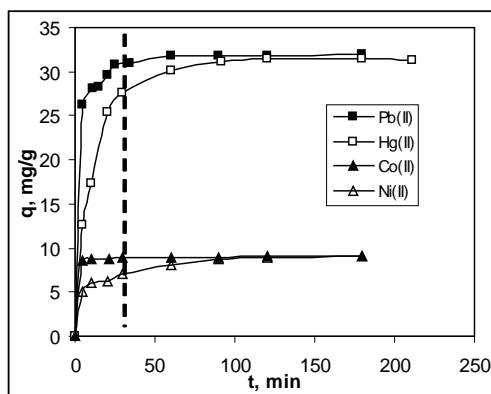


Figure 2. Influence of contact time on the adsorption of heavy metals onto peat moss.

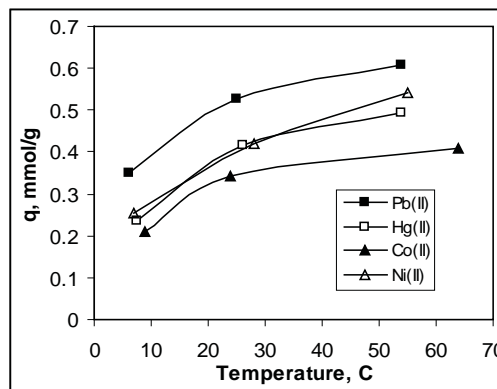


Figure 3. Influence of temperature on the adsorption of heavy metals onto peat moss.

The experimental data presented in Figure 2 indicate that the amount of heavy metal ions retained increase with the increasing of contact time and the sorption process reaches the equilibrium state after approximately 3 hours. The amount of heavy metal ions adsorbed increases sharply during the first 15 – 30 min of the process, when more than 85 % of metal ions were retained. After this initial step the rate of adsorption process becomes slower near to the equilibrium, which is practically obtained after 50-60 min (Table 1). No further significant adsorption is noted beyond 3 hours.

Temperature is also important for the retention of heavy metal ions, because this parameter dealing with the thermodynamics of the sorption process. It is known that temperature is directly related to the kinetic energy of the metal ions and it can account for the diffusion processes [22]. In order to study the effect of temperature, the adsorption experiments have been carried out at 6 – 65 °C, at optimum pH value and adsorbent dose of 5 g/L of peat moss. The equilibrium contact time was maintained between 3 and 4 hours, and the obtained experimental results related to the influence of these parameters are presented in Figure 3.

The results presented in Figure 3, show that the amount of heavy metal retained (q , mmol/g) increases with rise of temperature, during of the equilibrium time; and this effect is even more pronounced as the initial concentration of metal ions from aqueous solutions is higher. These results indicated the endothermic nature of heavy metals sorption on considered adsorbent, and may be due to the strengthening of adsorptive forces between superficial functional groups from peat moss and metal ions from aqueous solution. On the basis of these results, it was recommended that at large scale the removal of heavy metal ions from aqueous solutions by adsorption on peat moss to be performed at ambient temperature, and this is dictated especially from economical considerations.

In order to make the adsorption process more economical, it is necessary to regenerate the loaded-adsorbents. Different concentrations of aqueous solutions of mineral acids were tested in batch conditions for to desorb the heavy metals from loaded-peat moss. The obtained results (Table 2) have indicates that the most of heavy metal ions can be readily eluted with 0.1 mol/L HCl solution, and that a volume of 10 mL acid solution is enough to treat 1 g of loaded-adsorbent.

The adsorbent samples (washed with double distilled water and dried) were reuse in three sorption / desorption cycles, and the loss in the sorption capacity (see Table 2) was less than 8 % for studied heavy metal ions. This means that, peat moss could be repeatedly used in heavy metals retention without detectable losses in their initial sorption capacity. These studies further confirm that the adsorption of heavy metal ions on considered low-cost materials is mostly by

chemical nature, and that the interactions are stronger. The greatest part of the binding is reversible, so an ion exchange mechanism could explain the obtained results and share of other interaction forces is lower.

Table 2

Percent of heavy metals eluted from loaded-adsorbent by using 10^{-1} mol/L HCl solution [20].

Heavy metal	% eluted	% loss
Pb(II)	96.53	5.08
Co(II)	92.81	7.01
Ni(II)	91.24	7.53

Utilization of peat moss as low-cost material for the removal of oil products

The water contaminated with trace of oil products cannot be used as drinking water and in many cases this is not suitable as industrial water or irrigation water. As a consequence of several hazardous accidental oil spills in the previous decades, the interest for investigation of cleanup methods becomes one of the priorities among the directions of the environmental research. The sorption capacities of peat moss for LFO was determined in triplicate according to test, and the results are summarized in Table 3, together with average value and standard deviation data.

Table 3

Initial sorption capacity of peat for LFO, $T = 22 \pm 2$ °C [23].

	Run no.1	Run no.2	Run no.3	Average	Standard deviation
S (g/g)	7.387	7.472	7.878	7.579	0.214

The initial sorption capacity of 7.579 ± 0.214 g/g is given by the properties of sorbent such as porosity and capillaries as well as by the properties of oil product as viscosity, density and surface tension. The adsorption capacity of 7.579 g/g is relatively high suggesting that the retention of liquid phase into adsorbent matrix occurs due to adsorption and capillary phenomena.

The removal of oil products from water surface by sorption was investigated in our previous papers using the design of experiments (DoE) and response surface methodological (RSM) approach [23, 24]. The experimental design used for the modeling of adsorption process was carried out choosing three main factors (design variables), namely: the dosage of adsorbent, drainage time and the initial thickness of oil products on water surface. Since the cleanup process occurs on the top surface of water column it is appropriate to express the adsorbent dosage as amount of adsorbent per unit of surface area. Thus, in this application the adsorbent dosage was expressed as adsorbent amount in (g) per unit of polluted given in (dm^2), M (g/dm^2). The drainage time is given in seconds, t (s).

The application of peat as floating adsorbent for oil products (LFO) removal from water surface was investigated using the design of experiments and response surface methodology. The response surface plots indicate that the removal efficiency is influenced considerably by the adsorbent dosage and the initial thickness of oil slick on water. The optimal solution determined for adsorption process over the region of experimentation is as follows: adsorbent dosage of $4.89 \text{ g}/\text{dm}^2$, drainage time of 12 s and the initial thickness of oil products of 3.9 mm. In such conditions a maximal removal efficiency of 98.74% was obtained experimentally.

Conclusions

Adsorption of heavy metal ions and oil products from aqueous solutions on the low-cost adsorbent materials is a relative simple method that gained credibility in the last years, because it has good efficiency, minimize the obtaining of secondary (chemical or biological) wastes and low cost of these materials. In comparison with other methods, the adsorption on low-cost materials can be used for the removal of heavy metal ions and oil products in much higher volumes of aqueous solutions.

The experimental studies performed in this area have concerned the use of peat moss that is abundant in our region. This adsorbent was tested for the removal of some heavy metal ions (Pb(II), Hg(II), Co(II) and Ni(II)) and oil products, from aqueous media. The experimental results obtained in these studies have shown that: (i) the efficiency of adsorption processes are influenced by several experimental parameters, such as initial solution pH, adsorbent dose, contact time and temperature, and from this reason their study is important in order to found the optimum experimental conditions for to obtain a maximum removal yield; (ii) the heavy metal ions from loaded-adsorbent materials can be easily eluted by using a diluted mineral acids solutions (such as $0.1 \text{ mol}/\text{L}$ HCl solution), after that the regenerated materials can be used in other few adsorption / desorption cycles; (iii) in case of oil products the optimal solution determined for adsorption process is: adsorbent dosage of $4.89 \text{ g}/\text{dm}^2$, drainage time of 12 s and the initial thickness of oil products of 3.9 mm. The main practical drawback of the adsorption method for the removal of heavy metal ions and oil products from aqueous media is that such low-cost adsorbent materials can be used only in batch systems, which has a reduced applicability at industrial scale. The industrial utilization of the adsorption method requires the use of continuous systems. The solving of this problem remains in attention for the further research studies, in order to found some advantageous practical solutions.

References

1. Han, R.; Li, H.Y.; Zhang, J.; Xiao, H.; Shi, J. Biosorption of copper and lead ions by waste beer yeast. *Journal of Hazardous Materials*, 2006, 137, pp. 1569-1576.
2. Lyster, A.; Mody, K.; Jha, B.K. Biosorption of heavy metals by a marine bacterium. *Marine Pollution*, 2005, 50, pp. 175-179.
3. Montazer-Rahmati, M.M.; Rabbani, P.; Abdolali, A.; Keshtkar, A.R. Kinetics and equilibrium studies on biosorption of cadmium, lead, and nickel ions from aqueous solutions by intact and chemically modified brown algae. *Journal of Hazardous Materials*, 2011, 185, pp. 401-407.
4. Febrianto, J.; Kosasih, A.N.; Sunarso, J.; Ju, Y.H.; Indrawati, N.; Ismadji, S. Equilibrium and kinetic studies in adsorption of heavy metals using biosorbent: A summary of recent studies. *Journal of Hazardous Materials*, 2009, 162, pp. 616-645.
5. Kumar, Y.P.; King, P.; Prasad, V.S.R.K. Adsorption of zinc from aqueous solution using marine green algae-*Ulva fasciata* sp. *Chemical Engineering Journal*, 2007, 129, pp. 161-166.
6. Llanos, J.; Williams, P.M.; Cheng, S.; Rogers, D.; Wright, C.; Perez, A.; Canizares, P. Characterization of a ceramic ultrafiltration membrane in different operational states after its use in a heavy-metal ion removal process. *Water Research*, 2010, 44, pp. 3522-3530.
7. Cojocaru, C.; Macoveanu, M.; Cretescu, I. Peat-based sorbents for the removal of oil spills from water surface: Application of artificial neural network modeling. *Colloids and Surfaces A-Physicochemical and Engineering Aspects*, 2011, 384(1-3), pp. 675-684.
8. Wei, Q.F.; Mather, R.R.; Fotheringham, A.F.; Yang, R.D. Evaluation of nonwoven polypropylene oil sorbents in marine oil-spill recovery. *Marine Pollution Bulletin*, 2003, 46, pp. 780-783.
9. Annunziato, T.R.; Sydenstricker, T.H.D.; Amico, S.C. Experimental investigation of various vegetable fibers as sorbent materials for oil spills. *Marine Pollution Bulletin*, 2005, 50, pp. 1340-1346.
10. Babel, S.; Krniavan, T.A. Low cost adsorbents for the heavy metals uptake from contaminated water: a review. *Journal of Hazardous Materials*, 2003, B 97, pp. 219 - 243.
11. Coupal, B.; Spiff, A.I. The treatment of waste waters with peat moss. *Water Research*, 1999, 33(2), pp. 1071 - 1076.
12. Gogate, P.R.; Pandit, A.B. A review of imperative technologies for wastewater treatment II: hybrid methods. *Advanced Environmental Research*, 2004, 8, pp. 553 - 597.
13. Couillard, D. The use of peat in waste treatment. *Water Research*, 1994, 28(6), pp. 1261-1274.
14. Brown, P.A.; Gill, S.A.; Allen, S.J. Metal removal from waste waters using peat. *Water Research*, 2000, 34, pp. 3907-3916.
15. Bulgariu, L.; Cojocaru, C.; Robu, B.; Macoveanu, M. Equilibrium isotherms studies for the sorption of lead ions from aqua solutions using Romanian peat sorbent. *Environmental Engineering and Management Journal*, 2007, 6(5), pp. 425- 430.
16. Bulgariu, L.; Bulgariu, D.; Macoveanu, M. Kinetics and equilibrium study of nickel (II) removal using peat moss. *Environmental Engineering and Management Journal*, 2010, 9(5), pp. 659-666.
17. Bulgariu, L.; Ratoi, M.; Bulgariu, D.; Macoveanu, M. Adsorption potential of mercury (II) from aqueous solutions onto Romanian peat moss. *Journal of Environmental Science and Health, Part A*, 2009, 44, pp. 700-706.
18. Dean, J.A. *Analytical Chemistry Handbook*, 3rd Edition; McGraw-Hill Inc.: New York, 1995, 537 p.
19. Marques, P.A.S.S.; Rosa, M.F.; Pinheiro, H.M. pH effects on the removal of Cu^{+2} , Cd^{2+} and Pb^{2+} from aqueous solution by waste brewery biomass. *Bioprocess Engineering*, 2000, 23, pp. 135-141.
20. Bulgariu, L.; Bulgariu, D., Chapter 8: Removal of toxic heavy metals from aqueous media by sorption on low-cost materials, In: *Current topics, concepts and research priorities in environmental chemistry (II)*, Editor Carmen Zaharia; Alexandru Ioan Cuza University: Iasi, 2013, 153 p.
21. Aydin, H.; Bulut, Y.; Yerlikaya, C. Removal of copper (II) from aqueous solution by adsorption onto low-cost adsorbents. *Journal of Environmental Management*, 2008, 87, pp. 37-45.
22. Farooq, U.; Kozinski, J.A.; Khan, M.A.; Athar, M. Biosorption of heavy metal ions using wheat based biosorbents – A review of the recent literature. *Bioresource Technology*, 2010, 101, pp. 5043-5053.
23. Cojocaru, C.; Macoveanu, M.; Cretescu, I. Application of low-cost sorbent for oil spill sorption using response surface methodological approach, in *NATO Advanced Research Workshop on Role of Ecological Chemistry in Pollution Research and Sustainable Development*, Editor: A.M. Bahadir, Gh. Duca; Springer: Berlin, 2009, 109 p.
24. Cojocaru, C.; Cretu, V.C.; Preda, C.; Macoveanu, M.; Cretescu, I. Response surface methodology applied for investigation of diesel oil spill removal from water surface using textile sorbents. *Journal of Environmental Protection and Ecology*, 2010, 11(2), pp. 643-653.

QUANTIFICATION AND BIOREMEDIATION OF ENVIRONMENTAL SAMPLES BY DEVELOPING A NOVEL AND EFFICIENT METHOD

Mohammad Osama^{a*}, Felicia Armstrong^a, Peter Norris^b, Habiba Tahira Hussain^c

^aDepartment of Geological and Environmental Sciences, Youngstown State University, Ohio 44555, US

^bDepartment of Chemistry, Youngstown State University, Ohio 44555, US

^cDepartment of Microbiology, Jawaharlal Nehru Medical College and Hospital,
Aligarh Muslim University, Aligarh 202002, India

*e-mail: osama.alig@gmail.com

Abstract. *Pleurotus ostreatus*, a white rot fungus, is capable of bioremediating a wide range of organic contaminants including Polycyclic Aromatic Hydrocarbons (PAHs). Ergosterol is produced by living fungal biomass and used as a measure of fungal biomass. The first part of this work deals with the extraction and quantification of PAHs from contaminated sediments by Lipid Extraction Method (LEM). The second part consists of the development of a novel extraction method, Ergosterol Extraction Method (EEM), quantification and bioremediation. The novelty of this method is the simultaneous extraction and quantification of two different types of compounds, sterol (ergosterol) and PAHs and is more efficient than LEM. EEM has been successful in extracting ergosterol from the fungus grown on barley in the concentration range of 17.5-39.94 $\mu\text{g g}^{-1}$ ergosterol and the PAHs are much more quantified in numbers and amounts as compared to LEM. In addition, cholesterol usually found in animals, has also been detected in the fungus, *P. ostreatus* at easily detectable levels, which is a noteworthy point.

Keywords: ergosterol, cholesterol, gas chromatography-mass spectrometry (GC-MS), sediments, polycyclic aromatic hydrocarbons (PAHs), ergosterol extraction method.

Introduction

Mahoning River History

Contamination of soils, sediments, ground water and air with toxic materials has become a major concern today. The Mahoning River has received industrial waste since early 1900's from the steel industry. The lower branch of the Mahoning River starts at Winona, Ohio, extending towards Leavittsburg, and continues to south-east through Girard, Youngstown, Struthers and Lowellville into Pennsylvania. The Mahoning River joins with the Shenango River to form the Beaver River, which empties into the Ohio River. It was significantly altered by the construction of numerous large reservoirs and low-head dams. The dams were constructed to provide a reservoir of cooling waters for the hot steel and machinery in the steel industries that used the river as an 'industrial sewer' [1]. The sediment remained highly contaminated with PAHs and PCBs because of their tendency to bind to the sediment particles and their low solubility rates. When contaminants are introduced into aquatic environments, the sediments serve as a repository for the majority of these chemicals [2].

Polycyclic Aromatic Hydrocarbons

Polycyclic aromatic hydrocarbons (PAHs) are widespread contaminants in the environment and their fates in nature are of great environmental concern due to their potential toxicity, mutagenicity, teratogenicity and carcinogenicity [3,4]. Polycyclic aromatic hydrocarbons constitute a large and diverse class of organic compounds and are generally described as molecules which consist of two or more fused aromatic rings in various structural configurations [5]. The sources of PAHs include (i) mobile sources (e.g. cars, buses, trucks, ships and aircraft), (ii) industrial sources (e.g. power generation, steelworks, coke ovens, aluminium production, cement kilns, oil refining and waste incineration), (iii) domestic sources (e.g. combustion for heating and cooking especially solid fuel heaters using wood and coal), (iv) fires and smoke resulting from the burning of vegetation in agricultural processes, bushfires, grilling of food, or tobacco smoke [6-9]. Current research focuses on the effects of microbial biodegradation of PAHs composed of more than three rings. PAHs with more than three rings are often referred to as high-molecular-weight (HMW) PAHs [7,9]. Leaking storage containers on hazardous waste sites can release concentrated PAHs into soil and water making them especially dangerous to nursing infants living near hazardous waste sites [5,9]. PAH molecule stability and hydrophobicity are two primary factors which contribute to the persistence of HMW PAHs in the environment. Due to their lipophilic nature, PAHs have a high potential for biomagnifications through trophic transfers. Soil and sediment PAHs concentrations at contaminated and uncontaminated sites ranging from 1 $\mu\text{g kg}^{-1}$ to over 300 g kg^{-1} , have been reported [3,9]. A few PAHs are used in medicines, dyes, plastics, pesticides and road construction [3]. The potentially deleterious effects of PAHs on human health and their microbial biodegradation in the environmental system have prompted us to undertake this project. The very first goal of this research is to extract and measure the biodegradation of polycyclic aromatic hydrocarbons for the various samples collected from the sediments of Mahoning River using GC-MS by a Lipid Extraction procedure. A

new method is developed, the Ergosterol Extraction Method, with the aim that it should be useful in the extraction of both PAHs as well as ergosterol. The importance of this study is to discover the bioremediation potentiality of *Pleurotus ostreatus*, a white rot fungus in wet, unique, historically contaminated river sediment. It is inoculated in the contaminated sediments of Mahoning River with subsequent analysis of the effect of ergosterol as an indicator for fungal biomass. In the wider sense the main objectives of this research can be outlined as (i) to develop a single extraction method, Ergosterol extraction Method (EEM), that should be useful in the extraction of both PAHs as well as ergosterol using GC-MS, (ii) to compare the two methods for the extraction of PAHs and analyze which one gives the most productive results, and (iii) analyze the extracted ergosterol by GC-MS so that we can detect the degradation of PAHs at different time intervals by *Pleurotus ostreatus* from the sediments of Mahoning River.

Bioremediation by White Rot fungi (*Pleurotus ostreatus*)

Bioremediation is a managed or spontaneous technique where microbiological processes (bacteria, fungi) are used to degrade or transform contaminants to less toxic or nontoxic forms. Low molecular weight PAHs are usually readily degraded, but high molecular weight PAHs of five or more rings resist extensive bacterial degradation in soil and sediments [10]. Fungi might offer some advantages over bacteria for remediation due to their rapid colonization of substrates and high tolerance of the toxin [11]. These fungi display an extracellular degradation system that is capable of cleaving lignin.

Steroids

Sterols are essential structural and regulatory components of eukaryotic cell membranes. Ergosterol, the end product of the biosynthetic pathways and the main sterol in yeast and other fungi, is responsible for structural membrane features, such as fluidity and permeability similar to the way cholesterol is in mammalian cells [12]. Ergosterol is considered as the principal sterol of fungi and it plays an important role as a cell membrane component. Therefore, it has been proposed as a global indicator of mycological quality of foods and feeds.

Experimental

Standard of chemical compounds used was performed as 10.0, 20.0, 30.0, 40.0, and 50.0 µg/mL concentrations of the PAH mix, 20 µL of internal standard, and 50 µL of surrogate solution were added and the volume adjusted to 1.0 mL with hexane.

Part 1: Biodegradation of PAHs

Sample Collection

Sediment samples were collected from the shoreline of the Mahoning River in Lowellville, Ohio and stored at 4°C until use. Each sediment sample was analyzed for PAHs content using both lipid extraction and ergosterol extraction techniques to track the extraction efficiencies.

Fungal Growth

The white-rot culture was grown by on white-rot selective potato dextrose agar (PDA) plates [20]. The inoculated selective plates were placed in incubators at 25 °C for 72-120 h. Cores of the plates were taken and placed into sterile 250 mL Erlenmeyer flasks containing 125 mL of Potato Dextrose broth (Sigma). Broths were placed on a shaker at 250 rpm for 48-72 h at room temperature. After growth of inocula in 125mL of Potato Dextrose broth, 500 mL of grain was placed into spawn bag (Fungi Perfecti LLC) with 150 mL of deionized water. The spawn bag containing the grain and water mixture was sealed using an impulse sealer and autoclaved at 121 °C. Once autoclaved, the spawn bag was then inoculated with 125 mL of the Potato Dextrose broth containing the *P. ostreatus* inocula. Spawn bags were then placed in a 25 °C incubator for 72-120 h.

Sediment Incubation Set-up

One litre of the PAH contaminated Mahoning River sediment was transferred into 2 L glass containers ("fish bowls"). Eight experimental treatments were tested in triplicate in the laboratory during a 6 weeks period. The first treatment contained only sediment which was used as control. Treatment sediment was amended with sawdust (60% by volume), augmented with *Pleurotus ostreatus* (10% by volume) in the treatments and 10% by volume of inoculated grain was added to each bowl (containing sediment samples) as substrates for fungal growth. The second treatment (by volume) was 30% sediment with 60% sawdust augmented with *Pleurotus ostreatus* (10% by volume) and 10% of the inoculated grain as substrates for fungal growth was added to each bowl. To the treatments with sawdust (which provides carbon and nutrients to fungi), fungi (*Pleurotus ostreatus*) and additional nitrogen source (10% by volume) was added to stimulate fungal growth. A treatment free sediment sample was taken as control. The nitrogen sources included spawnmate, urea, peptone and tryptophan. Contents of the bowl were mixed to create a homogenous mixture. A glass petri dish filled with sterile water was suspended inside the glass bowl to keep the moisture content constant.

Incubation bowls were covered first with plastic wrap then aluminium foil and placed in an incubator at 25 °C. Initially, seven treatments were tested at time zero in July 2008. PAH extractions were done from these samples as a test of the lipid extraction method. The first controls contained sediment, saw dust (600 mL), grain (100 mL) and fungi (100 mL). In October 2008, eight more treatments were prepared and PAH extractions of each treatment were done at two different times: 0 d and 21 d.

Lipid Extraction Method

PAHs were extracted using a modified lipid extraction method [13] from the contaminated sediments of the Mahoning River. A mixture of dichloromethane (DCM), methanol, phosphate buffer (pH 7.4) and a surrogate solution were added to the samples, mixed well and extracted. The organic phase (DCM) containing PAHs was collected and purified over sodium sulfate columns. The sample was further concentrated by evaporating the solvent.

Part 2: Ergosterol Extraction Method

Steroids Extraction Procedure:

Much work is done for the extraction of PAHs and ergosterol separately using high performance liquid chromatography (HPLC) which can be time consuming and create higher amounts of waste [13-20]. Using a single extraction method to extract PAHs and ergosterol together is both less time consuming and produces less waste. Gas chromatography-mass spectrometry (GC-MS) is used for analysis instead of HPLC because it is more efficient and accurate due to its high degree of sensitivity and specificity. Sediment and reference ergosterol extraction and analysis were done using a method modified from the protocol described by Brodie et al. [21] with ethanol used as the extraction of alcohol because of its greater extraction efficiency reported by Padgett et al. [22]. The reference standard of sterols (ergosterol and cholesterol 98% purity, Sigma- Aldrich) was prepared in dichloromethane (DCM). During the extraction procedure of samples, KOH (1.50 M) in 96% ethanol was used for the saponification process. This caused de-esterification of the complexed ergosterol to its free form and to facilitate its detection. All extractions of sterol (ergosterol and cholesterol) were done in triplicate. The control mixtures were a combination of Sediment + Sawdust + Fungi grown on barley. The sample mixtures were fungi grown on PDA and barley and then mixed with sediment. The fungi were cultivated on barley in a bio-bag for approximately 3-weeks prior to sampling. The pure fungi were grown on PDA as described previously. Sediment was collected from Lowellville, Ohio, in September 2008. Fungi and sediment mixtures (controls and samples) were not incubated together; these were mixed just prior to sampling and analysis. A total of twenty-one treatments (control mixture and sample mixtures) were done in triplicate. Acetylation was done for samples containing pure fungi and samples containing sediment.

This helps to separate the sterols from other contaminants such as PAHs. GC requires that the compound should be in the gaseous phase, therefore to extract ergosterol (m.p.160 °C, b.p. 250 °C), its melting point should be lowered. Therefore, by doing acetylation its melting point is lowered and more easily detected on GC-MS. Another advantage of acetylation is that the original compound can be regenerated by hydrolysis.

Purification

Both the samples from the lipid extraction procedure and modified protocol from Brodie et al. [21] for sterols were concentrated and passed over silica gel columns. Any unwanted sediment waste adsorbs onto the activated silica, thus purifying the samples. The samples were further purified twice over the aminopropyl columns and analyzed by GC-MS after the internal standard was added (for PAHs analysis only).

Analysis of PAHs and steroids

Commercial ergosterol and cholesterol were analysed by GC-MS as standard references. When the samples collected from the Ergosterol Extraction Method was analyzed using GC-MS, 16 PAHs were detected. All analyses were performed on a Hewlett Packard 5890 Gas Chromatograph/ 5989A Mass Spectrometer equipped with a DB-5 column (30 m, 0.32 mm ID, and a HP 6890 Series Injector). The injector and the detector temperatures were set at 250 °C and 300 °C respectively. The oven temperature was held at 45 °C for 2 min, and then ramped at 20 °C per minute to 310 °C. The final temperature was held for 5.5 min.

Results and discussion

Part 1: Bioremediation and quantification of PAHs

The data are shown (Tables 2, 3 and 4) as a comparison of degradation patterns of low and high molecular weights PAHs ($\mu\text{g PAHs g}^{-1}$ sediment dry weight).

PAHs analyses

Of the detected PAHs, fluoranthene was of the highest concentration with $85.10 \mu\text{g g}^{-1}$ dry weight, followed by pyrene with $69.14 \mu\text{g g}^{-1}$ dry weight (Table 1).

Four treatments were done: (1) Control (2) Sawdust (3) Sawdust + fungi and (4) Sawdust + fungi + nitrogen. By the end of the experiment (21 *d*), nine of the eleven PAHs were detected which showed degradation in the sample with *Pleurotus ostreatus* + sawdust. The total PAH concentration was reduced by 58.6% from 253 $\mu\text{g g}^{-1}$ of dry weight on day 0 to 173 $\mu\text{g g}^{-1}$ on day 21.

When extractions were carried out in triplicate by the lipid extraction method for PAHs, only seven PAHs were detected, at time zero (Table 2) and only nine PAHs were detected, at time 21 *d* (Table 3) by GC-MS. The quantity of low molecular weight PAHs and high molecular weight PAHs varies from sample to sample when analyzed by GC-MS at time 0 and 21 *d*.

Table 1

PAHs detected in Mahoning river sediment by lipid extraction procedure.

No.	PAHs	Retention Time	Concentration $\mu\text{g g}^{-1}$ dry weight
1	Naphthalene	9.05	13.03
2	Acenaphthylene	11.26	1.23
3	Acenaphthene	11.49	3.03
4	Fluorene	12.19	11.76
5	Phenanthrene	13.55	39.37
6	Anthracene	13.55	46.64
7	Fluoranthene	15.20	85.10
8	Pyrene	15.53	69.14
9	1,2-Benzanthracene	17.42	17.48
10	Chrysene	17.42	15.10
11	2,3-Benzfluoranthene	19.79	40.19
12	3,4-Benzopyrene	0	N.D
13	1,2:5,6-Dibenzanthracene	0	N.D
14	Indeno(1,2,3-cd)pyrene	0	N.D
15	1,12-Benzoperylene	0	N.D

N.D – Not detected

Table 2

PAHs detected in Mahoning river sediment by lipid extraction procedure at time 0 days.

No.	PAHs	Retention Time	Concentration $\mu\text{g g}^{-1}$ dry weight
1	Naphthalene	9.05	N.D
2	Acenaphthylene	11.26	N.D
3	Acenaphthene	11.49	N.D
4	Fluorene	12.19	N.D
5	Phenanthrene	13.55	15.51
6	Anthracene	13.55	18.92
7	Fluoranthene	15.20	39.63
8	Pyrene	15.53	26.37
9	1,2-Benzanthracene	17.42	N.D
10	Chrysene	17.42	19.89
11	2,3-Benzfluoranthene	19.79	17.55
12	3,4-Benzopyrene	0	14.11
13	1,2:5,6-Dibenzanthracene	0	N.D
14	Indeno(1,2,3-cd)pyrene	0	N.D
15	1,12-Benzoperylene	0	N.D

N.D – Not detected

Table 3

PAHs detected in Mahoning river sediment by lipid extraction procedure at time 21 days.

No.	PAHs	Retention Time	Concentration $\mu\text{g g}^{-1}$ dry weight
1	Naphthalene	9.05	N.D
2	Acenaphthylene	11.26	0.48
3	Acenaphthene	11.49	N.D
4	Fluorene	12.19	8.65
5	Phenanthrene	13.55	12.09
6	Anthracene	13.55	24.72
7	Fluoranthene	15.20	19.23
8	Pyrene	15.53	3.65
9	1,2-Benzanthracene	17.42	8.32
10	Chrysene	17.42	5.92
11	2,3-Benzfluoranthene	19.79	13.78
12	3,4-Benzopyrene	0	N.D
13	1,2:5,6-Dibenzanthracene	0	N.D
14	Indeno(1,2,3-cd)pyrene	0	N.D
15	1,12-Benzoperylene	0	N.D

N.D – Not detected

Part 2: Bioremediation and quantification of PAHs and quantification of ergosterol

Sixteen PAHs were extracted using the modified ergosterol extraction method (Table 4), six of them being low molecular weight PAHs, namely naphthalene; acenaphthylene; acenaphthene; fluorine; phenanthrene and anthracene. Ten high molecular weight PAHs were detected which include fluoranthene; 1,2-Benzanthracene; pyrene; chrysene; 2,3-Benzfluoranthene; 11,12-Benzofluoranthene; 3,4-Benzopyrene; 1,2:5,6-Dibenzanthracene; Indeno(1,2,3-cd)pyrene and 1,12-Benzoperylene. The quantity of PAHs extracted from this method is much more than that extracted by the lipid extraction method (Table 2). The PAHs were extracted by the modified ergosterol extraction method done in triplicate from the samples having the treatment: fungi grown on barley (0.6207 g) + sediment (0.6199 g), fungi grown on barley (0.6143 g) + sediment (1.1886 g) and fungi grown on barley (0.6327 g) + sediment (0.5743 g). The extractions from these samples were analyzed by GC-MS without acetylation.

Table 4

Average PAHs detected in Mahoning river sediment (Controls) by Ergosterol Extraction Method.

No.	PAHs	RetentionTime	Concentration $\mu\text{g g}^{-1}$ dry weight
1	Naphthalene	9.71	7.36
2	Acenaphthylene	11.06	53.72
3	Acenaphthene	11.21	26.22
4	Fluorene	11.60	43.51
5	Phenanthrene	12.43	235.76
6	Anthracene	12.46	183.12
7	Fluoranthene	13.43	1013.57
8	Pyrene	13.63	858.76
9	1,2-Benzanthracene	14.66	385.04
10	Chrysene	14.70	224.34
11	2,3-Benzfluoranthene	15.83	375.29
12	11,12-Benzofluoranthene	15.83	328.76
13	3,4-Benzopyrene	16.17	336.57
14	1,2:5,6-Dibenzanthracene	18.05	68.71
15	Indeno(1,2,3-cd)pyrene	18.06	42.63
16	1,12-Benzoperylene	18.58	140.90

The concentrations of PAHs in the contaminated sediment samples were calculated (Eq. (1)).

$$(D \times X) / M = C \quad (1)$$

Where:

D = Amount of DCM with suspended PAHs extracted from the sample, mL;

X = Concentration of the sample given by GC-MS, $\mu\text{g mL}^{-1}$;

M = Mass of the sample before extraction, g;

C = Concentration of PAHs in the sample, $\mu\text{g g}^{-1}$.

The ergosterol was extracted and analyzed by GC-MS from the samples of pure fungi grown on PDA done in triplicate: pure fungi (0.5325 g), pure fungi (0.5247 g) and pure fungi (0.5225 g) (Figure 1a). The peak was detected at 397 a.m.u. which corresponds with ergosterol (Figure 1b). Acetylation of ergosterol was done after extraction of ergosterol.

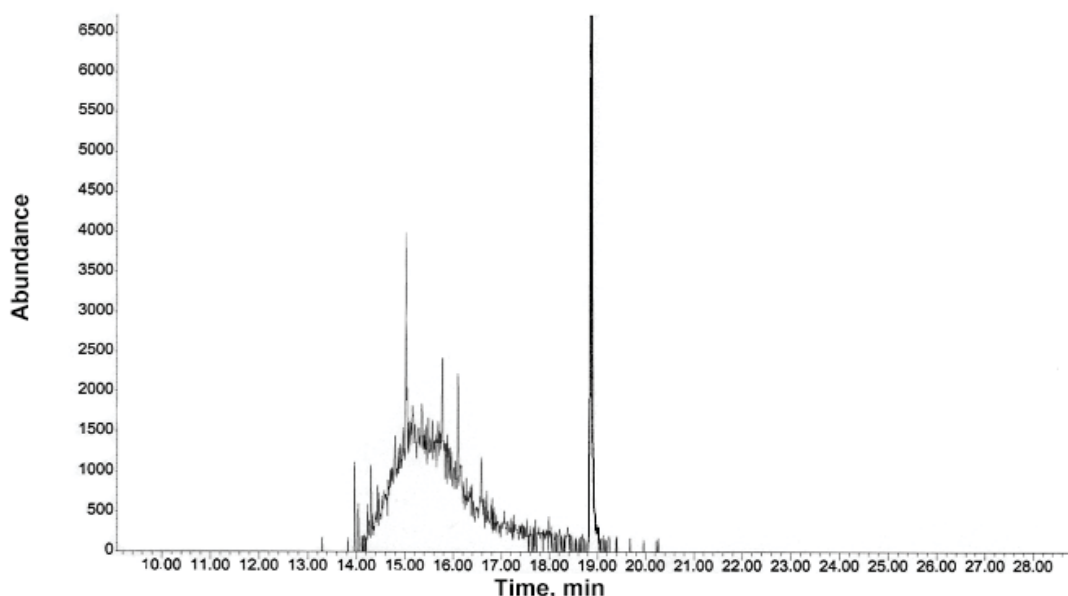


Figure 1a. MS chromatogram of ergosterol by EEM from fungi grown on potato dextrose agar, m/z 396.

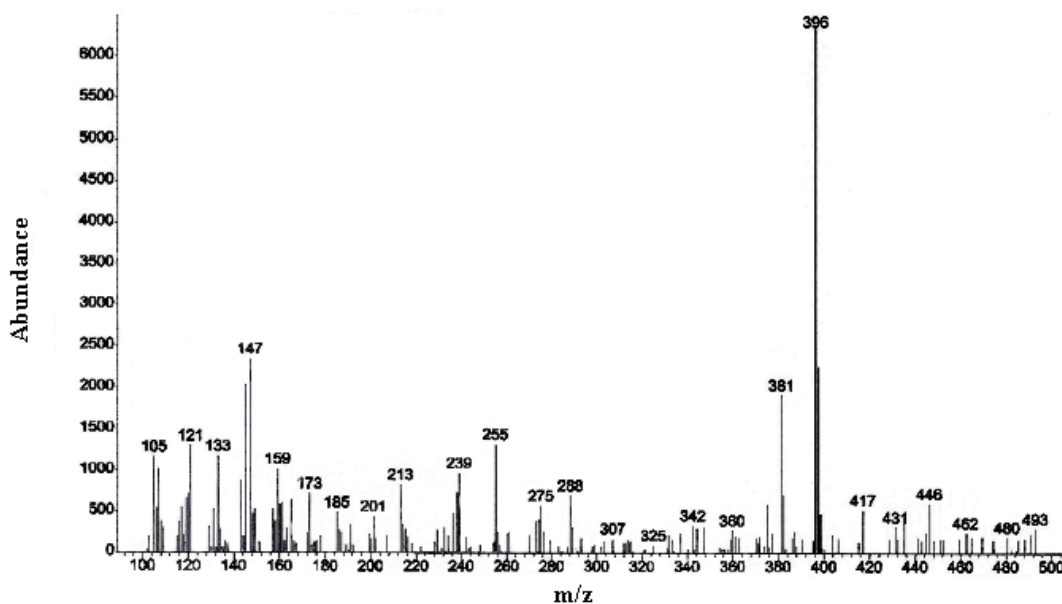


Figure 1b. Chromatogram of ergosterol by EEM from fungi grown on potato dextrose agar.

The extraction of samples done in triplicate taking pure fungi grown on PDA and sediment added separately: pure fungi (0.5283 g) + sediment (0.5880 g), pure fungi (0.54480 g) + sediment (0.5132 g) (Figures 2, 3 and 4) and pure fungi (0.6184 g) + sediment (0.5368 g). After the extraction, cholesterol and PAHs were detected from GC-MS, this is the first report for the occurrence of cholesterol (Figures 2 and 3). Cholesterol was seen after acetylation of sterol by GC-MS (Figure 3).

The extraction of pure fungi grown on PDA was done without acetylation and analyzed by GC-MS. Cholesterol and ergosterol were detected in high amounts with high intensity of peaks being observed for both sterols (Figures 3 and 4). The significant result is that cholesterol is usually found in animals but here it was detected in fungus *P. ostreatus* for the first time in good amount.

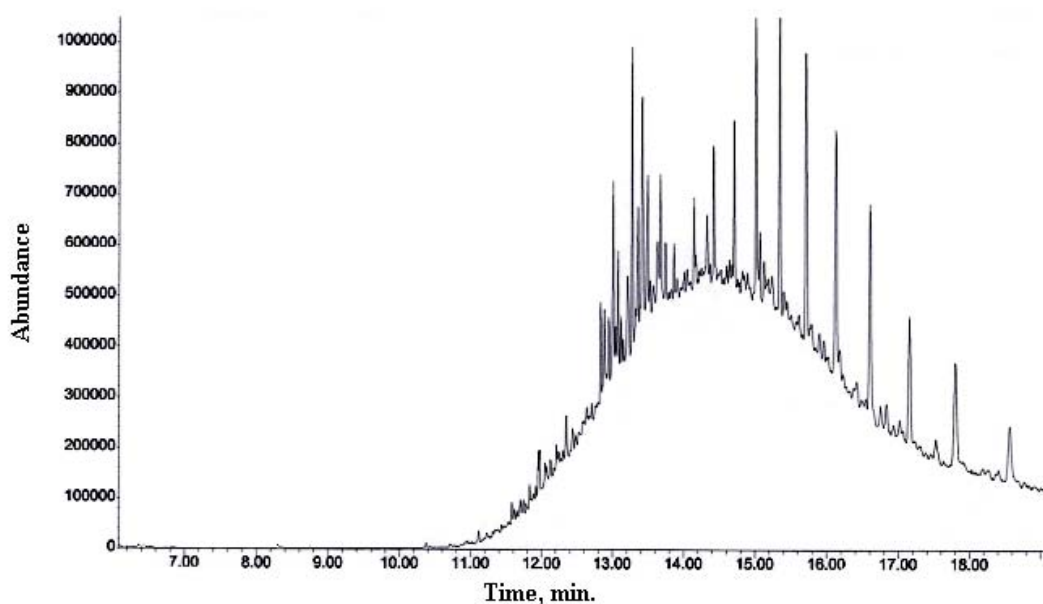


Figure 2a. MS chromatogram of PAHs by EEM from pure fungi plus sediment, m/z 105, 119, 128, 145, 159, 171, 183, 197, 251, 270, 284, 302.

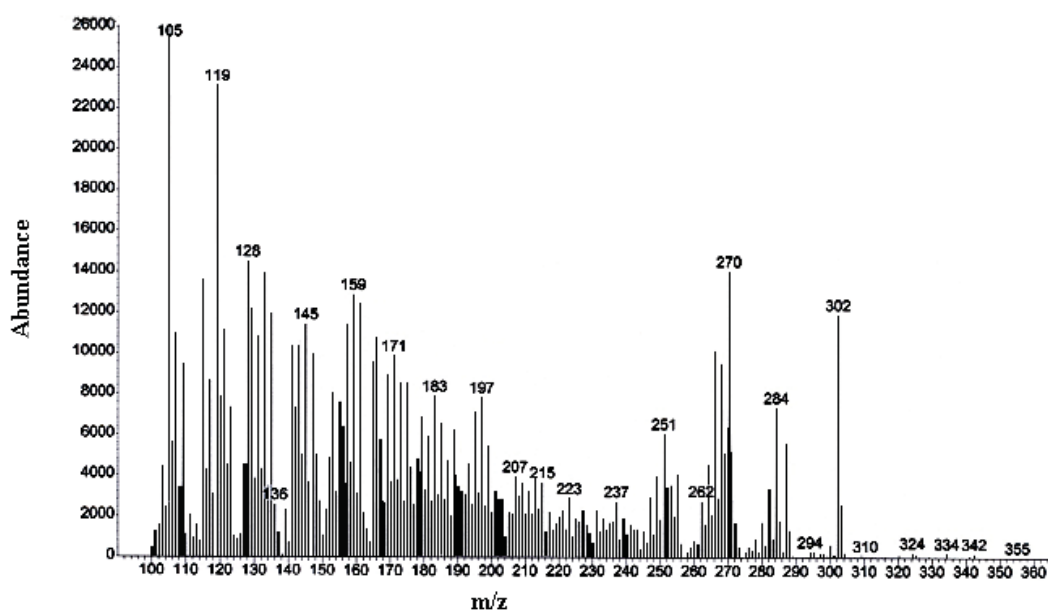


Figure 2b. Chromatogram of PAHs by EEM from pure fungi plus sediment.

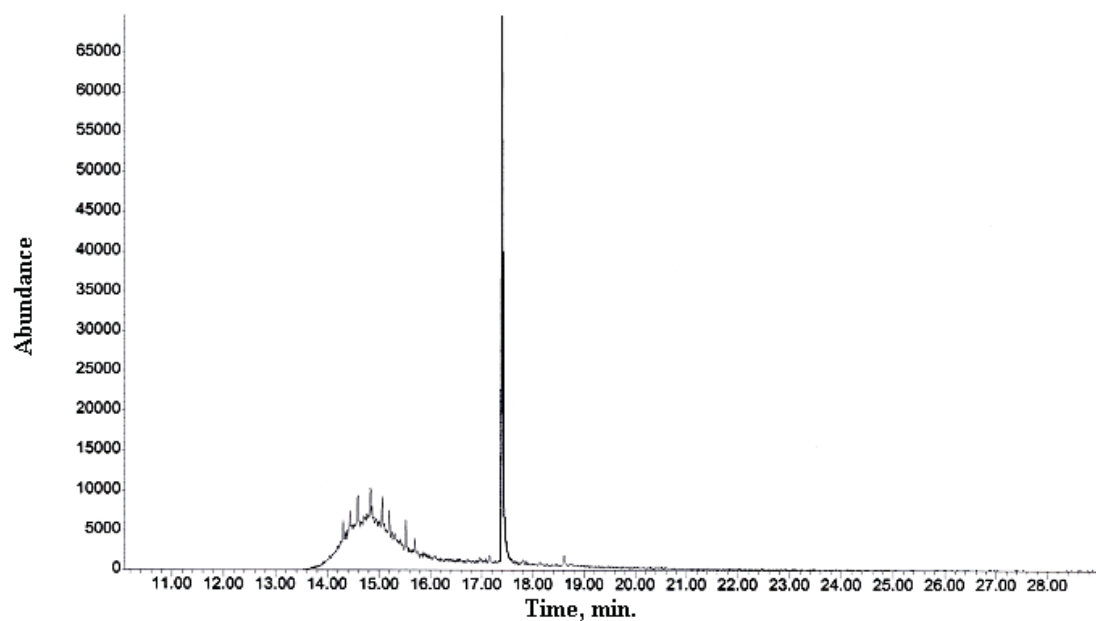


Figure 3a. MS chromatogram of cholesterol by EEM from pure fungi plus sediment, m/z 368.

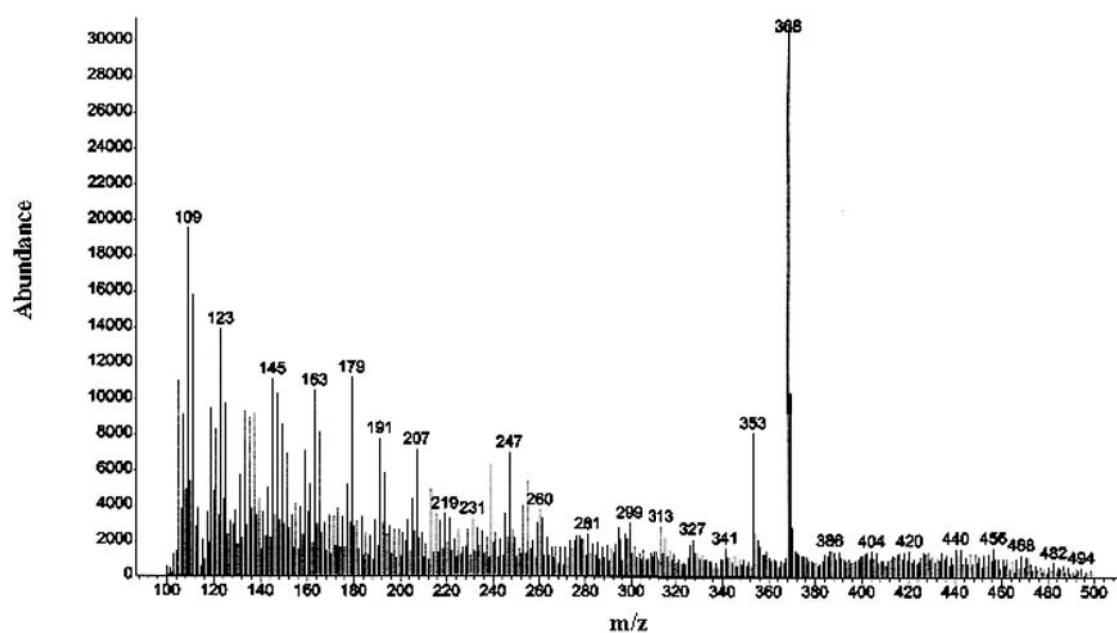


Figure 3b. Chromatogram of cholesterol by EEM from pure fungi plus sediment.

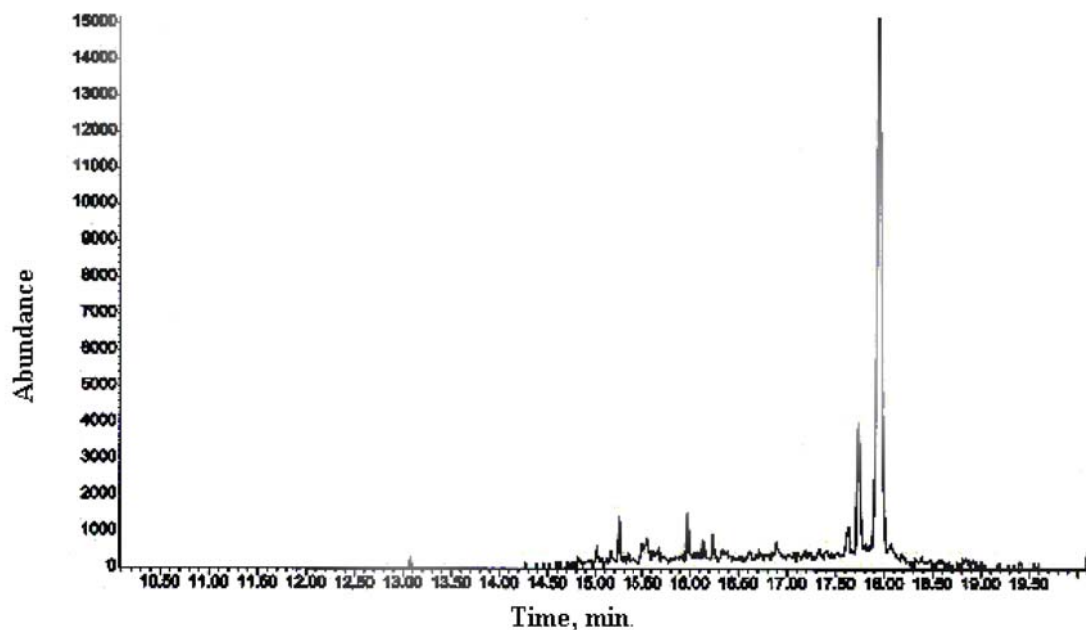


Figure 4a. MS chromatogram of ergosterol by EEM from the fungi *P. ostreatus* grown on potato dextrose agar, m/z 378.

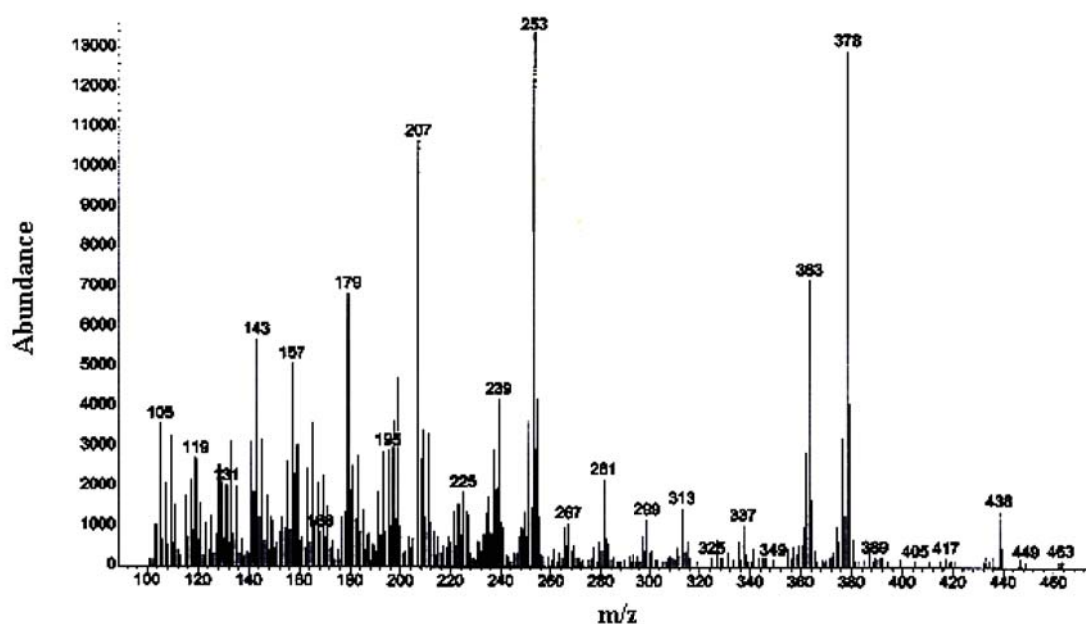


Figure 4b. Chromatogram of ergosterol extracted by EEM from the fungi *P. ostreatus* grown on potato dextrose agar.

The detection of cholesterol and ergosterol in fungi by GC-MS was analyzed from the peaks of standard reference spectra of commercial ergosterol and cholesterol. The cholesterol and ergosterol in fungi were also confirmed by the standard reference peaks of acetylated cholesterol and ergosterol, which were acetylated from the commercial cholesterol and ergosterol.

The detection of ergosterol by GC-MS from the samples done in triplicate and the amounts of ergosterol per gram of sample was analyzed after calculation: fungi grown on barley 0.67 g sample, 17.5 $\mu\text{g g}^{-1}$ of ergosterol was present (Figure 5); 0.53 g sample, 39.94 $\mu\text{g g}^{-1}$ of ergosterol was present (Figure 6) and 0.53 g sample, 21.58 $\mu\text{g g}^{-1}$ of ergosterol was present (Figure 7).

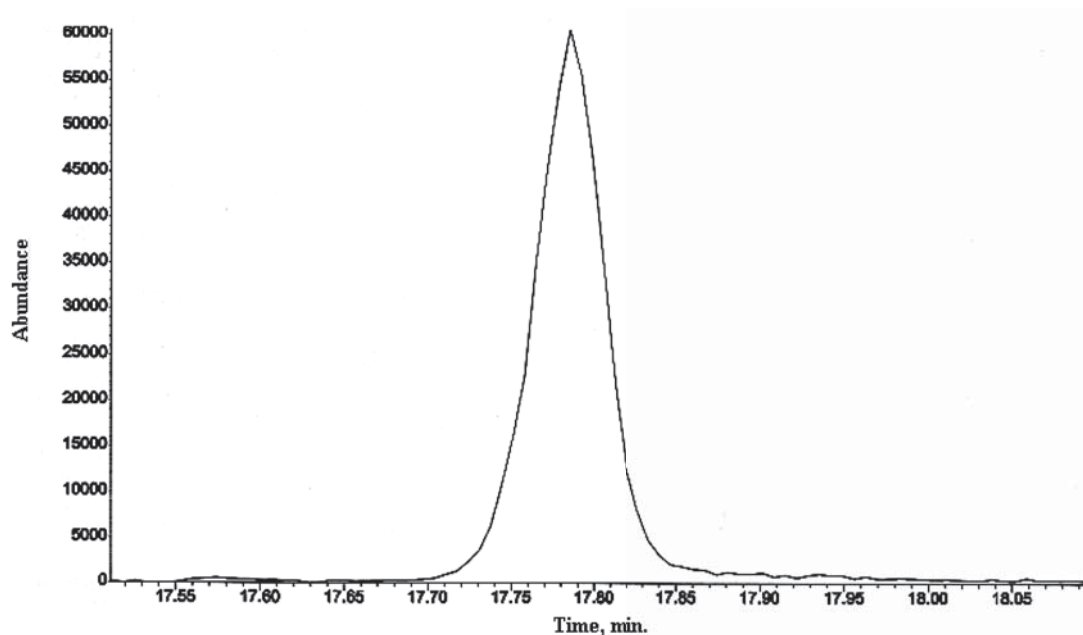


Figure 5a. MS chromatogram of ergosterol by EEM in *P. ostreatus* grown on barley is at m/z 396.

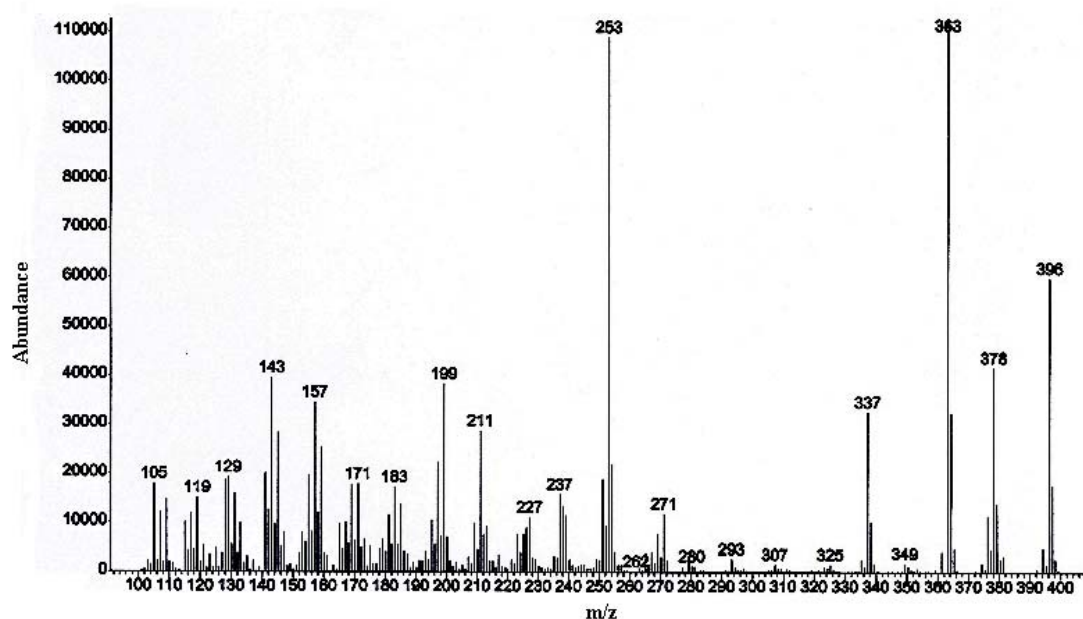


Figure 5b. Chromatogram of $17.5 \mu\text{g g}^{-1}$ ergosterol in *P. ostreatus* grown on barley.

The peaks of ergosterol were identified on the basis of retention times and spectral characteristics as compared to those of standard materials. The concentration of ergosterol samples ($\mu\text{g g}^{-1}$) were calculated (Eqs. (2) and (3)) as:

Calibration Std.:

$$\text{Calibration Factor} = \frac{\text{Area Counts of std. ergosterol}}{\text{Concentration of std. ergosterol } (\mu\text{g})} \quad (2)$$

For Sample:

$$\frac{\text{Area Count of ergosterol sample}}{CF} \times \frac{\text{Volume of extract (mL)}}{\text{Mass of sample (g)}} = \frac{\mu\text{g}}{\text{g}} \quad (3)$$

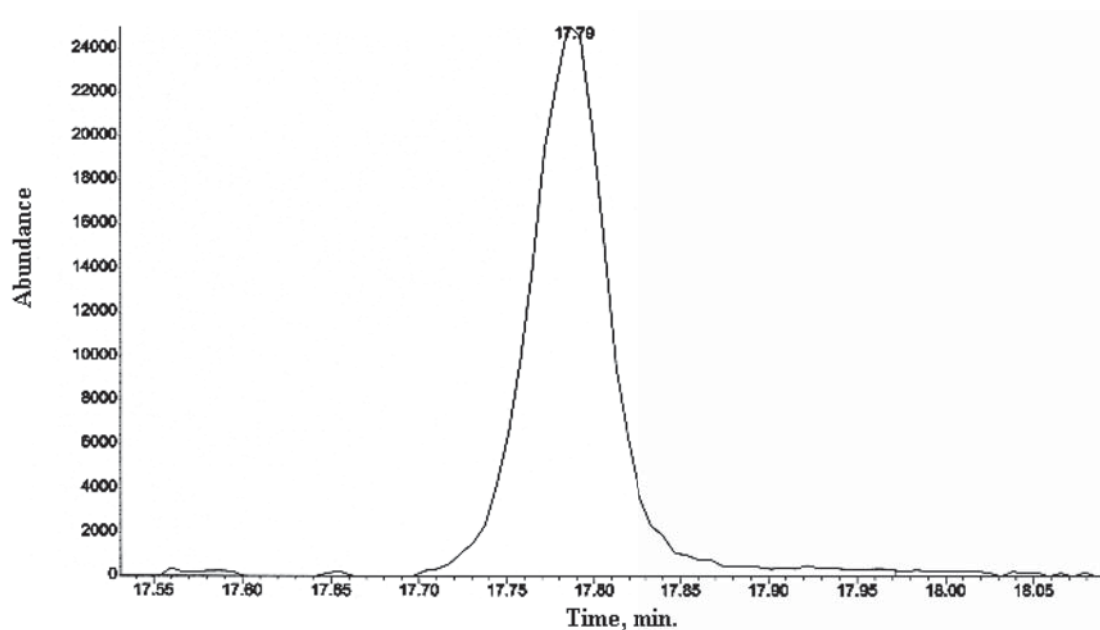


Figure 6a. MS chromatogram of ergosterol by EEM in *P. ostreatus* grown on barley, m/z 396.

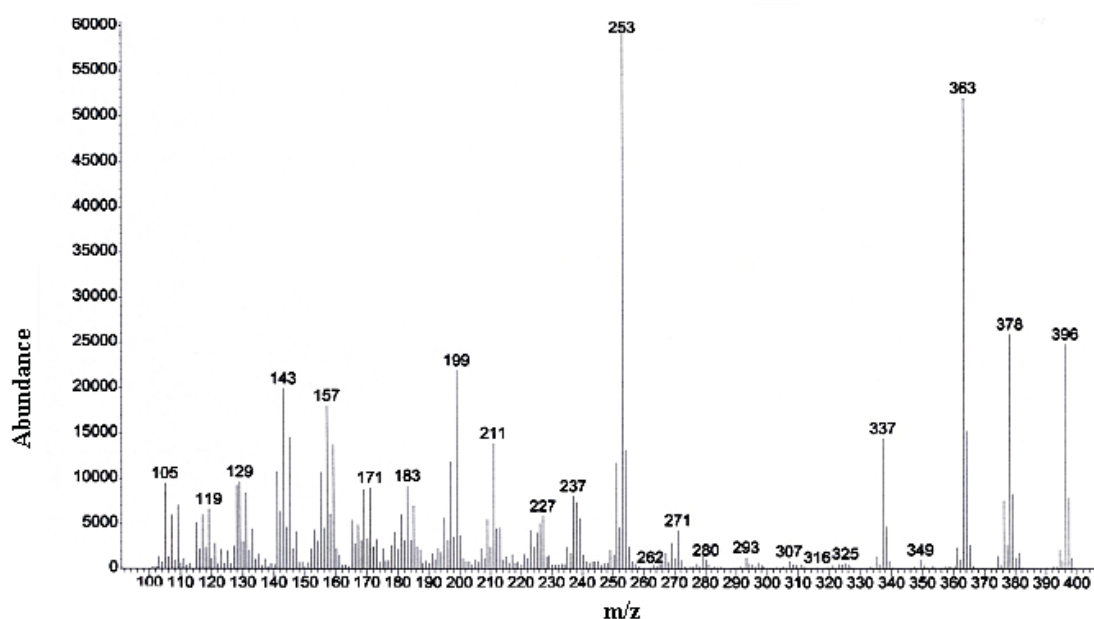


Figure 6b. Chromatogram of 39.94 $\mu\text{g g}^{-1}$ ergosterol in *P. ostreatus* grown on barley.

This method is useful for measuring the PAHs and ergosterol with great precision and accuracy without any hindrance. The extracts of the extractions for the samples which include sediments such as: pure fungi plus sediment and fungi (grown on barley) plus sediment, sterols were detected only after acetylation of the reaction mixture. This is because, acetylation was necessary to separate sterols from contaminants such as PAHs, these contaminants act as hindrance in analyzing extracts on GC-MS.

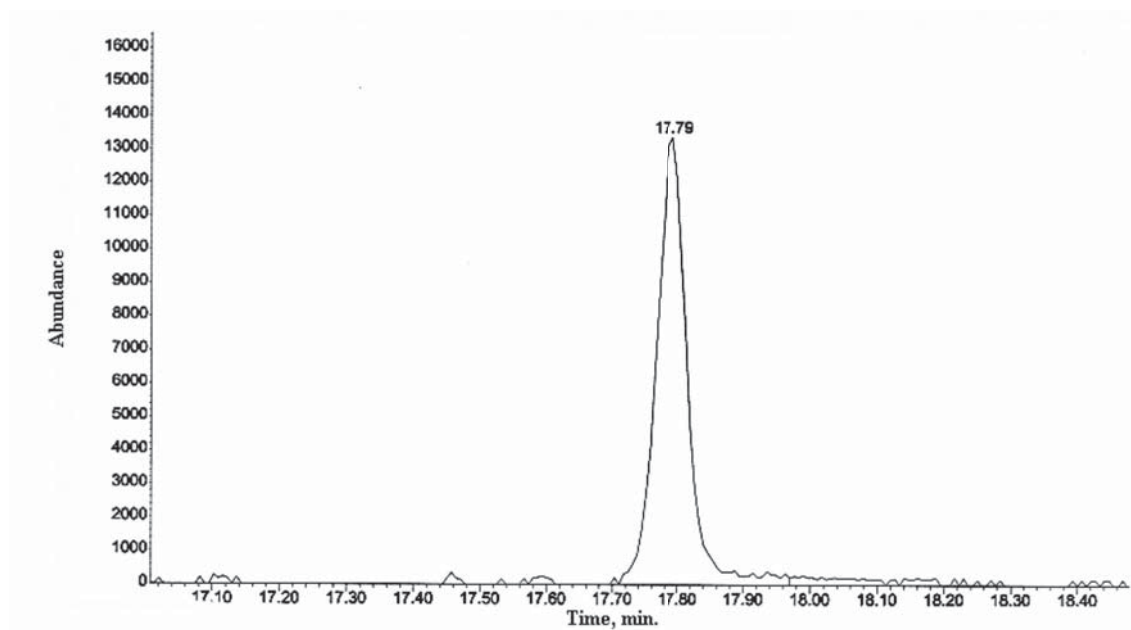


Figure 7a. MS chromatogram of ergosterol by EEM in *P. ostreatus* grown on barley, m/z 396.

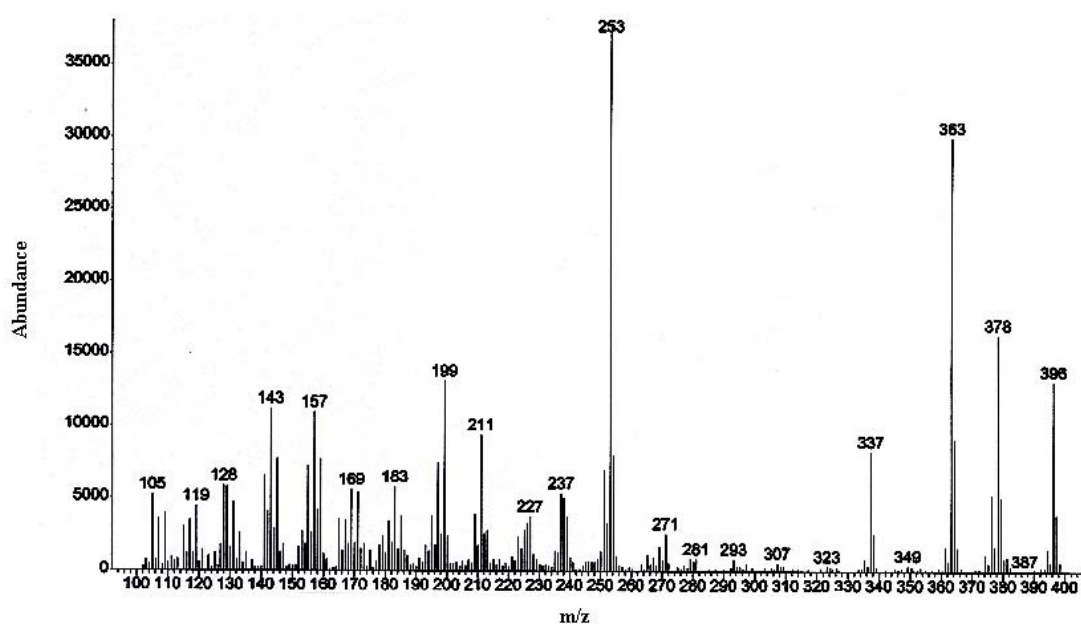


Figure 7b. Chromatogram of 21.58 µg g⁻¹ ergosterol in *P. ostreatus* grown on barley.

Comparison of Lipid Extraction Method and Ergosterol Extraction Method:

The solutes obtained from the extractions of the samples from these two methods were both analyzed by GC-MS. Eleven PAHs were detected in Mahoning River sediment using the modified Fang and Findlay lipid extraction procedure. A total of sixteen PAHs were detected by ergosterol extraction method (Figure 8). Ergosterol and cholesterol were also extracted and detected from this method. By Ergosterol Extraction Method both PAHs and sterols were detected with great efficiency and ease. It is also less time-consuming and does not require many solvents. Therefore, the Ergosterol Extraction Method is the most effective method both qualitatively and quantitatively for simultaneous analysis of PAHs and ergosterol.

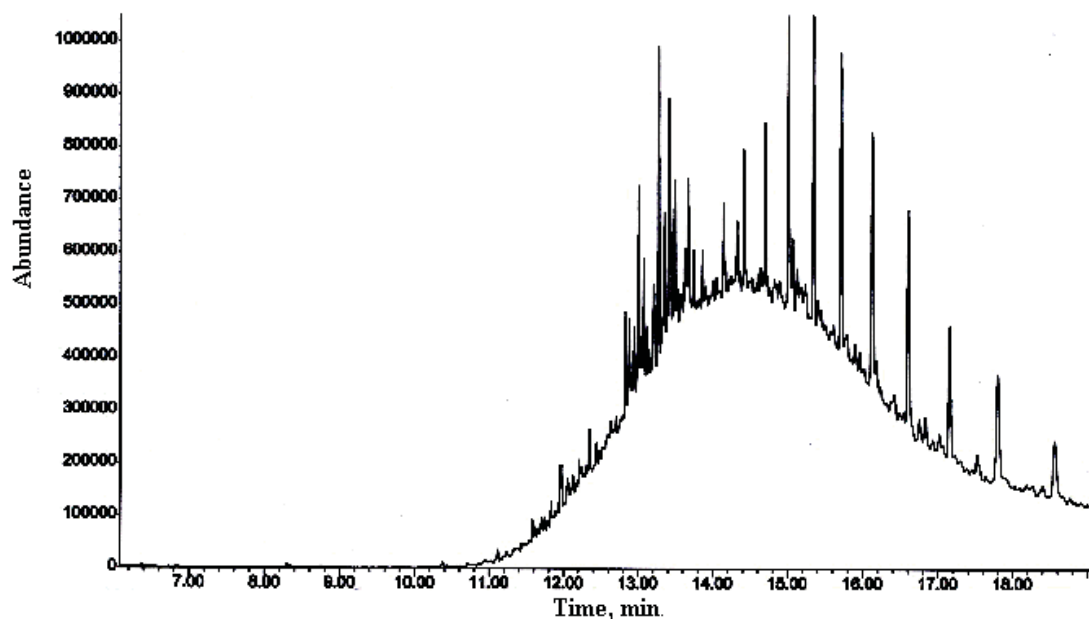


Figure 8a. MS chromatogram PAHs from sediment sample by EEM, m/z 119, 128, 136, 145, 159, 171, 197, 284, 270, 302.

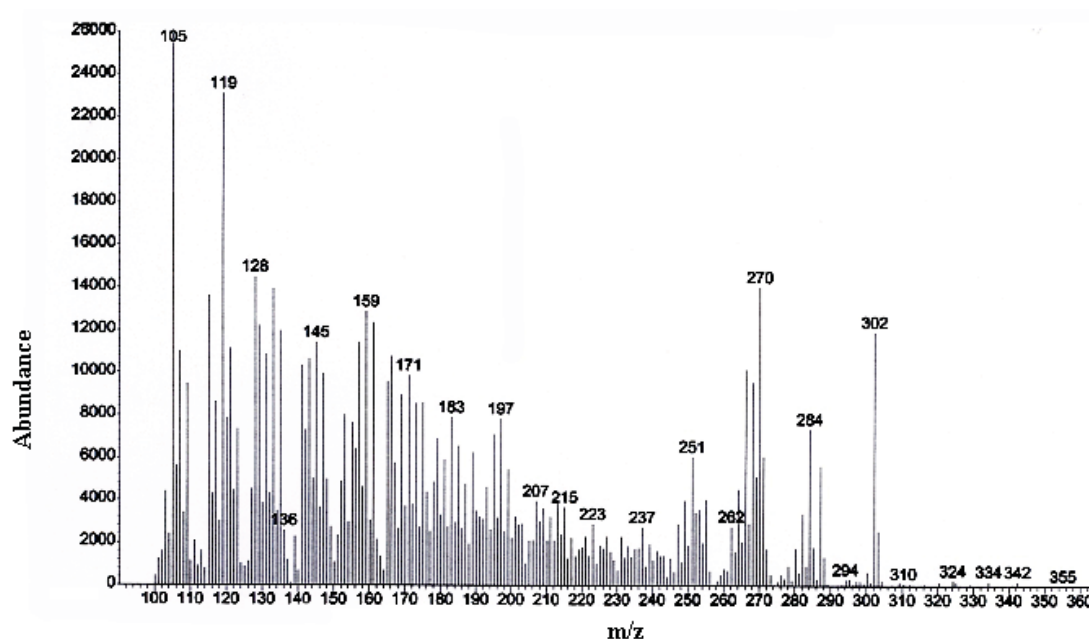


Figure 8b. Chromatogram of PAHs from sediment sample by EEM.

Conclusions

In conclusion, an efficient and high yielding Ergosterol Extraction Method was developed by which more PAHs were obtained than with the usual Lipid Extraction Method. Sediments were inoculated with *P.ostreatus*. Ergosterol Extraction Method was used as an effective tool for the extraction of ergosterol from *P.ostreatus* and bioremediation of contaminated sediment from PAHs by adding *P.ostreatus*. The detection of good amounts of ergosterol in white rot fungi, *P.ostreatus* confirms the fact that it acts as bioindicator of fungi. The growth of fungal mycelia can be increased by inoculating the treatment with a nitrogen source which serves as nutrients for fungi. EEM was particularly adapted

for studying ergosterol in various treatments and matrixes. EEM was used to quantitate and analyze the biodegradation of PAHs and the change in the amount of ergosterol in *Postreatus* at different treatments, at different times such as 0 d and 21 d. For ergosterol extraction, different treatments were set up with various amendments for at least three runs and every extraction was done in triplicate at two different times for these runs.

Degradation of PAHs should be seen in the future work by EEM at times 0 d and 21 d, also the change in the amounts of ergosterol must be seen at these time periods. For triplicate incubations, sediments from the same site and the same spot sampled at same time are recommended. *Pleurotus ostreatus* was found to be effective in removing PAHs from the contaminated sediment.

Acknowledgments

Use of Research Core Facilities and financial support were made possible by the Department of Geological and Environmental Sciences, Youngstown State University, Ohio. The author (MO) is thankful to the Department for Teaching Assistantship.

References

1. Ohio Environmental Protection Agency, Biological and water quality study of the Mahoning River Basin, OEPA Technical Report. 1996, MAS/1995-12-14, pp. 1-249.
2. Perera, F.P.; Rauh, V.; Whyatt, R.M.; Tsai, W.Y.; Tang, D.; Diaz, D.; Hoepner, L.; Barr, D.; Tu, Y.H.; Camann, D.; Kinney, P. Effect of Prenatal Exposure to Airborne Polycyclic Aromatic Hydrocarbons on Neurodevelopment in the First 3 Years of Life among Inner-City Children. *Environmental Health Perspective: Children's Health*, 2006, 114(8), pp. 1287-1292.
3. Luch, A. The Carcinogenic Effects of Polycyclic Aromatic Hydrocarbons. London: Imperial College Press. 2005, ISBN 1-86094-417-5, 516 p.
4. Spink, D.C.; Wu, S.J.; Skink, B.C.; Hussain, M.M.; Vakharia, D.D.; Pentecost, B.T.; Kaminsky, L.S. Induction of CYP1A1 and CYP1B1 by benzo(k)fluoranthene and benzo(a)pyrene in T-47D human breast cancer cells: Roles of PAH interactions and PAH metabolites. *Toxicology and Applied Pharmacology*, 2008, 226(3), pp. 213-224.
5. Zhang, C.; Li, X.; Li, P.; Lin, X.; Li, Q.; Gong, Z. Biodegradation of aged polycyclic aromatic hydrocarbons (PAHs) by microbial consortia in soil and slurry phases. *Journal of Hazardous Materials*, 2008, 150(1), pp. 21-26.
6. Bixian, M.; Jiamo, F.; Gan, Z.; Zheng, L.; Yushun, M.; Guoying, S.; Xingmin, W. Polycyclic aromatic hydrocarbons in sediments from the Pearl river and estuary, China: spatial and temporal distribution and sources. *Applied Geochemistry*, 2001, 16(11-12), pp. 1429-1445.
7. Kanaly, R.A.; Harayama, S. Biodegradation of high-molecular-weight polycyclic aromatic hydrocarbons by bacteria. *Journal of Bacteriology*, 2000, 182(8), pp. 2059-2067.
8. King, A.J.; Readman, J.W.; Zhou, J.L. Determination of polycyclic aromatic hydrocarbons in water by solid-phase microextraction–gas chromatography–mass spectrometry. *Analytica Chimica Acta*, 523(2), 2004. pp. 259-267.
9. Oren, A.; Aizenshtat, Z.; Chefetz, B. Persistent organic pollutants and sedimentary organic matter properties: A case study in the Kishon River, Israel. *Environmental pollution*, 2006, 141(2), pp. 265-274.
10. Field, J. A.; Jong, E. D.; Gumersindo, F. C.; Jan, A. M.; De, B. Biodegradation of polycyclic aromatic hydrocarbons by new isolates of white rot fungi. *Applied Environmental Microbiology*, 1992, 58(7), pp. 2219-2226.
11. Cerniglia, C.E. Biodegradation of polycyclic aromatic hydrocarbons. *Biodegradation*, 1992, 3, pp. 351-368.
12. Javitt, N.B. Bile acid synthesis from cholesterol: regulatory and auxiliary pathways. *FASEB Journal*, 1994, 8(15), pp. 1308-11.
13. Fang, J.; Findlay, R.H. The use of a classic lipid extraction method for simultaneous recovery of organic pollutants and microbial lipids from sediments. *Journal of Microbiological Methods*, 1996, 27(1), pp. 63-71.
14. Tardieu, D.; Bailly, J.D.; Bernard, G.; Guerre, P. Comparison of two extraction methods for ergosterol determination in vegetal feeds. *Revue de Medicine Veterinaire*, 2007, 158(8-9), pp. 442-446.
15. Headley, J.V.; Peru, K.M.; Verma, B.; Robarts, R.D. Mass spectrometric determination of ergosterol in a prairie natural wetland. *Journal of Chromatography A*, 2002, 958(1-2), pp. 149-156.
16. Axelsson, B.S.; Saraf, A.; Larsson, L. Determination of Ergosterol in organic dust by gas chromatography-mass spectrometry, *Journal of Chromatography B*, 666, 1995, pp. 77-84.
17. Parsi, Z.; Gorecki, T. Determination of ergosterol as an indicator of fungal biomass in various samples using non-discriminating flash pyrolysis. *Journal of Chromatography A*, 2006, 1130(1), pp. 145-150.
18. Stahl, P. D.; Parkin, T. B. Relationship of soil ergosterol concentration and fungal biomass. *Soil Biology and Biochemistry*, 1996, 28, pp. 847-855.
19. Yateem, A.; Balba, M.T.; Al-Awadhi, N. El-Nawawy, A.S. White rot fungi and their role in remediating oil contaminated soil. *Environmental International*, 1998, 24(1), pp. 181-187.

20. Dietrich, D.; Lamar, R. Selective Medium for Isolating *Phanerochaete chrysosporium* from Soil. *Applied and Environmental Microbiology*, 1990, 56, pp. 3088-3092.
21. Brodie, E.; Edwards, S.; Clipson, N. Soil fungal community structure in a temperate upland grassland soil. *FEMS Microbiology Ecology*, 2003, 45(2), pp. 105-114.
22. Padgett, D.E.; Posey, M.H. An evaluation of the efficiencies of several ergosterol extraction techniques. *Mycological Research*, 1993, 97, pp. 1476-1480.

REMOVAL OF REMAZOL ROSSO RB DYE FROM AQUEOUS EFFLUENTS BY HOMOGENOUS FENTON OXIDATION PROCESSES

Carmen Zaharia^{a*}, Victoria Fedorcea^a, Adrian Beda^a, Victor Amarandei^b
Augustin Muresan^b

^a“Gheorghe Asachi” Technical University of Iasi, Faculty of Chemical Engineering and Environmental Protection, Department of Environmental Engineering and Management, 73, Prof. dr. docent D. Mangeron Blvd., Iasi 700050, Romania

^b“Gheorghe Asachi” Technical University of Iasi, Faculty of Textiles, Leathers and Industrial Management,

53, Prof. dr. Docent D. Mangeron Blvd., Iasi 700050, Romania

*e-mail: czah@ch.tuiasi.ro or czaharia2003@yahoo.com;

phone: (+40 232) 27 86 83 ext 2175; fax: (+40 232) 27 13 11

Abstract. The paper presents some data from our laboratory-setup experiments of homogenous oxidative processes with hydrogen peroxide (*i.e.* advanced Fenton oxidation processes) applied for Remazol Rosso RB dye-containing aqueous systems, especially textile effluents. Therefore, some different operating parameters (including pH, concentration of dye, H₂O₂ and ferrous ions, oxidation time, temperature, stirring regime, among its) were tested for determination of the best performance in effluent discoloration and dye removal, meaning the optimal values of each studied parameters for highest discoloration or dye removal. For an effluent loaded with 50 mg/L Remazol Rosso RB dye, there were applied these optimal values that correspond to > 97 % discoloration efficiency performed with 88.24 mM H₂O₂, 0.18 mM FeSO₄, at pH (5.16), temperature of 19-20°C, continuous stirring regime (30 rpm) and minimum 25-30 minutes of homogenous advanced oxidation treatment. If there are not used additional chemical reagents for pH adjustment (minimization reason of treatment operating cost), the performance of this oxidative treatment is closed to above mentioned efficiency by after a higher oxidation time (> 90 min). These results are encouraging and sustain this oxidative process application and optimization for reducing the environmental impact of effluent discharging directly in different natural aquatic receptors and compliance with admissible limits imposed by environmental legislation as well.

Keywords: discoloration, Fenton reagent, homogenous advanced oxidation process, optimal operating parameter, Remazol Rosso RB dye, textile effluent treatment.

Introduction

In the whole world even in the most hardly accessible for tourist geographic zones, the water quality is negatively changing, and the pollution level of natural surface water resources is greatly increasing. One of the most important causes is the non-corresponding quality of final colored or not effluent discharged in natural water resources (water courses or accumulation lakes). Therefore, the wastewater or individual/final effluent treatment must continue to be one of priorities in environmental management (in terms of integrated production water management) even if an environmental prevention and control scheme was implemented in the productive/commercial unit for reduction of generated loaded wastewater amounts, among others. The treated effluents are indicated to be inside recycling/reuse for reduction of fresh water amount in each manufacturing process. One of recognized and viable emerging wastewater treatments in the scientific literature [1-4] is the advanced oxidation process (AOP) (or mineralization) of polluting compounds from wastewaters to carbon dioxides and/or other harmless species. A special attention was given for Fenton and/or Fenton-like oxidation processes applied for discoloration or dye removal purposes, together with its advantages (*i.e.* high efficiency, short operating time, simplicity in destroying the contaminants, stability to treat a wide range of polluting or not toxic species, non-necessity of special equipment and relatively small quantities of iron-based precipitates and sludge) and disadvantages (*i.e.* consumption of chemicals, necessity of iron-based precipitates/sludge separation with supplementary costs and treatment requirements) that select sometimes the environmental options of company management staff in terms of effluent quality and hourly load [5-8].

This research study continues the authors' works concerning the application of Fenton oxidation (FO) treatment using homogenous ferrous-based catalysts for discoloration purposes, and is summarized some results performed at laboratory set-up scale for some aqueous Remazol Rosso RB azo dye solutions concerning the influence of different FO operating parameters.

Experimental

Materials and reagents

Remazol Rosso RB is a commercial available textile azo dye used without further purification in preparation of dyeing bath for cotton fabrics manufacturing, having the following principal characteristics: chemical formula – C₂₀H₁₂N₆O₁₆S₅Na₄, molecular weight (MW) of 824 g/mol; maximum absorbance (λ_{max}) at 517 nm, purity of 82.60%. For further practical working, a stock solution of azo dye (600 mg/L) was prepared for obtaining of diluted samples (with distilled water) in dye content range of 50-100 mg/L [5-7].

- There were also used Fenton reagents (H_2O_2 / Fe^{2+} systems) and pH adjustment solutions, such as [5-6]:
- hydrogen peroxide (H_2O_2 30 %) purchased from S.C. Nordic Invest S.R.L. Company (Cluj Napoca, Romania).
 - ferrous catalyst (Fe^{2+}), prepared from ferrous sulphate ($\text{FeSO}_4 \cdot 7\text{H}_2\text{O}$) purchased from Fluka Analytical Co. (Germany) or Chemical SRL (Romania), i.e. aqueous stock solution of 20 g/L (2 mL of concentrated H_2SO_4 , purchased from Merck Co., were added in 500 mL solution of prepared ferrous sulphate).
 - pH adjustment solutions such as 0.1N H_2SO_4 and 0.1N NaOH (purchased from Chemical Co., RO).

Equipments and FO Procedure

Some series of homogenous Fenton oxidations of azo dye solutions were carried out in a 300 mL closed glass reactor under magnetic stirrer (AG-2) using the following working methodology [5-8]: in 50 mL-dye solution (known dye concentration) with stabilized temperature (5-45°C, mainly 20°C) and specific pH (2.16-10.50) is introduced with micropipette (EcoLine) a known volume of ferrous catalyst stock solution (0-2.5 mL), under continuous stirring or without stirring, and also a known volume of commercial H_2O_2 30% solution (0-2.5 mL H_2O_2 30%). The start of Fenton oxidation (FO) kinetic study was considering the moment when H_2O_2 was added in the dye solution ('zero' time). During kinetic oxidation experiment, samples (1-3 mL) were collected from FO reactor, and analysed in terms of two quality indicators: colour and dye content (after measurements, samples are quickly reintroduced in reactor for further continuing participation in Fenton oxidation, trying to keep the solution volume as constant as possible). The final inhibition of residual H_2O_2 oxidative activity in each collected sample after FO oxidation (experiment stop) is achieved by increasing of pH to alkaline range (9-12) with help of 5N NaOH solution, and optional by adding of solid MnO_2 (0.2 g MnO_2 for each sample) [6].

The colour and dye concentration were determined by absorbance measurements at different wavelengths [5-8]: (i) 436, 456 (Hazen unit - HU, 50 HU corresponds to an absorbance of 0.069 at 456 nm), 525 and 620 nm for colour, and (ii) 517 nm (λ_{max}) for dye content using a SP 830 Plus spectrophotometer (Metertech Inc.). The experimental data indicate the progress of dye removal or discoloration during homogenous Fenton oxidation process. The initial and final pH measurements were performed at a HACH One-Laboratory pH-meter (Hach Co., USA).

The dye removal and/or discoloration degree or FO efficiency in term of colour was expressed with the general known formula of a treatment degree (Eq.(1)) for colour or Remazol Rosso RB dye concentration (using the established calibration curve for this azo dye concentration at 517 nm) [5,7,8]:

$$\text{Dye removal or discoloration degree (\%)} = \frac{C_i - C_f}{C_i} \cdot 100 \quad (1)$$

where: C_i – the initial colour (HU) or dye concentration (mg/L), and C_f – the color (HU) or dye concentration (mg/L) at t time, mg/L.

Some notifications are necessary to be mentioned for complete understanding of experimental results:

- In further applications/stages from the textile technological manufacturing process (after FO treatment stage), the treated dye-containing solutions will be used in steps where the only imposed restriction is for color and pH, not for salts (fixed residues) and organic loads (toxic, refractory organics expressed by COD, and/or biodegradable organics expressed by BOD) that are important but not restrictively imposed. Therefore, the FO performance is firstly considered only for color (discoloration) or dye decomposition (expressed by dye removal).
- For the final individual or mixed effluent discharged in receptor from outside of plant emplacement is obligatory to have in view the total organic load (toxic and biodegradable ones) together with content of suspended solids, salts and color, and also in some technological manufacturing steps.
- This treated effluent by FO process will be considered only in further controlled activities/technological steps from in-side plant emplacement not individually discharged in nearby sewage system.

Results and discussion

The known mechanism of an advanced Fenton-like oxidative process is based on reaction of formed or existing hydroxyl radicals ($\text{HO}\cdot$) with ferrous ions (Fe^{2+}) or organics (ionic or molecular organic species - R) to form ferric ions (Fe^{3+}) and different final or intermediary oxidation products (P) (low molecular weight oxygenated compounds or, in some instances, CO_2 and H_2O). Hydroxyl radical generation is enhanced at low pH (2.5-5.0), and some sludge amounts can be formed (iron hydroxide precipitates).

Some previous authors' reports of homogenous Fenton-like oxidation processes [5-8] indicated that the principal factors influencing the FO-like processes in terms of discoloration or dye removal applied for different industrial wastewaters, especially textile effluents, depended on operating parameters such as initial pH, concentration of H_2O_2 , ferrous ions, temperature, (FO) oxidation time, stirring regime, etc.

pH Influence in FO Process

It is known that the pH affects greatly the FO process performance of azo dye-containing solutions, especially the HO \cdot generation/formation and availability of catalyst species (at pH > 5.3 can precipitate ferric and ferrous hydroxides or other iron hydroxo complexes) [5-8].

In the case of commercial Remazol Rosso RB azo dye, the pH influence vs. discoloration degree and dye removal is illustrated in Figure 1 (a, b) as results of different kinetic experiments of homogenous FO process applied for 50 mg/L-dye containing solutions, 120 min-working with 176.47 mM H₂O₂, 0.36 mM FeSO₄, at room temperature (20°C), under continuous stirring (30 rpm).

It is observed that the highest FO discoloration performance (*i.e.* 96.43% after 10 min of FO process, with decreasing behavior further at 83.48% after 60 min, or 84.375% after 120 min) and dye removal (*i.e.* 96.33% after 5 min of FO process, with decreasing at 82.45% after 60 min, or 83.27% after 120 min) were performed at pH 5.16 (no precipitates formed, no registered turbidity variation). The dye oxidation rate decreased for other pH values (*e.g.*, only 33.69–54.98% after 60 min at pH (8.93-10.50) or 9.52-63.74% at pH 2.45), excepting the pH value of 7.745 (*i.e.* 93.33% after 30 min, with in time-decreasing discoloration behavior until 83.59% after 60 min, or 69.79% after 120 min), because mainly of new types of ionic or molecular species formation/production (or lower catalytic activity of different iron ionic species in solution).

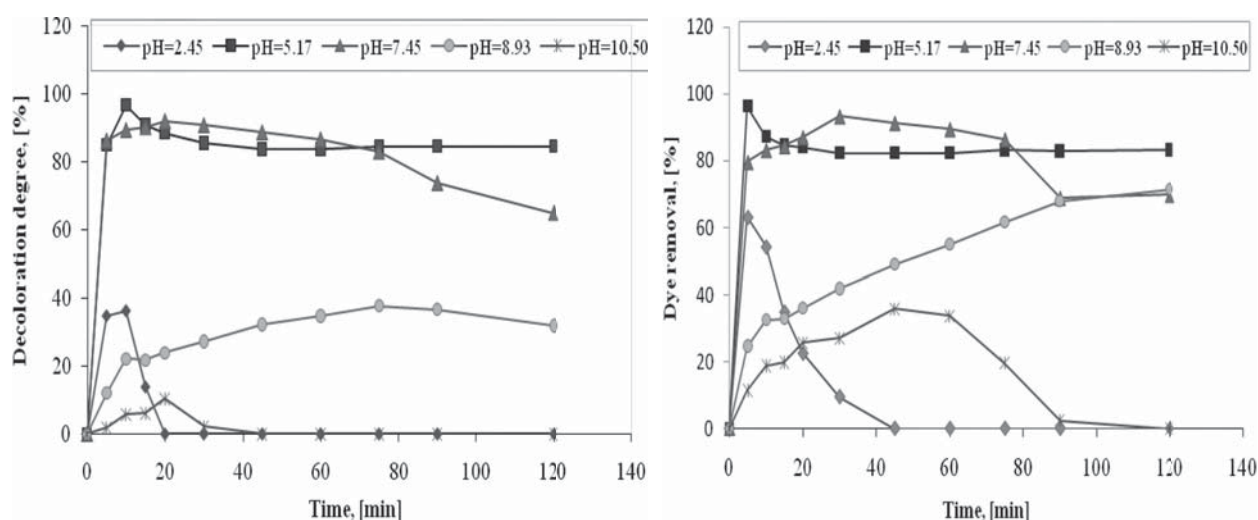


Figure 1. pH influence vs. homogenous FO process kinetic and performance of Remazol Rosso RB dye solution: (a) discoloration degree and (b) dye removal.

The most adequate pH for Remazol Rosso RB removal by FO process with ferrous sulphate as catalyst is 5.13-5.16, being obviously necessary a neutralization step before direct discharge of treated dye solution in different receptors or inside reuse, but good results can be performed at neutral pH of 7.47-7.745 (no neutralization step necessary, and no addition of chemical reagents for Fenton-like oxidation process).

H₂O₂ Concentration Influence in FO Process

Some kinetic experiments of Fenton oxidation process were performed with 50 mg/L-dye containing solutions, 120 min-working with 0.18 mM FeSO₄ and different H₂O₂ doses, at pH (7.47-7.745), temperature of 20°C, under continuous stirring (30 rpm).

All results were presented in Figure 2 (a, b) with clearly visual zones where competitive reactions take place in excess of hydrogen peroxide (HO \cdot) with acting of some inhibitory effects referring to dye removal or dye solution discoloration (*e.g.*, some inhibitory effect can appear at H₂O₂ doses in range of 44.12-264.71 mM H₂O₂ and type of oxidative process is changing, homogenous processes being competitive with Fenton-like processes).

Continuous increasing discoloration or dye removal is registered for H₂O₂ dose of 17.64 mM at pH 7.745 and room temperature (57.10% after 120 min), and also at the extreme testing H₂O₂ range working with 264.71 mM and 352.92 mM H₂O₂ (*i.e.* 45% and 69.47% after 120 min for discoloration degree, and 77.99% and 94.64% after 120 min for dye removal, respectively).

In Figure 3 (a, b) it is shown that relative high discoloration (37.91-100%) and also dye removal (6.89-100%) is registered in the first 10 min of FO process at pH 5.16 working in the H₂O₂ dose range of 17.67-264.71 mM with 0.18 mM FeSO₄. Complete discoloration at pH 5.16 (no precipitates formed, homogenous Fenton processes acting) was performed working with 88.24 mM and 176.47 mM H₂O₂.

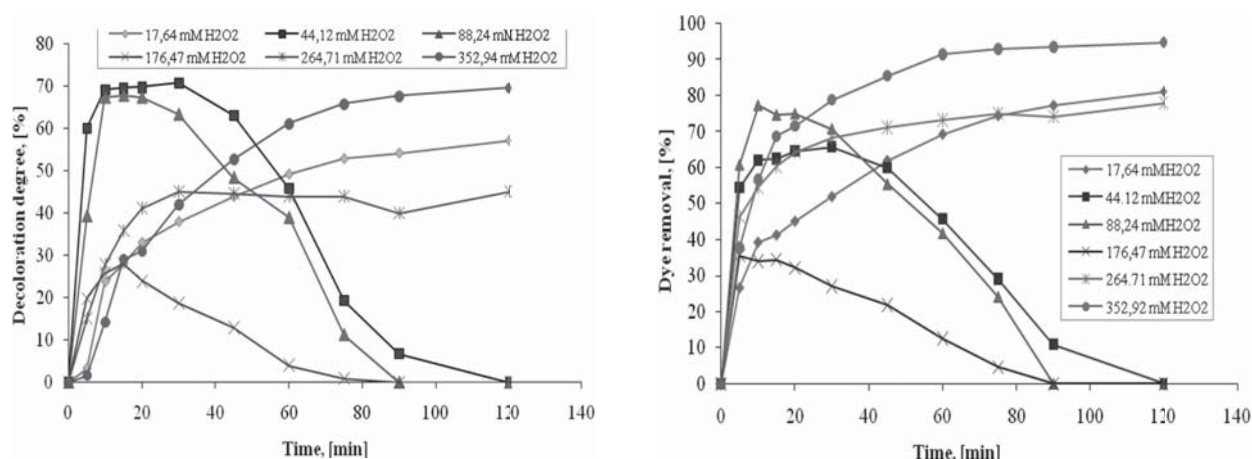


Figure 2. H_2O_2 dose influence vs. homogenous FO process kinetic and performance of Remazol Rosso RB dye solution (pH 7.745): (a) discoloration degree and (b) dye removal.

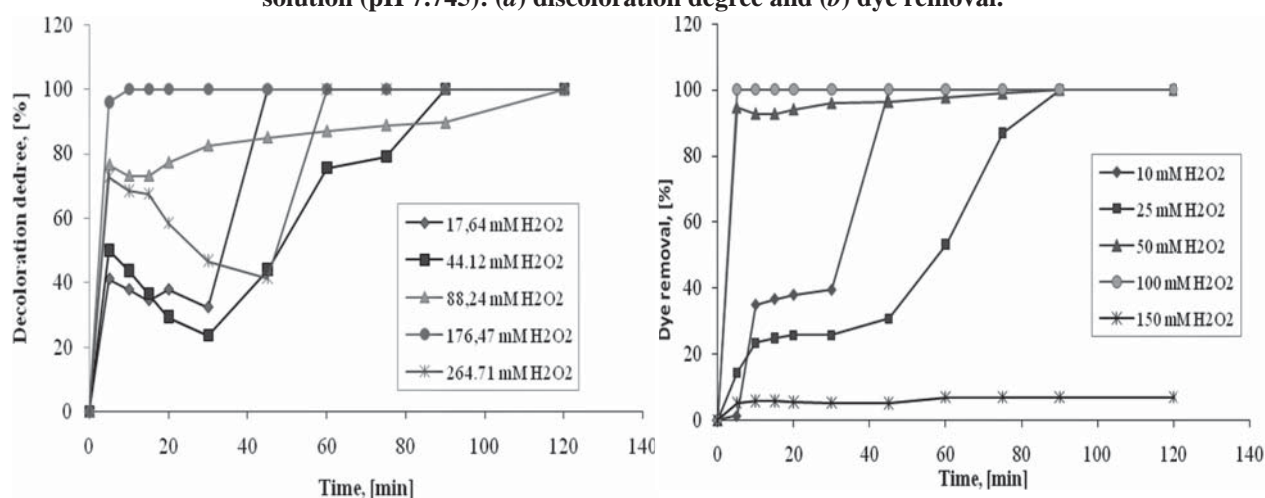


Figure 3. H_2O_2 dose influence vs. homogenous FO process kinetic and performance of Remazol Rosso RB dye solution (pH 5.16): (a) discoloration degree and (b) dye removal.

Ferrous Ions-Based Catalyst Influence in FO Process

Some kinetic experiments of homogenous Fenton oxidation process were performed with 50 mg/L-dye containing solutions, 120 min-working with 176.47 mM H_2O_2 and different $FeSO_4$ doses, at pH (5.13-5.16), room temperature (20°C), under continuous stirring (30 rpm), and the results are presented in Figure 4 (a, b).

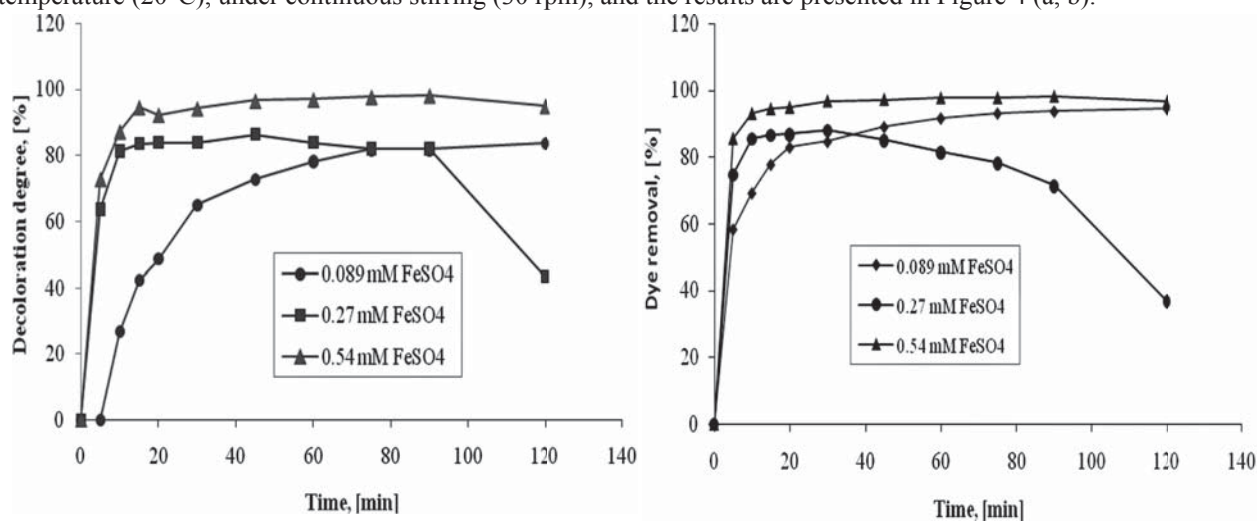


Figure 4. Ferrous catalyst dose influence vs. homogenous FO process kinetic and performance of Remazol Rosso RB dye solution (pH 5.16): (a) discoloration degree and (b) dye removal.

It seems that some increasing rates of FO process appear with ferrous catalyst concentration increases (adequate concentration range of 0.18-0.54 mM FeSO_4 at pH of 5.16). Higher ferrous catalyst concentration faster dye FO rate (more radical species formed), especially in the first FO period of (5-20 min) (*i.e.* discoloration of 81.25%-87.17% after 10 min of dye FO with 0.27 mM and 0.54 mM FeSO_4 , respectively). The treated aqueous solution can be discharged in natural receptor or urban sewerage system having admissible values of total iron concentration < 0.5 -1 mg/L, or mainly inside reuse.

The dye removal is rapid in the first 10-20 min and after a slow increasing progress until the maximal value of 86.33-98.05% in the range of 0.089-0.54 mM FeSO_4 . A little different behavior is remarked for a dose of 0.27 mM FeSO_4 , meaning a sharply increasing in the first 10 min followed by decreasing until 43.36% for discoloration degree, and 36.75% for dye removal after 120 min, respectively.

Temperature and Oxidation Time Influence in FO Process

The influence of temperature in dye FO oxidation is investigated at neutral (7.47-7.745) and low acid pH (5.13-5.16) in terms of discoloration degree or dye removal by performing some kinetic experiments with 50 mg/L dye, working with 88.24 mM H_2O_2 , 0.18 mM FeSO_4 , the results being illustrated in Figure 5 (a, b).

Higher part of discoloration or dye removal was rapidly performed in the first 5-30 min, but the maximal or complete discoloration after more than 60 min.

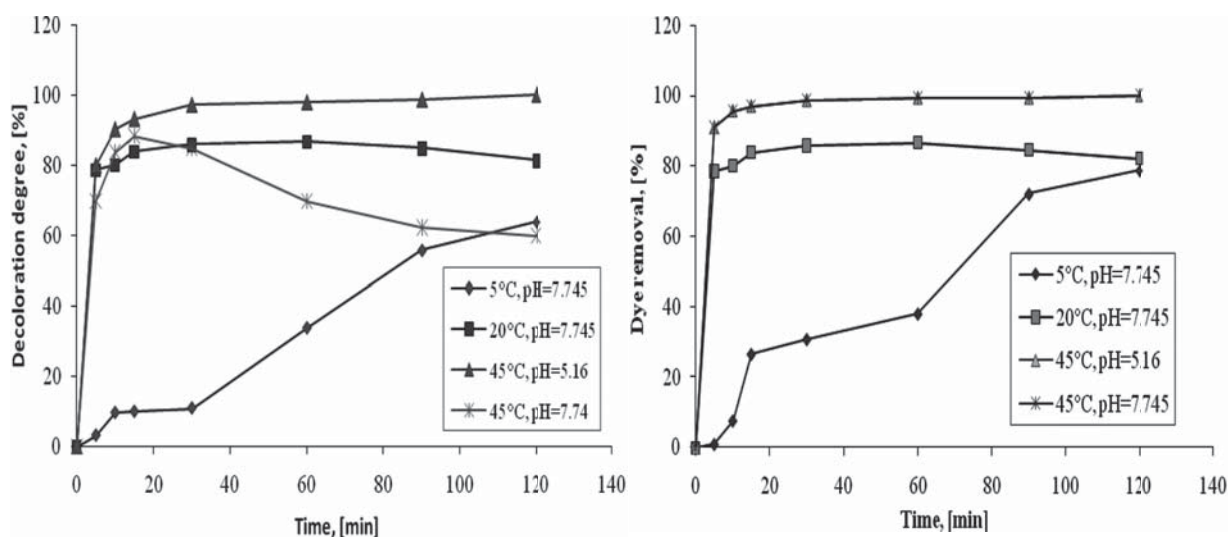


Figure 5. Temperature influence vs. homogenous FO process kinetic and performance of Remazol Rosso RB dye solution: (a) discoloration and (b) dye removal.

The dye FO kinetic results applied in the mentioned operating conditions (88.24 mM H_2O_2 , 0.18 mM FeSO_4 , pH 7.745 or 5.16, different temperatures, continuous stirring) were shown that the best performances were achieved at pH 5.16 and high temperature (45°C) for both discoloration degree and dye removal (100% after 15 min). Moreover, after only 15 min of FO process, there were performed discolorations and dye removals higher than 80% at pH 5.16 and 7.745 at 20° and 45°C, respectively.

These results indicated that even in cool season condition (5°C), the ferrous-based Fenton oxidation process can be achieved for aqueous solutions containing 50 mg/L Remazol Rosso RB azo dye.

Stirring Regime Influence in FO Process

Some kinetic experiments of homogenous Fenton oxidation process were performed with 50 mg/L-dye solutions, 120 min-working with 88.46 mM H_2O_2 and 0.18 mM FeSO_4 , at pH (5.16 and 7.745), room temperature (20°C), under continuous stirring (30 rpm) or without stirring.

The results are shown in Figure 6 (a, b), indicating that FO rate is increasing in time but a sharp increasing is registered only in the first 10-15 min, and after low increasing occurred.

In general, it seems that the continuous stirring with low rate (30 rpm) is beneficial for increasing of discoloration degree and dye removal, *i.e.* 26.566% at 5°C, 83.903% at 20°C, or 97.00% at 45°C after only 15 min of advanced FO oxidation, with maximal performance of 78.746% at 5°C, 82.11% at 20°C, and 100% at 45°C after 120 min. The treated dye solution can be safely discharge in any kind of aquatic receptor or urban sewerage system but mainly inside reuse, if necessary (the final pH value is not in the admissible range of 6.50-8.50), a neutralization stage is needed.

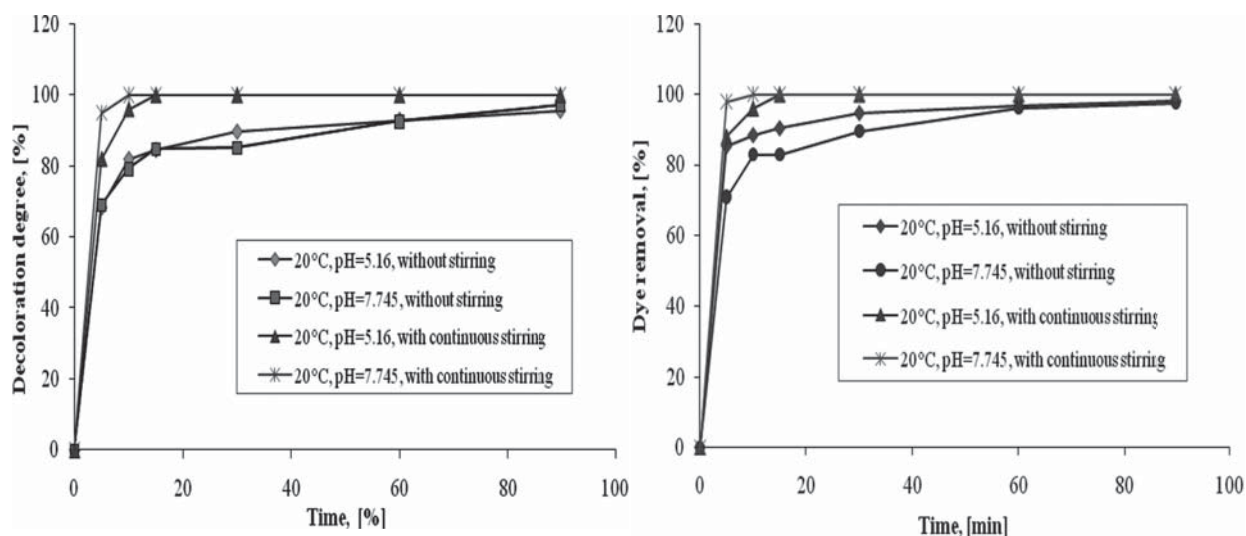


Figure 6. Stirring regime influence vs. homogenous FO process kinetic and performance of Remazol Rosso RB dye solution (pH 7.745, and 5.16): (a) discoloration degree and (b) dye removal.

Conclusions

The Remazol Rosso RB azo dye can be eliminated from aqueous systems by advanced ferrous-based Fenton oxidation processes (*i.e.* dye removal > 90%, even complete discoloration in specific operating conditions).

The influence of some FO operating parameters was investigated, *i.e.* pH, H_2O_2 and ferrous-based catalyst dose, temperature, operating oxidation time and stirring regime, for discoloration of 50 mg/L dye-containing solution. The recommended values for H_2O_2 and ferrous-based catalyst doses are 88.24–176.47 mM H_2O_2 and 0.36–0.54 mM $FeSO_4$ at a pH of 5.16, or 7.745, and temperature of 20°C.

The dye Fenton oxidation is indicated to be performed in low acidic conditions (*i.e.* 5.10–5.16) at room temperature, but good results (>70%) can be obtained also at pH 7.47–7.745 with no necessity of additional neutralization step (in rest, the dye oxidation rate diminished; changing of homogeneous Fenton oxidation type with competitive Fenton-like oxidative processes).

The advanced ferrous-based catalytic oxidation with hydrogen peroxide can be considered suitable treatment for discoloration purposes of industrial effluents, if the optimal operating conditions were established.

References

1. Anjaneyulu, Y.; Sreedhara, C.N.; Raj, D.S.S. Decolourization of Industrial Effluents – Available Methods and Emerging Technologies – A Review. *Reviews in Environmental Science and Bio/Technology*, 2005, 4, pp. 245–273.
2. Baban, A.; Yediler, A.; Ciliz, A.K. Integrated Water Management and CP Implementation for Wool and Textile Blend Processes, *Clean*, 2010, 38, pp. 84–90.
3. Meriç, S.; Kaptan, D.; Ölmez, T. Color and COD Removal from Wastewater Containing Reactive Black 5 Using Fenton's Oxidation Process, *Chemosphere*, 2004, 54, pp. 435–441.
4. Luo, Q. Oxidative Treatment of Aqueous Monochlorobenzene With Thermally-Activated Persulphate, *Frontiers of Environmental Science and Engineering*, 2014, 8(2), pp. 188–194.
5. Zaharia, C.; Suteu, D.; Muresan, A. Options and Solutions for Textile Effluent Decolourization Using Some Specific Physico-Chemical Treatment Steps, *Environmental Engineering and Management Journal*, 2012, 11(2), pp. 493–509.
6. Zaharia, C.; Luca, C.M.; Romaşcanu, A. Discoloration study of Remazol Arancio 3R azo dye from aqueous solutions by homogeneous Fenton-like oxidative processes, *Bul. Inst. Polit. Iaşi*, 2013, tom LIX (LXIII), f. 4, pp. 83–93.
7. Zaharia, C.; Dârţu, E.L. Preliminary Study of Decolourization of Some Textile Effluents by Homogenous Oxidative Processes. *Bul. Inst. Polit. Iaşi, s. Chemistry and Chemical Engineering*, 2010, tom LVI (LX), f. 4, pp. 63–71.
8. Zaharia, C.; Şuteu, D.; Mureşan, A.; Mureşan, R.; Popescu, A. Textile Wastewater Treatment by Homogenous Oxidation with Hydrogen Peroxide, *Environmental Engineering and Management Journal*, 2009, 8(6), pp. 1359–1369.

RADIATION CHEMICAL CONVERSION OF OIL DERIVED FROM OIL-BITUMEN ROCK

Lala Jabbarova^a, Islam Mustafaev^a, Rauf Rzayev^{a*}, Zarqalam Nabizade^a,
Navoi Ibadov^a, Saida Akhmedbekova^b

^a*Institute of Radiation Problems, National Academy of Sciences of Azerbaijan, 121, H. Javid ave., Baku AZ 1143, Azerbaijan*

^b*Institute of Petrochemical Processes, National Academy of Sciences of Azerbaijan, 30, N. Rafiev str.,
Baku AZ 1025, Azerbaijan*

*e-mail: r_rzayev80@mail.ru; Clala@mail.ru

Abstract. The results of research in the radiation processing of synthetic oil derived from oil-bitumen rock of the Balakhany deposit in Azerbaijan are presented. The study has been conducted on a ⁶⁰Co gamma-source at a dose rate of $P = 0.5$ Gy/s and various absorbed doses of $D = 43\text{--}216$ kGy. Samples of synthetic oil from natural bitumen rocks have been analyzed by chromatography, gas chromatography-mass spectrometry, and IR-spectroscopy, and their radiation resistance has been evaluated. The results of the study allow for both assessment of the feasibility of manufacturing petrochemicals for various applications by radiation processing and use of these materials for isolating radioactive sources to preclude their impact on the environment.

Keywords: oil-bitumen rock, synthetic oil, oxygen, hydrocarbon gases, radiation.

Introduction

Oil-bitumen rock (OBR) is a natural material formed from crude oil in the upper layers of the Earth crust as a result of the slow evaporation of light fractions from the oil, natural oil deasphalting, and the processes of interaction of its components with oxygen and sulfur. According to United Nations estimates, the world's geological reserves of OBR amount to ~360 billion tons on the hydrocarbon (HC) basis and are an alternative source of HC feedstock [1].

Large OBR accumulations were found in Canada, the United States, and the CIS countries. The reserves in Azerbaijan make 200 million tons in 11 deposits [2, 3].

In Russia there are 400 OBR deposits with total reserves of 7.2 billion tons. The total world production of oil from OBR is about 84 mb/d (million barrels per day). In Canada, there are plants for oil extraction from oil sands, one of which has a daily output of more than 140 thousand barrels of oil [4].

Experimental

The object of investigation was the synthetic oil derived from OBR of the Balakhany field of Azerbaijan. Experiments were carried out on an MRKh γ -30 ⁶⁰Co gamma-ray source at a dose rate of 0.5 Gy/s. By distillation in a Retort Heating Jacket apparatus at a temperature of 950 F (510°C), 50 mL of synthetic crude was obtained from 375 g. The rock composition (%) was as follows: oil 22, water 6, sand 72.

Samples of synthetic oil were irradiated to different absorbed doses in the range of 43–216 kGy in air or vacuum to follow the kinetics of the processes and to reveal the role of oxygen in the radiation resistance of the OBR. The samples of the synthetic oil intended for chromatographic analysis were dried with anhydrous sodium sulfate (Na₂SO₄) and diluted with dichloromethane (CH₂Cl₂); mass chromatograms in the m/z range of 35–400 (m/z is the ion mass to charge ratio) were recorded on a GCMS Trace DSQ instrument (Thermo Electron, Finnigan USA, 2005).

The sample notation was as follows: 12169, the initial synthetic oil; 12170, the synthetic oil irradiated for 96 h in air; and 12171, the synthetic oil irradiated for 96 h in a vacuum.

IR spectra of the samples were recorded on an M-80 spectrophotometer in the wave number range of 700–4000 cm⁻¹. The gaseous products were analyzed by gas chromatography.

Results and discussion

The components identified in the unirradiated synthetic oil are shown in Table 1.

The unirradiated oil samples predominately contain relatively light hydrocarbons, such as undecane, dodecane, tridecane, tetradecane, and hexadecane. After irradiation, an increase of the peak heights of heavier hydrocarbons, such as eicosane, allopregnane, and octadecane, is observed. This is due to the occurrence of complex radiation induced processes of polycondensation and rearrangement in the molecular structure of the synthetic oil.

The effect of γ -radiation on the structural group composition of the samples of synthetic bituminous oil was investigated.

Table 1

Liquid full scan.

No.	Component elution time, min	Identified components of initial synthetic oil	Formula
1	4.17	Toluene	C ₇ H ₈
2	7.37	p-Xylene	C ₈ H ₁₀
3	7.79	cis-2-Nonene	C ₉ H ₁₈
4	8.02	Nonane	C ₉ H ₂₀
5	9	Octane, 2,6-dimethyl-	C ₁₀ H ₂₂
6	9.65	1-Octyn-3-ol, 4-ethyl-	C ₁₀ H ₁₈ O
7	10.09	Benzene, 1-ethyl-3-methyl-	C ₉ H ₁₂
8	10.56	Benzene, (1-methylethyl)-	C ₉ H ₁₂
9	10.74	1-Decene	C ₁₀ H ₂₀
10	10.92	Decane	C ₁₀ H ₂₂
11	11.31	1-Octanol, 2-methyl-	C ₉ H ₂₀ O
12	11.75	Benzene, 1-ethyl-4-methyl-	C ₉ H ₁₂
13	13.3	1-Undecanol	C ₁₁ H ₂₄ O
14	13.46	Undecane	C ₁₁ H ₂₄
15	14.67	Undecane, 6-methyl-	C ₁₂ H ₂₆
16	14.93	Benzene, 1,2,4,5-tetramethyl-	C ₁₀ H ₁₄
17	15.58	Cyclopropane, nonyl-	C ₁₂ H ₂₄
18	15.73	Dodecane	C ₁₂ H ₂₆
19	15.97	Undecane, 2,6-dimethyl-	C ₁₃ H ₂₈
20	17.67	1-Tridecene	C ₁₃ H ₂₆
21	17.8	Tridecane	C ₁₃ H ₂₈
22	18.81	1-Pentadecanol	C ₁₅ H ₃₂ O
23	18.92	Cyclohexanol, 5-methyl-2-(1-methylethyl)-, [1R-(1à,2à,5à)]-	C ₁₀ H ₂₀ O
24	19.64	1-Tetradecene	C ₁₄ H ₂₈
25	19.75	Tetradecane	C ₁₄ H ₃₀
26	20.73	Naphthalene, 2,7-dimethyl-	C ₁₂ H ₁₂
27	20.81	Tetradecane, 2,6,10-trimethyl-	C ₁₇ H ₃₆
28	21.45	2,6-Dodecadien-1-ol, 3,7,11-trimethyl-, (E,E)-	C ₁₅ H ₂₈ O
29	21.58	Pentadecane	C ₁₅ H ₃₂
30	21.92	1H-Indene, 2,3,3a,4,7,7a-hexahydro-2,2,4,4,7,7-hexamethyl	C ₁₅ H ₂₆
31	22.64	Naphthalene, 1,6,7-trimethyl-	C ₁₃ H ₁₄
32	23.19	1-Hexadecanol	C ₁₆ H ₃₄ O
33	23.29	Hexadecane	C ₁₆ H ₃₄
34	24.84	1-Heptadecanol	C ₁₇ H ₃₆ O
35	24.92	Heptadecane	C ₁₇ H ₃₆
36	26.4	8-Heptadecene	C ₁₇ H ₃₄
37	26.47	Octadecane	C ₁₈ H ₃₈
38	27.95	Nonadecane	C ₁₉ H ₄₀
39	29.37	Eicosane	C ₂₀ H ₄₂
40	30.49	Octadecane, 3-methyl-	C ₁₉ H ₄₀
41	30.72	Heneicosane	C ₂₁ H ₄₄
42	32.74	Allopregnane	C ₂₁ H ₃₆
43	33.26	Octadecane, 3-ethyl-5-(2-ethylbutyl)-	C ₂₆ H ₅₄

The IR spectrum of the synthetic oil (initial) displayed an absorption band at 740 cm⁻¹ due to rocking vibration of the -CH₂ group and the 1380 cm⁻¹ bending and 2860 and 2960 cm⁻¹ stretching bands characteristic of the methyl group CH₃. The spectrum also contains bands characteristic of the =CH₂ group and the C=C bond of unsaturated hydrocarbons, corresponding to out-of-plane bending vibrations of the substituted benzene ring. The absorption band at 1720 cm⁻¹ corresponds to the carbonyl group C=O. In addition, there are absorption bands in the region of 1020–1160 cm⁻¹ with maxima at 1025, 1070, 1120, and 1160 cm⁻¹ corresponding to oxygen containing groups (C–O-, C–O–O-, O–H). Owing to the long-term occurrence in the environment, the bitumen rock has a high concentration of oxygenated compounds.

The presence of these reactive groups determines a higher adhesive strength of the binding components with the rock (adhesive properties) as compared with manmade compositions based on petroleum refining products; however, they are easily cleaved by irradiation. Irradiation reduces the concentration of oxygen containing groups as a result of their transfer to the heavier fractions.

The IR spectra of the synthetic oil derived from the bitumen rock are given in Figure 1. A comparison of the IR spectra of the samples (irradiated in air for 72 and 120 h) with the spectrum of the initial material shows that the intensities of the absorption bands of paraffinic, unsaturated, and aromatic hydrocarbons and oxygenated compounds are significantly reduced in the following order: unirradiated oil > oil irradiated in air for 72 h > oil irradiated in air for 120 h. As the absorbed dose increases, the optical density at the absorption bands of functional groups in the samples also decreases. The spectroscopic analysis data are presented in Figure 2.

To study the radiation resistance of BR, the samples of the synthetic oil were irradiated with absorbed doses of 43–216 kGy at a ^{60}Co γ -ray dose rate of $P = 0.5$ Gy/s. The rate curves of gas buildup during the γ -radiolysis of synthetic oil recovered from natural oil-bitumen rocks are given below in Figure 3.

For all the gases, oxygen enhances the radiation-chemical degradation of the synthetic oil, an effect that is associated with oxidative degradation reactions involving radiolytic radicals. This oil is characterized by a high concentration of cyclic structures, particularly aromatics, concentrated in middle distillates.

The average values of the radiation-chemical yield (molecule/100 eV) of gases from the synthetic bituminous oil are listed in Table 2.

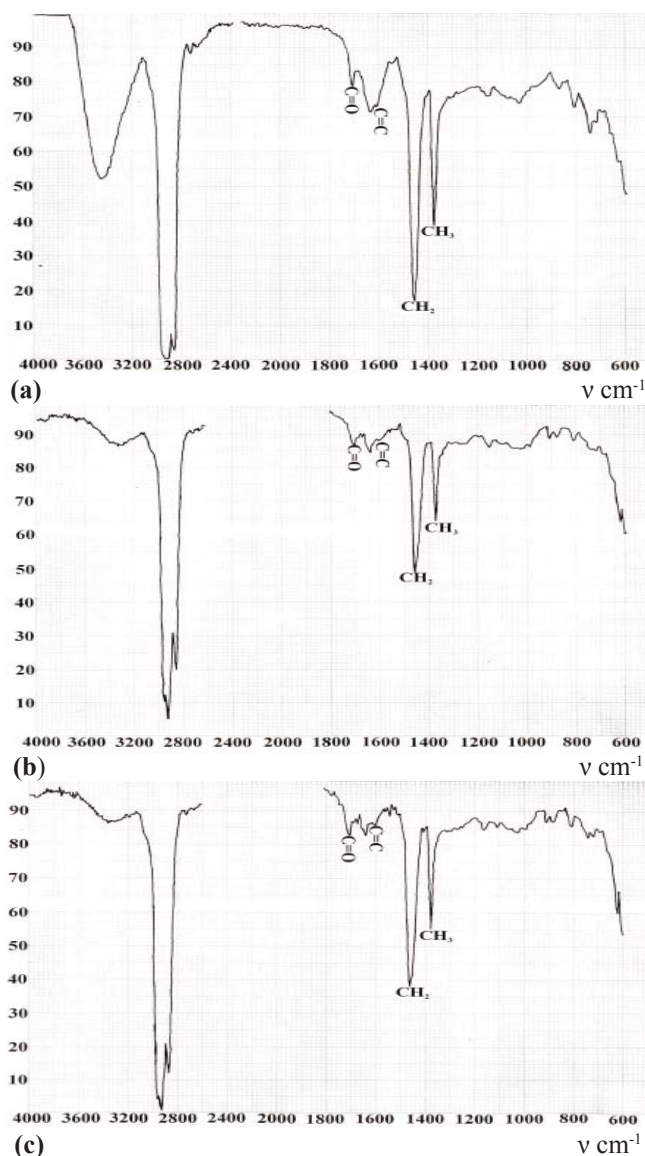


Figure 1. IR spectra of synthetic oil recovered from the bituminous rock: (a) the initial synthetic oil; and (b, c) the synthetic oil irradiated in air for 72 and 120 h, respectively.

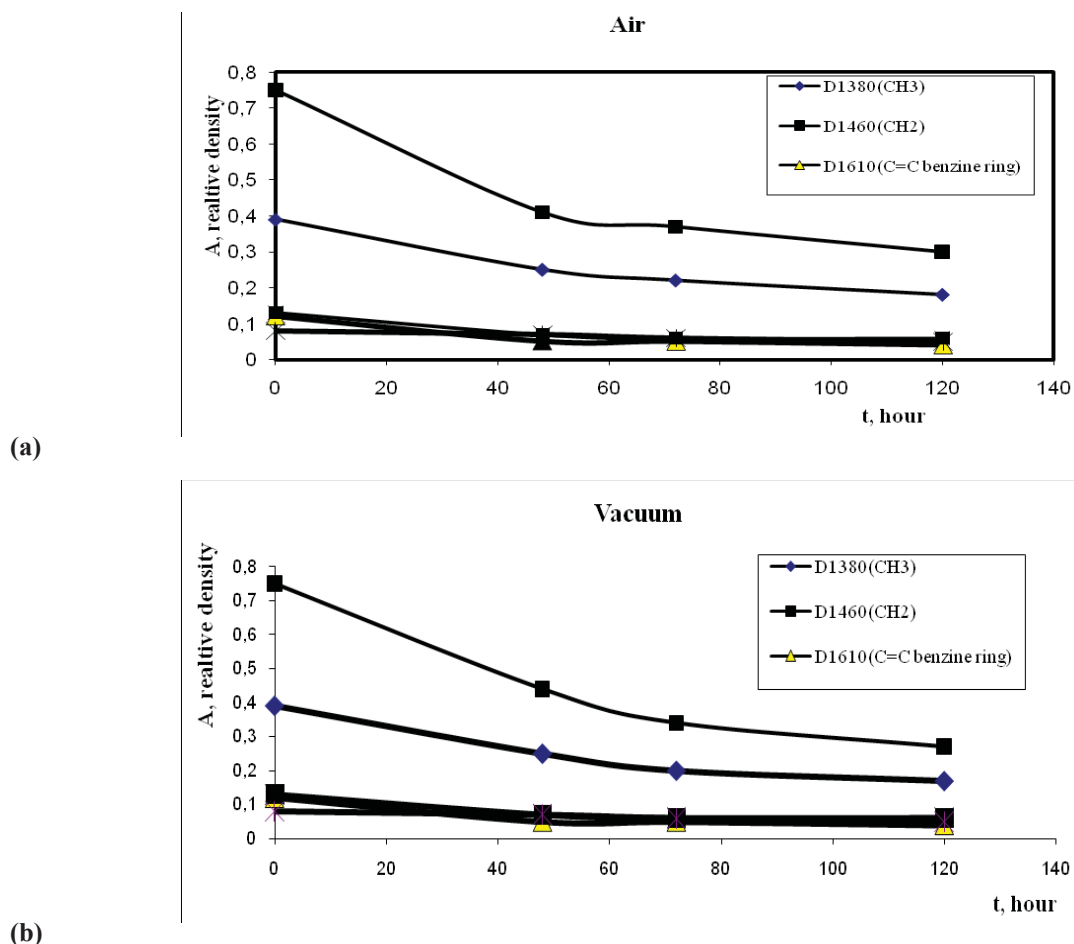


Figure 2. Dependence of the absorbance of samples of the synthetic oil recovered from the bituminous rock on the absorbed dose in (a) air and (b) vacuum.

Table 2

Average values of the radiation-chemical yield (molecule/100 eV) of gases from synthetic bituminous oil.

Average radiation-chemical yield of gas from BR synthetic oil (molecule/100 eV)	H ₂	CO	CO ₂	CH ₄	C ₂ H ₆	C ₂ H ₄	C ₃	C ₄	C ₅	C ₆	C ₇
air	0.31	0.85	0.66	0.06	0.05	0.024	0.13	0.33	0.32	0.16	0.04
vacuum	0.37	0.26	0.67	0.03	0.02	0.005	0.014	0.022	0.176	0.13	0.06

It should be noted that paraffinic and polycyclic aromatic hydrocarbons exhibit a relatively high stability against radiation. However, functional groups (especially, oxygen containing groups) and olefins have a low radiation resistance. The stability of these organic compounds towards radiation depends on their excitation and ionization potentials. In the presence of polyconjugated aromatic structures, the none of the vibrational degrees of freedom gets a sufficient energy for breaking chemical bonds. The energy can also be dissipated before the decomposition of the molecule [5]. The irradiation of these samples in an air medium leads to slight enhancement of the degradation process, but the product yields remain relatively low. In order to increase the radiation chemical yield of gases and ensure the chain mechanism of degradation of hydrocarbons in such systems, it is necessary to apply a high temperature. At elevated temperatures, the substrate degradation processes proceed effectively owing to abstraction reactions involving radiolytic hydrocarbon radicals. In the case of joint heat and radiation treatment, in order to preclude the recombination processes of chain termination, it is necessary to choose appropriate temperature and dose rate at which the radiation effect is maximal [6].

Conclusions

The relatively high radiation resistance of the synthetic oil, recovered from the OBR, in vacuum and air below 50°C is associated with the presence of paraffins, polynuclear aromatic hydrocarbons, and resin asphaltene substances in its composition. This makes it possible to use the synthetic oil as a feedstock for manufacturing a waterproof material applicable in radiation fields, including the disposal of radioactive waste. The organic matter of the OBR may serve as a promising source material for manufacturing various fuels, lubricating oils, coke, and asphalt. Hydrogen, hydrocarbon gases, and olefin hydrocarbons can be produced from the synthetic oil by the joint ionizing radiation and heat treatment at consistent values of the temperature and the dose rate.

References

1. Golberg, I.S. Proceedings of All Union Meeting on Comprehensive Processing and Use of Bituminous Rocks, Alma-Ata: Nauka, 1982, pp. 48-54 (in Russian).
2. Oil Sands and Oil Shales of Azerbaijan: Collection of Articles of Institute of Geology, National Academy of Sciences of Azerbaijan, Baku: Elm, 1990, pp. 149-157 (in Russian).
3. Nadirov, S.G.; Aliev, G.M. Proceedings of All Union Meeting on Comprehensive Processing and Use of Bituminous Rocks, Alma-Ata: Nauka, 1982, 116 p. (in Russian).
4. Devlikamova, V.V.; Khabibulin, Z.A. Abnormal Crude Oils, Moscow: Nedra, 1975, 198 p. (in Russian).
5. Pikaev, A.K. Modern Radiation Chemistry. Radiolysis of Gases and Liquids, Moscow: Nauka, 1986, 440 p. (in Russian).
6. Jabbarova, L.Y. Radiation–thermal transformations of bituminous rocks, Ph.D. Thesis, Institute of Radiation Problems, Baku, Azerbaijan, 2007.

THE DIMINISHING OF THE CONTENT OF TEXTILE DIRECT DYES AND AUXILIARY COMPOUNDS DURING THEIR CATALYTIC OXIDATION

Maria Gonta^{a*}, Gheorghe Duca^b, Vera Matveevici^a, Larisa Mocanu^a

^aMoldova State University, 60, Alexei Mateevici str., Chisinau MD-2009, Republic of Moldova

^bAcademy of Sciences of Moldova, 1, Stefan cel Mare blvd., Chisinau MD-2001, Republic of Moldova

*e-mail: mvgonta@yahoo.com; phone: (+373 22) 57 75 53; fax: (+373 22) 57 75 53

Abstract. Advanced oxidation methods of organic compounds lead to their partial mineralization and increase of the adsorption process efficiency on the surface of oxidized activated carbon. We have studied the oxidation process using model solutions containing mixture of dye direct brown (DB), ethylene glycol (EGL) and sodium lauryl sulfate (SLS) under the action of Fenton reagent, in the presence and absence of UV irradiation or under the action of electric current (in the electrochemical cell). The same studies were performed by replacing the iron (II) ion with titanium dioxide. We have found that the degree of oxidation and mineralization increases by photocatalytic oxidation and decreases the concentration of organic compounds. Due to the oxidation of dye molecules and other auxiliary components, by strong oxidation ability of free OH* radicals, which evolve to the formation of carbon dioxide, water and low molecular organic compounds (alcohols, ketones, organic acids) are forming. The decrease of the concentration of mixture of organic compounds (for the values of COD-Cr) depends on the nature of catalysts and the presence of electric current. The degree of oxidation is greater in the presence of iron (II) ions than in the presence of titanium dioxide after oxidation of the mixture of organic compounds with hydrogen peroxide in model solutions. This is explained by the fact that UV irradiation increases the concentration of free OH* radicals as iron ions further decompose hydrogen peroxide, but in the presence of titanium dioxide, the leading band electrons are accepted by free OH* radicals, converting these radicals to ions, as shown in the mechanism by Garcia J., et al. This leads to a decrease of the concentration of OH* radicals in model solution and reducing the effect of oxidation, respectively. On the contrary, in the presence of electric current electrons are accepted by the electrode, and the OH* radicals concentration does not decrease, but increases, and this leads to the enhancement of the oxidation effect and mineralization of organic compounds.

Keywords: disperses dye, anionic surfactant, textile wastewater, chemical and electrochemical oxidation, adsorption, TiO₂, ZrO₂.

Introduction

The main pollutants in waste waters generated during the technologic coloring of different types of fabrics are diverse classes of dyes as well as auxiliary compounds such as surfactants, polyalcohols, dye fixing agents and others.

Dyes and surfactants are chemically stable compounds that hardly interact with oxidants and cannot be treated by biochemical processes. As a result of discharge into natural water bodies, the disturbance of self-purification processes takes place while the water becomes toxic for water inhabitants. The removal of residues of dyes and surfactants as well as the compliance with sanitary norms is achieved through application of combined methods of treatment that ensure a better oxidation, retention and elimination of pollutants [1]. The methods described in literature [2] refer to adsorption of surfactants by activated charcoal or other synthetic brands of natural adsorbents. The combined processes of treatment of surfactants [1] by means of extraction through flotation and further degradation during the second phase of treatment were investigated as well.

The advanced oxidation methods applied till present rely on degradation of organic compounds into more simple ones or their oxidation with formation of carbon dioxide and water. These pollutants are degraded by OH· radicals obtained from photochemical decomposition of hydrogen peroxide [3-8]. Due to hydrogen peroxide decomposition the concentration of OH radicals increases, which respectively increases the rate of oxidation and mineralization of both dyes and surfactants. The rate of oxidation and mineralization is influenced largely by the length and structure of hydrophobic or hydrophilic radicals generated by molecules of surfactant or colorings agents and by the structure of dyes. The increase of the length of hydrocarbon radicals and of the polarity of hydrophilic groups causes the increase of the ratio of oxidation and mineralization. The degree of mineralization of surfactants can reach 60.0-80.0% [8]. However the removal of surfactants from waste waters from textile industry is impaired by the simultaneous presence of textile dyes and their stabilization by other auxiliary substances that are used in the technological process of coloring of textiles. Application of adsorption methods of removal by activated charcoals is limited due to inefficient removal of only 2.0-4.0% of surfactants and dyes due to the limited access of associated particles of pollutants to micropores and mesopores [9]. That is why in the first phase of treatment of textile waste waters the coagulation with iron and aluminum salts most often is used. This process consists of iron and aluminum salts dissolution and formation of colloidal particles that are capable to neutralize and sediment surfactants and dyes. The next phases of treatment are applied depending on the chemical oxygen demand, which depends on the remaining pollutants.

Consequently, the process of treatment and purification of residual waters is a complex task that can be solved only through efficient combined mechanical, chemical, physicochemical and biological methods.

The above mentioned task was addressed through a study of removal of textile coloring mixtures and auxiliary substances through catalytic and photocatalytic oxidation with hydrogen peroxide followed by absorption of residues on activated charcoals depending on the concentration direct dyes, time of catalytic oxidation in the presence of iron (II) ions, titan oxide and zirconium oxide. The mixture was irradiated with UV rays with or without application of electric current.

Experimental laboratory investigations were determined by the increased interest in environmental protection from developing industries. In the Republic of Moldova the problem of efficient purification of wastewaters from textile industry that are discharged in natural water bodies is still not properly solved. It is still necessary to investigate the oxidation of pollutants in systems that simulate the real concentrations of dyes and auxiliary substances. However, literature refers predominantly to treatment of dyes containing methylene blue and methylene orange that have a simple molecular structure and their concentration in solutions is lower than 60 mg/L, and time of treatment is about 4 hours.

Experimental

The reagents were pure for analysis grade and were acquired from Aldrich Company and other providers.

Chemical processes of removal of colorants and auxiliary substances

Chemical and electrochemical methods of advanced oxidation in the presence of catalysts such as Fenton reagent, $\text{TiO}_2/\text{H}_2\text{O}_2$, $\text{ZrO}_2/\text{H}_2\text{O}_2$, UV irradiation at 254, 365 nm were applied.

The investigations were carried out on simulation solutions with 50, 100 and 200 mg/L of colorants, because the range of concentrations of residues in wastewaters can reach 200-250 mg/L.

A mixture of chemical organic compounds consisted of direct textile dye (direct brown (DB)), tensioactive substance (anionic surfactant – sodium lauryl sulfate) and polyalcohol (ethylene glycol). The simulation solutions were chosen according to the content of waste waters. The initial concentration of direct dye varied within the limits from 50 mg/L till 200 mg/L, while the anionic surfactant constituted 60 mg/L.

The degree of oxidation of textile dyes and mixtures of colorants with surfactants and ethylene glycol were determined according to the COD-Cr method.

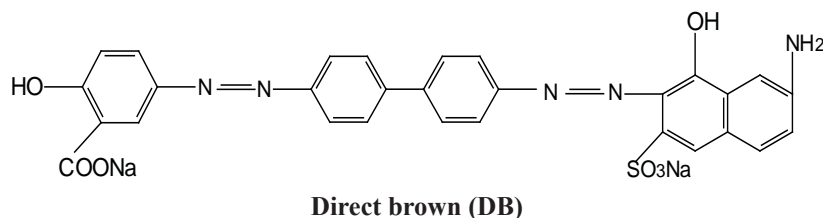
The investigation of the catalytic and photocatalytic oxidation followed by absorption of products of oxidation by activated charcoal (KAU-1) was realized according to the method described in the literature [10].

The results of catalytic oxidation in the presence of hydrogen peroxide along with Iron (II) ions and UV radiation have allowed calculation of the degree of oxidation and mineralization ($\text{Min.}, \%$) of textile dyes and mixtures investigated according to Eq.(1):

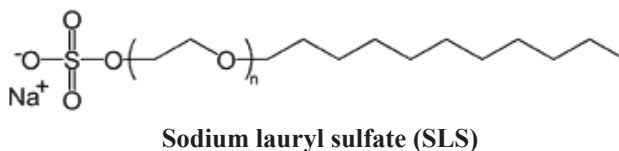
$$\text{Min, \%} = \frac{\text{COD} - \text{Cr}_0 - \text{COD} - \text{Cr}_{\text{rem.}}}{\text{COD} - \text{Cr}_0} \cdot 100\% \quad (1)$$

where $\text{COD} - \text{Cr}_{\text{rem.}}$ represents the residues of organic compounds after one hour of treatment.

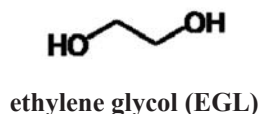
A direct textile dye, direct brown (DB), has been used in this study:



Besides textile dyes, different classes of surfactants that ameliorate the dying of textile fabrics are present in the waste waters. This work focuses also on the oxidation of anionic surfactant – sodium lauryl sulfate that has the following chemical structure:



The polyalcohols are hygroscopic and hydrosoluble compounds and have the role of fixation, dissolving and penetration of dyes into the fabrics. The polyalcohol used in current investigation is ethylene glycol (EGL), which has the following structure:



Methodology

In a 250 mL flask a solution of brown direct dye (0.5 mg/L), anionic surfactant (20 g/L) and ethylene glycol (3 g/L) were added. The final simulation solution contained 200 mg/L of colorant, along with 60 mg/L of surfactant and ethylene glycol. The pH was adjusted (Consort C 3030 pH-meter) with a solution of sulfuric acid during stirring with a WiseStir device. The process of oxidation was investigated at various concentrations of hydrogen peroxide (3×10^{-3} - 8×10^{-3} mol/L) and iron (II) ions (3×10^{-4} mol/L).

Titanium oxide and zirconium oxide powders were added the system, and UV radiation was generated by a VL-4.LC that assures two wavelengths (254 and 365 nm).

The electrochemical treatment was carried out in electrochemical cells with graphite anodes and iron mesh that covers the anode and serves as cathode. The cells were powered by electric generators TEC 14 that assured an intensity of current equal to 0.4 A. In order to launch the electrochemical oxidation 50 mL of a 0.1 mol/L sodium sulfate solution were added to the cell. The solutions were stirred permanently for 10, 20, 40 and 60 minutes on magnetic stirrers. Each consecutive stirring was followed by sampling of 5 mL of solution, that were transferred into test tubes containing 3 mL of $K_2Cr_2O_7$ (0.025 N) each, and addition of 7 mL of Ag_2SO_{4conc} .

The test tubes were covered with glass caps and placed in a heating stove (Pol-Eko, Nitech) and stored for 2 h at 150°C in accordance with the method described in [8].

The obtained solutions were tested spectrophotometrically (T60+UV/Vis) at $\lambda = 600$ nm. The obtained results were used for calculation of the degree of oxidation and mineralization (*Min.*, %, Equation 1) of textile dyes and mixtures in different conditions.

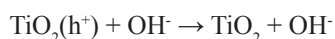
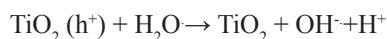
Results and discussion

The process of diminishing of the content of mixtures of direct dye and auxiliary compounds on simulation solutions was investigated in the presence of various catalysts. In order to assure the comparison of the results the oxidation of the pure compound was investigated. Figure 1 shows the oxidation of pure surfactant sodium lauryl sulfate for one hour in the presence of Fenton reagent, hydrogen peroxide and titanium dioxide powder. The optimal amounts of iron(II), hydrogen peroxide and titanium oxide were established experimentally. The analysis of results depicted from Figure 1 allow us to conclude that the process of oxidation of anionic surfactant takes place at a higher rate during the first 20 min of the experiment both in presence of iron ions as well as in the presence of titanium oxide. In both cases the chemical oxygen demand of residues is three times lower than the original concentration of substrate, while the rest of treatment time up to one hour does not affect it significantly.

After one hour of oxidation, in the second phase, the adsorption on activated charcoal was performed. The remaining compounds were again tested according to the COD-Cr procedure (4.0 – 6.0 mgO₂/L) and comply with the standards for allowed emissions in waste waters discharged into natural water bodies. The maximum allowed concentration is 6.0-7.0 mgO₂/L.

The results presented in Figure 1 prove that oxidation of the anionic surfactant sodium lauryl sulfate is more intensive in the presence of Fenton reagent than in the presence of titanium oxide.

The mechanism that describes the majority of techniques of advanced oxidation is based on generation of hydroxyl radicals (OH·) in solution. The hydroxyl radical is a strong oxidation agent that interacts non-selectively with organic compounds. The formation of OH· radicals occur as a result of irradiation with UV ($\lambda_{max} = 365$ nm) due to interactions of valence band holes with molecules of water or OH⁻ ions [10].



A decreased efficiency of catalytic oxidation in the case of application of TiO_2 powder (500 mg/L) is caused by the adsorption of surfactants on the surface of the catalysts, thus blocking the active catalytic centers.

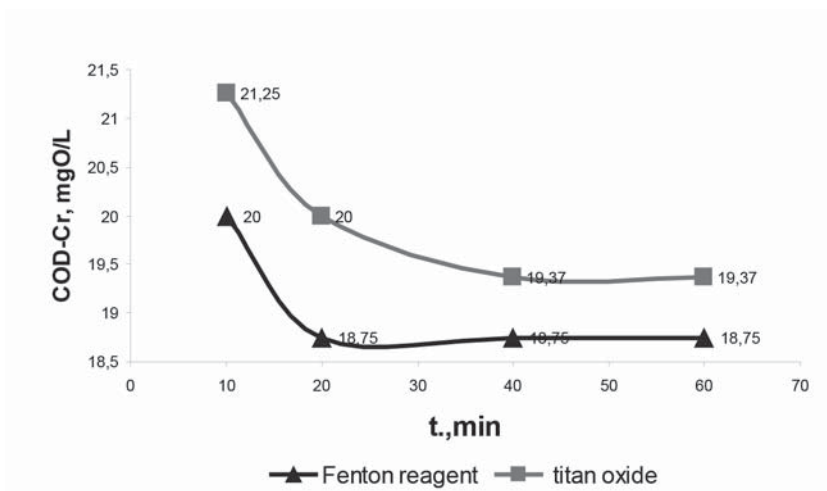
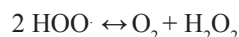
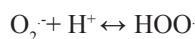
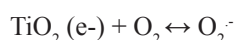


Figure 1. Efficiency of catalytic oxidation in the case of application of TiO_2 powder and reagent Fenton.
 $[\text{anion.surf.}] = 60 \text{ mg/L}$, $[\text{H}_2\text{O}_2] = 3 \times 10^{-3} \text{ mol/L}$, $[\text{Fe}^{2+}] = 3 \times 10^{-4} \text{ mol/L}$, $\text{pH} = 2.0-2.5$, $[\text{TiO}_2] = 500 \text{ mg/L}$, $\text{pH} = 4.0$,
 $\lambda = 365 \text{ nm}$, $\text{COD-Cr}_0 = 75 \text{ mgO}_2/\text{L}$.

The mechanism of photocatalytic degradation in the presence of titanium oxide involves as well formation of superoxide radicals. Due to interactions between O_2 and electrons generated by photons in the conduction band the $\text{O}_2^{\cdot-}$ radicals are formed which act as oxidants in reactions with pollutants [10]:



The degree of mineralization of anionic surfactant SLS after 60 min of oxidation is $18.75 \text{ mgO}_2/\text{L}$ in case of Fenton reagent and $19.37 \text{ mgO}_2/\text{L}$ for TiO_2 . It has been found that during photochemical treatment in the presence of selected catalysts does not achieve the maximum admissible concentration according to COD-Cr. Further, it was studied the adsorption process of remanent compounds from preliminary reactions on active charcoal and results have been reached MAC for COD-Cr.

During the treatment of direct dye the TiO_2 and ZrO_2 catalysts were used. The aquatic solutions were irradiated at $\lambda_{\text{max}} = 365 \text{ nm}$ in the presence of H_2O_2 with a concentration of $3 \times 10^{-3} \text{ mol/L}$. The concentration of the dye in the system consisted 200 mg/L . At concentrations equal to 50 and 100 mg/L the process of advanced oxidation is complete. However, the concentration of textile dye in wastewaters is significantly higher.

The initial COD-Cr level for the investigated system constituted $220 \text{ mgO}_2/\text{L}$. During the first 10 min an intensive process of DB oxidation takes place: in the case of TiO_2 the COD-Cr diminishes down to $59.38 \text{ mgO}_2/\text{L}$, while for ZrO_2 a more advanced decrease down to $28.75 \text{ mgO}_2/\text{L}$ is observed (Figure 2).

In order to determine the efficiency of catalytic oxidation of organic compounds the Equation 1 for assessment of the degree of mineralization was used.

The results presented in Figure 2 show that in the cases of systems with titanium oxide the oxidation of DB occurs at a lower rate in comparison with oxidation catalyzed by zirconium oxide.

The rinsing cycle of fabrics that follows the process of dyeing requires application of auxiliary components including active surfactant agents and organic solvents. Additionally, optional ingredients such as thick co-emollients and ether oils can be added. The emollient (organic solvent) is constitutes 40% by weight of the fixation microemulsions. The organic solvents added include aliphatic alcohols that have between 1 and 6 atoms of carbon, or aliphatic polyalcohol compounds such as ethylene glycol, polypropylene- and butylene glycol.

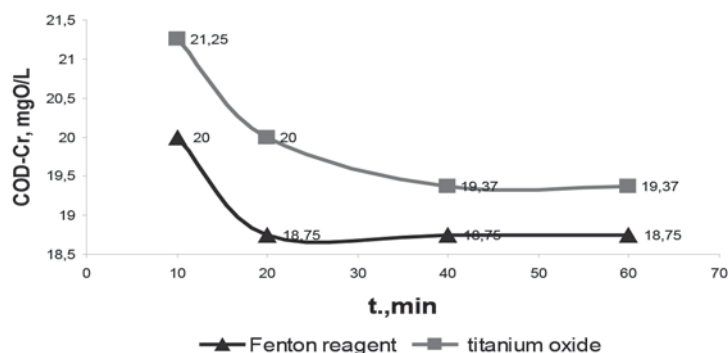
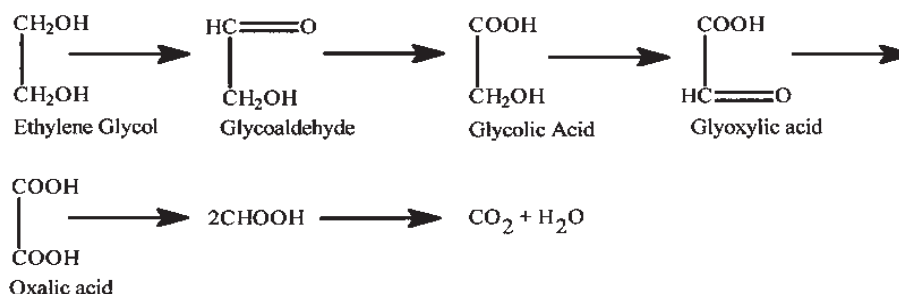


Figure 2. Model systems oxidized titanium oxide and zirconium oxide.
 [DB]=200 mg/L, [TiO₂] and [ZrO₂]=500 mg/L, pH=4.0, [H₂O₂]=3×10⁻³ mol/L, λ=365 nm.

From the literature reference [3] was found that EGL is oxidized with formation of various organic acids that further on are mineralized down to CO₂ and H₂O, although this process is very slow:



The ethylene glycol in the system was oxidized through irradiation with UV in the presence of titanium oxide and H₂O₂. Figure 3 shows that during the first 10 minutes, the oxygen demand decreases by three times (from 66.5 to 20.62 mgO₂/L). The compounds formed in the process of photocatalytic oxidation still persist in the solution for one hour of treatment. In these conditions EGL cannot be mineralized below the maximum admissible concentration in waste waters that has to be discharged.

The results of the experiment have demonstrated a decrease of the content of organic compounds caused by photocatalytic oxidation of ethylene glycol molecules by OH-forming compounds of more simple structure (alcohols, ketones, organic acids) while a part of it is transformed in carbon dioxide and water which contribute mineralization and decrease of chemical oxygen demand.

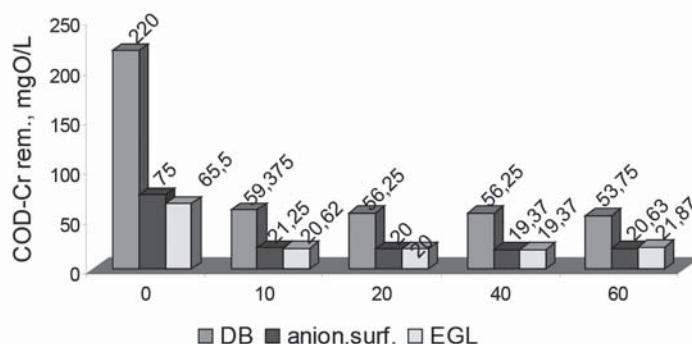
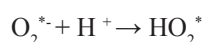
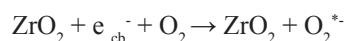
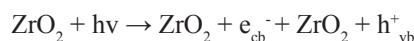


Figure 3. Model system containing dye and auxiliary compounds oxidized titanium oxide.
 [DB]=200 mg/L, [EGL]=60 mg/L, [anion.surf.]=60 mg/L, [H₂O₂]=3×10⁻³ mol/L,
 [TiO₂]=500 mg/L, pH=4.0, λ=365 nm.

In order to bring the content of simulation solutions closer to the state of real waster waters a mixture of similar pollutants including direct dye, EGL and surfactant SLS was investigated. The photocatalytic oxidation was performed for one hour in the presence of ZrO_2 with and without addition of H_2O_2 . The experimental results are presented in Figure 4.

The results of the experimental investigations have proved that addition of H_2O_2 takes place at a lower rate in comparison with the mixtures where was not added. The mechanism of formation of free radicals during photocatalytic oxidation when zirconium oxide was used without addition of H_2O_2 can be represented as follows:



The mechanism of the process that do not use H_2O_2 can be explained by the transfer of electrons from the valence band of zirconium to the conduction band and their gain by oxygen molecules and not by hydrogen peroxide that are responsible for generation of OH^{\bullet} radicals. Therefore, in the systems that do not contain H_2O_2 instead of OH^{\bullet} radical formation the formation of HO_2^{\bullet} radicals takes place, while in the systems where the H_2O_2 was added the formation of OH^{\bullet} occurs under the influence of UV rays.

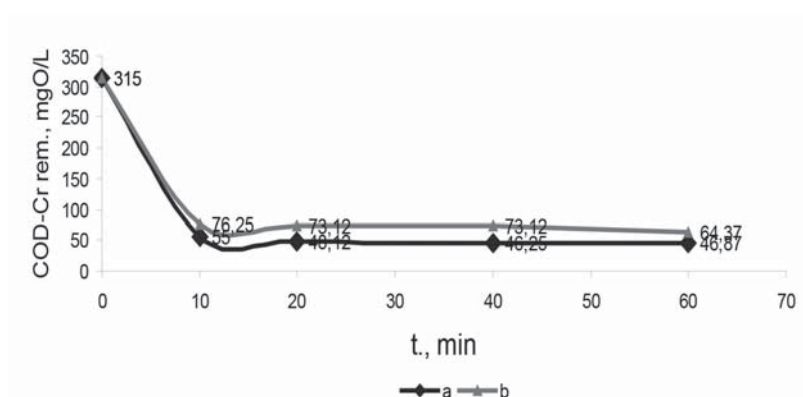
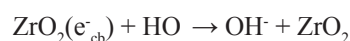
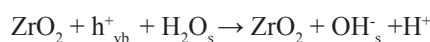


Figure 4. Photocatalytic oxidation in the presence of ZrO_2 with and without the addition of H_2O_2 .
a – without H_2O_2 , b- with H_2O_2 , [DB]=200 mg/L, [EGL]=60 mg/L, [anion. surf.]=60 mg/L, [ZrO₂]=500 mg/L, pH=4.0, [H_2O_2]= 3×10^{-3} mol/L, $\lambda = 365$ nm.

In the absence of gaining oxidants, the electron from the conduction band can be gained by OH^{\bullet} radicals which leads to diminishing of the content of oxidative panicles in solution:



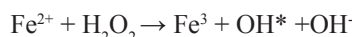
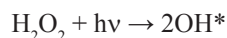
It became known that the absence of hydrogen peroxide the rate of oxidation and mineralization are increased both in the presence of zirconium oxide and titanium oxide. In order to diminish the negative effect of electrons from the conduction band additional oxygen is pumped into the water.

The effect of diminishing of the content of organic compounds in mixtures during oxidation in the presence of hydrogen peroxide is influenced by the amount of direct dyes in the mixture, the nature of catalyst and presence of UV radiation. The experimental investigations summarized in Table 1 show that oxidation effect and rate of mineralization is affected by the nature of catalyst.

The remaining content of degradable compounds decreases for the duration of one hour as follows: utilization of Fenton reagent decreases the level of COD-Cr from 300 mgO₂/L to 96.87 mgO₂/L, while the rate of oxidation and mineralization constitutes 67.71 mgO₂/L.

During utilization of Fenton reagent the COD-Cr decreases from 300 mg/L to 35.0 mg/L, and the rate of oxidation and mineralization constitutes 88.22 mgO₂/L.

The mineralization and oxidation effect is affected also by the presence of UV rays, since in this case the concentration of OH· radicals produced from decomposition of hydrogen peroxide is increasing in accordance with the following mechanism:



In this case the concentration of OH· is increased and respectively is increased the rate of oxidation and mineralization of dyes and surfactants. According to estimations based on measuring of COD-Cr and the rate of oxidation, the utilization of TiO₂ + UV catalyst is less effective than application of Fenton reagent. In the presence of hydrogen peroxide the process takes place with formation of an additional amount of OH· radicals that is influenced by the content of titanium oxide, wavelength of UV radiation and time of irradiation:



When acceptor oxidants are not present the electrons from the conduction band can be gained by OH· which leads to diminishing of their content in solution:

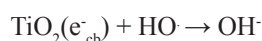


Table 1

The diminishing of the content of dye and auxiliary compounds at treatment in the presence of various catalysis. [DB]=200 mg/L, [anion.surf.]=60 mg/L, [H₂O₂]=3×10⁻³ mol/L, [Fe²⁺]=3×10⁻⁴ mol/L, pH=2.0-2.5, [TiO₂]=500 mg/L, pH=3.5-4.0, λ=365 nm.

t, min.	Fenton		Fenton + UV		TiO ₂ +UV	
	COD-Cr, mgO ₂ /L	Min., %	COD-Cr, mgO ₂ /L	Min., %	COD-Cr, mgO ₂ /L	Min., %
Chemical treatment, COD-Cr ₀ mixt.= 315 mgO ₂ /L						
10	104	65.33	45.00	85.00	60.00	80.00
20	98.75	67.08	42.50	85.83	50.00	83.33
40	97.5	67.50	38.75	87.08	36.25	87.92
60	96.87	67.71	35.00	88.33	36.25	87.92
AC	5.62	98.13	5.00	98.33	5.62	98.13

In all the cases the COD-Cr exceeds the admissible concentration requested for waste waters. Taking this into account, the process of adsorption of residues of oxidation on active charcoal (AC) with a concentration of 500 mg/L was investigated. Following the adsorption (Table 1) the COD-Cr for all the samples of oxidation has decrease to 5 mgO₂/L, while the rate of oxidation has risen by 98.0 %. Thus, the conditions for a complete treatment were optimized that would assure the compliance with sanitary norms of divers waste waters.

Similarly the electrochemical oxidation of organic compounds in simulation solutions containing mixtures of direct textile dye along with anionic surfactant SLS and ethylene glycol was investigated and proved according to COD-Cr. The experiment results show that organic components content decreases as a result of electrochemical oxidation in the presence of hydrogen peroxide catalyzed with Fenton reagent, titanium oxide or photo-Fenton at irradiation with ultraviolet rays (UV) at the optimal wavelength of 365 nm. The results obtained are presented in Figure 6 and Table 2.

Table 2

Diminishing of the concentration of dye and auxiliary compounds with different catalysts. [DB]=200mg/L, [anion. surf.]=60 mg/L, [H₂O₂]=3×10⁻³ mol/L, [Fe²⁺]=3×10⁻⁴ mol/L, [TiO₂]=500 mg/L, λ=365 nm.

t, min.	Fenton, pH=2.0-2.5		Fenton + UV, pH=2.0-2.5		TiO ₂ +UV, pH=3.5-4.0	
	COD-Cr, mgO ₂ /L	Min., %	COD-Cr, mgO ₂ /L	Min., %	COD-Cr, mgO ₂ /L	Min., %
Electrochemical treatment, COD-Cr ₀ mixt. = 315 mgO ₂ /L						
10	47.5	84.17	32.5	89.17	63.75	78.75
20	28.75	90.42	31.25	89.58	50.00	83.33
40	24.37	91.88	30.63	89.79	41.87	86.04
60	11.87	96.04	23.75	92.08	40.62	86.46
AC	0.62	99.79	5.63	98.12	28.75	90.42

From Figure 6 it is observed that the process of catalytic oxidation with hydrogen peroxide through electrochemical method in the presence of titanium dioxide at higher concentrations of direct dye takes place with a lower rate in comparison with Fenton and photo-Fenton methods. After the chemical and electrochemical treatment, during the second phase the active charcoal was used for adsorption in order to reach the maximum admissible concentration for certain mixtures.

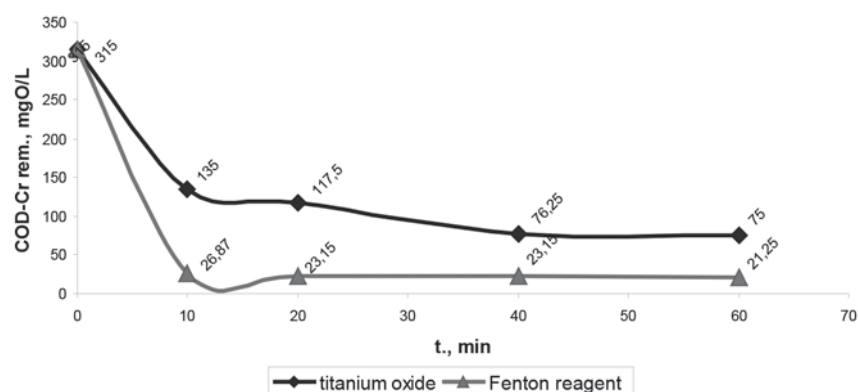


Figure 6. Electrochemical treatment (0.4 A), [DB]=200mg/L, [EGL]=60 mg/L, [anion. surf.]=60 mg/L, [TiO₂]=500 mg/L, pH=4.0, [Fe²⁺]=3×10⁻⁴ mol/L, pH=2.0-2.5, [H₂O₂]=8×10⁻³mol/L, λ=365 nm.

Conclusions

The mixture of direct dye DB and anionic surfactant SLS and EGL is oxidized more efficiently through Fenton and photo-Fenton methods in comparison with application of titanium oxide as catalyst.

It was identified that the oxidation for one hour of a mixture of DB, ethylene glycol and anionic surfactant SLS in model solutions using the photo-Fenton and electrochemical methods, the degree of oxidation and mineralization can reach 91.0-95.0%.

It has been proved that direct dye DB, surfactant SLS and ethylene glycol can be removed from waste water through combined methods of photocatalytic oxidation with hydrogen peroxide, electrochemical treatment and adsorption of degraded compounds on active charcoal.

Acknowledgements

It is acknowledged the Government of Republic of Moldova and Academy of Sciences of Moldova for financial support.

References

- Alcantara, M. T.; Gomez, J.; Pazos, M.; Sanroman, M. A. Combined treatment of PAHs contaminated soils using the sequense extrasionn with surfactant- electrochemical degradation. *Chemosphere*, 2008, 70, pp. 1438-1444.
- Bouras, O.; Bollinger, J.; Baudu, M.; Khalay, H. Adsorption of diuron and its degradation products from aqueous solution by surfactant –modified pillared clays. *Applied Clay Science*. 2007, 37, pp. 240-250.
- Dietrick McGinnis, B.; Dean Adams, V. Degradation of ethylene glycol using Fenton's reagent and UV. *Chemosphere*, 2001, 45, pp. 101-108.
- Fabiana, M.; Paschoal, M.; Marc. A.; Anderson, A.; Valnice, M.; Zanoni, B. Fotoelectrocatalytic oxidation of anoinic surfactant used in leather industry on nanoporous Ti/TiO₂ electrodes. *Journal of the Brazilian Chemical Society*. 2008, 19(4), pp. 603-810.
- Hidaka, H.; Ajisaka, K.; Harikoshi, S.; Oyama, T.; Takauchi, K. Comparative assessment of the efficiency of TiO₂/OTE thin film electrodes fabricated by three deposition methods. *Photoelectrochemical degradation of the DBS anionic surfactant. Journal of Photochemistry and Photobiology, A. Chemistry*. 2001, 138, pp. 185-192.
- Ma, C.W.; Chu, W. Photodegradation mechanism and rate improvement of chlorinated aromatic dye in non-ionic surfactant solutions. *Water Resources*. 2001, 35(10), pp. 2453-2459.
- Matveevici, V.; Duca, Gh.; Gonta, M.; Isac, T.; Mocanu, L. Studying the process of reducing the concentration of active dyes in model solutions by applying physico - chemical methods. *Studia Universitatis, series "Natural Sciences"*, 2010. 31(1), pp. 162 - 172 (in Romanian).
- Michitaka, O.; Hirofurni, S.; Hiroyuki, F.; Koichi, E. Intramolecularly selective decomposition of surfactant molecules on photocatalytic oxidative degradation over TiO₂ photocatalyst. *Journal of Molecular Catalysis A. Chemical*, 2000, 155, pp. 122-129.
- Lupascu, T. Activated carbons from vegetal raw materials; Chisinau: Stiinta, 2004, 224 p. (in Romanian).
- Lu, P.; Chien, C.-W.; Chen, T.-S.; Chern, Jia-Ming. Azo dye degradation kinetics in TiO₂ film-coated photoreactor. *Chemical Engineering Journal*, 2010, 163, pp. 28-34.

MIXED-METAL COMPLEXES OF MIXED-VALENT DINUCLEAR RUTHENIUM(II,III) CARBOXYLATE AND TETRACYANIDONICKELATE(II)

Masahiro Mikuriya^{a*}, Yusuke Tanaka^a, Daisuke Yoshioka^a, Makoto Handa^{b*}

^aDepartment of Chemistry and Research Center for Coordination Molecule-based Devices, School of Science and Technology, Kwansei Gakuin University, 2-1 Gakuen, Sanda 669-1337, Japan

^bDepartment of Chemistry, Interdisciplinary Graduate School of Science and Engineering, Shimane University, 1060 Nishikawatsu, Matsue 690-8504, Japan

*e-mail: junpei@kwansei.ac.jp, phone: (+81 79) 565 83 65; fax: (+81 79) 565 90 77

Abstract. Mixed-metal chain complexes constructed from lantern-type dinuclear ruthenium(II,III) carboxylate unit and tetracyanonickelate(II), $(\text{PPh}_4)_n[\text{Ru}_2(\text{O}_2\text{CCH}_3)_4\text{Ni}(\text{CN})_4]_n \cdot n\text{H}_2\text{O}$ (**1**) and $(\text{PPh}_4)_n[\text{Ru}_2\{\text{O}_2\text{CC}(\text{CH}_3)_3\}_4]_n[\text{Ni}(\text{CN})_4]_{2n} \cdot 2n\text{H}_2\text{O}$ (**2**), were synthesized and characterized by elemental analysis, IR, and UV-vis spectroscopies. These data are in accordance with the formation of the chain complex with an alternative arrangement of the dinuclear Ru_2 unit and tetracyanonickelate(II). A broad band at near-IR and a band at visible region (1058 and 452 nm for **1** and 1082 and 454 nm for **2**) were observed in the diffused reflectance spectra and ascribed to a $\delta(\text{Ru}_2) \rightarrow \delta^*(\text{Ru}_2)$ and a $\pi(\text{RuO}, \text{Ru}_2) \rightarrow \pi^*(\text{Ru}_2)$ transitions, respectively. Temperature-dependence of magnetic susceptibility (4.5–300 K) showed that the antiferromagnetic interaction between the dinuclear units is weak ($zJ = -0.2 \text{ cm}^{-1}$) with D value of 75 cm^{-1} for both complexes.

Keywords: dinuclear ruthenium(II,III) carboxylate, magnetic property, mixed-metal complex, tetracyanido nickelate(II).

Introduction

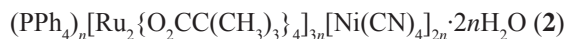
The chemistry of dinuclear metal carboxylates has attracted much attention over the past five decades because of the unique lantern-type (or paddlewheel-type) dinuclear core [1-5]. Among the dinuclear metal carboxylates, mixed-valent ruthenium(II,III) carboxylates $[\text{Ru}_2(\text{O}_2\text{CR})_4]^+$ are interesting, because these dinuclear systems are paramagnetic with three unpaired electrons on the $\pi^*\delta^*$ orbitals in the metal–metal bonds and with large zero-field splitting (ZFS) [3–37]. The dinuclear ruthenium carboxylates show various interesting features such as liquid crystalline properties [25] as well as the paramagnetic properties. We prepared many metal-assembled complexes from dinuclear species to one-dimensional chain compounds by application of linking ligands to dinuclear ruthenium carboxylates and found that most of them are antiferromagnetic between the dinuclear ruthenium units and the strength of the antiferromagnetic interaction depends on the linking ligands [16-29]. About ten years ago, we and Miller's group reported that the dinuclear ruthenium carboxylates form polymeric mixed-metal complexes with hexacyanometalate ion $[\text{M}(\text{CN})_6]^{3-}$ ($\text{M} = \text{Fe}, \text{Co}$, and so on) and found some of them show an antiferromagnetic interaction between the dinuclear ruthenium units through the diamagnetic hexacyanometalate ion and a ferrimagnetic interaction among the hetero metal ions [30-35]. Recently, our continuing study on these systems led us to mixed-metal complexes with octacyanometalate ions $[\text{M}(\text{CN})_8]^{4-}$ ($\text{M} = \text{W}$) [36,37]. In these mixed-metal systems, a ferrimagnetic interaction between the dinuclear Ru_2 spins and octacyanometalate spins was observed for $[\{\text{Ru}_2(\text{O}_2\text{CC}(\text{CH}_3)_3)_4\}_3(\text{H}_2\text{O})\text{W}(\text{CN})_8]_n$ [37]. Therefore, it is important to develop these mixed-metal systems to find interesting molecular magnetic compounds. In this study, we extended these systems to mixed-metal complexes with tetracyanometalate ion by using tetracyanonickelate(II) ion $[\text{Ni}(\text{CN})_4]^{2-}$ in order to obtain new metal-assembled complexes of ruthenium(II,III) carboxylate. The isolated complexes were characterized by elemental analysis, IR, UV-vis spectra, and temperature dependence of magnetic susceptibilities (4.5–300 K). Here, we report on the preparation and structural characterization of these new systems.

Experimental

Synthesis: $[\text{Ru}_2(\text{O}_2\text{CCH}_3)_4(\text{H}_2\text{O})_2]\text{BF}_4$ and $[\text{Ru}_2\{\text{O}_2\text{CC}(\text{CH}_3)_3\}_4(\text{H}_2\text{O})_2]\text{BF}_4$ were synthesized by literature methods [6,7]. Other reagents and solvents were purchased from commercial sources and were used without further purification.

$(\text{PPh}_4)_n[\text{Ru}_2(\text{O}_2\text{CCH}_3)_4\text{Ni}(\text{CN})_4]_n \cdot n\text{H}_2\text{O}$ (**1**)

Tetraphenylphosphonium chloride (6.7 mg, 0.018 mmol) and potassium tetracyanonickelate(II) (2.3 mg, 0.0088 mmol) were dissolved in 4 mL of H_2O , respectively. To an aqueous solution (2 mL) of $[\text{Ru}_2(\text{O}_2\text{CCH}_3)_4(\text{H}_2\text{O})_2]\text{BF}_4$ (10.0 mg, 0.0178 mmol) were added these solutions, stirred for 1 min. The resulting precipitate was filtered, washed with 9 mL of water, and dried *in vacuo*. Yield: 5.4 mg (62%). Anal. Found: C, 45.15; H, 3.44; N, 5.87%. Calcd. for $\text{C}_{36}\text{H}_{34}\text{N}_4\text{NiO}_9\text{PRu}_2$: C, 45.11; H, 3.58; N, 5.85%. IR (KBr): $\nu(\text{Ar-H})$ 3060, 3100, $\nu(\text{CN})$ 2130, $\nu_{\text{as}}(\text{CO}_2^-)$ 1442, $\nu_{\text{s}}(\text{CO}_2^-)$ 1403. Diffuse reflectance spectrum: λ_{max} 338, 452, 1058, 1670 nm.



Tetraphenylphosphonium chloride (5.1 mg, 0.014 mmol) and potassium tetracyanonickelate(II) (1.8 mg, 0.0070 mmol) were dissolved in 5 mL of H_2O , respectively. To an aqueous solution (5 mL) of $[\text{Ru}_2\{\text{O}_2\text{CC}(\text{CH}_3)_3\}_4(\text{H}_2\text{O})_2]\text{BF}_4$ (10.0 mg, 0.0137 mmol) were added these solutions, stirred for 1 hr. The resulting precipitate was filtered, washed with 9 mL of water, and dried *in vacuo*. Yield: 6.5 mg (77%). Anal. Found: C, 43.70; H, 5.29; N, 4.46%. Calcd. for $\text{C}_{92}\text{H}_{132}\text{N}_8\text{Ni}_2\text{O}_{26}\text{PRu}_6$: C, 43.83; H, 5.28; N, 4.45%. IR (KBr): $\nu(\text{Ar-H})$ 3061, 3085, $\nu(\text{CN})$ 2128, $\nu_{\text{as}}(\text{CO}_2^-)$ 1487, $\nu_{\text{s}}(\text{CO}_2^-)$ 1421. Diffuse reflectance spectrum: λ_{max} 346, 454, 1082, 1676 nm.

Measurements: Elemental analyses for carbon, hydrogen, and nitrogen were done using a Thermo-Finnigan FLASH EA1112 series CHNO-S analyzer. Infrared spectra were measured with a JASCO MFT-2000 FT-IR Spectrometer in the 4000—600 cm^{-1} region. Electronic spectra were measured with a Shimadzu UV-vis-NIR Recording Spectrophotometer (Model UV-3100). Magnetic susceptibilities were measured with a Quantum Design MPMS-XL7 SQUID susceptometer operating at a magnetic field of 0.5 T over a range of 4.5—300 K. The susceptibilities were corrected for the diamagnetism of the constituent atoms using Pascal's constants. The effective magnetic moments were calculated from the equation $\mu_{\text{eff}} = 2.828\sqrt{\chi_{\text{M}}T}$, where χ_{M} is the molar magnetic susceptibility per mole of dinuclear ruthenium(II,III) unit.

Results and discussion

Reaction of the mixed-valent dinuclear ruthenium(II,III) acetate and ruthenium(II,III) pivalate with tetracyanonickelate(II) ion in the presence of tetraphenylphosphonium ion gave orange and brown precipitates, respectively. The formulation of the mixed-metal systems of dinuclear ruthenium(II,III) carboxylate with tetracyanonickelate(II), $(\text{PPh}_4)_n[\text{Ru}_2(\text{O}_2\text{CCH}_3)_4\text{Ni}(\text{CN})_4]_n \cdot n\text{H}_2\text{O}$ (**1**) and $(\text{PPh}_4)_n[\text{Ru}_2\{\text{O}_2\text{CC}(\text{CH}_3)_3\}_4]_{3n}[\text{Ni}(\text{CN})_4]_{2n} \cdot 2n\text{H}_2\text{O}$ (**2**), was confirmed by the elemental analyses, infrared and electronic spectra, and temperature dependence of magnetic susceptibility data (4.5—300 K).

In the infrared spectra, two strong bands were observed at 1442 and 1403 cm^{-1} assignable to asymmetric and symmetric stretching vibrations of the *syn-syn* acetate bridges, respectively, for **1**, whereas two strong bands observed at 1487 and 1421 cm^{-1} assignable to asymmetric and symmetric stretching vibrations of the *syn-syn* pivalate bridges, respectively, for **2** (Figure 1). The sharp bands at 2130 cm^{-1} in **1** and 2128 cm^{-1} in **2** may be attributed to $\nu(\text{CN})$ stretching band of the tetracyanonickelate(II) ion. These bands appeared at a little higher energy region compared with that of $\text{K}_2[\text{Ni}(\text{CN})_4]$ ($\nu(\text{CN})$: 2125 cm^{-1}), suggesting the bridging of the tetracyanonickelate(II) to the dinuclear ruthenium carboxylate unit [38,39]. The C-H stretching vibrations of aromatic rings were observed at 3100 and 3060 cm^{-1} for **1** and at 3085 and 3061 cm^{-1} for **2**, respectively, in agreement with the presence of the tetraphenylphosphonium ions.

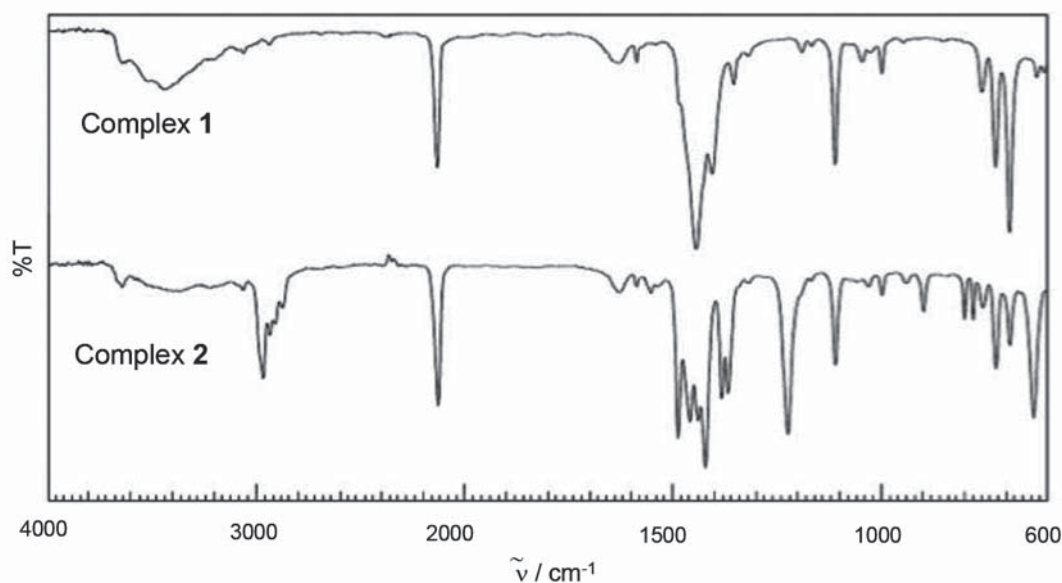


Figure 1. Infrared spectra of **1** and **2**.

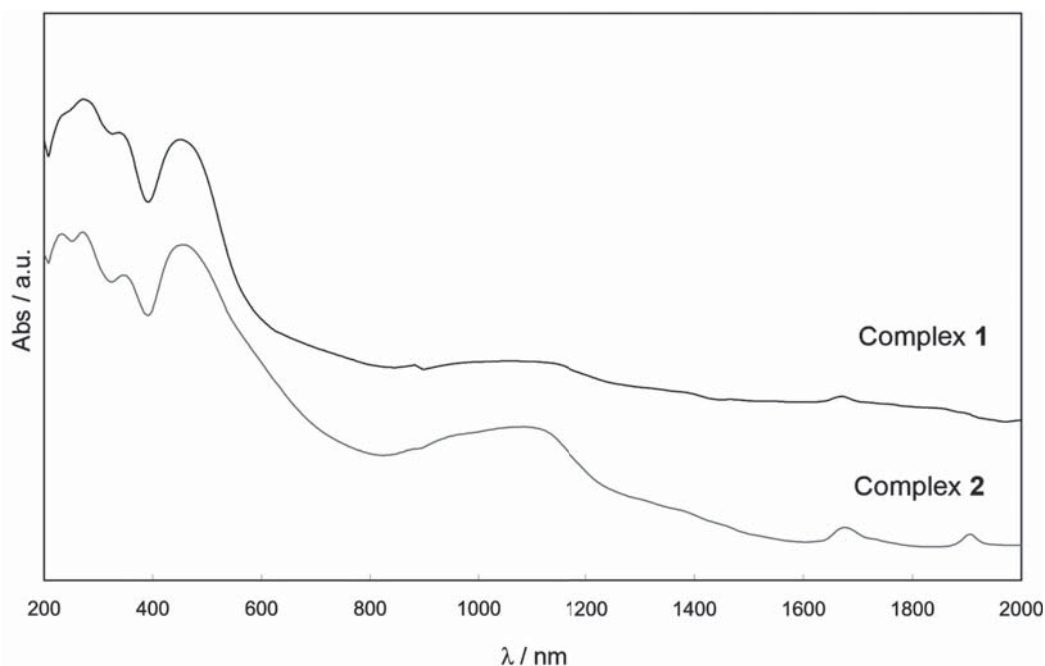


Figure 2. Diffused reflectance spectra of **1** and **2**.

The diffused reflectance spectra of **1** and **2** are shown in Figure 2. The paddlewheel-type dinuclear structure of the mixed-valent dinuclear ruthenium(II,III) carboxylate can be considered to be maintained in these mixed-metal complexes, because the spectra contain the characteristic bands of dinuclear ruthenium(II,III) carboxylate. A weak broad absorption band around 1058 and 1670 nm in solid is typical for ruthenium(II,III) carboxylates and can be attributed to a $\delta(\text{Ru}_2) \rightarrow \delta^*(\text{Ru}_2)$ and $\pi^*(\text{Ru}_2) \rightarrow \delta^*(\text{Ru}_2)$ transitions, respectively, within ruthenium(II,III) dinuclear core [8]. A medium band at 452 nm may be due to $\pi(\text{RuO}, \text{Ru}_2) \rightarrow \pi^*(\text{Ru}_2)$ transition [11,12]. The spectra contain another feature due to the presence of tetracyanonickelate(II) moiety. The bands at 338 and 452 nm can be assigned to the $^1A_{1g} \rightarrow ^1A_{2g}$ and $^1A_{1g} \rightarrow ^1B_{2g}$ transitions, respectively, of the tetracyanonickelate(II) moiety [38,39]. Similar spectral feature was observed for **2**: 1082 ($\delta(\text{Ru}_2) \rightarrow \delta^*(\text{Ru}_2)$), 1676 ($\pi^*(\text{Ru}_2) \rightarrow \delta^*(\text{Ru}_2)$), 454 ($\pi(\text{RuO}, \text{Ru}_2) \rightarrow \pi^*(\text{Ru}_2)$), $^1A_{1g}(\text{Ni}) \rightarrow ^1A_{2g}(\text{Ni})$, 346 ($^1A_{1g}(\text{Ni}) \rightarrow ^1B_{2g}(\text{Ni})$) nm.

Temperature dependence of effective magnetic moments is shown in Figure 3.

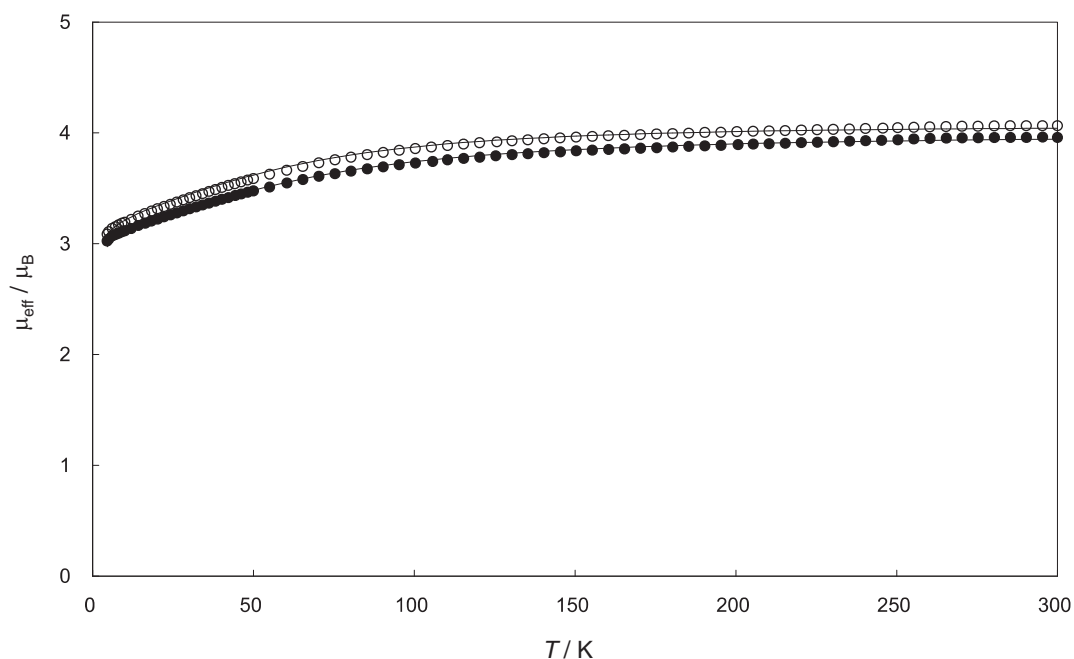


Figure 3. Temperature dependence of the magnetic moments of **1** (●) and **2** (○).

The magnetic moments of **1** and **2** are 3.98 and 4.07 μ_B , respectively, at 300 K per dinuclear ruthenium(II,III) unit, which are slightly higher than the spin-only value of $S = 3/2$ (3.87 μ_B). The magnetic moments gradually decrease with lowering of temperature until reaching 3.02 and 3.09 μ_B , respectively, at 4.5 K, being typical of dinuclear ruthenium(II,III) carboxylates [3-5].

The magnetic data were analyzed by a molecular field approximation [40] considering the ZFS effect to estimate the magnitude of the antiferromagnetic interaction [9,10]. This approximation has been commonly applied for dinuclear ruthenium(II,III) carboxylates using the following equations:

$$\chi' = \chi / \{1 - (2zJ / Ng^2\mu_B^2)\chi\}$$

$$\chi = (\chi_{||} + 2\chi_{\perp}) / 3$$

$$\chi_{||} = (Ng^2\mu_B^2 / kT)[1 + 9\exp(-2D / kT)] / 4\{1 + \exp(-2D / kT)\}$$

$$\chi_{\perp} = (Ng^2\mu_B^2 / kT)[4 + (3kT / D)\{1 - \exp(-2D / kT)\}] / 4\{1 + \exp(-2D / kT)\}$$

where zJ is the exchange integral multiplied by the number of interacting neighbors, χ is the magnetic susceptibility of the individual dinuclear unit, and D is the ZFS parameter.

The D parameter was fixed at 75 cm^{-1} which is a normal value for dinuclear ruthenium(II,III) carboxylates [3]. The g value was treated as isotropic. Best fitting curve was obtained with the parameters; $zJ = -0.20 \text{ cm}^{-1}$, $g = 2.06$ for **1**. The similar parameters $zJ = -0.20 \text{ cm}^{-1}$, $g = 2.09$ were obtained for **2**. These results show that a weak antiferromagnetic interaction is operating between the dinuclear ruthenium units, being consistent with a long separation of the dinuclear ruthenium units through the tetracyanidonickelate(II) bridge for the present complexes.

From the above results, we can assume a chain structure with an alternated arrangement of dinuclear ruthenium units and tetracyanidonickelate(II) ions shown in Figure 4 (a) for **1**, whereas one- or two-dimensional array of dinuclear ruthenium units and tetracyanidonickelate(II) ions such as Figures 4 (b) and 4 (c) for **2**. There are two types of CN groups for the tetracyanidonickelate(II) moieties: bridging and non-coordinating. We can see the overlapping of these CN stretching bands in the infrared spectra as shown in Figure 5.

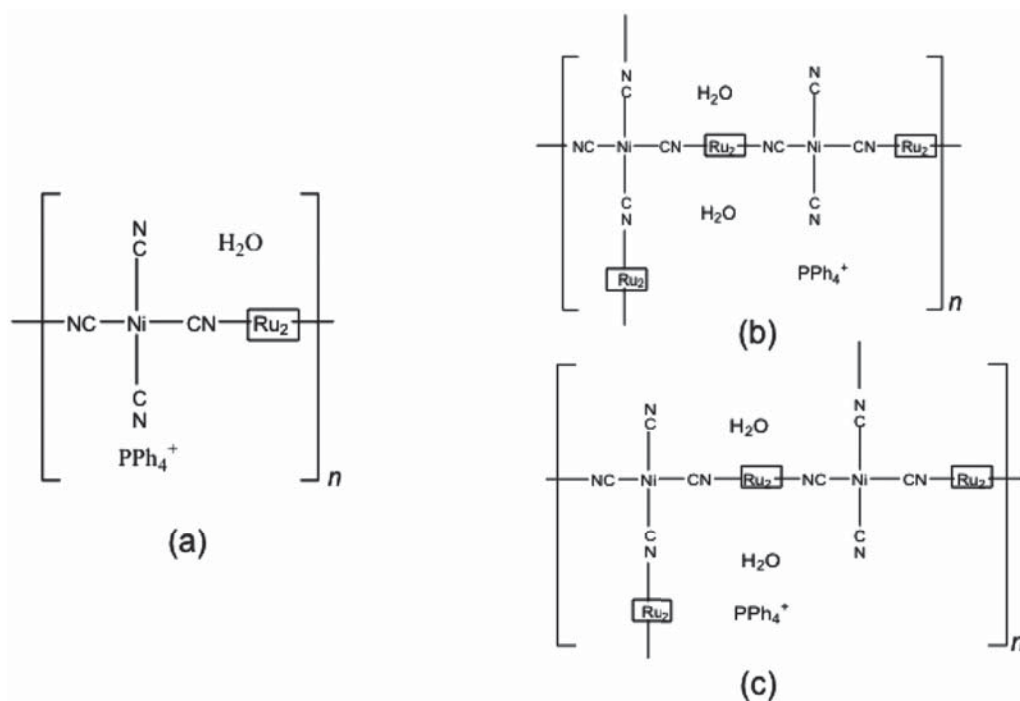


Figure 4. Proposed structures (a) for **1** and (b) and (c) for **2**, respectively.
The Ru_2 unit denotes the dinuclear ruthenium carboxylate.

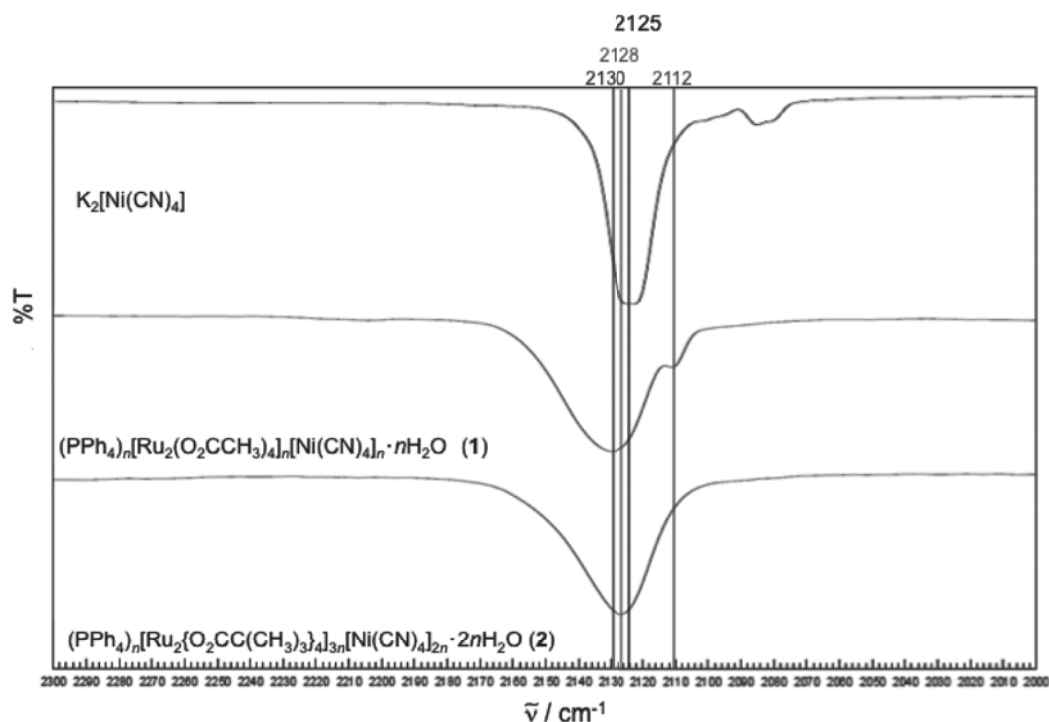


Figure 5. Infrared spectra of $K_2[Ni(CN)_4]$ and the present complexes in the CN stretching band region.

Conclusions

By using tetracyanidonickelate(II), the preparation of the mixed-metal chain complexes of dinuclear ruthenium(II,III) carboxylate, $(PPh_4)_n[Ru_2(O_2CCH_3)_4][Ni(CN)_4]_n \cdot nH_2O$ (**1**) and $(PPh_4)_n[Ru_2\{O_2CC(CH_3)_3\}_4]_{2n}[Ni(CN)_4]_{2n} \cdot 2nH_2O$ (**2**), was achieved successfully. The analytical data, infrared spectra, UV-vis-NIR spectra, and temperature dependence of magnetic susceptibilities are consistent with one- or two-dimensional chain structures with an alternated arrangement of dinuclear ruthenium units and tetracyanidonickelate(II) ions. In accordance with the structural feature, a weak antiferromagnetic interaction through the tetracyanidonickelate(II) ion was observed for the present complexes.

Acknowledgements

The present work was partially supported by Grant-in-Aid for Scientific Research No. 26410080 from the Ministry of Education, Culture, Sports, Science and Technology (MEXT, Japan) and the NEXT-Supported Program for the Strategic Research Foundation at Private Universities, 2010-2014.

References

1. Cotton, F.A.; Murillo, C.A.; Walton, R.A. Multiple Bonds between Metal Atoms. 3rd ed. Springer Science and Business Media: New York, 2005, 818 p.
2. Mikuriya, M. Copper(II) acetate as a motif for metal-assembled complexes. Bulletin of the Japanese Society of Coordination Chemistry, 2008, 52, pp. 17-28 (in Japanese).
3. Mikuriya, M.; Yoshioka, D.; Handa, M. Magnetic interactions in one-, two-, and three-dimensional assemblies of dinuclear ruthenium carboxylates. Coordination Chemistry Reviews, 2006, 250, pp. 2194-2211.
4. Aquino, M.A.S. Recent developments in the synthesis and properties of dinuclear tetracarboxylates. Coordination Chemistry Reviews, 2004, 248, pp. 1025-1045.
5. Aquino, M.A.S. Diruthenium and diosmium tetracarboxylates: synthesis, physical properties and applications. Coordination Chemistry Reviews, 1998, 170, pp. 141-202.
6. Stephenson, T. A.; Wilkinson, G. New ruthenium carboxylate complexes, Journal of inorganic and nuclear Chemistry, 1966, 28, pp. 2285-2291.
7. Barral, M. C.; Jiménez-Aparicio, R.; Priego, J. L.; Royer, E.C. Polyhedron, 1992, pp. 2209-2215.
8. Norman, G.J.; Renzoni, G.E.; Case, D.A. Electronic structure of $Ru_2(O_2CR)_4^+$ and $Rh_2(O_2CR)_4^+$ complexes, Journal of the American Chemical Society, 1979, 101, pp. 5256-5267.
9. Telser, J.; Drago, R.S. Reinvestigation of the electronic and magnetic properties of ruthenium butyrate chloride. Inorganic Chemistry, 1984, 23, pp. 3114-3120.

10. Telser, J.; Drago, R.S. Correction: Reinvestigation of the electronic and magnetic properties of ruthenium butyrate chloride. *Inorganic Chemistry*, 1985, 24(26), p. 4765.
11. Miskowski, V.M.; Loehr, T.M.; Gray, H.B. Electronic and vibrational spectra of $\text{Ru}_2(\text{carboxylate})_4^+$ complexes. Characterization of a high spin metal-metal ground state. *Inorganic Chemistry*, 1987, 26, pp. 1098–1108.
12. Miskowski, V.M.; Gray, H.B. Electronic spectra of $\text{Ru}_2(\text{carboxylate})_4^{4+}$ complexes. Higher energy electronic excited states, *Inorganic Chemistry*, 1988, 27(14), pp. 2501–2506.
13. Ishida, H.; Handa, M.; Mikuriya, M. Synthesis and crystal structure of aqua adduct of dinuclear ruthenium(II,III) 3,4,5-tri(ethoxy- d_3)benzoate tetrafluoroborate, X-Ray Structure Analysis Online, 2014, 30, pp. 9-10.
14. Sayama, Y.; Handa, M.; Mikuriya, M.; Nukada, R.; Hiromitsu, I.; Kasuga, K. Mixed-valent ruthenium pivalate and its nitroxide adduct. *Coordination Chemistry at the Turn of the Century*. Ed. by Ondrejovic, G.; Sirota, A. Slovak Technical University Press: Bratislava, 1999; pp. 447-452.
15. Sayama, S.; Handa, M.; Mikuriya, M.; Hiromitsu, I.; Kasuga, K. Chain compound of mixed-valent ruthenium dimers linked by hydrogen-bonding between the axially coordinated nitronyl nitroxide and water molecules, *Chemistry Letters*, 1999, pp. 453-454.
16. Handa, M.; Yoshioka, D.; Sayama, Y.; Shiomi, K.; Mikuriya, M.; Hiromitsu, I.; Kasuga, K. A new “dimer-of-dimers” complex derived from axial coordination of 7,7,8,8-tetracyanoquinodimethane to $\text{Ru}(\text{II,III})$ cation dimer, *Chemistry Letters*, 1999, pp. 1033-1034.
17. Yoshioka, D.; Handa, M.; Azuma, H.; Mikuriya, M.; Hiromitsu, I.; Kasuga, K. Synthesis and magnetic property of adducts of ruthenium(II,III) pivalate with 9,10-anthraquinone, *Molecular Crystal and Liquid Crystal*, 2000, 342, pp. 133-138.
18. Sayama, Y.; Handa, M.; Mikuriya, M.; Hiromitsu, I.; Kasuga, K. Structures and magnetic properties of ruthenium(II,III) pivalate cation dimers axially coordinated by pyridyl nitronyl nitroxide radicals through their pyridyl nitrogen atoms, *Bulletin of the Chemical Society of Japan*, 2000, 73, pp. 2499-2504.
19. Sayama, Y.; Handa, M.; Mikuriya, M.; Hiromitsu, I.; Kasuga, K. Synthesis and magnetic properties of ruthenium(II,III) pivalate dimers axially coordinated by nitronyl nitroxide radicals $[\text{Ru}_2(\text{O}_2\text{CCMe}_3)_4(\text{L})_2]\text{BF}_4$ and $[\{\text{Ru}_2(\text{O}_2\text{CCMe}_3)_4(\text{L})_2\}\{\text{Ru}_2(\text{O}_2\text{CCMe}_3)_4(\text{H}_2\text{O})_2\}]_n(\text{BF}_4)_{2n}$, $\text{L} = 2,4,4,5,5$ -pentamethyl-4,5-dihydro-1*H*-imidazol-1-oxyl-3-*N*-oxide and 2-ethyl-4,4,5,5-tetramethyl-4,5-dihydro-1*H*-imidazol-1-oxyl-3-*N*-oxide, *Bulletin of the Chemical Society of Japan*, 2003, 76, pp. 769-779.
20. Handa, M.; Yoshioka, D.; Mikuriya, M.; Hiromitsu, I.; Kasuga, K. Coordination polymers of ruthenium(II) acetate with pyrazine, 4,4'-bipyridine, and 1,4-diazabicyclo[2.2.2]octane, *Molecular Crystal and Liquid Crystal*, 2002, 376, pp. 257-262.
21. Yoshioka, D.; Mikuriya, M.; Handa, M. Synthesis and characterization of polynuclear chain and tetranuclear complexes of mixed-valent ruthenium(II,III) pivalate with *N,N'*-didentate ligands. *Bulletin of the Chemical Society of Japan*, 2004, 77, pp. 2205–2211.
22. Handa, M.; Ishida, H.; Ito, K.; Adachi, T.; Ikeue, T.; Hiromitsu, I.; Mikuriya, M.; Kasuga, K. Synthesis and magnetic properties of polymeric complexes containing ruthenium(II)-ruthenium(III) tetracarboxylato units linked by cyanato, thiocyanato, and selenocyanato ligands. *Chemical Papers*, 2008, 62, pp. 410–416.
23. Yoshioka, D.; Handa, M.; Mikuriya, M.; Kasuga, K. Coordination polymers of ruthenium pivalate dimer with tetracyanoethylene, 7,7,8,8-tetracyanoquinodimethane, and 2,5-dimethyl-*N,N'*-dicyanobenzoquinonediimine. *Advances in Coordination, Bioinorganic and Inorganic Chemistry*. ed. by Melnik, M.; Sima, J.; Tatarko, M. Slovak Technical University Press: Bratislava, 2005; pp. 218-223.
24. Mikuriya, M.; Tanaka, K.; Handa, M.; Hiromitsu, I.; Yoshioka, D.; Luneau, D. Adduct complexes of ruthenium(II,III) propionate dimer with pyridyl nitroxides, *Polyhedron*, 2005, 24, pp. 2658-2664.
25. Ishida, H.; Handa, M.; Hiromitsu, I.; Ujiie, S.; Mikuriya, M. Synthesis and magnetic properties of polymer complexes of ruthenium(II,III) 3,4,5-trioctanoxybenzoate linked by chloro and cyanato ligands with liquid-crystalline behavior. *Achievements in Coordination, Bioinorganic and Applied Inorganic Chemistry*. ed. by Melnik, M.; Sima, J.; Tatarko, M. Slovak Technical University Press: Bratislava, 2007; pp. 121-127.
26. Ishida, H.; Handa, M.; Hiromitsu, I.; Mikuriya, M. Synthesis, magnetic and spectral properties, and crystal structure of mixed-valence ruthenium(II,III) 3,4,5-tributanoxymbenzoate. *Insights into Coordination, Bioinorganic and Applied Inorganic Chemistry*. Ed. by Melnik, M.; Segl'a, P.; Tatarko, M. Slovak Technical University Press: Bratislava, 2009; pp. 197-203.
27. Ishida, H.; Handa, M.; Ikeue, T.; Taguchi, J.; Mikuriya, M. Synthesis, crystal structure, and ^1H NMR spectra of a chloride-bridged chain complex of dinuclear ruthenium(II,III) 3,4,5-tri(ethoxy- d_3)benzoate. *Chemical Papers*, 2010, 64, pp. 767–775.
28. Ishida, H.; Handa, M.; Hiromitsu, I.; Mikuriya, M. Fastener effect on magnetic properties of chain compounds of dinuclear ruthenium carboxylates. *Chemical Papers*, 2013, 67, pp. 743–750.

29. Ikeue, T.; Karino, K.; Iida, M.; Yamaji, T.; Hiromitsu, I.; Sugimori, T.; Yoshioka, D.; Mikuriya, M.; Handa, M. Structural, magnetic, and ^1H NMR spectral study on lantern-type *cis*- and *trans*-diruthenium(II,III) complexes with two formamidinato and two acetato bridges. *Inorganic Chemistry Communications*, 2013, 33, pp. 133-137.
30. Yoshioka, D.; Mikuriya, M.; Handa, M. Molecular-assembled complexes of mixed-valent ruthenium dimer with hexacyanoferrate(III) and hexacyanocobaltate(III) ions, *Chemistry Letters*, 2002, 31, pp. 1044-1045.
31. Vos, T.E.; Liao, Y.; Shum, W.W.; Her, J.-H.; Stephens, P.W.; Reiff, W.M.; Miller, J.S. Diruthenium tetraacetate monocation, $[\text{Ru}^{\text{II/III}}_2(\text{O}_2\text{CMe})_4]^+$, building blocks for 3-D molecule-based magnets, *Journal of the American Chemical Society*, 2004, 126, pp. 11630-11639.
32. Vos, T.E.; Miller, J.S. Building blocks for 2D molecule-based magnets: the diruthenium tetrapivalate monocation $[\text{Ru}^{\text{II/III}}_2(\text{O}_2\text{CtBu})_4]^+$, *Angewandte Chemie International Edition*, 2005, 44, pp. 2416-2419.
33. Miller, J. S. Magnetically ordered molecule-based assemblies, *Dalton Transaction*, 2006, pp. 2742-2949.
34. Kennon, B.S.; Her, J.-H.; Stephens, P.W.; Miller, J.S. Diruthenium teracarboxylate trianion, $[\text{Ru}^{\text{II/III}}_2(\text{O}_2\text{CO})_4]^{3-}$, based molecule-based magnets: three-dimensional network structure and two-dimensional magnetic ordering, *Inorganic Chemistry*, 2009, 48, pp. 6117-6123.
35. Kennon, B.S.; Miller, J.S. Observation of magnetic ordering for layered (2-D) potassium diruthenium tetracarboxylate, $\text{K}_3[\text{Ru}^{\text{II/III}}_2(\text{O}_2\text{CO})_4]$: a rare second row transition, *Inorganic Chemistry*, 2010, 49, pp. 5542-5545.
36. Matoga, D.; Mikuriya, M.; Handa, M.; Szklarzewicz, J. Self-assembly of Mixed-valent ruthenium(II,III) pivalate and octacyanotungstate(V) building blocks. *Chemistry Letters*, 2005, 34, pp. 1550-1551.
37. Mikuriya, M.; Yoshioka, D.; Borta, A.; Luneau, D.; Matoga, D.; Szklarzewicz, J.; Handa, M. Molecule-based magnetic materials based on dinuclear ruthenium carboxylate and octacyanotungstate. *New Journal of Chemistry*, 2011, 35, pp. 1226-1233.
38. Zhan, S.-Z.; Guo, D.; Zhang, X.-Y.; Du, C.-X.; Zhu, Y.; Yang R.-N. The design, assembly, properties and crystal structure of one-dimensional polymeric cyanide-bridged nickel(II)/nickel(II) complexes, *Inorganica Chimica Acta*, 2000, 298, pp. 57-62.
39. Smekal, Z.; Cisarova, I.; Mrozinski, J. Cyano-bridged bimetallic complexes of copper(II) with tetracyanonickelate(II). Crystal structure of $[\text{Cu}(\text{dpt})\text{Ni}(\text{CN})_4]$, *Polyhedron*, 2001, 20, pp. 3301-3306.
40. O'Connor, C.J. Magnetochemistry—Advances in theory and experimentation, *Progress in Inorganic Chemistry*, 1982, 29, pp. 203-283.
41. Terazzi, E.; Torelli, S.; Bernardinelli, G.; Rivera, J.-P.; Bénech, J.-M.; Bourgogne, C.; Donnio, B.; Guillon, D.; Imbert, D.; Bünzli, J.-C. G.; Pinto, A.; Jeannerat, D.; Piruet, C. Molecular control of macroscopic cubic, columnar, and lamellar organizations in luminescent lanthanide-containing thermotropic liquid crystals, *Journal of the American Chemical Society*, 2005, 127, pp. 888-903.

MIXED-VALENT TETRANUCLEAR $\text{Mn}^{\text{II}}\text{Mn}^{\text{III}}$ COMPLEX WITH 1,3-DIAMINO-2-HYDROXYPROPANE- N,N',N'',N''' -TETRAACETIC ACID

Masahiro Mikuriya^{a*}, Nobuyuki Nagao^a, Satoshi Kurahashi^a, Atsushi Tabuchi^a,
Seiki Tomohara^a, Motohiro Tsuboi^a, Daisuke Yoshioka^a, Hiroshi Sakiyama^b, Akira Fuyuhiko^c

^aDepartment of Chemistry and Research Center for Coordination Molecule-based Devices, School of Science and Technology,
Kwansei Gakuin University, 2-1 Gakuen, Sanda 669-1337, Japan

^bDepartment of Material and Biological Chemistry, Faculty of Science, Yamagata University, 1-4-12 Kojirakawa,
Yamagata 990-8560, Japan

^cDepartment of Chemistry, Graduate School of Science, Osaka University, Toyonaka, Osaka 560-0043, Japan

*e-mail: junpei@kwansei.ac.jp; phone: (+81 79) 565 83 65; fax: (+81 79) 565 90 77

Abstract. Mixed-valent tetranuclear $\text{Mn}^{\text{II}}\text{Mn}^{\text{III}}$ complex with 1,3-diamino-2-hydroxypropane- N,N',N'',N''' -tetraacetic acid (H_5dhpta), $\text{Ca}_2[\text{Mn}_4\{\mu\text{-OHO}\}(\text{dhpta})_2(\text{CH}_3\text{COO})_2] \cdot 13\text{H}_2\text{O}$ (**1**), was synthesized and characterized by elemental analysis, IR and UV-vis-NIR spectroscopy, and temperature dependence of magnetic susceptibilities (4.5–300 K). Single-crystal X-ray crystallography revealed a trapezoid tetranuclear core with $\mu\text{-(OHO)}$, $\mu\text{-alkoxido}$, $\mu\text{-acetato}$ bridges. Magnetic data analysis showed considerable antiferromagnetic interactions among these four manganese atoms with $J(\text{Mn}^{\text{III}}\text{-Mn}^{\text{III}})$ of -35.02 cm^{-1} , $J'(\text{Mn}^{\text{III}}(\text{Mn}^{\text{II}})\text{-Mn}^{\text{III}})$ of -4.82 cm^{-1} , and $J''(\text{Mn}^{\text{II}}\text{-Mn}^{\text{III}})$ of -4.61 cm^{-1} .

Keywords: manganese complex, tetranuclear complex, magnetic property, mixed-valent complex.

Introduction

Tetranuclear manganese complexes have received much attention as model complexes of tetranuclear manganese center of oxygen-evolving complex (OEC) since such system was discovered in the active site of OEC of photosystem II [1-4]. Especially, mixed metal complexes with calcium ions are most interesting in relation to the OEC active site. We have engaged in chemistry of manganese complexes, paying attention to their magnetic properties with a variety of unpaired electrons depending on the oxidation state of manganese ion. So far, we and others synthesized some manganese complexes from mononuclear to tetranuclear and polynuclear species by the use of organic ligands [5-30]. Gorun *et al.* reported that tetranuclear and hexadecanuclear manganese complexes with barium or calcium ions can be isolated by the use of polydentate organic ligand, 1,3-diamino-2-hydroxypropane- N,N',N'',N''' -tetraacetic acid (H_5dhpta) shown in Figure 1 [31-33]. In this study, we examined reaction of H_5dhpta with manganese salt by the use of calcium acetate as counter ion in the hope of obtaining new polynuclear manganese complexes. We isolated a tetranuclear manganese complex with calcium

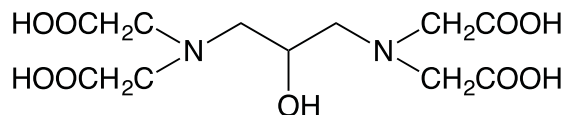


Figure 1. Polydentate organic ligand, H_5dhpta .

ions similar to Gorun's tetranuclear manganese complex. The isolated complex was characterized by elemental analysis, IR and UV-vis-NIR spectroscopies, measurement of temperature dependence of magnetic susceptibilities (4.5–300 K), and single-crystal X-ray crystallography. Herein, we report on the crystal structure, spectral features, and magnetic property of this complex.

Experimental

All reagents and solvents were obtained from commercial sources and were used without further purification.

$\text{Ca}_2[\text{Mn}_4\{\mu\text{-OHO}\}(\text{dhpta})_2(\text{CH}_3\text{COO})_2] \cdot 13\text{H}_2\text{O}$ (**1**)

Calcium acetate monohydrate (23 mg, 0.15 mmol) and H_5dhpta (32 mg, 0.10 mmol) were dissolved in 4.5 mL of H_2O . To this solution was added a methanol solution (3 mL) of manganese(II) chloride tetrahydrate (40 mg, 0.20 mmol). After the pH of the solution was brought to *ca.* 8 with 1 M NaOH solution, 0.1 mL of 30% H_2O_2 was added dropwise with stirring, giving a dark brown solution. *N,N*-Dimethylformamide (10 mL) was layered onto this solution and the mixture was allowed to stand at room temperature for several days. Dark brown crystals separated, and were collected by filtration, washed with small amount of methanol, and dried *in vacuo*. Yield: 25 mg (38%). Anal. Found: C, 23.81; H, 4.71; N, 4.61%. Calcd. for $\text{C}_{26}\text{H}_{50}\text{Ca}_2\text{Mn}_4\text{N}_4\text{O}_{37}$: C, 23.66; H, 4.51; N, 4.25%. IR (KBr): $\nu(\text{OH})$ 3381, $\delta(\text{H}_2\text{O})$ 1616, $\nu_{\text{as}}(\text{CO}_2^-)$ 1560sh, $\nu_{\text{s}}(\text{CO}_2^-)$ 1400. Diffuse reflectance spectrum: λ_{max} 292, 478, 566(sh), 858, 1096(sh) nm.

Measurements: Elemental analyses for carbon, hydrogen, and nitrogen were done using a Thermo-Finnigan FLASH EA1112 series CHNO-S analyzer. Infrared spectra were measured with a JASCO MFT-2000 FT-IR Spectrometer in the 4000–600 cm^{-1} region. Electronic spectra were measured with a Shimadzu UV-vis-NIR Recording Spectrophotometer (Model UV-3100). Magnetic susceptibilities were measured with a Quantum Design MPMS-XL7 SQUID susceptometer operating at a magnetic field of 0.5 T over a range of 4.5–300 K. The susceptibilities were

corrected for the diamagnetism of the constituent atoms using Pascal's constants. The effective magnetic moments were calculated from the equation $\mu_{\text{eff}} = 2.828\sqrt{\chi_M T}$, where χ_M is the molar magnetic susceptibility per mole of tetranuclear manganese unit.

X-Ray Crystallography: Preliminary X-ray diffraction data were taken by a Rigaku R-Axis RAPID diffractometer using graphite-monochromated Mo K α radiation at 200 K. X-Ray diffraction data were collected on a Bruker SMART APEX CCD diffractometer (Mo K α radiation) at 90 K and indexed using the SMART software. Crystal data and details concerning data collection are given in Table 1. The cell parameters were refined by full-matrix least-squares on F^2 . Integrated intensity information for each reflections was obtained and corrected using the SAINT+ program package including the reduction program SAINT and the empirical absorption correction program SADABS. The structure was solved using the SHELXTL program. The structure was solved by direct methods, and the residual non-hydrogen atoms were located by D-Fourier synthesis. All of non-hydrogen atoms were refined by full-matrix least-squares on F^2 . One of the two acetato groups was found to be disordered into two positions with half occupations. The hydrogen atoms except for those of water molecules were inserted at their ideal positions and fixed there. All of the calculations were carried out on a Pentium IV Windows 2000 computer utilizing the SHELXTL software package. CCDC 996784 for **1** contains supplementary crystallographic data for this paper. The data can be obtained free of charge at www.ccdc.cam.ac.uk/conts/retrieving.html [or from the Cambridge Crystallographic Data Centre, 12 Union Road, Cambridge CB12 1EZ, UK; fax: (internet.) +44 1223 336033; E-mail: deposit@ccdc.cam.ac.uk].

Table 1

Crystal and experimental data.

Parameter	Value
Chemical formula	C ₂₆ H ₆₇ Ca ₂ Mn ₄ N ₄ O ₄₁
Formula weight	1391.76
Temperature, (K)	90
Crystal system	monoclinic
Space group	$P2_1/m$
Z	2
a, (Å)	11.291(2)
b, (Å)	20.601(4)
c, (Å)	11.563(2)
β , (°)	98.678(3)
V, (Å ³)	2658.7(9)
D _x , (g/cm ³)	1.738
Radiation: Mo K α , λ , (Å)	0.71073
μ (Mo K α), (mm ⁻¹)	1.235
F ₀ (000)	1438
Crystal size, (mm ³)	0.73 x 0.64 x 0.10
No. of reflections collected	15723
No. of independent reflections	6157
θ range for data collection, (°)	1.81 - 28.22
Data/Restraints/Parameters	6157/0/371
Goodness-of-fit on F^2	1.050
R indices [$I > 2\sigma(I)$]	$R1 = 0.0832$, $wR2 = 0.2275$
R indices (all data)	$R1 = 0.1033$, $wR2 = 0.2427$
$(\Delta/\sigma)_{\text{max}}$	0.000
$(\Delta\rho)_{\text{max}}$, (eÅ ⁻³)	2.547
$(\Delta\rho)_{\text{min}}$, (eÅ ⁻³)	-1.957
Measurement	Bruker Smart APEX CCD diffractometer
Program system	SHELXTL
Structure determination	Direct methods (SHELXS-97)
Refinement	full matrix least-squares (SHELXL-97)
CCDC deposition number	996784

Results and discussion

Reaction of manganese(II) chloride tetrahydrate with the polydentate ligand H_3dhpta in the presence of calcium ions gave dark brown crystals. The formulation of the mixed-metal system of tetranuclear $Mn^{II}Mn^{III}_3$ complex with calcium(II), $Ca_2[Mn_4\{\mu-OHO\}(dhpta)_2(CH_3COO)_2]$, was confirmed by the elemental analyses, infrared and electronic spectroscopies, single-crystal X-ray structure analysis, and magnetic susceptibility measurement. The analytical data were obtained from the dried sample containing different amount of crystal water molecules from the single crystals for X-ray structure analysis. In the infrared spectra of **1**, one strong shoulder band at 1560 nm and one strong band at 1400 cm^{-1} may be assigned to antisymmetric and symmetric stretching vibrations of the *syn-syn* acetato bridges [34], respectively, as shown in Figure 2. The broad bands at 3381 and 1616 cm^{-1} in **1** may be attributed to $\nu(OH)$ stretching band and $\delta(H_2O)$ bending mode of water molecules, respectively [34].

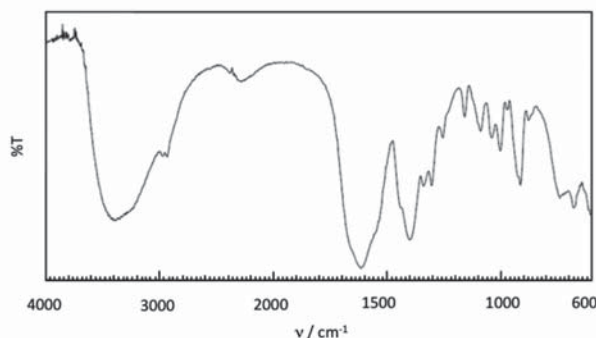


Figure 2. Infrared spectra of **1**.

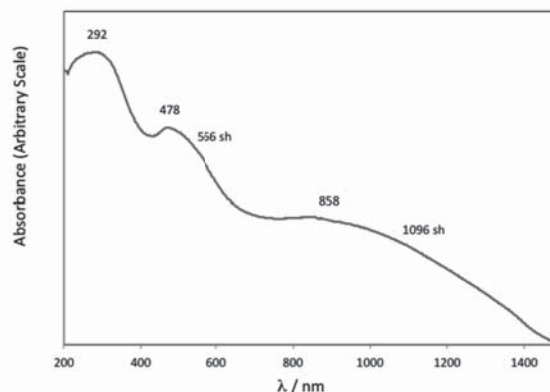


Figure 3. Diffused reflectance spectra of **1**.

The diffused reflectance spectra of **1** are shown in Figure 3. Two or three broad absorption bands around 292 and 478 (possibly, and 566 shoulder) nm in solid can be attributed to LMCT charge-transfer transitions in origin [5,6,8]. A broad band at 858 nm with shoulder at 1096 may be due to d-d transitions of manganese(III) ions [5,6,8]. The spectral feature is in harmony with the mixed-valent state of the present complex, because d-d transitions of manganese(II) are spin-forbidden and the intervalence bands of the mixed-valence should be in the broad band in the NIR region.

Single crystals of **1** were obtained by crystallization from the reaction solution. X-ray crystal structure analysis revealed that the present complex has a tetranuclear manganese core similar to Gorun's structure [32]. The structure of the tetranuclear complex drawn by ORTEP is shown in Figure 4. The four manganese atoms are located in a trapezoid form. The molecule has a crystallographic mirror plane intersecting the O13, O14, C12, C13, and H(O14) atoms. The Mn1 atom is coordinated by two monodentate acetato-oxygen atoms (O1, O3), amino-nitrogen atom (N1), and alkoxido-oxygen atom (O5) of $dhpta^{5-}$, one acetato-oxygen atom (O10) of *syn-syn*-bridging acetate ion, and oxido-oxygen atom (O13) in an axially compressed octahedral geometry, suggesting the Jahn-Teller distortion due to Mn^{III} , whereas the Mn2 atom is coordinated by two monodentate acetato-oxygen atoms (O6, O8), amino-nitrogen atom (N2), and alkoxido-oxygen atom (O5) of $dhpta^{5-}$, one acetato-oxygen atom (O11 or O12') of *syn-syn*-bridging acetate ion, and hydroxido-oxygen atom (O14) in a distorted octahedral geometry. The bond distances around the Mn2 atom are mostly longer than those of the Mn1 atom in accordance with the mixed-valence $Mn^{II}Mn^{III}$ state of the Mn2 and Mn2' atoms.

Temperature dependence of effective magnetic moments is shown in Figure 5. The magnetic moment of **1** is $9.72\mu_B$ at 300 K per tetranuclear $Mn^{II}Mn^{III}_3$ unit, which is lower than the spin-only value ($10.34\mu_B$). The magnetic moments gradually decrease with lowering of temperature until reaching $3.74\mu_B$ at 4.5 K, being typical of antiferromagnetic behavior [3, 11-14, 17-20, 25-28]. The magnetic data were analyzed with magnetic susceptibility equation based on the Heisenberg model $H = -JS_{31}\cdot S_{32} - J'(S_{31}\cdot S_{21} + S_{31}\cdot S_{33} + S_{32}\cdot S_{21} + S_{32}\cdot S_{33}) - J''S_{21}\cdot S_{33}$ by a scheme shown in Figure 6 considering the mirror symmetry of this system. The g value was treated as isotropic and $g(Mn^{III}) = g(Mn^{II})$. Best fitting curve was obtained with the parameters; $J = -35.02\text{ cm}^{-1}$, $J' = -4.82\text{ cm}^{-1}$, $J'' = -4.61\text{ cm}^{-1}$, $g = 2.08$, and $N\alpha = 2500 \times 10^{-6}\text{ cm}^3\text{ mol}^{-1}$. This result shows that a strong antiferromagnetic interaction is operating between the two Mn^{III} atoms ($Mn1-Mn1'$) with weak antiferromagnetic interactions between $Mn^{III}-Mn^{II}(Mn^{III})$ ($Mn1-Mn2$, $Mn1-Mn2'$, $Mn1'-Mn2$, $Mn1'-Mn2'$) or $Mn^{II}-Mn^{III}$ ($Mn2-Mn2'$) atoms, being consistent with the wide angles of the bridging groups ($Mn1-O13-Mn1'$ $137.7(3)^\circ$, $Mn2-O14-Mn2'$ $136.0(4)^\circ$, $Mn1-O5-Mn2$ $132.85(18)^\circ$) between these manganese atoms preferring antiferromagnetic interaction for the present complex.

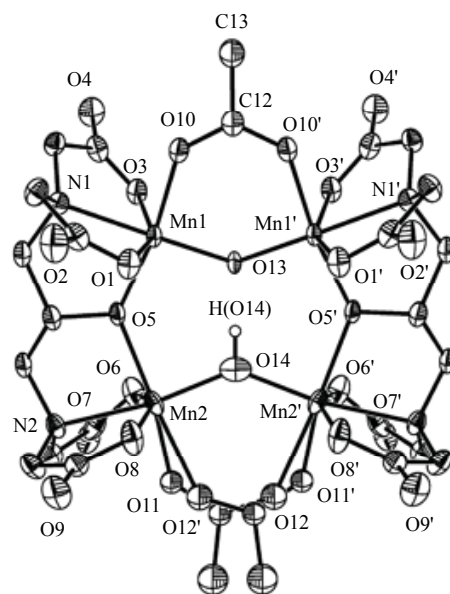


Figure 4. ORTEP drawing of the structure of the tetranuclear manganese complex anion showing the 50% probability level thermal ellipsoids.

Selected bond lengths (Å) and angles (°): Mn1···Mn1' 3.382(2), Mn2···Mn2' 3.565(2), Mn1···Mn2 3.719(1), Mn1-O1 2.150(4), Mn1-O3 2.188(4), Mn1-O5 1.953(4), Mn1-O10 1.969(4), Mn1-O13 1.813(2), Mn1-N1 2.114(4), Mn2-O5 2.103(4), Mn2-O6 2.172(4), Mn2-O8 2.133(4), Mn2-O12' 2.323(11), Mn2-O11 1.851(9), Mn2-O14 1.923(3), Mn2-N2 2.193(4), Mn1-O13-Mn1' 137.7(3), Mn2-O14-Mn2' 136.0(4), Mn1-O5-Mn2 132.85(18). Prime denotes the equivalent position (x, 1/2–y, z).

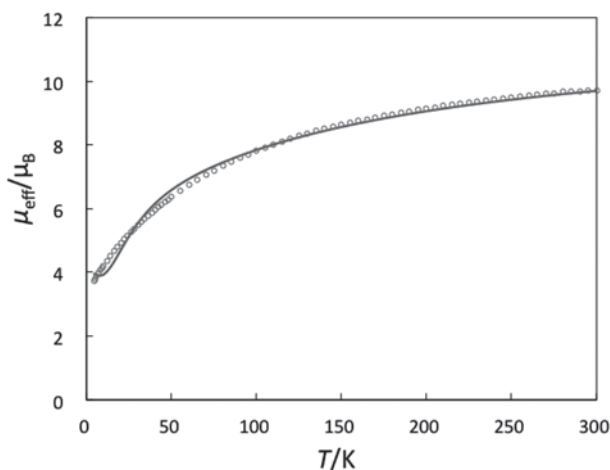


Figure 5. Temperature dependence of magnetic moment of 1.

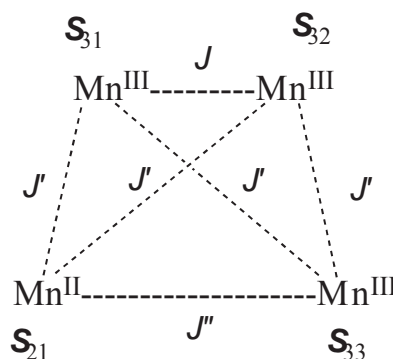


Figure 6. Magnetic interactions in trapezoid tetranuclear Mn^{II}Mn^{III}₃ core.

Conclusions

By using 1,3-diamino-2-hydroxypropane-*N,N',N'',N'''*-tetraacetic acid, a tetranuclear mixed-valent Mn^{II}Mn^{III}₃ complex, Ca₂[Mn₄{μ-OHO}(dhpta)₂(CH₃COO)₂], was isolated. The crystal structure revealed a trapezoid tetranuclear core with μ-(OHO), μ-alkoxido, μ-acetato bridges. In accordance with the structural feature, a considerable antiferromagnetic interaction was observed for the present complex.

Acknowledgements

The present work was partially supported by Grant-in-Aid for Scientific Research No. 26410080 from the Ministry of Education, Culture, Sports, Science and Technology (MEXT, Japan) and the NEXT-Supported Program for the Strategic Research Foundation at Private Universities, 2010–2014.

References

1. Pecoraro, V. L., Eds. Manganese Redox Enzymes. VHC Publishers: New York, 1992, 290 p.
2. Uemura, Y.; Kawakami, K.; Shen, J.R.; Kamiya, N. Crystal structure of oxygen-evolving photosystem II at a resolution of 1.9 Å. *Nature*, 2011, 473, pp. 55-60.
3. Mikuriya, M. Mononuclear and Oligonuclear Manganese Complexes with Organic Multidentate Ligands. *Nihon Kessho Gakkaishi*, 2011, 53, pp. 193-200 (in Japanese).
4. Mikuriya, M. X-ray Crystal Structure Analysis in Coordination Chemistry Laboratory—Multinuclear Metal Complexes. *Advances in X-Ray Chemical Analysis Japan*, 2012, 43, pp. 89-102 (in Japanese).
5. Mikuriya, M.; Takebayashi, H.; Matsunami, K. A Manganese(III) Complex with 1-[(2-Hydroxyethyl)amino]-2-(salicylideneamino)ethane. *Bulletin of the Chemical Society of Japan*, 1994, 67, pp. 3128-3130.
6. Mikuriya, M.; Nukada, R.; Tokami, W.; Hashimoto, Y.; Fujii, T. Synthesis and Characterization of Manganese(III) Complexes with 2-{*N*-[2-(4-Imidazolyl)ethyl]iminomethyl}phenol or 2-{*N*-[2-(2-Pyridyl)ethyl]iminomethyl}phenol. *Bulletin of the Chemical Society of Japan*, 1996, 69, pp. 1573-1578.
7. Mikuriya, M.; Hatano, Y.; Asato, E. Synthesis and Structural Characterization of Manganese(II) Complexes with *N,N'*-Bis(2-pyridylmethylene)-1,3-diaminopropane-2-ol or *N,N'*-Bis(2-Pyridylmethylene)-1,3-propanediamine. *Bulletin of the Chemical Society of Japan*, 1997, 70, pp. 2495-2507.
8. Shongwe, M. S.; Mikuriya, M.; Nukada, R.; Ainscough, E. W.; Brodie, A. M.; Waters, J. M. A series of heteroleptic complexes of the type *fac*-[Mn^{III}L₂]⁻ [H₂L = derivatives of *N*-(2-hydroxybenzyl)glycine or *N*-(5-nitro-2-hydroxybenzyl)sarcosine] possessing unusual Mn(III) co-ordination spheres. *Inorganica Chimica Acta*, 1999, 290, pp. 228-236.
9. Mikuriya, M.; Dai, J.; Kakuta, Y.; Tokii, T. Synthesis and Characterization of a Series of Mononuclear Manganese(IV) Complexes with *o*-(Salicylideneaminomethyl)phenol and its Substituted Derivatives. *Bulletin of the Chemical Society of Japan*, 1993, 66, pp. 1132-1139.
10. Suzuki, R.; Chiba, Y.; Yamaguchi, R.; Yoshioka, D.; Mikuriya, M.; Sakiyama, H. Synthesis and Crystal Structure of a Trigonally Compressed Hexakis-DMF Manganese(II) Complex, X-ray Structure Analysis Online, 2013, 29, pp. 11-12.
11. Torihara, N.; Mikuriya, M.; Okawa, H.; Kida, S. Binuclear Metal Complexes. XXXI. Synthesis and Magnetic Property of Binuclear Manganese(III) Complexes with 3-Salicylideneamino-1-propanol and Its Homologues. *Bulletin of the Chemical Society of Japan*, 1980, 53, pp. 1610-1613.
12. Mikuriya, M.; Torihara, N.; Okawa, H.; Kida, S. Binuclear Metal Complexes. XXXVII. Crystal and Molecular Structure of a Binuclear Manganese(III) Complex Bridged by Two Alkoxo Oxygens and Two Bidentate Acetate Ions. *Bulletin of the Chemical Society of Japan*, 1981, 54, pp. 1063-1067.
13. Suzuki, M.; Mikuriya, M.; Murata, S.; Uehara, A.; Oshio, H.; Kida, S.; Saito, K. Synthesis and Characterization of Dinuclear Manganese(II,II) and Manganese(II,III) Complexes with Phenolate and Two Carboxylate Bridges. *Bulletin of the Chemical Society of Japan*, 1987, 60, pp. 4305-4312.
14. Mikuriya, M.; Yamato, Y.; Tokii, T. 1,3-Bis(salicylideneamino)-2-propanol as the Ligand for Manganese(III) Ions. *Bulletin of the Chemical Society of Japan*, 1992, 65, pp. 1466-1468.
15. Mikuriya, M.; Yamato, Y.; Tokii, T. Ferromagnetically Coupled Dimanganese(III) Complex and Antiferromagnetically Coupled Diiron(III) Complex with Unsymmetrical Ligands. *Chemistry Letters*, 1992, 21(8), pp. 1571-1574.
16. Mikuriya, M.; Nakadera, K.; Tokii, T. Novel elimination reaction of a hydroxyethyl group in a manganese complex. Formation of a binuclear manganese(II) complex with a Robson-type macrocyclic ligand. *Inorganica Chimica Acta*, 1992, 194, pp. 129-131.
17. Mikuriya, M.; Fujii, T.; Tokii, T.; Kawamori, A. Synthesis and Characterization of Mononuclear (Mn(II) and Mn(III)) and Dinuclear (Mn(II)Mn(II) and Mn(II)Mn(III)) Complexes with 2,6-Bis[*N*-(2-pyridylethyl)iminomethyl]-4-methylphenol. *Bulletin of the Chemical Society of Japan*, 1993, 66, pp. 1675-1686.
18. Mikuriya, M.; Fukumoto, H.; Kako, T. Novel dinuclear manganese(II) complexes with monocapped trigonal prism geometries: implication of Mn-Mn distance on the catalase activity of dinuclear manganese center. *Inorganic Chemistry Communication*, 1998, 1, pp. 225-227.
19. Mikata, Y.; So, H.; Yamashita, A.; Kawamura, A.; Mikuriya, M.; Fukui, K.; Ichimura, A.; Yano, S. Quinoline-based tetradentate nitrogen ligands stabilize the bis(μ-oxo) dinuclear manganese(III,III) core. *Dalton Transaction*, 2007, 30, pp. 3330-3334.
20. Wada, S.; Mikuriya, M. Synthesis and Structural Characterization of Dinuclear Manganese(III) Complexes with Cyclam-Based Macrocyclic Ligands Having Schiff-base Pendant Arms as Chelating Agents. *Bulletin of the Chemical Society of Japan*, 2008, 81, pp. 348-357.
21. Mikuriya, M.; Majima, K.; Yamato, Y. Alkoxo-Bridged Trinuclear Manganese(III) Complex with an Isosceles Triangle Core. *Chemistry Letters*, 1992, 21(10), pp. 1929-1932.
22. Tanase, T.; Tamakoshi, S.; Doi, M.; Mikuriya, M.; Sakurai, H.; Yano, S. Novel Mn^{II}Mn^{III}Mn^{II} Trinuclear Complexes

- with Carbohydrate Bridges Derived from Seven-Coordinate Manganese(II) Complexes with *N*-Glycoside. *Inorganic Chemistry*, 2000, 39, pp. 692-704.
23. Yoshino, A.; Miyagi, T.; Asato, E.; Mikuriya, M.; Sakata, Y.; Sugiura, K.; Iwasaki, K.; Hino, S. Construction of a mixed valence trinuclear $Mn^{II}Mn^{III}Mn^{II}$ aggregate into a large macrocyclic ligand. *Chemical Communications*, 2000, 16, pp. 1475-1476.
24. Nakai, M.; Funabiki, T.; Ohtsuki, C.; Harada, M.; Ichimura, A.; Tanaka, R.; Nishioka, T.; Kinoshita, I.; Mikuriya, M.; Guo, J.; Benten, H.; Ohkita, H.; Ito, S.; Obata, M.; Nakabayshi, Y.; Yano, S. Synthesis, structures, and photochemical properties of $(\mu_3-O)tris\{bis(\mu-carboxylato)\}$ trimanganese complexes with naphthylacetate ligands with relevance to artificial solar energy-harvesting systems. *Inorganica Chimica Acta*, 2013, 406, 130-137.
25. Mikuriya, M.; Yamato, Y.; Tokii, T. Synthesis, Properties, and Crystal Structures of a Series of Dinuclear Manganese(III) Complexes with 1,5-Bis(salicylideneamino)-3-pentanol and Various Anions: Formation of a Tetranuclear Manganese(III) Complex. *Bulletin of the Chemical Society of Japan*, 1992, 65, pp. 2624-2637.
26. Mikuriya, M.; Nakadera, K.; Kotera, T.; Tokii, T.; Mori, W. Synthesis and Characterization of tetranuclear Manganese(III) Complexes with 2,6-Bis(salicylideneaminomethyl)-4-methylphenol. *Bulletin of the Chemical Society of Japan*, 1995, 68, pp. 3077-3083.
27. Mikuriya, M.; Hashimoto, Y.; Kawamori, A. Synthesis of a Tetranuclear Manganese Complex with a Cubane Core at the $Mn^{II}Mn^{III}Mn^{II}Mn^{III}$ Oxidation Level. *Chemistry Letters*, 1995, 12, pp. 1095-1096.
28. Mikuriya, M.; Kotera, T. Novel Thiolato-Bridged Tetranuclear Manganese(II) and Iron(II) Complexes with Adamantane-like Cores, *Chemistry Letters*, 1998, pp. 971-972.
29. Mikata, Y.; Wakamatsu, M.; So, H.; Abe, Y.; Mikuriya, M.; Fukui, K.; Yano, S. *N,N,N',N'*-Tetrakis(2-quinolylmethyl)-2-hydroxy-1,3-propanediamine (Htqhpn) as a Supporting Ligand for a Low-Valent $(\mu-O)_2$ Tetranuclear Manganese Core. *Inorganic Chemistry*, 2005, 44, pp. 7268-7270.
30. Mikuriya, M.; Adachi, F.; Iwasawa, H.; Handa, M.; Koikawa, M.; Okawa, H. Synthesis and Characterization of Thiolate-Bridged Manganese(II) Complexes with NNS-Tridentate Thiolic Ligands. *Bulletin of the Chemical Society of Japan*, 1994, 67, pp. 3263-3270.
31. Stibrany, R. T.; Gorun, S. M. Synthesis, Structure, and Catalase-Type Activity of a Novel Oxo-Bridged tetranuclear manganese Aggregate Exhibiting Short O...O Interactions. *Angewandte Chemie International Edition*, 1990, 29, pp. 1156-1158.
32. Gorun, S. M.; Stibrany, R. T.; Lillo, A. Supramolecular Mn-Ca Aggregates as Models for the Photosynthetic water Oxidation Complex. *Inorganic Chemistry*, 1998, 37, 836-837.
33. Lee, J.; Chasteen, N. D.; Zhao, G.; Papaefthymiou, G. C.; Gorun, S. M. Deuterium Structural Effects in Inorganic and Bioinorganic Aggregates. *Journal of the American Chemistry*, 2002, 124, pp. 3042-3049.
34. Nakamoto, K. *Infrared and Raman Spectra of Inorganic and Coordination Compounds Part B*; John Wiley & Sons: Hoboken, 2009, 408 p.

STUDY OF PROPERTIES OF SOME POLYETHYLENE-CLAY NANOCOMPOSITES: INFLUENCE OF PREPARATION METHOD ON THE DEGREE OF CLAY INTERCALATION/EXFOLIATION

Fulga Tanasa*, Madalina Zanoaga

"Petru Poni" Institute of Macromolecular Chemistry, 41A, Grigore Ghica Voda Alley, Iasi 700487, Romania

**e-mail: ftanasa@icmpp.ro; phone (+40 232) 21 74 54; fax (+40 232) 21 12 99*

Paper dedicated to the 65th anniversary of the

"Petru Poni" Institute of Macromolecular Chemistry of Romanian Academy, Iasi, Romania

Abstract: New nanocomposites based on high density polyethylene (HDPE) and organically modified nanoclay (Cloisite 20A) were obtained by two different methods, namely melt compounding and solution blending, and their properties were comparatively studied by XRD, DSC, POM and SEM in order to establish the dependence of the clay degree of exfoliation/intercalation on the preparation procedure. Nanocomposites prepared in molten state under shear stress were found to possess the most extensive dispersion of nanometric clay particles and high levels of exfoliation.

Keywords: polymer-clay nanocomposites, preparation, properties, exfoliation, intercalation.

Introduction

Thermoplastic composites play an important role in our society, as their properties respond to a wide range of specific demands. They have, therefore, attracted considerable interest from both industry and academic media.

When clays and polymers are compatible, the properties conferred by the filler to the polymer matrix are comparable or exceed those of traditional materials. High levels of exfoliated layered silicate may be difficultly reached when highly hydrophobic materials, such as polyethylene (PE) and polypropylene (PP), are used. Maleic anhydride (MA) grafting proved to be the most efficient method to grant compatibility to PE and PP towards organoclays. Modern approaches use not only such compatibilizing agents (PP-g-MA and PE-g-MA), but also organically modified clays [1].

The high aspect ratio of the nanoclays provides a great interfacial area, thus enhancing reinforcing properties. Silicates, such as montmorillonite, hectorite, and saponite, have a layered structure that, upon exfoliation, leads to composites with very high stiffness and strength [2].

The most known methods for preparing polymer-clay nanocomposites are melt intercalation, *in situ* polymerization, and solution dispersion. The melt intercalation method is the most convenient at industrial scale due to the continuous nature of the process and economic factors. It was found that the orientation of clay in compatibilized polymer matrices (polymers grafted with maleic anhydride) increased with increasing shear rate. The hydrogen bridges between polymeric maleic anhydride units and oxygen-containing groups in the silicates may significantly contribute to the clay intercalation. But for an effective clay exfoliation, the shear stress addition was required.

The solution blending is a procedure of lesser importance compared to melt compounding, as it requires toxic/aggressive solvents. Even so, significant levels of intercalation or exfoliation were achieved for linear low density polyethylene (LDPE) or polypropylene (PP) nanocomposites prepared from solution without compatibilizers [3,4] and only microcomposites are known to be produced from the same components by melt-compounding [5,6]. Other studies reported that only un-intercalated microcomposites were obtained by this procedure, although a wide range of solvents was employed, and regardless the method applied for solvent removal (evaporation or precipitation in different non-solvents) [7]. It was also reported [8,9] that nanocomposites prepared in molten state were the only ones displaying high degrees of exfoliation.

From a scientific point of view, a comparative study of the structure and morphology of polymer-clay composites obtained through different procedures is very useful when it comes to explain composites properties and behavior; it is also of great importance to understand the mechanisms and influence of the different parameters, such as the shear stress in melt compounding, the temperature, the polymer-organoclay compatibility, etc., on the intercalation/exfoliation processes.

New nanocomposites based on high density polyethylene (HDPE) and organically modified nanoclay (Cloisite 20A) were obtained by two different methods, namely melt compounding and solution blending, and their properties were comparatively studied in order to establish the dependence of the clay degree of exfoliation/intercalation on the preparation procedure.

Results and discussion

The structure of phyllosilicates (nanoclays) (Figure 1) was extensively studied in correlation with their applications in polymer nanocomposites in order to reveal their effects on polymeric materials [1,10,11].

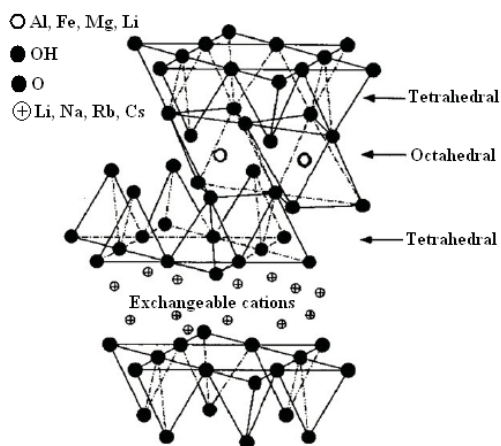


Figure 1. Structure of phyllosilicates (nanoclays).

Surface modification of clay has commonly been used to achieve a better compatibility of the clay and polymer. Ion exchange of Na^+ or Ca^{2+} cations present in the clay galleries by alkylammonium ions from organic modifiers is frequently used [10].

The thermal gravimetric analysis (TGA) of the unmodified montmorillonite displayed three mass loss stages: below 100°C , at 135°C and at 450°C [11]. They were attributed to water desorption from clay, dehydration of the hydrated cations inside galleries and to the dehydroxylation of the montmorillonite, respectively. The presence of organic cations increases the number of decomposition steps, as follows: the first step is up to 66.9°C and is attributed to the desorption of water; the second occurs from 135.5°C to 310°C and is assigned to the loss of hydration water from Na^+ cations; the third one corresponds to the removal of the surfactant at approx. 440°C ; the last mass loss stage is associated to the loss of structural hydroxyl groups from clay and occurs around 580°C . This is an indication of the thermal stability of modified clays [11].

DSC data for the neat polymers are presented in Table 1. HDPE-g-MA has lower melting temperature, melting heat and degree of crystallinity than HDPE, due to the presence of maleic anhydride groups that disrupt the order of the crystalline structure of polyethylene macromolecular chains.

Table 1

DSC data for neat polymers.

Polymer	Melting point ($^\circ\text{C}$)	Melting heat (J/g)	Crystallinity (%)
HDPE	135.9	196.1	64.7
HDPE-g-MA	133.7	173.3	57.6

The crystallization of nanocomposite samples prepared by solution dispersion or by melt blending has been studied according to a literature procedure [9], by isothermal DSC analysis in the range of crystallization temperatures of 120 - 124°C (Table 2).

Table 2

Crystallization times for composite samples prepared by melt blending and from solution.

Half crystallization time ($t_{0.5}$, s)

Crystallization temperature ($^\circ\text{C}$)	Composite samples			
	HDPE 5 melt	HDPE-g-MA 10 melt	HDPE-g-MA 10 sol	HDPE-g-MA 15 sol
124	255	308	202	170
123	197	179	117	119
122	165	141	93	73
121	109	101	65	52
120	91	80	45	49

It is known that clay remains in solid state over the whole selected range of temperature during the DSC measurements. Thus, the recorded isothermal DSC traces consist of single exothermic peaks. As presented in Table 2, the addition of Cloisite 20A into HDPE and HDPE-g-MA matrices (melt blending) slightly modified the half-crystallization times of the corresponding polymers. For solution mixing samples, the presence of clay particles decreased the half crystallization times of the polymer matrix. These results are in good concordance with reported data [9].

The XRD patterns of the Cloisite 20A and of some of the composites prepared by melt blending are shown in Figure 2, while those for composites obtained by solution mixing are presented in Figure 3.

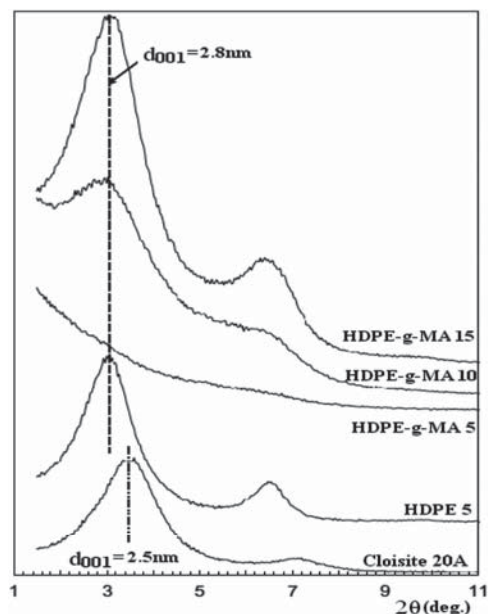


Figure 2. XRD patterns of Cloisite 20A and of some composites obtained by melt blending.

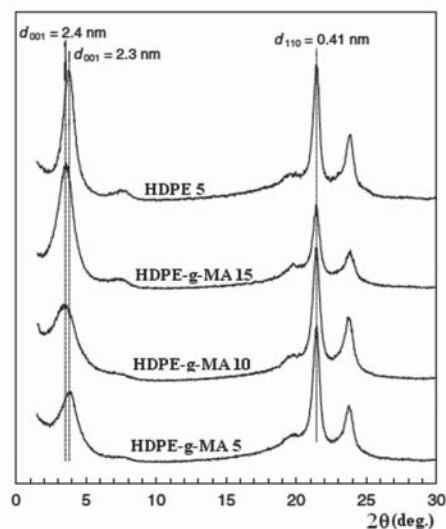


Figure 3. XRD patterns of some composites prepared by solution mixing.

The basal reflection at $2\theta = 3.5^\circ$ ($d_{001} = 2.5$ nm) characteristic to Cloisite 20A (Figure 2) is slightly shifted to lower angles ($2\theta = 3.1^\circ$, $d_{001} = 2.8$ nm) in the XRD spectrum of HDPE-3. Most authors agree that different PE grades yield in conventional microcomposites when melt blended with commercial organoclays [5,8,12,13]; thus, shifts of the basal reflection toward lower or wider angles have often been observed and were attributed to limited intercalation, interlayer reorganization, or to thermal decomposition of the surfactant inside the galleries [14]. In our case, the slight gallery expansion observed for HDPE 5 and HDPE-g-MA composites obtain by melt blending might be caused by the limited penetration of polyolefin macromolecules inside the clay galleries, observation consistent with literature data [14].

The behavior of the HDPE and HDMA composites prepared from solution is illustrated by the XRD patterns in Figure 3. It is known that the unbound surfactant of an organoclay, added in excess with respect to the CEC of the clay during the cation exchange, can be removed by solvent extraction (*e.g.*, with alcohols) [15,16]. It was also shown that an ethanol extraction of Cloisite 20A yielded in a product characterized by lower organic content (from 38.5 to 35.9 wt%) and interlayer distance (from 2.53 to 2.42 nm) [7].

In our experiments, composites were prepared from solution by room-temperature solvent removal and the corresponding XRD patterns showed they contain a more or less intense basal reflection approximately at the same angular position as clay. Comparing Figures 2 and 3, it seems that HDPE-g-MA 15 composites are highly exfoliated when prepared in molten state, but contain ordered platelets stacks when prepared from solution.

Literature data showed the clay sheets, which are predominantly delaminated in the xylene dispersion [15,16], tend to aggregate back into stacks during solvent evaporation. This is a well documented phenomenon, known in literature as the secondary aggregation which occurs due to the processing conditions [17]. Such phenomenon takes place along with the expulsion of the polymer chains, so that unintercalated silicate stacks are formed. A comparison of Figures 2 and 3 shows that the interlayer spacing of the HDPE 3 and HDPE-g-MA 15 composites obtained from solution is smaller than that of the same composites prepared in molten state, which is evidence in favor of intercalation for the latter.

Primary examination of composites morphology was performed by POM and the selected images of HDPE-g-MA 10 samples are shown in Figure 4.

The image corresponding to the composite prepared by melt compounding appears almost completely dark, in agreement with the XRD suggestion that this is a highly exfoliated nanocomposite characterized by homogeneous

dispersion of nanometric clay particles. The other image, corresponding to the composite prepared from solution, reveals the presence of birefringent particles quite uniformly distributed over the entire field. The SEM analysis results confirm these observations (Figure 5).

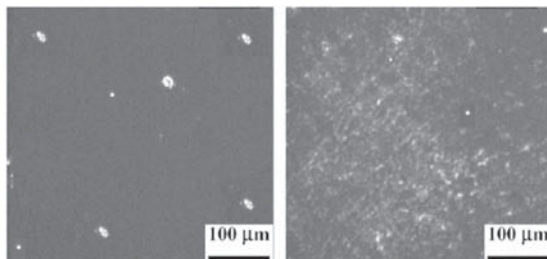


Figure 4. POM images of HDPE-g-MA 10 prepared by melt blending (left) and from solution (right).

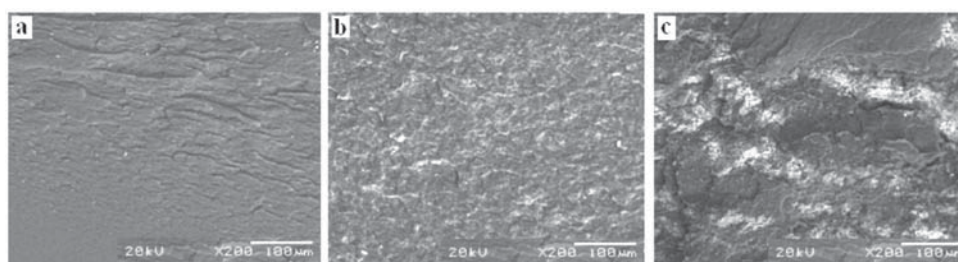


Figure 5. SEM micrographs of composite samples: a - HDPE 5 (melt blending), b - HDPE-g-MA 10 (melt blending), c - HDPE-g-MA 10 (from solution).

Micrographs of melt blended samples (Figure 5a and b) showed a fairly homogeneous distribution of filler inside the polymer matrix, despite the relatively high amount of clay in the corresponding formulations. This suggests a nanometric dispersion of exfoliated nanoparticles up to a certain degree, higher than that obtained through solution mixing, as suggested by micrograph 5c which shows a completely different texture, with rough areas (attributed to secondary agglomeration of clay platelets) distributed in an inhomogeneous manner in the polymer matrix.

This hypothesis was demonstrated in literature by SEM micrographs obtained for cryo-fractured samples after they were burned in order to remove the organic material (the polymer matrix), so that the inorganic phase was the only one remaining and it retained the initial shape from the corresponding composite [8]. In this way, it was possible to show the extensive local parallelism of the clay layers inside the melt compounded nanocomposites, which is completely absent in those obtained from solution.

A deeper insight into the morphology of these composites we presented in this study, by the means of transmission electron microscopy (TEM), is required in order to fully demonstrate the local parallelism between individual silicate platelets and tactoids, or thin stacks present in the matrix. These investigations are currently underway and will be published in a future article.

Conclusion

Nanocomposites based on HDPE and HDPE-g-MA, as matrix, and Cloisite 20A, as filler, were obtained by two different methods, namely melt compounding and solution mixing. Their properties were comparatively studied (DSC, XRD, POM and SEM) in order to establish the correlation between the preparation method and the degree of clay intercalation/exfoliation.

Solution mixing failed to produce intercalated composites, as long as solvent removal is made at room temperature. The organoclay is predominantly exfoliated when dispersed in a good solvent relative to the polymer, such is hot xylene, but it tends to aggregate during processing (when solvent is removed by evaporation), leading to the homogeneous dispersion of small amounts of unintercalated tactoids in the polymer matrix.

Still, microscopic analysis demonstrated that the preparation approach has a marked influence on the composites morphology. Thus, the presence of poorly dispersed, micron-sized, yet intercalated clay particles was revealed in composites prepared from solution, whereas the nanocomposites prepared in the melt under shear stress were found to possess the most extensive dispersion of nanometric clay particles and high levels of exfoliation.

The results were attributed to different patterns of clay dispersion and degrees of intercalation/exfoliation achieved during different preparation procedures. They are relevant in terms of tailoring nanocomposites properties as to meet particular application demands.

Experimental

Materials

For this study, the following materials were used:

- HDPE (MFI 2 g/10min and density 0.96 g/cm³) was donated by LyondellBasell and HDPE-g-MA (Fusabond® E100) (MFI 2 g/10min, density 0.96 g/cm³, melting point 134°C and MA content 0.9 %) was provided by DuPont;
- the organoclay was Cloisite® 20A which is dimethyl bis(hydrogenated tallow) quaternary ammonium chloride montmorillonite (hydrogenated tallow is a blend of saturated alkyl chains and contains ~65% C18, ~30% C16 and ~5% C14), supplied by Southern Clay Products, Inc., having the following characteristics: organic load 95 mequiv/100 g clay; organic content 39.6 wt%; density 2.83 g/cm³, d_{001} =24.2 Å by XRS; particle size distribution: <15 µm (90%); moisture <2%.

Six composite formulations were prepared by two different methods, using the same amounts of organoclay: 5, 10 and 15 wt%, respectively. Thus, they were identified as HDPE 5, HDPE 10, HDPE 15, and HDPE-g-MA 5, HDPE-g-MA 10, HDPE-g-MA 15, respectively.

Composites preparation

Solution mixing

About 5 g of polymer and 200 mL of xylene were placed in a flask equipped with stirrer and reflux condenser, which was immersed in an oil bath and held at 120°C under stirring until complete polymer dissolution. The appropriate volume of a dispersion of clay in the same solvent (2 wt%), prepared by gentle heating at 60°C for 2 h under stirring, was then added to the polymer solution, stirring continued. The solution was placed in an aluminium pan and evaporated at room temperature, first at atmospheric pressure and then under vacuum.

Melt blending

The polymer pellets and the clay were dried in a vacuum oven at 60°C over the night and then fed to a HAAKE RHEOCORD 9000 mixer (equipped with two internal roller mixers and a capacity of mixing chamber of 50 cm³). As the mixing head is volume sensitive, the feeding amount is calculated by considering the volume of the cavity, density of the material and 85% of the capacity utilization. The molten composites were removed from the mixer and cooled naturally in air, at room temperature.

Characterization techniques

Differential scanning calorimetric (DSC) thermograms were recorded using a Pyris Diamond DSC (Perkin Elmer, USA) at a heating rate of 10°C/min under dry N₂ atmosphere. The specimens were heated up to 190°C and kept at this temperature for 5 min in order to destroy the polyethylene crystal nuclei. The DSC cooling traces were recorded at a rate of 10°C/min. The degree of crystallinity was calculated from the crystallization enthalpy, normalized to the amount of polymer.

XRD patterns were recorded on a Bruker AD8 Advance diffractometer. The spacing basal of the samples was observed at room temperature (40 kV, 30 mA) using CuKα radiation ($\lambda = 0.154$ nm) at the rate of 2°/min. All diffractograms were reported as observed.

Polarized optical microscopy (POM) observations were made using an Olympus BH-2 polarized light microscope equipped with a THMS600/HSF9I heating stage. The optical observations were performed by using clean untreated glass slides.

The morphology of the fracture surface of the nanocomposites was investigated by using a scanning electron microscope (SEM) VEGA II SBH instrument manufactured by TESCAN (Brno, Czech Republic). Samples were cryogenically fractured by immersion in liquid nitrogen for 30-50 minutes. Shortly after fracturing, the rupture surfaces were coated with a thin gold layer (of about 50 nm) prior to examination under the electron beam. An operating voltage of 30kV was used.

Acknowledgements

Authors gratefully acknowledge the scientific contribution of Dr. Luminita Marin.

References

1. Bhattacharya, S. N.; Kamal, M.; Gupta, R. Polymeric Nanocomposites: Theory and Practice. Carl Hanser Verlag: Munich, 2008, 383 p.
2. Hetzera, M.; De Keea, D. Wood/polymer/nanoclay composites, environmentally friendly sustainable technology: A review. Chemical Engineering Research and Design, 2008, 86, pp. 1083-1093.

3. Qiu, L.; Chen, W.; Qu, B. Morphology and thermal stabilization mechanism of LLDPE/MMT and LLDPE/LDH nanocomposites. *Polymer*, 2006, 47, pp. 922–930.
4. Chiu, F. C.; Chu, P. H. Characterization of solution-mixed polypropylene/clay nanocomposites without compatibilizers. *Journal of Polymer Research*, 2006, 13, pp. 73–78.
5. Chiu, F. C.; Lai, S. M.; Chen, J. W.; Chu, P.H. Combined effects of clay modifications and compatibilizers on the formation and physical properties of melt-mixed polypropylene/clay nanocomposites. *Journal of Polymer Science Part B: Polymer Physics*, 2004, 42, pp. 4139–4150.
6. Hotta, S.; Paul, D. R. Nanocomposites formed from linear low density polyethylene and organoclays. *Polymer*, 2004, 45, pp. 7639–7654.
7. Filippi, S.; Mameli, E.; Marazzato, C.; Magagnini, P. Comparison of solution-blending and melt-intercalation for the preparation of poly(ethylene-co-acrylic acid)/organoclay nanocomposites. *European Polymer Journal*, 2007, 43, pp. 1645–1659.
8. Filippi, S.; Marazzato, C.; Magagnini, P.; Famulari, A.; Arosio, P.; Meille, S. V. Structure and morphology of HDPE-g-MA/organoclay nanocomposites: Effects of the preparation procedures. *European Polymer Journal*, 2008, 44, pp. 987–1002.
9. Minkova, L.; Filippi, S. Characterization of HDPE-g-MA/clay nanocomposites prepared by different preparation procedures: Effect of the filler dimension on crystallization, microhardness and flammability. *Polymer Testing*, 2011, 30, pp. 1–7.
10. Hetzer, M.; De Kee, D. Wood/polymer/nanoclay composites, environmentally friendly sustainable technology: A review. *Chemical Engineering Research and Design*, 2008, 86, pp. 1083–1093.
11. Singla, P.; Mehta, R.; Upadhyay, S. N. Clay modification by the use of organic cations. *Green and Sustainable Chemistry*, 2012, 2, pp. 21–25.
12. Spencer, M. W.; Cui, L.; Yoo, Y.; Paul, D. R. Morphology and properties of nanocomposites based on HDPE/HDPE-g-MA blends. *Polymer*, 2010, 51, pp. 1056–1070.
13. Shah, R. K.; Paul, D. R. Organoclay degradation in melt processed polyethylene nanocomposites. *Polymer*, 2006, 47, pp. 4075–4084.
14. Paul, D. R.; Zeng, Q. H.; Yu A. B.; Lu, G. Q. The interlayer swelling and molecular packing in organoclays. *Journal of Colloid and Interface Science*, 2005, 292, pp. 462–468.
15. Ho, D. L.; Briber, R. M.; Glinka, C. J. Characterization of organically modified clays using scattering and microscopic techniques. *Chemistry of Materials*, 2001, 13, pp. 1923–1931.
16. Ho, D. L.; Glinka C. J. Effects of solvents solubility parameters on organoclay dispersions. *Chemistry of Materials*, 2003, 15, pp. 1309–1312.
17. Dorigato, A.; Dzenis, Y.; Pegoretti, A. Filler aggregation as a reinforcement mechanism in polymer nanocomposites. *Mechanics of Materials*, 2013, 61, pp. 79–90.

HOLOGRAPHIC INFORMATION MEDIA BASED ON AZO-POLYMERS WITH DIFFERENT STRUCTURES

Irina Davidenko

Kiev Taras Shevchenko National University, 64, Volodymyrs'ka str., Kiev 01601, Ukraine
email: irynadavydenko@gmail.com

Abstract. Azobenzene polymer compositions are extensively studied now due to wide perspectives of their applications in optoelectronics and information technologies. Some possibilities of modification of their properties by chemical methods are analyzed in the present work. These methods allow to improve information characteristics of the media. Electrooptical effect is investigated and possibilities of polarization sensitive holographic recording is demonstrated in copolymer octyl methacrylate with incorporated azo dyes and its complex with Co ions.

Keywords: azobenzene, metallic polycomplexes, polymer composition, electrooptical effect, polarization holography.

Introduction

Films of polymeric compositions (PC) containing azobenzene dyes or azobenzene lateral groups [1,2] are of interest due to possibility of their use as optically active media [3,4], in particular as electrooptical or magneto-optical light controlling elements and polarization sensitive media for optical holographic recording. Induced polarization appears in the PC films under influence of linearly polarized light which is absorbed by the azobenzene groups and causes changes of isomeric structures. The photoinduced polarization can be conserved at the room temperature during quite a long time. Changes of the polarization are possible under influence of external thermal or mechanical treatments, illumination with light and in external electric or/and magnetic fields. Rotation of the dipole moments happens in an external electric field.

Sensitization of this effect is possible by changing chemical structure of azobenzene groups or by using of different dopants. As it follows from numerous theoretical and experimental investigations [5,6] linearly polarized light is absorbed by the azobenzene groups resulting in changes of isomeric structure. Photoinduced anisotropy of the polarization appears in the films due to changes of concentration of *trans*- and *cis*-isomers of the azobenzene groups. Rotation of the dipole moments is possible in an external electric field involving changes of the conditions of interaction between light and PC. This is a fundamental reason of experimentally observed electrooptical effect.

Since the mechanism of external electric influence is determined by the arisen forces orienting the dipole moments of the azobenzene compounds, one can suppose that introduction of metallic ions chemically connected to the polymer could strengthen the electrooptical effect. Also addition of magnetic nanoparticles into the PC could result in external magnetic field influence on photoinduced optical anisotropy [7]. Physical properties of such doped PCs are not completely investigated so far as well as their information properties, i.e. the possibility of registration the diffraction grating, its maximal achievable diffraction efficiency, its control by external electric and magnetic fields.

Azobenzene containing PC are also considered as the perspective media for polarization holography [6,8] due to dependency of the photoinduced optical anisotropy on light polarization. Polarization holography technique [9,10] has many unique properties and possibilities as compared to the scalar holography. These ones result in more flexible opportunities of light beam control when using light polarization sensitive photoactive media.

Investigations of electrooptical properties of PC films, based on azobenzene of different structure depending on presence of coordinated metallic ions as well as on other dopants is the aim of the present work. Holographic information properties of the PC with and without metallic ions are also studied.

Experimental

Polymer 4-methacryloyloxy-(4'-carboxy-3'-oxy)azobenzene (A1), its polycomplex with cobalt (A1-Co) and polycomplex 4-methacryloyloxy-(4'-carboxy-3'-hydroxy)-2-chlorineazobenzene with cobalt (A1-Co,Cl) were synthesized and investigated (Figure 1). Their characterization accordingly to chemical standards and the full scheme of synthesis is presented by authors [11]. Structural formulas of the polycomplexes A1, A1-Co and A1-Co,Cl are shown below.

There is inter-chain coordination of metallic ions in the polycomplexes A1-Co. The polycomplex A1-Co,Cl contains chlorine increasing dipole moment of the azobenzene fragment. The samples were prepared as the structures with free surface of the polymeric film: glass substrate – polymeric film. The thickness of the polymeric film was 1.8–2.0 μm .

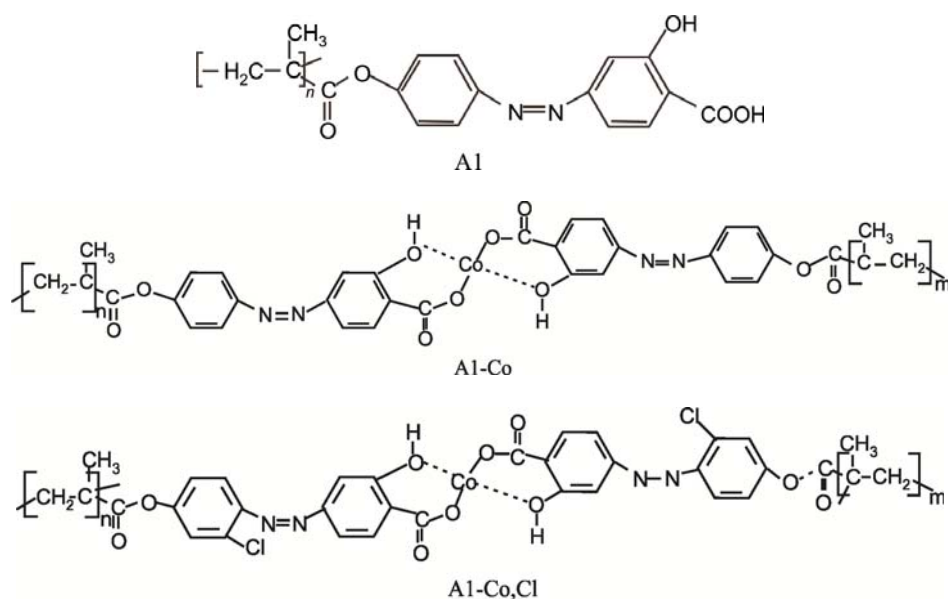


Figure 1. Polymer 4-methacryloyloxy-(4'-carboxy-3'-oxy)azobenzene (A1), its polycomplex with cobalt (A1-Co) and polycomplex 4-methacryloyloxy-(4'carboxy-3'-hydroxy)-2-chlorineazobenzene with cobalt (A1-Co,Cl).

Results of investigation of an influence of external electric field on the transmission of the films A1 and A1-Co are presented in Figure 2. Here, I_0 and I_E are the intensities of light before and after application of the external electric field respectively. External electric field $E = 1 \times 10^8$ V/m in the PC film was produced by a crown discharge in a special device. The field was oriented normally to the film surface. It was observed [12] that influence of electric field increases when the samples were previously illuminated with linearly polarized light from the band of absorption of azobenzene groups ($\lambda < 550$ nm). The most pronounced changes of I_0 when switching on external electric field were observed for the time of preliminary illumination $t > 30$ s. External electric field involves decrease of the intensity of light passed through the samples with compound A1 (Figure 2, curve 1) and its growth for the samples with A1-Co (Figure 2, curve 2). All measurements were done when the investigated samples were placed between crossed polarizers.

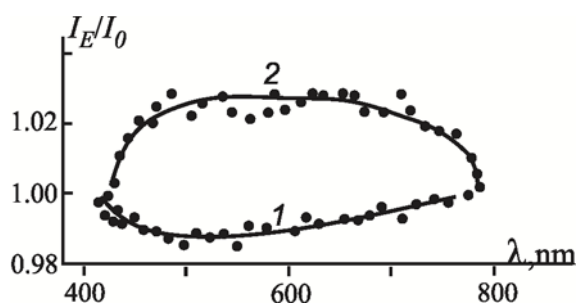


Figure 2. Spectral dependencies of I_E/I_0 in the samples with A1 (1), A1-Co (2).

Recording of the polarization holographic gratings in the samples with the polycomplex A1-Co,Cl can be considered as an example. Nd^{3+} : YAG laser with light wavelength $\lambda = 532$ nm and maximal power 100 mW was used. Usual setup for registration of the holograms of flat wave front [9,13] was used in the experiments. Kinetics of recording and relaxation of the holographic gratings for the both cases mutually parallel and perpendicular polarization vectors of recording and reference light beams are shown in Figure 3. The ratio between intensities of the beams was 1:1. The diffraction efficiency η was determined as the ratio between light intensity in -1 diffraction order and intensity of the reference beam passed through the sample. The spatial frequency of the hologram of flat wave front was 1500 mm^{-1} .

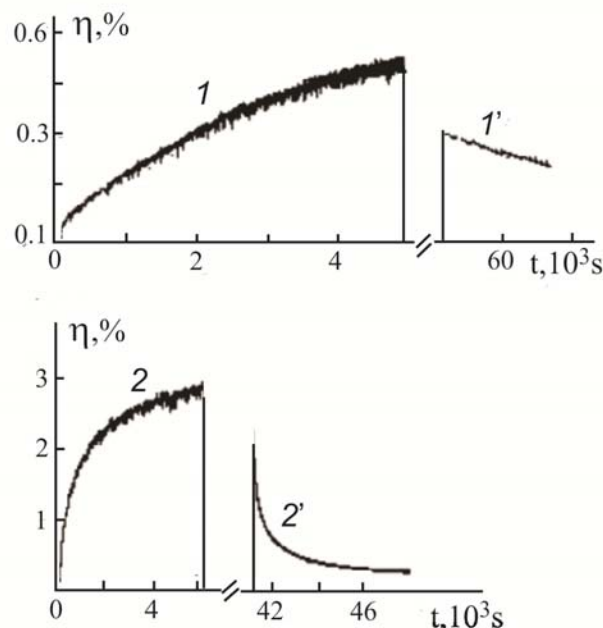


Figure 3. Kinetics of recording (1, 2) and relaxation (1', 2') of the holograms for the cases $\vec{e}_1 \parallel \vec{e}_2$ (1, 1') and $\vec{e}_1 \perp \vec{e}_2$ (2, 2') in the sample with A1-Co,Cl. The curves 1', 2' were registered using reference beam after exposure and keeping of the recording medium in darkness.

The case when light polarization vectors \vec{e}_1 and \vec{e}_2 of the object and reference beams are parallel $\vec{e}_1 \parallel \vec{e}_2$ corresponds to spatial distribution of the light intensity along the sample surface. When these vectors are mutually perpendicular spatial distribution of ellipticity and orientation of polarization ellipse of the total light beam along the sample surface takes place. After registration of the holograms their relaxation occurs, and its velocity increases when the samples is illuminated with continuous light. For $\vec{e}_1 \parallel \vec{e}_2$ diffraction efficiency η is less and relaxation time is greater as compare to $\vec{e}_1 \perp \vec{e}_2$. For the first case recorded holograms can be conserved at the room temperature during few months.

Polycomplex of azobenzene with intrachain coordination of Co ion (A2-Co) was synthesized and investigated to compare electrooptical properties of this one and polycomplex of azobenzene with interchain coordination of Co ion (A1-Co) (Figure 4).

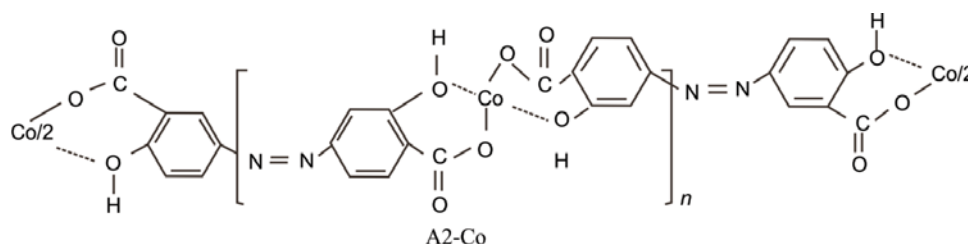


Figure 4. Polycomplex 4- carboxy-3-oxy-3'-carboxy-4'-oxyazobenzene with cobalt.

Spectral dependencies of δI_E in the samples with PC A1-Co (curve 1) and A2-Co (curve 2) are shown in Figure 5. Here, $\delta I_E = (I_E - I_0) / I_0$ where I_E and I_0 are the intensities of light before and after application of the external electric field respectively. Measurements were done for crossed polarizers. The samples were preliminary illuminated with linearly polarized light from the band of absorption of azobenzene groups $\lambda < 550$ nm.

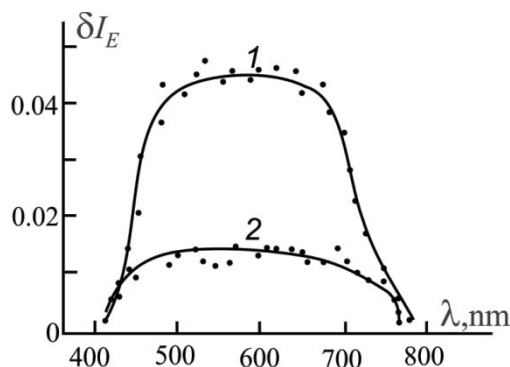


Figure 5. Spectral dependencies of δI_E in the films with A1-Co (1) and A2-Co (2) for crossed polarizers after preliminary illumination with linearly polarized light $\lambda < 550$ nm during 60 min.

Results and discussion

Opposite sign of influence of external electric field on the intensity of light passed through the samples with PC A1 and A1-Co can be explained by the peculiarities of interaction of these compounds with external electric field. In the films A1 an external electric field provokes alignment of the photoinduced dipoles along the force lines of the field. As a result, interaction between polarized light and these dipoles is weaker and $\delta I_E < 0$ for crossed polarizers. In the films A1-Co in the external electric field polarized light undergoes more intensive dispersion and depolarization resulting in positive δI_E . This fact is probably caused by more effective interaction between the Co^{2+} ions and the electric field as compared to dipoles interaction with the field. These ions are bonded to the azobenzene groups indirectly, and the direction of the bond and the photoinduced dipole moment do not coincide. Hence, change of orientation of the photoinduced dipoles bonded to the metallic ions in the sample with A1-Co in the external electric field could be opposite to the change in the sample with A1. These experimental results can be qualitatively described within the scope of phenomenological theoretical model [12].

The samples with polycomplex A1-Co,Cl was chosen as an example for holographic recording. It is once more chemical modification of investigated azobenzene polycomplexes with cobalt ions. It is characterized by increased dipole moment of azobenzene fragment due to presence of chlorine ions. Recording of two types of interference field of the recording and reference beams was accomplished: spatial distribution of light intensity ($\vec{e}_1 \parallel \vec{e}_2$) and spatial distribution of light polarization state ($\vec{e}_1 \perp \vec{e}_2$). Difference of the relaxation times (Figure 3) in the both cases can be attributed to the difference of the structural rearrangement of the polymeric matrix which happens in the polymeric film containing azobenzene polycomplexes while intensive *trans*–*cis*-isomerization of the azobenzene groups occurred. Similar effects were observed before [14,15] and it was concluded that exactly rearrangement of the polymeric matrix is the reason of long time conservation of the holographic recording. Moreover, long-lived photoinduced surface relief [6,16] can contribute in the observed effect.

Co ions coordinated by chelate groups (A2-Co) participate in electrooptical effect and create additional mechanical obstacles for isomerization of azobenzene groups and their rotation in the external electric field. Therefore, we observed weaker electrooptical effect in the films with A2-Co where azobenzene group is bonded to two Co ions (Figure 5).

Conclusions

Azobenzene polymers now are widely considered as the perspective media for information technologies. Their physical and information properties are extensively studied. Analyzing few experimental results presented in this paper one can conclude that these properties can be varied depending on practical necessities by appropriate chemical modifications, namely by introduction of coordinated metallic ions, by changes of the dipole moment of azobenzene fragments, by change of coordination of the metallic ions. Introduction of coordinated metallic ions in the investigated PC opens additional possibilities of control of the properties of the photoactive medium, allows increasing of their sensitivity in external fields. Special conditions can be chosen when presence of metallic ions and/or change of dipole moment of azobenzene groups intensify the effect of photoinduced polarization.

Moreover, physical and information properties of PC containing azobenzene compounds can be changed by introduction of organic merocyanine dyes into their structure [17]. Their influence in the PC reveals itself in sensitization of electrooptical effect. Also increase of the length of “spacers” and possibility to form hydrogen bonds between substitutes in azobenzene groups reduce time and increase magnitude of the changes of optical characteristics of the films under influence of external electric field [18]. Since influence of external electric field is explained by appearance of the forces effecting on the dipole moments of azobenzene groups and metallic ions increase of the dipole moments of azobenzene groups by chemical methods provokes decrease of the metallic ions influence on the electrooptical properties. This effect was observed by authors [19] introducing donor and acceptor substitutes into the structure of azobenzene groups.

Thus, polymer composites with azobenzene dyes and their metallic complexes have wide perspectives for practical applications such as for holographic information recording and in optoelectronics due to possibilities to vary their properties particularly by chemical methods. Some of these methods are analyzed in this paper.

References

1. Yesodha, S.K.; Sadashiva, C.K.; Pillai, P.; Tsutsumi, N. Stable polymeric materials for nonlinear optics: a review based on azobenzene systems. *Progress in Polymer Science*, 2004, 29, pp. 45-74.
2. Yaroshchuk, O.; Tereshchenko, A.; Zakrevskyy, Yu.; Shanski, I. 3D Orientational Structures in Azopolymers Studied by UV Absorption Method. *Molecular Crystals and Liquid Crystals*, 2001, 361, pp. 187-192.
3. Camorani, P.; Cristofolini, L.; Fontana, M.P.; Angiolini, L. Comparative Study of Photomechanical Effects in Linear and Star Azo-Polymers. *Molecular Crystals and Liquid Crystals*, 2009, 500, pp. 1-9.
4. Ishitobi, H.; Tanbe, M. The anisotropic nanomovement of azo-polymers. *Optics Express*, 2007, 15, pp. 652-659.
5. Lefin, P.; Fiorini, C.; Nunziy, J.-M. Anisotropy of the photo-induced translation diffusion of azobenzene dyes in polymer matrices. *Pure Appl. Opt.*, 1998, 7, pp. 71-82.
6. Bublitz, D.; Fleck, B.; Wenke, L. A model for surface-relief formation in azobenzene polymers. *Applied Physics B*, 2001, 72, pp. 931-936.
7. Borsch, A.A.; Volkov, V.I.; Lyakhovetskii, V.R.; Kutsenko, A.S. Nonlinear refraction in an epoxy-based polymer with 4-aminoazobenzene caused by the orientation of azobenzene molecules upon pulsed laser excitation. *Quantum Electronics*, 2003, 33, pp. 441-445.
8. Eickman, J.; Bieringer, T.; Kostromine, S.; Berneth, H.; Thoma, R. Photoaddressable Polymers: A New Class of Materials for Optical Data Storage and Holographic Memories. *Japanese Journal of Applied Physics*, 1999, 38, pp. 1835-1840.
9. Todorov, T.; Nikolova, L.; Tomova, N. Polarization holography. 1: A new high-efficiency organic material with reversible photoinduced birefringence. *Applied Optics*, 1984, 23, pp. 4309-4312.
10. Yang, Q.; Wei, Z.; Zhang, Y.; Sun, G.; Li, F. Polarized-light-controlled holographic recording in an azobenzene-doped polymer film. *Applied Physics B*, 2001, 72, pp. 855-858.
11. Davidenko, N.A.; Davidenko, I.I.; Pavlov, V.A.; Popenaka, A.N.; Savchenko, I.A.; Shumeluk, A.N. Recording medium based on a polymer azobenzene complex with cobalt for polarization holography. *Theoretical and Experimental Chemistry*, 2009, 45, pp. 54-57.
12. Davidenko, N.A.; Davidenko, I.I.; Savchenko, I.A.; Popenaka, A.N.; Baath, L.B. Electrooptical effect in films of azobenzene polycomplexes with cobalt. *Journal of Applied Physics*, 2008, 103, pp. 094223-094227.
13. Caulfield, H.J. *Handbook of Optical Holography*; Academic Press: New-York, 1979, 480 p.
14. Freiberg, S.; Lagugne-Labarthe, F.; Rochon, P.; Natansohn, A. Synthesis and Characterization of a Series of Azobenzene-Containing Side-Chain Liquid Crystalline Polymers. *Macromolecules*, 2003, 36, pp. 2680-2688.
15. Davidenko, I.I.; Savchenko, I.A.; Popenaka, A.N.; Shumelyuk, A.N.; Bedarev, V.A. Holographic recording and electrooptical effect in the films of azobenzene polycomplexes with cobalt. *Ferroelectrics*, 2007, 352, pp. 158-163.
16. Viswanathan, N.K.; Balasubramanian, S.; Li, L.; Sukant, K.; Tripathy, K.; Kumar, J. A Detailed Investigation of the Polarization-Dependent Surface-Relief-Grating Formation Process on Azo Polymer Films. *Japanese Journal of Applied Physics*, 1999, 38, pp. 5928-5937.
17. Davidenko, N.A.; Davidenko, I.I.; Savchenko, I.A.; Popenaka, A.N.; Derevyanko, N.A.; Ishchenko, A.A.; Kulinich, A.V. Sensitization of the Electrooptical Effect by a Merocyanine Dye in Polymers of Azobenzene Derivatives. *High Energy Chemistry*, 2008, 42, pp. 123-126.
18. Davidenko, N.A.; Davidenko, I.I.; Popenaka, A.N.; Savchenko, I.A.; Studzinskii, S.L. Effect of the interaction of azobenzene groups in polymeric composites on their electrooptical characteristics. *Theoretical and Experimental Chemistry*, 2009, 45, pp. 349-354.
19. Davidenko, N.A.; Davidenko, I.I.; Popenaka, A.N.; Savchenko, I.A. Electrooptical properties of the films of azopolymers and polycomplexes with donor and acceptor substitutes. *Optical Journal*, 2008, 75, pp. 70-73 (In Russian).

HOLOGRAPHIC RECORDING MEDIA BASED ON ELECTRONS DONOR OLIGOMERS

Nicolay Davidenko^{a*}, Irina Davidenko^a, Nicolay Chuprina^a, Yuriy Getmanchuk^a,
Leonid Kostenko^b, Elena Mokrinskaya^a, Valeriy Pavlov^a,
Sergey Studzinsky^a, Larisa Tonkopieva^a

^aKiev Taras Shevchenko National University, 64, Volodymyrs'ka str., Kiev 01601, Ukraine

^bL.M. Litvinenko Institute of Physics Organic Chemistry and Coal Fuel Chemistry NAS of Ukraine
70, R. Luksemburg str., Donetsk 83114, Ukraine

*email: ndav@univ.kiev.ua

Abstract. Information properties of the recording media for photothermoplastic technique with the films of oligomer composites based on carbazole containing cooligomers of linear and radial structures with branching center on silicon atoms are investigated. It was ascertained that the media based on the radial oligomers possess higher holographic sensitivity due to higher plasticity and ability to accumulate volume electric charge during the exposure. Examples of practical application of the investigated recording media are presented.

Keywords: carbazole, oligomer, photothermoplastic, holographic recording.

Introduction

Development of the new materials possessing photoconductivity in the visible and near IR parts of spectrum is very actual question for their practical applications in the equipment for recording, storage and processing of optical information. Along with inorganic semiconductors it seems to be attractive to use organic oligomers and based on them compositions (OC) [1–7]. These OC were tested in the holographic recording media (HRM) for the photothermoplastic technique (PTT) of information recording [8]. HRM for PTT holographic recording have to possess following characteristics: low electric conductivity; high absorption coefficient close to the irradiation maximum of used light sources; high quantum yield of photogeneration of charge carriers; high mobility of non-equilibrium charge carriers. Basically, photoconductivity of the OC films is provided by presence of the molecules of three types: donors, acceptors and centers of photogeneration of charge carriers [8, 9]. Absorption of light quantum occurs in the photogeneration center resulting in its transition from the ground state into excited one. The dye molecules, the molecules of organic compounds with intramolecular charge transfer, the intermolecular complexes with charge transfer (CCT) [9, 10] can be considered as such centers. The excited state of the photogeneration center is characterized by empty limit orbitals, notably by presence of one electron on the high occupied molecular orbital (HOMO) and one electron on low unoccupied molecular orbital (LUMO). Photogeneration of charge carriers happens as the result of intermolecular electron transitions. Electron can transit from LUMO of the excited photogeneration center into LUMO of the molecule with electron acceptor properties. Electron from valent orbital of the molecule with electron donor properties can transit to empty HOMO of the photogeneration center. If the ionization potential of the electron donor molecules is I_{gd} (HOMO energy is proportional to this one) and affinity energy of the acceptor molecules is A_{ea} [11] (LUMO energy is proportional to this one), then the molecules of photogeneration centers are chosen to satisfy the conditions $|I_{gc}| > |I_{gd}|$, $|A_{ec}| < |A_{ea}|$, where I_{gc} and A_{ec} are respectively ionization potential and affinity energy of the molecule of photogeneration centre. These conditions determine formation of electron – hole pair (EHP) in the molecule of photogeneration centre after absorption of light quantum and intermolecular electronic transitions. EHP can consist of either donor cation-radical and anion-radical of the photogeneration centre, or cation-radical of the photogeneration centre and acceptor anion-radical, or donor cation-radical and acceptor anion-radical. EHP dissociation involves appearance of free charge carriers.

The most important requirement of appearance of the photoconductivity effect in the OC films is existence of the charge carriers transport in the OC film volume [9]. The transport is provided by increase of the concentration of the donor and/or acceptor fragments in the OC films. The concentration growth enhances overlap of the wave functions of neighboring fragments and increases probability of intermolecular electron transitions. Oligomers with electron donor substitutes are used for production of the OC with hole conductivity type. π -conjugated closed systems (condensed aromatic cycles) can be employed as such substitutes. These systems are able to return electron but does not able to capture electron due to positive LUMO energy.

Aspects of influence of the oligomers structure on above notified properties are not clearly understood till now. Hetero-chain electron donor oligomers were synthesized and used before for production of photosensitive information media. That allows to develop HRM with optimal rheological properties. The oligomers do not possess high-elastic state. This fact allows to transit from solid vitreous state of the film into liquid state with low viscosity and backward very quickly. Time of development decreases until microseconds, the film functions in real time scale. The film has

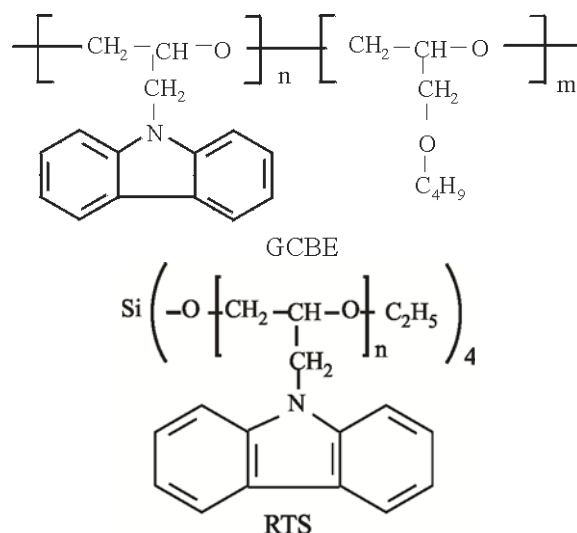
to possess enough elasticity for its using on flexible substrate. Such forced elasticity below the temperature of glass transition can be reached only due to conformational transitions in separate oligomer links consisting of, as a rule, donor multinuclear conjugated substitutes.

Not only structure of the macromolecule chain has significant influence on rheological properties of the polymers and oligomers, but also its shape, particularly branching. One can conclude from the results of our investigation that sensitivity and diffraction efficiency of the HRM considerably increases for the radial oligomers as compare to linear ones. Recently we have made [12] new oligomer: radial tetrasubstituted silan (RTS). Films of these oligomers possess improved rheological properties.

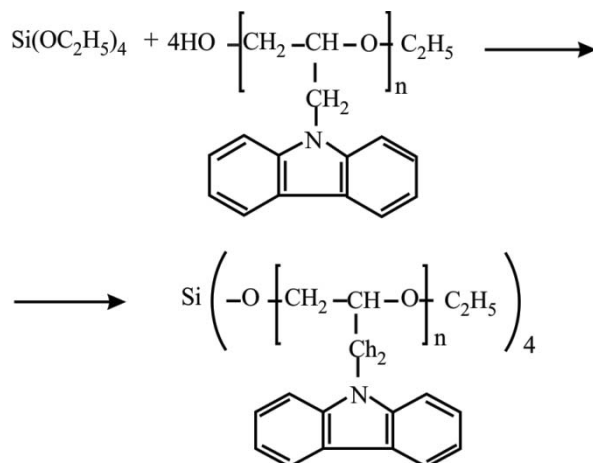
The present work is aimed at fulfilling of comparative analysis of information properties of HRM based on the oligomers with linear and radial molecular structures.

Experiments

Cooligomer of glycidylcarbazole with butylglycidyl ether (GCBE) of linear structure and radial oligomer RTS were used as the OC base:

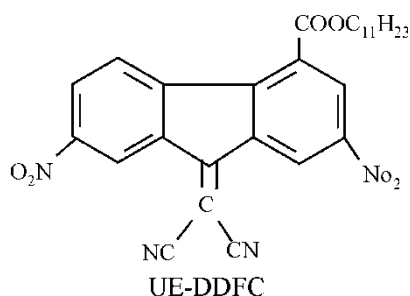


The synthesis of RTS was carried out according to the following scheme:



The 0.5 g (0.2 M) of tetraethoxysilane, 10 g (1 M) of oligoglycidylcarbazole, and 0.05 g of sodium was added to the four-neck 0.5 L reactor with a stirrer, the reflux condenser, and the thermometer. The starting compounds were dissolved in 5 mL of *o*-xylene and were heated (on boiling) and stirred for two hours. The residual xylene was distilled off, and then reaction mixture was separated from the sodium and xylene by washing with ethanol. The product was purified by recrystallisation from the mixture of benzene with petroleum ether or dry acetone. The main product is a white powder (yield 90%, softening point $T_m = 95-105\text{ }^{\circ}\text{C}$).

Acceptor undecyl ether 2,7- dinitro -9-dicyanmethylenefluorene-4-carboxylic acids (UE-DDFC) was used as the sensitizer of HRM photosensitivity:



Intermolecular complexes with charge transfer (CCT) arise while contacting acceptor UE-DDFC molecules with carbazole fragments of the oligomers (in liquid solutions and in solid films). Appearance of new wide absorption band is evidence of CCT arising. This band is absent in electronic spectra of OC individual components [9, 13]. The normalized spectra of optical density (D) of the OC films based on GCBE, RTS and RTG with the same UE-DDFC are practically identical within visible range of spectrum (Figure 1). This is evidence of formation of identical CCT in these films.

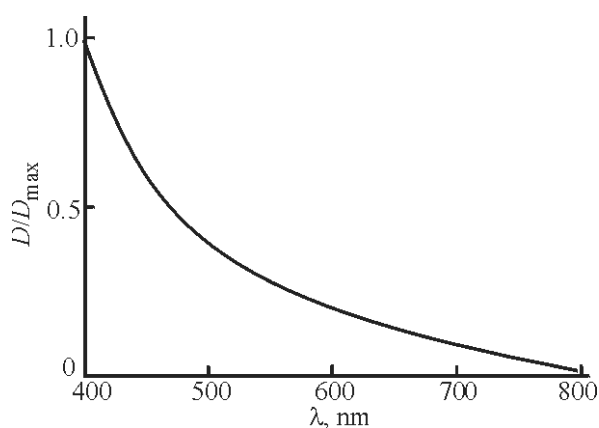


Figure 1. Normalized absorption spectrum of the films GCBE, RTS containing 3 mas.% UE-DDFC.

For holographic recording by PTP method HRM were prepared similarly to [4, 10] as thin OC film deposited onto transparent conducting layer $\text{SnO}_2\cdot\text{In}_2\text{O}_3$ (ITO) with resistance 20 Ohm/square. Ratio between the components in OC was following: oligomer – 97 mas.%, UE-DDFC – 3 mas.%. The thickness (L) of the OC films was 1.1 – 1.2 μm which is optimal for HRM.

Measurements of photothermoplastic characteristics of OC were done using known technique [14] of registration of the hologram of flat wave front. Spatial frequency was 500 mm^{-1} , light wavelength of the used semiconductor laser was 650 nm, ratio between light intensities in the reference and object beams was 1:1. Diffraction efficiency (η) of the reconstructed image of the hologram of flat wave front in -1 diffraction order was measured continuously during development process. Photodetector was used for these purposes, signal from which was registered by memory oscilloscope Tektronix TDS1001B. The process of the hologram development was not ceased when maximal η value was reached, heating of OC was continued during the duration of current pulse until full erasing of the hologram. Dependency of the maximal η value on the exposure $I \cdot t$ was measured, where I is the light intensity, t is the time of the HRM exposure. Experiments on our small-sized holographic device [15] were carried out to test the possibilities of employing of the produced HRM in the technique of holographic interferometry.

Results and discussion

It was observed that the value η increases at 1.5 times respectively in transition from HRM with GCBE to HRM with RTS (Figure 2). Maximal value η was reached for short durations of the pulse of development of latent image for HRM with OC based on RTS as compare to HRM based on GCBE. This fact indicates that evolution of geometrical surface relief of the OC films with RTS during the hologram development occurs at lower temperatures as compared to GCBE. Low noise level of the reconstructed holographic images is evidence of good rheological properties of OC.

However, growth of the holographic sensitivity at transition from HRM with OC based on GCBE to RTS can be attributed to once more reason. It was observed in experiments that investigated HRMs possess “memory” effect for preliminary illumination with light before charging of the surface of OC film in crown discharge. Investigations of the η dependency on time (t_1) of exposure before start of charging cycle and development of the latent holographic image, as well as η dependency after long-time exposure of the HRM on time (t_2) of delay before start of the charging cycle and development of the latent image were carried out. In these experiments only reference laser beam was used for measurements, the object beam was cut off. Before each next measurement charging of the surface of OC film was done in darkness and few long-time current pulses propagated for heating of the OC film. These operations allow being convinced in absence of the “memory” effect.

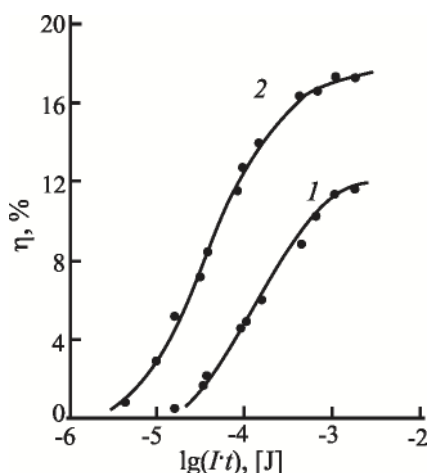


Figure 2. Dependencies of the maximal η value on light energy absorbed in HRM during holographic recording for HRM based on GCBE (1) and RTS (2).

Additional investigations were fulfilled for ascertainment of the reason of the “memory” effect. The samples of sandwich structure glass substrate / ITO / OC film / Ag were prepared for these investigations. The concentration (Q) of non-equilibrium electric charge was measured in the samples. It appears in the volume of the OC film after its illumination with light without application of external electric voltage. Method of Q determination and technique of measurement of Q dependencies on time (t_1) of illumination and time (t_2) after illumination was ceased are illustrated by the diagrams in Figure 3.

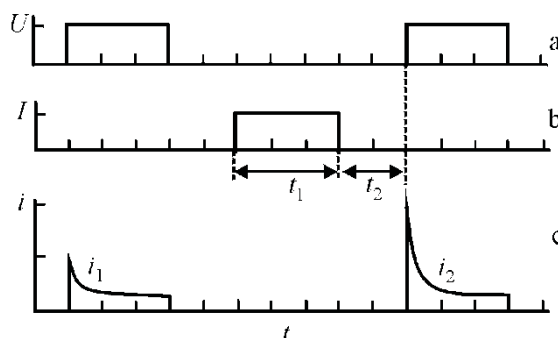


Figure 3. Diagrams demonstrating sequence of electric voltage application (a), illumination with light (b) and measurement of the current in the samples ITO / OC / Ag (c).

At first, electric voltage (U) was applied to the sample in darkness and current (i_1) kinetics was registered using memory oscilloscope. Next, electric contacts were disconnected and the sample was illuminated with light during the time t_1 , light was switched off, after the time interval t_2 the electric contacts were connected, electric voltage U was applied to the sample and current (i_2) kinetics was registered. From these measurements Q accumulation and relaxation were determined using relation $Q = \int (i_2 - i_1) dt / eSL$, where e is the charge of electron, S is the square of the sample of sandwich structure. The samples were illuminated from the side of ITO layer. U value was measured within the range 20 – 300 V. The measurements were done at room temperature. Dependencies of η on durations t_1 and t_2 measured in the HRM samples with OC based on RTS and RTG are shown in Figure 4.

Saturation of the “memory” effect (reaching of the stationary value in the dependency $\eta(t_1)$) occurs quicker (curve 1 in Figure 4) than its relaxation (dependency $\eta(t_2)$) (curve 2 in Figure 4). Besides, kinetic curves of the dependencies $\eta(t_1)$ and $\eta(t_2)$ are similar to the dependencies $Q(t_1)$ and $Q(t_2)$ (Figure 4). The value Q increases with U growth and does not depend on the polarity of applied voltage. The last fact testifies that the “memory” effect is attributed to accumulation and relaxation of the volume electric charge in the OC films as the result of their illumination with light. In the HRM samples with OC based on GCBE the “memory” effect and Q accumulation were not observed.

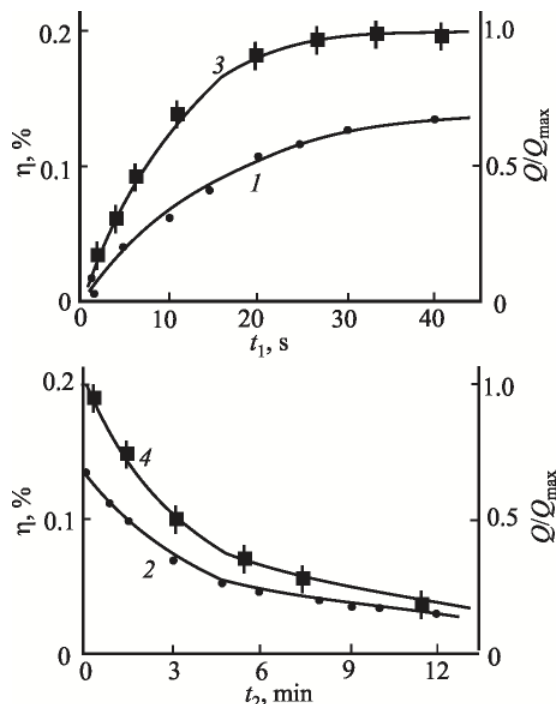


Figure 4. Dependencies $\eta(t_1)$ (1) and $\eta(t_2)$ (2) in HRM with OC based on RTS and dependencies $Q/Q_{\max}(t_1)$ (3) and $Q/Q_{\max}(t_2)$ (4) in the samples ITO / OC / Ag with OC based on RTS.

It is generally known that radial (starlike) polymers possess unusual low viscosity even having very high molecular mass. Radial polymers with hard chain always are more plastic as compare to their linear analogs even having significantly higher molecular mass. Similar properties are characteristic for oligomers also. The film of linear cooligomer starts to deform slowly within the wide temperature range 35 – 80°C and then flows quickly. The film of radial oligomer turns into liquid state quickly at temperature ≥ 60 °C. These peculiarities involve increase of the sensitivity and diffraction efficiency of the material when radial oligomer is used. Small growth of the sensitivity for exposure time $\sim 1 - 2$ s also can involve accumulation of the volume electric charge in the OC volume. However, under long-time illumination of the samples non-equilibrium electric charge appears in the OC films based on the radial oligomers. It relaxes during long time after light switching off. This volume charge can be leveled as a result of application of external electric field or by temperature increase.

Appearance of the volume electric charge in the OC films after their illumination with light can be attributed at least to two reasons. Firstly, if $|I_{gc}| > |I_{gd}|$ then after photoexcitation of the photogeneration centre and generation of hole on carbazolil oligomer fragment energetic barrier exists for opposite transition of non-equilibrium electron from the molecule of photogeneration centre to cation-radical of the carbazolil fragment. It is proportional to the difference of energies $|I_{gc}| - |I_{gd}|$. Such effect was observed before [16] when compounds with intramolecular charge transfer (CICT) were used as the photogeneration centers. $|I_{gc}| > |I_{gd}|$ for CICT. Not excited CICT molecules do not interact with the carbazolil fragments of oligomers, absorption spectra of OC based on different oligomers practically coincide and are similar to absorption spectra of CICT liquid solutions. However, in our case CCTs consisting of carbazolil fragments serve as the photogeneration centers. These fragments are similar to ones through which transport of non-equilibrium holes in external electric field occurs. As it was shown before, the barrier for holes recombination during EHP annihilation in such system is small and life time of geminate EHP is $\sim 10^{-7}$ s.

The second reason can be attributed to energetic traps which are able to capture the photogenerated charges and hold them during long time. Physical dimers (excimers) of the carbazolil fragments of sandwich structure can be considered as such traps. For them $|I_{gd}|$ is ~ 0.3 eV less than in the carbazolil fragments which are not included in the

dimers [9]. In carbazoyl containing polymers and oligomers the dimers are formed by end carbazoyl groups due to more favorable steric location for interaction with neighboring fragments. In the molecules of radial oligomer RTS number of the end carbazoyl fragments is 2 times more as compare to linear GCBE. Therefore, probability of the dimers formation in the films of radial oligomers also is higher. This fact explains presence of the “memory” and formation of the long-living photoinduced volume electric charge in OC based on RTS and its absence (or much less value) in OC based on GCBE.

Conclusions

Fulfilled investigations testify that optimal properties of OC for GRM depend not only on the ratio between ionization potential of the donor and affinity of acceptor to electron but also on the shape of their macromolecules. Plastic and rheological properties of the films become better when radial oligomers are used instead linear ones. Increase of the number of end carbazoyl fragments in oligomer macromolecules provokes effect of holographic “memory”. This effect is explained by accumulation of photoinduced volume charge in energetic traps formed by dimers of the end carbazoyl groups. This effect can be used for development of new information media, in particular for holographic recording with few exposures allowing to increase recording density. Besides, possibility of formation of long-lived photoinduced volume charge in the OC films is of interest for development of new materials for optoelectronics and molecular electronics.

References

1. Huang, C.; Wang, N.; Li, Y.; Li, C.; Li, J.; Liu, H.; Zhu, D. A new class of conjugated polymers having porphyrin, poly(p-phenylenevinylene), and fullerene units for efficient electron transfer. *Macromolecules*, 2004, 39, pp. 5319–5325.
2. Lanzi, M.; Paganin, L.; Caretti, D. New photoactive oligo- and poly-alkylthiophenes. *Polymer*, 2008, 49, pp. 4942–4948.
3. Davidenko, N.A.; Ishchenko, A.A.; Kulinich, A.V.; Studzinsky, S.L. Effect of concentration of anionic polymethine dye in poly-N-epoxypropylcarbazole polymer film composite on the spectral-luminescent properties and photoconductivity. *Spectrochimica Acta Part A: Molecular and Biomolecular Spectroscopy*, 2012, 98, pp. 271–274.
4. Davidenko, N.A.; Dekhtyarenko, S.V.; Getmanchuk, Yu.P.; Ishchenko, A.A.; Kozinetz, A.V.; Kostenko, L.I.; Mokhrinskaya, E.V.; Studzinskii, S.L.; Skryshevskii, V.A.; Skulskii, N.A.; Tretyak, O.V.; Chuprina, N.G. Photoconducting properties of holographic media based on ferrocenyl-containing cooligomers of glycidyl carbazole with these oligomers sensitized organic dye. *Semiconductors*, 2009, 43, pp. 1473–1478.
5. Davidenko, N.A.; Ishchenko, A.A.; Kozinets, A.V.; Kostenko, L.I.; Kurdyukova, I.V.; Mokhrinskaya, E.V.; Studzinskii, S.L.; Chuprina, N.G. Sensitization of photoconductivity in ferrocene-containing oligomer by squarylium and merocyanine dyes. *Journal of Applied Spectroscopy*, 2011, 78, pp. 129–133.
6. Davidenko, N.A.; Dehtarenko, S.V.; Getmanchuk, Yu.P.; Ishchenko, A.A.; Kozinetz, A.V.; Kostenko, L.I.; Mokhrinskaya, E.V.; Studzinskii, S.L.; Skryshevskii, V.A.; Tretyak, O.V.; Chuprina, N.G.; Sensitization of Photoconducting Properties of Holographic Recording Media Based on Glycidylcarbazole Cooligomers by Organic Dyes. *Molecular Crystals and Liquid Crystals*, 2011, 535, pp. 148–155.
7. Hariharan, P. *Basics of Holography*; Cambridge University Press: Cambridge, 2002, 411 p.
8. Davidenko, N.; Davidenko, I.; Ishchenko, A.; Kulinich, A.; Pavlov, V.; Studzinskii, S.; Chuprina, N. Reversible holographic recording media based on polymeric composites and their use in energy-saving technologies. *Applied Optics*, 2012, 51, pp. C48–C54.
9. Pope, M.; Swenberg, C. *Electronic Processes in Organic Crystals and Polymers*, 2nd ed; Oxford University: Oxford, 1999, 278 p.
10. Davidenko, N.; Ishchenko, A.; Kostenko, L.I.; Kuvshinskii, N.; Kulinich, A.; Melenevskii, D.; Mysyk, D.; Mysyk, R.; Pavlov, V.; Chuprina, N. Holographic Recording Media Based on Systems with Intramolecular and Intermolecular Charge Transfer. *High Energy Chemistry*, 2005, 39, pp. 254–262.
11. Danovich, D.; Apeloig, Y.; Shaik, S. A Reliable and Inexpensive Method for Calculating Ionization Potentials and Electron Affinities of Radicals and Molecules. *Journal of Chemical Society, Perkin Trans.*, 1993, 2, pp. 321–330.
12. Getmanchuk, Yu.P.; Davidenko, N.A.; Kunitskaya, L.R.; Mokhrinskaya, E.V. Information media based on electron donor oligomers. *Polymer Science, Ser. B*, 2013, 55, pp. 88–94.
13. Schaffert, R.M. *Electrophotography*; Wiley: New York, 1981, 318 p.
14. Rosen, J. ed. *Holography, Research and Technologies*; InTech: Rijeka (Croatia), 2011, 477 p.
15. Holographic Interferometer. http://www.youtube.com/watch?v=EZynG_qkGvM.
16. Davidenko, N.; Ishchenko, A.; Kuvshinskii, N. *Photonics of Molecular Semiconductor Composites Based on Organic Dyes*; Naukova Dumka: Kiev, 2005, 296 p. (in Russian).

AMINOSILICA NANO- AND SUBMICROSPHERES: ANALYSIS OF FACTORS INFLUENCING MORPHOLOGY, STRUCTURE AND PROPERTIES

Inna Melnyk

*Chuiko Institute of Surface Chemistry of NAS of Ukraine, 17, General Naumov str., Kyiv 03164, Ukraine
e-mail: melnyk@isc.gov.ua; phone: (+38) 044 422 96 09; fax: (+38) 044 424 35 67*

Abstract. Current paper focuses on the analysis of influence of main factors (stages of the synthesis, the ratio of the reacting components, the order of their introduction, the concentration of water and ammonia, the synthesis temperature) on the morphology, size and content of functional groups of aminosilica nano- and submicrospheres. The recommendations for the synthesis of particles with predetermined properties were done. It is shown, that the ratio of the reacting components mainly affects the content of 3-aminopropyl functional groups and the temperature of the hydrolytic polycondensation reaction - the size of the particles.

Keywords: silica nanoparticles and submicrospheres, aminopropyl groups, Stöber method.

Introduction

Silica nanoparticles are prominent in research, as they are easy to synthesize and are widely used in various fields such as catalysis [1], adsorption (including adsorption of pigments) [2], medicine [3], manufacturing of electronic and thin supports, and electronic insulation materials [4]. The quality of most of these products is largely dependent on the size and size distribution of the particles and the nature, content, and stability of their functional groups. The formation of silica nanoparticles and their size are controlled by the rate of two reactions: alkoxysilanes hydrolysis to form oligomers with silanol groups $\text{Si}(\text{OR})_4 + \text{H}_2\text{O} \rightarrow \text{Si}(\text{OH})_4 + 4\text{ROH}$, and condensation of oligomers to form siloxane bonds $2\text{Si}(\text{OH})_4 \rightarrow 2(\text{O}-\text{Si}-\text{O}) + 4\text{H}_2\text{O}$.

In 1968 Stöber et al. described the synthesis of monodisperse spherical silica nanoparticles by hydrolytic polycondensation of silicon alkoxides in aqueous alcohol solutions in the presence of ammonia [5]. So, there were synthesized silica particles ranging in size from 50 nm to 1.5 microns with narrow size distribution. In the same publication, it was shown that with increasing concentration of ammonia, the size of silica particles decreases. With respect to the concentration of water and alcohol, it was necessary to select specific conditions. Later [6], there was determined the effect of temperature and the nature of solvent on the particle size, and in [7] - the impact of the components ratio and components addition order during the reaction. Thus, so far, there were suggested techniques for obtaining silica nanoparticles and some of the factors that affect their properties were determined.

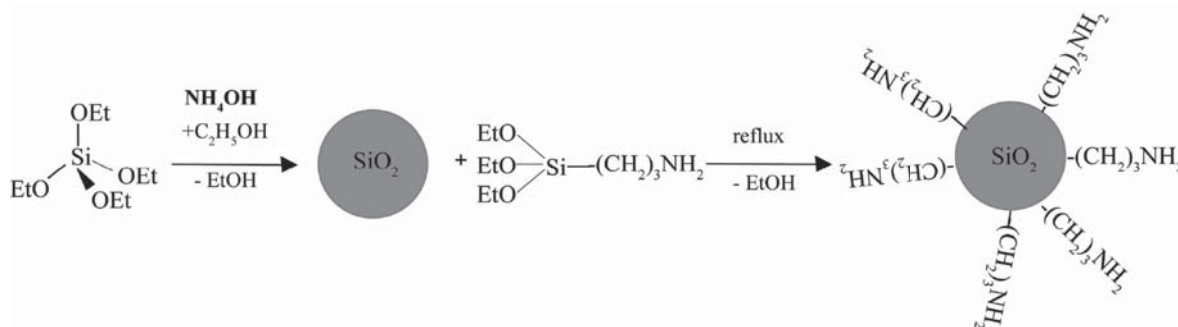
Functionalization of surfaces of such materials significantly extends their applications. Recently, more and more silica microspheres, especially containing 3-aminopropyl groups are used for adsorption of biomolecules [8] and metal ions [9]. This is due to the participation of amino groups in hydrogen bonds and the formation stable metal complexes. It is not surprising, that already in the 1990th, there appeared publications about functionalization of silica particles [10-12]. However, there still lacks the systematization of the material, and there are no answers to such important questions as which ratios of ingredients, temperature, amount of catalyst, etc. should be used to obtain silica particles of a certain size and with the required content of functional groups. Therefore, the subject of this paper is such analysis.

Methods of synthesis: one-step and two-steps

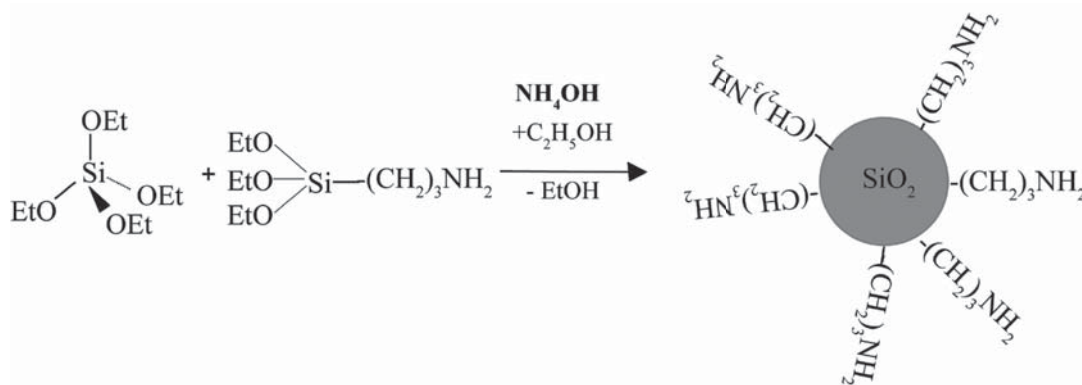
The search for the techniques of synthesis of spherical silica particles with 3-aminopropyl groups in their surface layers was launched in [10]. Some authors suggested two- (scheme 1) and single-stage (scheme 2) [11] techniques.

The two-stage method included the formation of pure silica nanoparticles (either extracted or not from their reaction solution) with their subsequent modification with 3-aminopropyl groups. For example, Badley et al. first prepared silica nanoparticles in water-ethanol-ammonia solution, then the solvent was removed and the reaction between silica and 3-aminopropyltrimethoxysilane (APTMS) was held in DMF by heating to 100°C. Such sample contained 0.81 mmol/g of amino groups at components ratio $\sim 4/1$ ($\text{SiO}_2/\text{APTMS}$) [10]. Using the same ratio of alkoxysilanes in water-ethanol-ammonia solution, Badley et al. also prepared sample with groups content of 0.61 mmol/g, firstly adding TEOS to the reaction mixture, and after 5 h - APTMS. Moreover, the stirring with APTMS was accompanied by ultrasonic treatment for 20 h [10]. Scientists [2] also produced spheres via two-stage method. But the presence of amino groups in them was not proved, their content was not specified and the TEOS/APTES (3-aminopropyltriethoxysilane) ratio was ~ 500 . Blaaderen et al. in [11], except for one-stage synthesis, also conducted surface modification of silica particles. Modification was carried out at TEOS/APTES ratios equal to 1/3 and $\sim 1/1$, by the addition of APTES to alkosol and stirring the mixture for 1 h at room temperature followed by boiling for 2 h and partial stripping of the solvent. Thus, the

authors obtained particles of 9 and ~ 70 nm in size, but only the former (according ^{29}Si MAS NMR spectroscopy data) contained T^3 and T^2 structural units, indicating a consolidation of functional groups on the surface of these particles, according to elemental analysis their content was 1.5 mmol/g.



Scheme 1. Two-steps synthesis of functionalized silica nanoparticles.



Scheme 2. One-step synthesis of aminofunctionalized silica nanoparticles.

We performed similar syntheses (surface modification of nanoparticles using APTES) at room temperature, but according to IR spectroscopy and acid-base titration did not observe the presence of amino groups in the particles [13]. However, authors in [14] describe the preparation of silica particles with amino groups at room temperature. Thus, the suspension of synthesized silica particles initially was stirred for 24 h, and after that, another 24 h with APTES (ratio of components was 1/1). The content of functional groups was not determined, but they were identified by ^{13}C and ^{29}Si MAS NMR spectroscopy.

One-step method of synthesis was also considered in [11], where alkoxy silanes (first APTES, and after 1 min - TEOS) at a ratio of about 1/1 were added to water-ethanol-ammonia solution. The resulting particles were about 100 nm in size with 3.2 mmol/g of amino groups. That is, there was developed one-step method of obtaining silica nanoparticles with high content of 3-aminopropyl groups. However, the sample contained both spherical particles, and non-spherical impurities [13]. Therefore, we examined in more detail the peculiarities of obtaining silica particles with 3-aminopropyl functional groups. It was established that the addition of APTES to ethanol-ammonia solution containing already formed silica particles does not lead to the fixation of amino groups on their surface. This requires boiling of the suspension or changing of the sequence alkoxy silanes introduction (first APTES and then TEOS). Moreover, it was stated in [12] that stirring APTES in water-ethanol-ammonia solution does not result in visible changes of the reagent, and adding TEOS after stirring for 24 h forms a gel-like substance.

The variation of the ratio of the reaction components

References of such specifically conducted research were not found. But in the paper [11], changing the components ratio from 1/3 to 1/1 determined the decrease in the particle size from ~ 10 nm to ~ 70 nm and the drop in the contents of amino groups from 3.2 mmol/g to 0.2 mmol/g (at the margins of the experimental error) in obtaining two-stage particles. Thus, it is clear that amino groups, having basic properties, affect the size of the obtained particles. In [12], it was shown that for one-stage synthesis under the same conditions an increase in particle size - 120 nm, 140 nm and 182 nm was observed by changing the component ratio from 1.5/1, 2/1 to 3/1, respectively. Our research

[13] confirmed such trend (Figure 1). Moreover, it was found, that the increase in the molar ratio of TEOS/APTES also improves morphological characteristics of the samples. However, the content of functional groups significantly decreased with increasing ratio to 6/1.

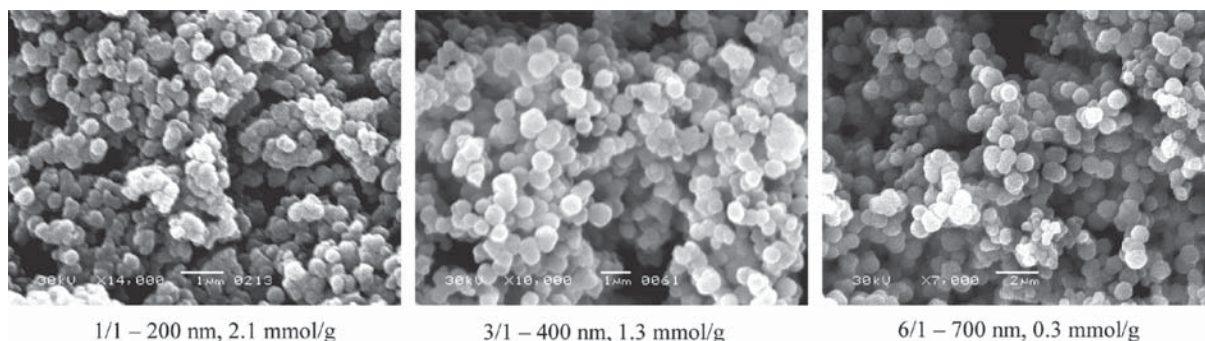


Figure 1. The influence of the ratio of reacting of alkoxysilanes (TEOS/APTES).

Effect amount of water and ammonia on the morphology and concentration of 3-aminopropyl groups

Some authors believe, that the amount of water in the synthesis must be greater [10,11], and others - that the water from ammonia solution is sufficient for the reaction of hydrolytic polycondensation [12]. Our studies have shown [13] that the extra amount of water does not affect the particle size and the content of functional groups.

In [5,7] the influence of the concentration of water and ammonia was considered in detail for silica nanoparticles (Figure 2). From this figure, it is evident that if there is a direct dependence between particle size and concentration for the ammonia, initially increasing concentration of water promotes the increase in particle size, followed by its sudden decrease. In addition, it was noticed that heterodispersed particle size distribution is observed in small quantities of alcohol. As for particles with 3-aminopropyl groups, it should be noted that the amino group itself creates an alkaline environment. In addition, the order of adding ammonia as a catalyst to the reaction solution is also very important. When ammonia is injected into the water-ethanol solution before alkoxysilyl components, APTES should be added first, or the synthesis should be conducted with heating, otherwise, amino groups would not be fixed on the surface of particles [10,11]. However, co-condensation of two alkoxysilanes (TEOS and APTES) can be used to form aminospheres at room temperatures by mixing components and adding ammonia as a catalyst to this mixture [12]. We also showed that silica microspheres with 3-aminopropyl groups formed without the use of ammonia [13]. Adding ammonia only improved particle size distribution, the content of functional groups did not change (Figure 3), but the size of the formed particles increased. Therefore, there was not observed simple dependence between the concentration of ammonia and particle size for aminosilica.

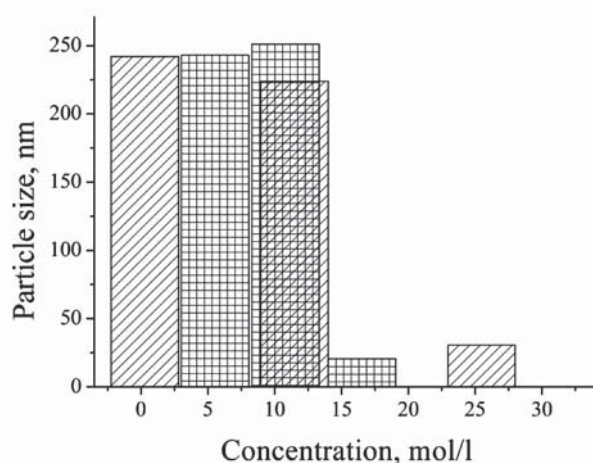


Figure 2. The effect of ammonia (lines) and water (cells) on silica particle size [7].

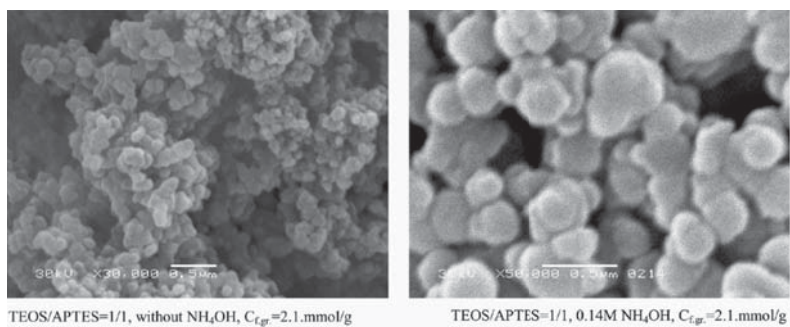


Figure 3. The effect of ammonia for aminosilica particles.

Effect of synthesis temperature

As shown in Figure 4 [6], the particle size decreases with increasing temperature for the silica particles. The most important result is that silica spheres can be synthesized in a wide size range (0.2-2.0 μm) using TEOS and alcohol solvent by changing the reaction temperature. The synthesized particles are relatively monodisperse and size distribution becomes broader with increasing temperature. Other authors [7] extended these studies and the effect of temperature on the particle size of the silica was studied at different concentrations of ethanol. These comparative studies were conducted from 30 to 70°C. The authors concluded that the particle size increases with increasing temperature in less dilute solutions (solvent - ethanol), respectively, reducing the particle size was observed with increasing temperature in the more dilute solutions [7]. These dependencies are represented in the literature for aminosilica particles. Only [10] refers to the fact that heating the suspension to 100°C for 24 h does not contribute to the consolidation of more groups on the surface but contributes to the stability of the surface layer by modifying silica particles with APTES.

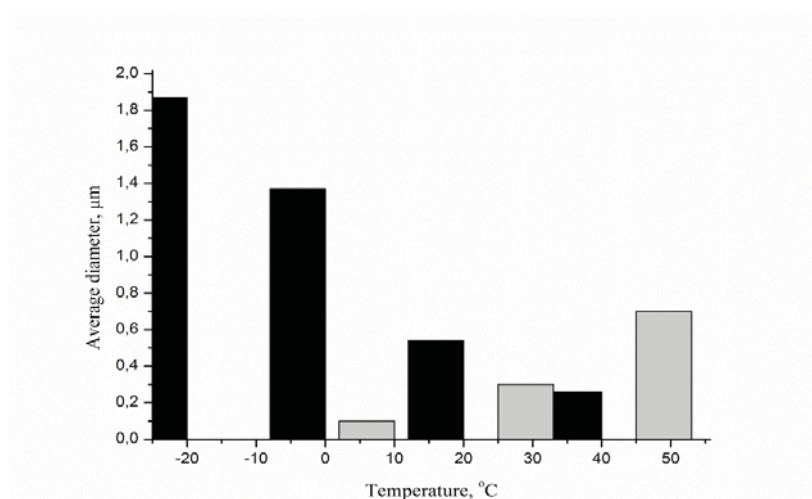


Figure 4. The average diameter of silica spheres (black) [6] and aminosilica spheres (gray) obtained using different temperatures.

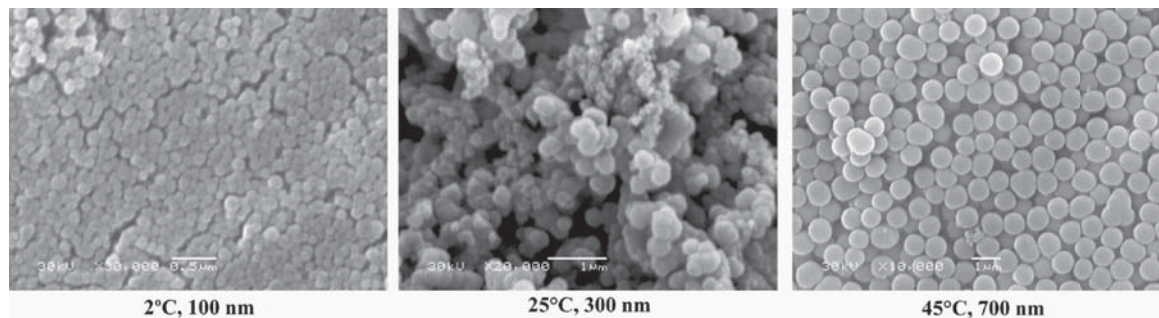


Figure 5. SEM images of aminosilicas at different temperatures.

We studied the influence of the synthesis temperature on particle size and content of functional groups. The synthesis was performed by mixing alkoxysilanes and adding ammonia after the appearance of opalescence at different temperatures - 2°C, 25°C and 45°C [13]. Comparing these samples to their size (Figure 5), it is easy to conclude that the increase in temperature of an ice bath ($\approx 2^\circ\text{C}$) to 45°C leads to the 7 times increase in the diameter. This increases the content and functional groups.

Conclusions

There was analyzed the influence of such factors as components addition order, reacting alkoxysilanes ratio, temperature, amount of water and solvent on the morphology and functional groups content in aminosilica microspheres. It was determined, that contrary to “pure” silica spheres, ammonia has no decisive influence on the particle size of aminosilica microspheres, and there is an inverse temperature relationship: namely, with growing temperature, particle size is not decreasing but increasing. Two-component system TEOS/APTES significantly differs from one-component because here the formation of functionalized particles can occur without introducing ammonia solution. Modification of silica particles with 3-aminopropyltriethoxysilane in ammonia-alcohol solution does not lead to fixation of the groups on the surface of silica particles (at room temperature), because the processes of condensation dominates over hydrolysis in alkaline environment. It was shown that the synthesis temperature has a significant impact on the shape and size of the particles, and the ratio of the reacting alkoxysilanes on the content of the 3-aminopropyl groups.

Acknowledgments

This work was carried out within the framework to the State Target Scientific and Technical Program of NASU “Nanotechnologies and Nanomaterials” (project No 6.22.5.42).

References

1. Banerjee, S.; Santra, S. Remarkable catalytic activity of silica nanoparticle in the bis-Michael addition of active methylene compounds to conjugated alkenes. *Tetrahedron Letters*, 2009, 50(18), pp. 2037–2040.
2. Wu, Z.; Xiang, H.; Kim, T.; Chun, M.-S.; Lee, K. Surface properties of submicrometer silica spheres modified with aminopropyltriethoxysilane and phenyltriethoxysilane. *Journal of Colloid and Interface Science*, 2006, 304, pp. 119–124.
3. Knopp, D.; Tang, D.; Niessner, R. Review: Bioanalytical applications of biomolecule-functionalized nanometer-sized doped silica particles. *Analytica Chimica Acta*, 2009, 647, pp. 14–30.
4. Aspen Aerogels. <http://www.aerogel.com/ehs.html>.
5. Stöber, W.; Fink, A.; Bohn, E. Controlled growth of monodisperse silica spheres in the micron size range. *Journal of Colloid and Interface Science*, 1968, 26, pp. 62–69.
6. Tan, C.G.; Bowen, B.D.; Epstein, N. Production of monodisperse colloidal silica spheres: effect of temperature. *Journal of Colloid and Interface Science*, 1987, 118(1), pp. 290–293.
7. Rao, K. S.; El-Hami, K.; Kodaki, T.; Matsushige, K.; Makino, K. A novel method for synthesis of silica nanoparticles. *Journal of Colloid and Interface Science*, 2005, 289, pp. 125–131.
8. Enrichi, F. Luminescent amino-functionalized or erbium-doped silica spheres for biological applications. *Annals of the New York Academy of Sciences*, 2008, 1130, pp. 262–266.
9. Najafi, M.; Yousefi, Y.; Rafati, A.A. Synthesis, characterization and adsorption studies of several heavy metal ions on amino-functionalized silica nano hollow sphere and silica gel. *Separation and Purification Technology*, 2012, 85, pp. 193–205.
10. Badley, R.D.; Ford, W.T.; McEnroe, F.J.; Assinks, R.A. Surface modification of colloidal silica. *Langmuir*, 1990, 6, pp. 792–801.
11. Bergna, H.E. Ed. *The Colloid Chemistry of Silica Advances in Chemistry Series 234*, American Chemical Society: Washington, DC, 1994; pp. 83–111.
12. Van Blaaderen, A.; Vrij, A. Synthesis and characterization of monodisperse colloidal organo-silica spheres. *Journal of Colloid and Interface Science*, 1993, 156, pp. 1–18.
13. Melnyk, I.V.; Tomina, V.V.; Zub, Yu.L. Synthesis submicro- and nanoscale spherical silica particles with 3-aminopropyl groups in the surface layer. The 3rd International Conference Nanomaterials: Application and Properties, 16–21 September, 2013: Proceedings of the international conference nanomaterials: applications and properties, Alushta, the Crimea, Ukraine, 2(1), pp. 02PCN40-1 -02PCN40-3.
14. Berriozabal, G.; R. de Miguel, Y. Synthesis and characterisation of silica nanoparticles bearing different functional groups obtained via a two-stage method. *Physica Status Solidi C* 7, 2010, 11–12, pp. 2692–2696.

SYNTHESIS AND CHARACTERIZATION OF CdSe COLLOIDAL QUANTUM DOTS IN ORGANIC SOLVENT

Ion Geru^{a,*}, Olga Bordian^{a,b}, Constantin Loshmansky^c, Ion Culeac^{a,b}, Constantin Turta^a

^a*Institute of Chemistry of Academy of Sciences of Moldova, 3, Academiei str., Chisinau MD 2028, Republic of Moldova*

^b*Institute of Applied Physics of Academy of Sciences of Moldova, 5, Academiei str., Chisinau MD 2028, Republic of Moldova*

^c*University of the Academy of Sciences of Moldova, 3/2, Academiei str., Chisinau MD 2028, Republic of Moldova*

*e-mail: iongeru11@gmail.com

Abstract. In this paper we present experimental results on preparation and characterization of colloidal CdSe quantum dots in organic solvent. CdSe QDs were synthesized following a modified literature method. CdSe QDs were isolated by adding acetone to the cooled solution followed by centrifugation. CdSe QDs have been characterized by UV-Vis absorption and photoluminescent (PL) spectroscopy. The average CdSe particles size estimated from the UV-Vis absorption spectra was found to be in the range 2.28-2.92 nm which is in good agreement with PL measurements.

Keywords: colloidal quantum dots, semiconductor, cadmium selenide, nanocrystals, photoluminescence.

Introduction

Among various semiconductor quantum dots (QDs) extensive research efforts have been developed over the last decade in the case of CdSe QDs because of their attractivity for various application in optoelectronics, photonics, medicine, etc. [1-3]. In spite of the problems related to the toxicity of Cd compounds, the possibility of tuning of the optical parameters of CdSe QDs makes them very attractive for technological development as well as for optoelectronics and biomedical applications. The size of QDs can be easily controlled by different ways, for example by variation of the reaction time, or the temperature of the solvents, by variation of the concentration of the reaction solvents, etc. This means a relatively simply and convenient technology for controlling the optical parameters of the nanocomposite structures for practical exploitation. For example, PL emission from colloidal CdSe quantum dots can be adjusted in a relatively wide spectral range from 465 to 670 nm [2]. The technology makes it possible to prepare different sized nanocrystals with high PL efficiency and narrow PL band, while PL emission may cover a narrow spectral band, tuned from blue to red and even up to near infrared. Control and improvement of optical properties of CdSe quantum dots remain on the agenda of research in the field of nanotechnology.

Experimental details

The technology of preparation of the CdSe nanodots is well described in details in the literature and an extended list of publications in this field can be consulted. Colloidal semiconductor QDs described in this paper were prepared via a chemical route.

Materials

Cadmium oxide (99.999%), oleic acid (90%), selenium (99.5%, 100 mesh), trioctylphosphine (90%), 1-octadecene (90%), tributylphosphine (90%), were purchased from Aldrich and used without further purification.

Synthesis

CdSe semiconductor nanocrystals were synthesized in a three-neck flask equipped with condenser, magnetic stirrer, thermocouple, and heating mantle. Typically the synthesis of the nanocrystals CdSe was carried out at 170°C by the following method. At the first step the stock solution was prepared, containing 180 mg of Se powder, 3 mL of 1-octadecene (ODE), 2 mL tributylphosphine (TBP) and 0.8 mL of trioctylphosphine (TOP) are mixed with intense stirring. The Cd precursor solution was prepared from 80 mg of CdO powder, 3 mL of 1-octadecene, 1 mL of TBP (tributylphosphine) and 4 mL of oleic acid. These compositions were mixed together by vigorous stirring. At the next step at the temperature 170 °C 2 mL of the Stocks solution was quickly injected into the hot Cd precursor solution and then this mixture was kept at 170 °C. Different-sized QDs were obtained varying the reaction time. The colloidal quantum dots solutions were collected at determined reaction time interval after the injection, for obtaining the desired size of quantum dots. The obtained CdSe QDs were further isolated and purified by adding acetone to the cooled solution followed by centrifugation at 8000 rpm for about 30 min.

Characterization

CdSe nanoparticles have been characterized by UV-Vis absorption and photoluminescent (PL) spectroscopy. The average CdSe particles size for three selected samples was estimated from the position of the first excitonic peak in the UV-Vis absorption spectrum and was found to be in the range 2.28 - 2.92 nm which correlates with PL experimental data. PL spectra were measured under excitation of a laser beam 337 or 405 nm using a MDR-23 monochromator and a photon counting module H9319-12 connected to a PC.

Results and discussion

Figure 1 shows the image of the prepared CdSe quantum dots dispersed in chloroform. From right to left the particle size increases, as well as the suspension color changes from light orange to reddish. This is a good illustration of the effect of the particle size on optical absorption of the quantum dots.

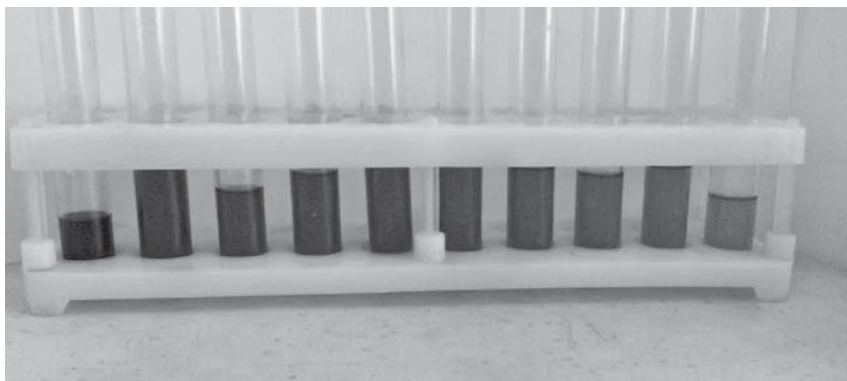


Figure 1. Size-dependent color of luminescent CdSe nanoparticles.
The particle size increases from right to left.

Figure 2 illustrates the absorbance spectra of the colloidal chloroform solution of the prepared QDs with different particles size. The absorption peaks appear very clear on each curve, indicating the presence of CdSe QDs. The reaction time for selected samples 1, 2, 3 increases by 50 s, and the absorption peak red-shifts from 494.7 up to 543 nm, sequentially. The absorption edge is relatively sharp, indicating a relatively narrow size distribution of the nanoparticles.

From the peak positions, one can estimate the average size of CdSe QDs. From the position of the first excitonic peak the size of nanoparticles have been evaluated through the empirical relation [3]:

$$d = (1.6122 \times 10^{-9})\lambda^4 - (2.6575 \times 10^{-6})\lambda^3 + (1.6242 \times 10^{-3})\lambda^2 - (0.4277)\lambda + 41.57 \quad (1)$$

where d (nm) is the average diameter of the CdSe QDs and λ (nm) is the wavelength of the first excitonic peak of the corresponding sample.

The size of CdSe quantum dots was varied for samples 1 - 3 by changing the reaction time, and was calculated as 2.28, 2.42 and 2.92 nm respectively. This QDs size implies the strong confinement of the charge carriers, while the confinement energies of the electron and hole are larger than the Coulomb interaction [3-5].

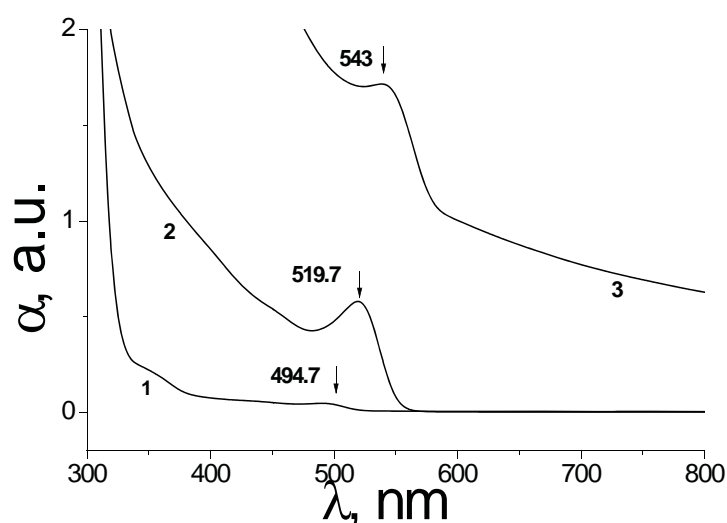


Figure 2. UV-Vis absorption spectra of suspension of CdSe quantum dots in chloroform grown at various reaction times. The plots 1 - 3 correspond to three dots samples collected at 50 s time interval from the injection. The reaction time, t : (1) t_0 ; (2) $t_0 + 50$ s; (3) $t_0 + 100$ s.

We can compare the energy of the main excitonic peak E as a function of the size of the nanocrystal from the relation [5-7]:

$$E = E_g + \frac{\hbar^2 \pi^2}{2R^2} \left(\frac{1}{m_e^*} + \frac{1}{m_h^*} \right) - \frac{1}{R} \left(\frac{1.8e^2}{4\pi\epsilon_0\epsilon_r} \right) \quad (2)$$

where E_g is the energy gap of bulk CdSe ($E_g = 1.7$ eV, R is the size of the nanoparticle, m_e^* and m_h^* are the effective masses of the electron and hole. The corresponding values for the effective masses are as reported elsewhere [5,8]: $\frac{m_e^*}{m_0} = 0.13$ and $\frac{m_h^*}{m_0} = 0.45$ and the dielectric constant $\epsilon_r = 10.6$, ϵ_0 is the permittivity of free space and e is the electron charge. If we take the particles diameter calculated from the absorption spectra in Figure 2 as 2.28 nm (1), 2.42 nm (2) and 2.92 nm (3), then the calculated exciton energies are respectively 2.31, 2.24 and 2.05 eV. On the other side, the positions of the excitonic peaks determined from the absorption spectra in Figure 2 are a bit higher, and represent 2.5, 2.39 and 2.28 eV respectively. The difference in the values of E calculated from (2) and the values determined from the absorption spectra in Figure 2 is determined basically by the error related to Eq.(1) as well as by approximations involved in the theoretical model based on the effective mass approximation with the electron-hole pair confined at the center of an infinite spherical potential wall [5,7].

The energy values calculated from (2) and Figure 2 are higher than E_g of the bulk CdSe (1.7 eV at 300 K) which is indicative of a blue shift of the absorption edge. The increase of the band gap is determined by the quantum size effect of small crystallites, and the calculated values for the diameter of the nanocrystals are less than the bulk CdSe exciton Bohr radius 5.6 nm [9,10]. As far as the size of quantum dots investigated here are smaller than their Bohr radius, they exhibit size-dependent properties [3,6]. Eq.(2) illustrates the quantum confinement effect of quantum dots. In this equation the second term in represents the quantum confinement term which is proportional to R^{-2} , and shifts E to higher energy when the diameter of the nanoparticle decreases. The third term in Eq.(2) represents the Coulomb term, which is proportional to R^{-1} . It shifts E to lower energy as the radius of the nanoparticles decreases. Consequently, when the particles size decreases the energy gap increases [3,6,7].

The PL emission spectra have been registered at room temperature under the excitation of laser beam 405 nm (Figure 3). The PL emission spectra of CdSe colloidal QDs solution in chloroform are represented in Figure 3, which shows a Stokes red-shift for each sample. From these spectra one can suggest that for moderate reaction times there one can obtain good PL characteristic with narrow emission peaks. While at longer reaction times, the PL intensity is substantially reduced. We can suggest that at moderate growth times one can obtain better emission characteristics and monodispersed size distribution.

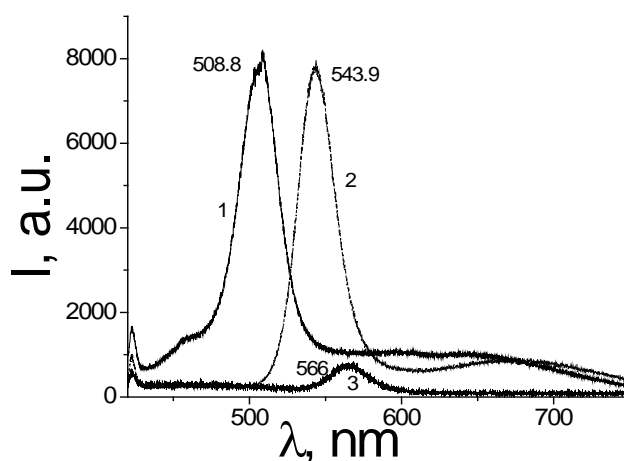


Figure 3. PL spectra of CdSe colloidal quantum dot samples dissolved in chloroform, collected at 50 sec time interval. The plots 1 - 3 correspond to three dots samples, as indicated in Figure 2. The excitation light is a N_2 laser beam 337 nm.

These experimental results are consistent with previous work on CdSe QDs [4, 8-10]. The PL spectrum for CdSe nanodots can be characterized by an almost Gaussian line with the peak maximum shifting from 508 nm to 566 nm in dependence of the CdSe nanoparticle size. The PL emission of CdSe QDs is dominated by a near-band-edge emission; while a weak broad band in the near IR can be related to the surface shallow trap emission is markedly suppressed. The

PL spectrum for the sample 2 can be deconvoluted in a major Gaussian line, positioned at 508 nm and other two low intensities bands shifted toward red wavelengths (Figure 4). While the CdSe QDs size tends to increase with increasing the reaction time, the PL bands shifts from 508 to 566 nm (Figure 3), which correlates with the position of the main excitonic peak shifting in the absorption spectrum (Figure 2). The narrow line width of the main PL band suggests that particles have a narrow size distribution, while the low intensity emission from surface trap states at longer wavelengths suggests low concentration of surface defects.

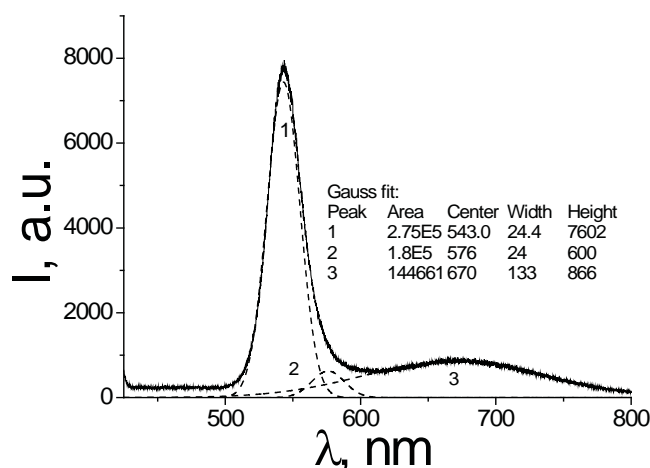


Figure 4. Deconvolution of the PL spectrum for sample 2.
The peaks are situated at 543, 576 and 670 nm.
The FWHM for the main band at 543 is ~ 24 nm.

Conclusions

We present experimental results on preparation and characterization of colloidal CdSe quantum dots. CdSe nanoparticles were synthesized following a modified literature method. CdSe QDs were isolated by adding acetone to the cooled solution followed by centrifugation. CdSe QDs have been characterized by UV-Vis absorption and photoluminescent (PL) spectroscopy. The average CdSe QDs size estimated from the UV-Vis absorption spectrum was found to be in the range 2.28-2.92 nm which is in good agreement with PL emission spectra registered at room temperature.

References

1. Somers, R.C.; Bawendi, M.G.; Nocera, D.G. CdSe nanocrystal based chem-/bio- sensors, *Chemical Society Reviews*, 2007, 36, pp. 579–591.
2. Jorge, P.; Martins, M.A.; Trindade, T.; Santos, J.-L.; Farahi, F. Optical Fiber Sensing Using Quantum Dots, *Sensors*, 2007, 7, pp. 3489-3534.
3. Yu, W.W.; Qu, L.; Guo, W.; Peng, X. Experimental Determination of the Extinction Coefficient of CdTe, CdSe, and CdS Nanocrystals, *Chemistry of Materials*, 2003, 15, pp. 2854-2860.
4. Nguyen, H.Q. Synthesis and optical properties of CdSe nanocrystals and CdSe/ZnS core/shell nanostructures in non-coordinating solvents, *Advances in Natural Sciences: Nanoscience and Nanotechnology*, 2010, 1, doi:10.1088/2043-6254/1/2/025004.
5. Bawendi, M.G.; Steigerwald, M.L. and Brus, L.E. The Quantum Mechanics of Larger Semiconductor Clusters ("Quantum Dots"), *Annual Review of Physical Chemistry*, 1990, 41, pp. 477-496.
6. Wang, Y.; Herron, N. Nanometer-Sized Semiconductor Clusters: Materials Synthesis, Quantum Size Effects, and Photophysical Properties, *The Journal of Physical Chemistry*, 1991, 95, pp. 525-532.
7. Brus, L. Quantum crystallites and nonlinear optics, *Applied Physics A*, 1991, 53(6), pp. 465-474.
8. Biswas, A. and Ghosal, A. Hole Transport Characteristics of CdSe Single Quantum Wells at Low Temperatures, *Journal of Electron Devices*, 2011, 10, pp. 444-447.
9. Meulenbergh, R.W.; Lee, J.R.I.; Wolcott, A.; Zhang, J.Z.; Terminello L.J.; van Buuren, T. Determination of the Exciton Binding Energy in CdSe Quantum Dots, *ACS Nano*, 2009, 3 (2), pp. 325–330.
10. Jarosz, M. The physics and Chemistry of Transport in CdSe Quantum dot Solids, Ph.D. Thesis, Massachusetts Institute of Technology, USA, 2004.

BIOMATERIALS BASED ON NANOHYDROXYAPATITE

Gabriela Ciobanu^{a*}, Constantin Luca^a, Octavian Ciobanu^b

^a“Gheorghe Asachi” Technical University of Iasi, Faculty of Chemical Engineering and Environmental Protection,
63, Prof. dr. docent Dimitrie Mangeron Rd., Iasi 700050, Romania

^b“Grigore T. Popa” University of Medicine and Pharmacy, Faculty of Medical Bioengineering,
16, Universitatii str., Iasi 700115, Romania

*email: gciobanu03@yahoo.co.uk; phone (+40 741) 02 51 63; fax (+40 232) 27 13 11

Abstract. In this study, the porous hydroxyapatite-filled cellulose acetate scaffolds were prepared via dry-wet phase inversion method by dispersing hydroxyapatite nanoparticles in the polymeric matrix. The calcined hydroxyapatite prepared by wet precipitation method has the crystal size smaller than 50 nm. The unfilled and hydroxyapatite-filled cellulose acetate scaffolds have an asymmetric structure consisting of two layers, the dense top layer (active layer) supported by the porous sub-layer (substructure). The cross-sectional SEM images revealed that hydroxyapatite nanoparticles were well dispersed in the cellulose acetate matrix.

Keywords: hydroxyapatite, cellulose acetate, scaffold.

Introduction

In the biological hard tissues the calcium phosphates are the most important inorganic constituents. From the calcium phosphate family, the hydroxyapatite $\text{Ca}_{10}(\text{PO}_4)_6(\text{OH})_2$ is an important representative being present in bone, teeth, and tendons to give these organs stability, hardness and function [1]. The hydroxyapatite has many practical applications in the medicine and chemistry fields. In biomedical applications, the hydroxyapatite has been used as bioceramics due to its excellent biocompatibility and osteoconductivity properties [2]. The hydroxyapatite provides bioactivity but is brittle, particularly in highly porous scaffolds which may also exhibit low strength [3]. Therefore, dense or porous polymer-hydroxyapatite composites have been investigated for synthetic bone graft substitutes and bone tissue engineering scaffolds [4,5]. Recently, many research efforts are focused on combining the characteristics of both hydroxyapatite and polymers to create hybrid materials to be used for hard tissue replacement applications [6]. The polymer/hydroxyapatite composites have attractive features as candidates for novel bone substitutes because they may show bone-bonding capacity and mechanical performances derived from the organic substrate.

In this work, hydroxyapatite and cellulose acetate are combined to form hydroxyapatite-filled cellulose acetate scaffolds with applications in the biomedical field. The hydroxyapatite nanocrystals were dispersed within the cellulose acetate matrix for improving their properties. The effects of hydroxyapatite loading on the morphology and properties of the resultant scaffolds were investigated.

Experimental

The hydroxyapatite nanopowder was synthesized by wet chemical precipitation method, as described elsewhere [7]. Calcium nitrate $\text{Ca}(\text{NO}_3)_2 \cdot 4\text{H}_2\text{O}$, ammonium phosphate dibasic $(\text{NH}_4)_2\text{HPO}_4$, HNO_3 and NaOH were purchased by Sigma-Aldrich (Germany). All reagents were of analytical grade and were used as received without further purification. Experiments were performed in distilled and deionized water. The $\text{Ca}(\text{NO}_3)_2 \cdot 4\text{H}_2\text{O}$ and $(\text{NH}_4)_2\text{HPO}_4$ were used as calcium source and as phosphorous source, respectively. An aqueous solution of 250 mL of $\text{Ca}(\text{NO}_3)_2 \cdot 4\text{H}_2\text{O}$ (0.01 M) was added drop-wise to an appropriate amount of $(\text{NH}_4)_2\text{HPO}_4$ (0.05 M) aqueous solution to achieve predetermined Ca/P atomic ratio of 1.67. The suspension was adjusted to pH=11 by adding small portions of 1 M NaOH and matured for 3 h at approximately 70 °C under magnetic stirring. The powder obtained was removed from the solution, washed with deionized water, dried at 110 °C for 24 h and calcined at a temperature of 800 °C during 3 h. The phase composition of the hydroxyapatite powder was characterized by X-ray diffraction (XRD) with X'PERT PRO MRD diffractometer (PANalytical, Netherlands) using monochromatic $\text{CuK}\alpha$ radiation ($\lambda=0.15418$ nm), operating at 40 kV and 50 mA over a 2θ range from 2° to 70°. The average crystallite size (D) of the hydroxyapatite powder was calculated from XRD data by the Scherrer equation, using the peak at $2\theta=25.9^\circ$ for (002) reflection. The morphology and chemical composition of the sample were studied by scanning electron microscopy (SEM) coupled with energy dispersive X-ray spectroscopy (EDX) with QUANTA 200 3D microscope (FEI, Netherlands). Silver sputtering was used to make the coating surfaces conductive for the SEM investigations. The pH measurements were realized with a Multi-Parameter Consort C831 (CONSORT, Belgium).

The pure cellulose acetate scaffold (denoted CA-HA-0) was prepared by the phase inversion method using cellulose acetate (CA) polymer and acetone as solvent, as described elsewhere [8]. The CA polymer and acetone were purchased by Sigma-Aldrich (Germany). The CA solution was made by dissolving a suitable quantity of CA polymer (20 wt.%) in acetone at atmospheric pressure and 22 °C for 3 h. Then, the polymer solution was casted on a glass plate at

a designated wet thickness using a casting knife at ambient temperature and left subsequently for 15 min in order to form the skin layer. After that, the cast film was dried at 70 °C for 24 h to remove residual solvents. The composite scaffolds were obtained by adding a calculated amount of HA into the CA polymer solution and mixing thoroughly before casting. The weight percentages of HA loaded in each scaffold were varied as stipulated in Table 1. The casting and curing of the composite samples are identical with those of the pure CA scaffolds.

Table 1

The characteristics of the unfilled and hydroxyapatite-filled cellulose acetate scaffolds.

Sample	HA content (%)	Thickness ^a (μm)	Pore diameter in active layer ^b (μm)	Pore diameter in substructure ^a (μm)	Porosity (%)	Density (g/cm ³)
CA-HA-0	0	208	1.33	99.3	69.7	0.209
CA-HA-10	10	178	1.08	70.1	65.2	0.314
CA-HA-20	20	127	0.97	42.7	51.8	0.327
CA-HA-30	30	86	0.94	20.9	40.1	0.342

a) by SEM method;

b) by Bubble-point method.

The morphology and chemical composition of the samples were elucidated by scanning electron microscopy (SEM) coupled with energy dispersive X-ray spectroscopy (EDX), with QUANTA 200 3D Dual Beam scanning electron microscope (FEI Co., USA). For the SEM-EDX investigations, gold sputtering was used to create a conductive coating surface. The pore diameters have been determined by Bubble-point method with a laboratory instrument. The porosity (ε) of the scaffolds was estimated by gravimetric method by the weight of liquid (isopropanol) contained in the scaffold pores, using the following equation:

$$\varepsilon = \frac{w_w - w_d}{\rho_w \cdot A \cdot L} \cdot 100 \quad (1)$$

where w_d is the weight of the dry sample (g), w_w is the weight of the wet sample after dipping into isopropanol for 2 h (g), ρ_w is the isopropanol density (0.785 g/cm³) at room temperature, A is the effective area of the sample (m²) and L is the sample thickness (m).

The feature characteristics of the prepared scaffolds are summarized in Table 1.

Results and discussion

The XRD method was applied to characterize the phase structure and crystallite size of the hydroxyapatite sample. The wide-angle XRD pattern (Figure 1a) indicate that the calcined hydroxyapatite powder has the characteristic peaks in the 2θ regions of 21°–29°, 32°–34°, 39°–41°, 46°–54°, in good agreement with the hexagonal hydroxyapatite phase (JCPDS Data Card 09–0432). The average crystallite size (D) of the hydroxyapatite powder was calculated from XRD data using the Scherrer equation, being of 49 nm.

The SEM and EDX methods were performed in order to determine the morphology and surface elemental composition of the hydroxyapatite. Figure 1b shows the SEM micrographs of the calcined sample. It is seen that the hydroxyapatite powder is composed of nanosized primary particles which tends to form agglomerates with intergranular micropores. The EDX analysis (Figure 1c) of the sample confirms the presence of the Ca, P, and O elements in HA crystallites. The Ca/P mole ratio was of 1.675 mostly close to 1.67 corresponding to the stoichiometric hydroxyapatite [1].

The formation of CA asymmetric scaffold is the result of microphase separation phenomena that occur during an evaporation step and/or quench step of an initially thermodynamically stable polymer solution. Consequently, the scaffold structure is affected by the conditions of scaffold preparation [9–11].

The unfilled and hydroxyapatite-filled cellulose acetate scaffolds with an asymmetric and interconnected porous structure were obtained by applying a phase inversion process. These asymmetric scaffolds have a very thin skin layer supported by a more open porous substructure, as seen in Figure 2. The formation of skin layer was attributed to the solvent evaporation during the microphase separation process. The size of the pores in the skin layer is very small compared to that in the substructure (Table 1). The CA scaffolds have internal micropores and macropores. At external surface of the scaffold, on the skin layer, many nanopores were formed during phase inversion process.

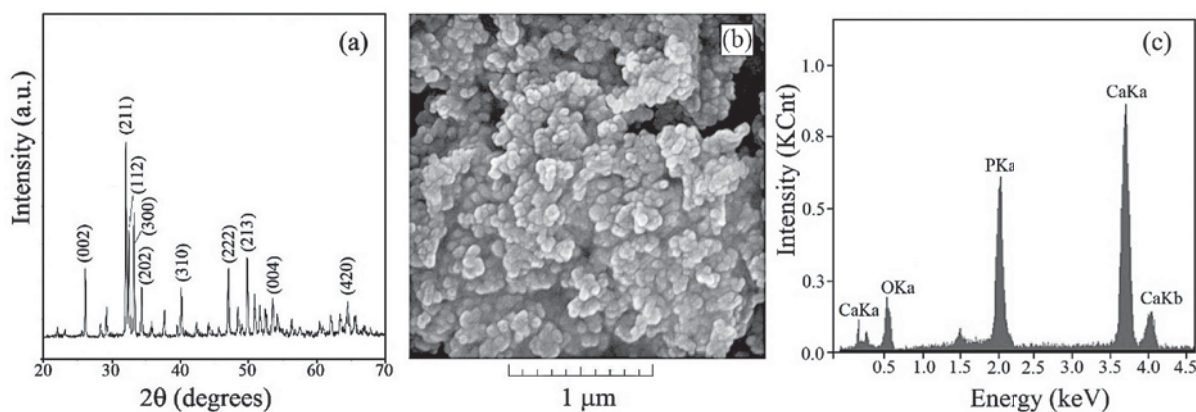


Figure 1. XRD pattern (a), SEM image (b) and EDX spectrum (c) of the hydroxyapatite sample.

The porosity of the scaffolds is high, and therefore this porous structure provides a good microenvironment for cell adherence, growth and proliferation. As shown in Table 1, the porosity of the composite samples decreases with the addition of the hydroxyapatite. The SEM images of the scaffolds in the cross-section (Figure 2) confirm the good incorporation of the hydroxyapatite in the polymeric matrix. Hydroxyapatite crystals can be seen spread over the internal surface of the scaffold as white spots. The most hydroxyapatite particles were dispersed uniformly within the scaffolds substructure, excepting for very few clusters that might have been resulting from nanosized particles coalescing in the polymeric matrix. We assume that the occurrence of these clusters is due to the fact that the surface of the hydroxyapatite contains OH functionalities (hydrophilic P–OH groups) causing inherent hydrophilicity to these particles. Therefore, some hydroxyapatite nanoparticles tend to adhere to each other via hydrogen bonding forming some irregular agglomerations within scaffold. This could reduce the efficiency of the dispersion process especially in the samples with higher hydroxyapatite particle contents (> 30 %).

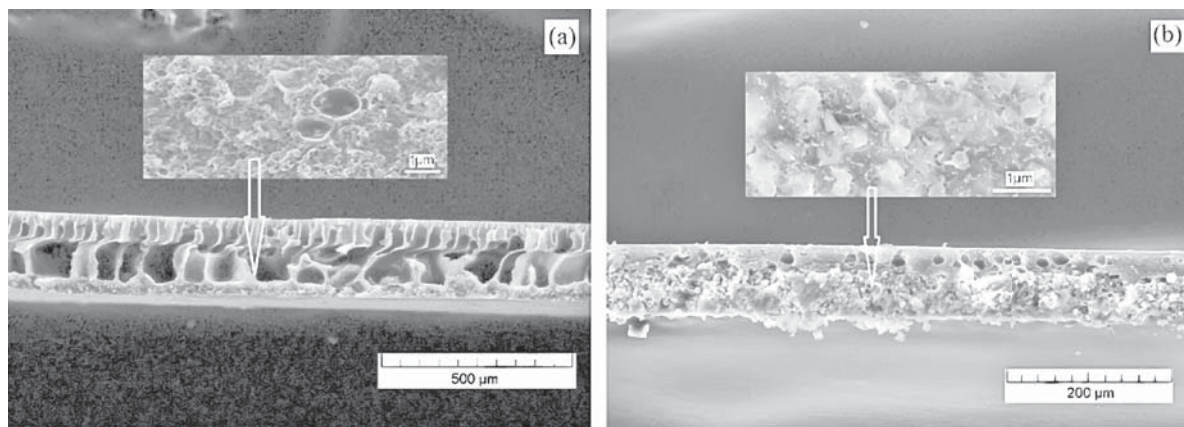


Figure 2. The SEM images of the scaffolds in the cross-section: a) CA-HA-0 and b) CA-HA-30 samples.

The incorporation of the hydroxyapatite crystals in CA matrix induces some changes into scaffold morphology. A good dispersion of the hydroxyapatite is important but difficult to obtain especially when small particles of hydroxyapatite are used. Interactions exist between hydroxyapatite and the used polymer. The hydroxyapatite acted as a cross-linker on the CA polymer and, finally resulted material being a reinforced scaffold.

The brittleness of the final scaffolds was influenced by the amount of hydroxyapatite in the scaffold. When the amount of hydroxyapatite particles in the composites was less than 30 %, the obtained scaffolds were intact and strong. On the other hand, when the amount of hydroxyapatite was higher than 30 %, the scaffolds possessed a relatively coarse surface becoming brittle.

Finally, the results of the present study indicate that the asymmetric hydroxyapatite-filled cellulose acetate scaffolds could be obtained by phase inversion method.

Conclusions

The hydroxyapatite nanopowder was produced by coprecipitation reactions. The XRD pattern of the hydroxyapatite sample display well-defined and sharp peaks in agreement with a high degree of crystallinity. The porous hydroxyapatite-filled cellulose acetate scaffolds were prepared via dry-wet phase inversion method. The unfilled and hydroxyapatite-filled cellulose acetate scaffolds have an asymmetric structure consisting of two layers: the dense top layer supported by the porous sub-layer. The SEM-EDX studies of the composites confirm the presence of the hydroxyapatite nanocrystals in the cellulose acetate matrix. The most hydroxyapatite particles were dispersed uniformly within the scaffolds substructure, excepting for very few clusters that might have been resulting from nanosized particles coalescing in the cellulose acetate matrix. The porosity of the scaffolds is high, and therefore this porous structure provides a good microenvironment for cell adherence, growth and proliferation.

References

1. Dorozhkin, S.; Epple, M. Biological and Medical Significance of Calcium Phosphates. *Angewandte Chemie International Edition*, 2002, 41, pp. 3130–3146.
2. Kong, L.; Gao, Y.; Lu, G.; Gong, Y.; Zhao, N.; Zhang, X. A study on the bioactivity of chitosan/nanohydroxyapatite composite scaffolds for bone tissue engineering. *European Polymer Journal*, 2006, 42, pp. 3171–3179.
3. Kane, R.; Roeder, R. Effects of hydroxyapatite reinforcement on the architecture and mechanical properties of freeze-dried collagen scaffolds. *Journal of the Mechanical Behavior of Biomedical Materials*, 2012, 7, pp. 41–49.
4. El-Kady, A.M.; Mohamed, K.R.; El-Bassyouni, G.T. Fabrication, characterization and bioactivity evaluation of calcium pyrophosphate/polymeric biocomposites. *Ceramics International*, 2009, 35, pp. 2933–2942.
5. Habraken, W.J.; Wolke, J.G.; Jansen, J.A. Ceramic composites as matrices and scaffolds for drug delivery in tissue engineering. *Advanced Drug Delivery Reviews*, 2007, 59, pp. 234–248.
6. Yarlagadda, P.; Chandrasekharan, M.; Shyan, J.Y.M. Recent advances and current developments in tissue scaffolding. *Bio-Medical Materials and Engineering*, 2005, 15, pp. 159–177.
7. Ciobanu, G.; Ilisei, S.; Harja, M.; Luca, C. Removal of Reactive Blue 204 dye from aqueous solutions by adsorption onto nanohydroxyapatite. *Science of Advanced Materials*, 2013, 5, pp. 1090–1096.
8. Ciobanu, G.; Carja, G.; Ciobanu, O. Preparation and characterization of polymer–zeolite nanocomposite membranes. *Materials Science and Engineering C - Materials for Biological Applications*, 2007, 27, pp. 1138–1140.
9. Ciobanu, G.; Carja, G.; Ciobanu, O. Use of SAPO-5 zeolite–filled polyurethane membranes in wastewater treatment. *Desalination*, 2008, 222, pp. 197–201.
10. Hou, Q.P.; Grijpma, D.W.; Feijen, J. Porous polymeric structures for tissue engineering prepared by a coagulation, compression moulding and salt leaching technique. *Biomaterials*, 2003, 24, pp. 1937–1947.
11. Guan, J.; Fujimoto, K.; Sacks, M.; Wagner, W. Preparation and characterization of highly porous, biodegradable polyurethane scaffolds for soft tissue applications. *Biomaterials*, 2005, 26, pp. 3961–3971.